SHAKEDOWN AND COLLAPSE OF SOME AXISYMMETRIC PRESSURE VESSEL HEADS AND NOZZLES

by

Ventura José Ortigão de MELLO SAMPAYO, Dipl.Eng.(I.S.T.)

A Thesis submitted for the degree of Doctor of Philosphy in the Faculty of Engineering

Department of Mechanical Engineering,
City and Guilds College,
Imperial College of Science and Technology,
University of London

November 1973

ABSTRACT

Computations of the elastic and elastic-plastic behaviour of some symmetrical pressure vessel heads and nozzle-sphere junctions is described; comparison of the stress concentration factors of the two geometries are made with previous published results.

The computed plastic strain values for a particular head are compared with experimental results in order to demonstrate the validity of the computational methods, and a collapse mechanism derived from the computed values is given.

From the computed results, the elastic-plastic behaviour for a series of nozzles:

(a) having a specified radius of toroidal knuckle and continuous thickness,

(b) for a specified radial nozzle-on-sphere having different geometries of the toroidal knuckle and a sphere thickness double that of the cylinder, is described.

A comparison is made of collapse and shakedown results using different criteria and work-hardening rules, and also using available results from a limit analysis for flush cylindrical nozzles.

It was generally found that the use of work-hardening in the calculation gave only a slight improvement in the predicted values for shakedown behaviour, using the ellipse of yield moving towards the stress state reached, In the case of radial nozzles on spheres, the ellipse expanding with work-hardening is also considered.

Tests concerning shakedown behaviour were carried out with a circular plate with a central hole, and with an almost symmetrical radial nozzle-on-sphere, both plate and nozzle-on-sphere being made of mild steel.

The results of these tests are presented and discussed; those for the nozzle-on-sphere case are compared with computed values of the elastic-plastic behaviour of rigid-plastic and work-hardening materials.

ACKNOWLEDGEMENTS

I would like to thank the Calouste Gulbenkian Foundation, the University of Lourenço Marques and the Instituto de Alta Cultura (Ministério de Educação Nactional) for support during the work reported here. Particular thanks should go to Dr. J.A. Blomfield, late of Imperial College, now with the Central Electricity Generating Board, to Dr. L.C. Laming and Dr. R.T. Smith, both of Imperial College and to Mr. Poynor, Babcock and Wilcox Ltd., for their advice and help and interest in this project.

I would also like to record my special thanks to my research supervisor, Dr. C.E. Turner, B.Sc.(Eng.), Ph.D., D.Sc.(Eng.), M.I.Mech.E. for his encouragement, help and interest.

Thanks are due to Mr. K. Walker for his help during the course of the experimental work and to Mr. C.E. Noad for his help in the preparation of this thesis.

Finally many thanks to my family for their presence in London with me all the time during the course of this work.

CONTENTS

TABLES

NOMENCLATURE AND ABBREVIATIONS

Nomenclature

a	material constant or geometry constant
A_n	constants of integration for the cylinder ($n = 1, \ldots 4$)
A', A''	constants of integration for the plate
b	material constant or geometry constant or suffix for shallow shell
ber, bei	Kelvin function
B', B''	constants of integration for the plate
c	suffix for cylinder or for collapse or material constant
C_i	variable in a non-linear strain distribution through the thickness, $i = \ell, \varphi$, or constants of integration for the sphere, ($i = 1, .. 4$)
d	mean diameter of cylinder, Figs. 3 to 5
D_o	mean diameter of sphere, Figs. 3 and 4
D	flexural rigidity [$= 2h^3E/3(1 - \nu^3)$]
e	strain with suffixes ℓ, φ, i and j
$\bar{e}_p$	equivalent plastic strain
E	Young's modulus
f	variable in a non-linear strain distribution through thickness
F	radial force per unit length, Fig. 1a; with suffix b for shallow sphere
g_1, g_2	series used in the Kelvin function
h	half thickness of shell, Fig. 1a, or height of the head
H'	slope of the equivalent stress v plastic strain curve ($= d\sigma_e/d\bar{e}_p$)
i,j	suffixes ($=\ell,\varphi$)
k	constant describing the cylindrical shell [$= \sqrt[4]{12(1 - \nu^2)/d^2t^2}$]
K_1	elastic stress concentration factor; ratio of maximum von Mises' equivalent stress to membrane equivalent stress (SCF)
K_1^*	elastic stress concentration factor; ratio of maximum shear stress to membrane shear stress [the * notation also applies to K_2 and K_3]
K_2	ratio of shakedown pressure to membrane yield stress ($= P_s^*/k_1$)

K_3	ratio of collapse pressure to membrane yield stress ($= P^*_c/k_1$)
ker,kei	Kelvin function
ℓ	meridional suffix and meridional length
L	axial load
L_y	axial load to cause yield
M	bending moments per unit length, with suffixes, ℓ, φ, i and j, Fig. 1b or work hardening case in Tables 1 to 12
N	direct force per unit length, with suffixes, ℓ, φ, i and j, Fig. 1a
p,P	pressure (numerically positive for internal), Fig. 1a, or with suffixes c, s and y
$\bar{\bar{p}}_m$	variable used in spherical heads
P_y	pressure for first yield at any point in the vessel
P^*	ratio of pressure to first yield pressure
P^*_c	ratio of collapse pressure to first yield pressure
P^*_s	ratio of shakedown pressure to first yield pressure
r	radius perpendicular to shell axis, Fig. 2b, or radius of Toroidal knuckle
R	mean radius of the sphere or non-work hardening case in Tables 1 to 12
s	suffix, either for the sphere or for shakedown load
SCF	stress concentration factor
t	cylinder thickness
T	either sphere or plate thickness
u	radial displacement, Fig. 2a
U_i	variable in non-linear strain distribution through the thickness ($i = \ell, \varphi$)
v	axial displacement, Fig. 2a
V	constant of integration for axial loading, per unit radian
x	meridional coordinate for the cylinder, Figs. 3 to 5
X	applied radial force per unit length, Fig. 1a
Y	applied axial force per unit length, Fig. 1a
y	suffix for equivalent stress limit of elasticity
W	axial force per unit length, Fig. 1a

α	complementary angle of $\theta(= \pi/2 - \theta)$, Fig. 3 and 4
β	shell thickness taper $(= dh/d\ell)$
γ	variable used in shallow shells $[= \sqrt[4]{(4\lambda^4 - \nu^2)/4}]$
δ	increment
ϵ	variable used for spherical shell
φ	circumferential suffix
ϕ	rotation of the meridional direction, Fig.2b
ϕ_i	change in curvature $(i = \ell, \varphi)$
χ	variable used for shallow shells $(= \gamma\, \alpha \sqrt{2})$
θ	angle between shell-wall normal and the radial direction, Fig. 1a
θ_o	the value of θ on a point on the sphere, defined by the intersection of cylinder-sphere geometries
θ_{A^i}	particular value of θ_o corresponding to points marked by A^i $(i = ' \; '' \; ''' \; 'v)$ on Figs. 19-21
λ	parameter describing spherical shell $(= \sqrt[4]{3(1 - \nu^2)}\ \sqrt{D_o/2T})$
ρ	smaller radii of curvature of the shell
σ	direct stress, with suffixes, ℓ, φ, i, j, c, m and y
σ_e	equivalent stress (von Mises' criterion)
σ'	deviatoric stress, with suffixes ℓ, φ, i and j
σ^*_m	ratio of meridional stress to yield or proof stress
σ^*_c	ratio of circumferential stress to yield or proof stress
σ_y	yield or proof stress
τ	shear stress
ν	Poisson's ratio
ω	nozzle parameter (Ref. 13) $(d/\sqrt{2D_oT})$, and variable used for spherical shell
$-$	mid-wall values
$=$	membrane values

Abbreviations (for further details see text, Chapter 2)

In connection with shakedown, based on:

SEM elastic calculations by the method of Macfarlane and Findlay, Ref. 12

SPC elastic-plastic computations with the ellipse of yielding moving along the path of the elastic stress ratios

SPT elastic-plastic computations with the ellipse of yielding moving along the radius, to the actual stress point considered

SPW elastic-plastic computations with the ellipse of yielding increasing in size with work-hardening

In connection with incipient collapse:

Intersection of the elastic line with the tangent drawn to a particular point on a given curve defined by:

C3I a line of one third the elastic slope intersecting an individual strain curve

C3E a line of one third the elastic slope intersecting an equivalent strain curve

C3D a line of one third the elastic slope intersecting the overall deflection curve

Based on the pressure to cause:

BSLY large increase in rate of spreading of local yield

C5I 5% individual maximum strain on the outer surface

C5E 5% equivalent maximum strain on the outer surface

C15I 1.5% individual maximum strain

C15E 1.5% equivalent maximum strain

CMEO large jump of the position of maximum equivalent strain on the outer surface

CSP the turning point on the stress path to the last anti-clockwise movement around an ellipse of yield (applied to nozzles)

INTRODUCTION

Design of pressure vessels has in the past been restricted to a "strength of materials" approach. With the demands of modern industry, the designer must now consider higher static and cyclic loading on the structure; he is also obliged to produce a more efficient design.

The methods of elasticity have been developed and applied to the design of pressure vessels but, although approximations to the correct solution have been used, the effort to present better approximations is still a subject demanding a great deal of research.

The improvement in knowledge of material behaviour beyond the elastic limit has made possible the development of some theories of plastic design i.e. design for structures loaded beyond this limit. The theorems of limit analysis and of slip line field have given to the designer the assistance of the theory of plasticity in the design of structures. Limit analysis was extended to plates by Hopkins and Prager [22]* in 1953 and to cylindrical shells by Drucker [80] in 1954; since then, limit analysis has been the object of much research and has lately been successfully applied to some cases of plastic design of pressure vessels e.g. [33] to [36]. Only in the late 1950's was limit analysis applied to nonsymmetrically loaded shells, although very few relevant works are available, e.g. [72]. Limit analysis is basically an approximate theory, since it considers the structure as having a mechanism of plastic deformation, and the material as having perfectly plastic behaviour. The effect of changes in geometry in increasing the limit pressure of some nozzles has also been studied [70]. Limit analysis has been used to assess the collapse level by determining the upper and lower limits of loading in which collapse of the component must occur, in the absence of work-hardening.

---

*Numbers in square brackets are references.

Cyclic loading of a structure implies the possibility of cyclic failure either by incremental collapse or by low or high cycle fatigue.

The necessity of avoiding incremental collapse, or low cycle fatigue behaviour, restricts the extent of permissible plastic flow due to the cyclic loading of the structure. These types of behaviour are in principle cycle-dependent, and must be so treated if a limited life design is proposed. The concept of shakedown arises when the above-mentioned types of failure are to be avoided in circumstances in which not all the variables, with their effects, are known. Shakedown behaviour is associated with entirely elastic behaviour after some initial plastic flow has been undergone by the structure, This has become an accepted criterion. Shakedown behaviour was well known in structural design, but Symonds [54] and Koiter [55] extended Melan's theorem to continuous media. Leckie [61] has described a method of estimating the lower limit of the shakedown pressure for a flush cylinder-sphere intersection, by applying Melan's theorem, using the results from an elastic analysis, and the Tresca yield criterion [61]. Fox et al have applied Leckie's method to ellipsoidal heads [23]. Macfarlane and Findlay have described a simple technique for calculating shakedown loads on pressure vessels by using Leckie's method [12]. Findlay and Spence however explained how shakedown loads may be determined from the post-yield behaviour of the pressure vessel [53], although Crisp describes a computer program which provides a rapid and accurate means of computing post-yield stresses and the shakedown limit from experimental data, assuming an elastic-perfectly plastic material [57]. Taylor has investigated the effect of shakedown with regard to strain hardening materials. In the above-mentioned approximations to shakedown analysis, the Bauchinger effect has in all the cases been neglected, and the unloading path is considered parallel to the elastic. Very little experimental

work has been reported on shakedown behaviour; Procter and Flinders [59], have carried out shakedown investigations on partial penetration welded nozzles in a spherical shell, and Findlay, Moffat and Stanley [56] have carried out limit-pressure and shakedown investigations on torispherical drum heads.

The development of electronic digital computers has made the elastic-plastic analysis of pressure vessels a reality. In the last four years, much work has been done on the improvement of the elastic-plastic solutions by the use of methods of numerical analysis and of the equivalent plastic stress-strain curve of the material under consideration. In a collapse or limit pressure study, elastic-perfectly plastic material is very often considered, [3],[7],[9] and [73], but more appropriate stress-strain curves, as an approximation to the real static equivalent plastic stress-strain curve for the material, are, when available, used in order to obtain a better approximation to the collapse behaviour of the structure, [6],[7] and [24]. In a low cycle fatigue study, Blomfield [6] has demonstrated that a settled down equivalent plastic stress-strain curve would give very reasonable results in pipe bend studies. In shakedown studies, the material has always been considered as elastic-perfectly plastic for an elastic-plastic analysis [9] and [73].

The object of the present work is to extend the study of collapse and shakedown behaviour by means of an elastic-plastic computer program. The feasibility of such studies has been shown by earlier work, [3],[7], [8] and [42]. Comparisons of elastic stress concentration factors are made between the analytical results and the numerical results from an elastic computer program for symmetrically loaded shells of revolution. Calculated elastic-plastic strains are compared with the available experimental data for the case of Head A [3] in order to assess the

reasonableness of the elastic-plastic computer program used in this work. Some shakedown investigations were carried out on a plate with a central hole, and on a knuckle of cylindrical nozzle on spherical pressure vessel. The elastic-plastic behaviour given by the computer program was compared with the experimental results from the test nozzle in order to assess the feasibility of the shakedown criteria described in this thesis, and in [24].

CHAPTER 1

THE ELASTIC-PLASTIC ANALYSIS OF SYMMETRICALLY LOADED SHELLS OF REVOLUTION

1.1 Elastic Theory

1.1.1 Introduction

In Figs. 1 and 2 an element of a symmetrically loaded thin shell of revolution is shown in which the geometrical parameters are defined, and the applied and resultant forces and moments are presented.

In Appendix A, the basic equations for the theoretical study of the distribution of elastic stresses and strains are described; they are based on the thin shell theory defined previously by Love, Ref.[77] and used later by other researchers, e.g. Refs. [1],[4],[13] to [20]. The derivation of the equations in Appendix A has its origin in Ref. [1], and is based on the four following assumptions:

(a) The ratio of thickness of the shell to the smaller of the radii of curvature is small compared to unity.

(b) Plane sections normal to the mid-surface of the shell in the unloaded state remain plane after the application of the load.

(c) The stresses normal to the mid-surface are negligible in comparison with those acting in the plane of the mid-surface.

(d) The magnitude of the displacements is small.

These four assumptions, together with Hooke's law as applied to isotropic and homogeneous materials, form the basis for the derivation of the equations in Appendix A, are the same as those used in Ref. [2], and [3], with minor differences, in Ref. [1]. These equations have proved to give good agreement with results when compared with experimental work, as long as the ratio $2h/\rho$ is less than or equal to 1/10, as defined by Flügge, Ref. [14], and Timoshenko, Ref. [15]. It is noteworthy that Novozhilov, Ref. [16], has 1/20 as the upper limit to $2h/\rho$.

Because this work is concerned with shell geometries containing some region where the condition $2h/\rho \leqslant .1$ is not satisfied, as in knuckles of small radius of curvature in the meridional plane, a "thick curved bar" theory or "Winkler's curved beam" theory, Ref. [11], was used where the above condition was not satisfied. This approximation allows an elastic stress pattern to develop, that is non-linear across the thickness (as in "Winkler's theory", Ref. [11]), but nevertheless ignores shear and through thickness deformations. This approximation is shown and described in Appendix D. The improvement gained with this approximation can be seen in Refs. [3] and [9], but, for ratios of $2h/\rho$ greater than $\frac{1}{2}$, this approximation over-estimates results, Ref. [9].

1.1.2 Theoretical Analysis

The governing equations, presented in Appendix A, are for a symmetrically loaded thin shells of revolution theory, and they must be simplified in order to obtain an analytic solution for each particular case.

It is known that each simplification, in a system of differential equations, brings a corresponding limitation to the solution. Hence the simplification must be made with the geometry and system of applied loading to the structure in mind.

In Appendix B, the analytic solutions for internally pressurised cylinder-sphere intersections, Figs. 3 to 5, are shown, bearing in mind the limitations presented by the sphere solution, either when the sphere can be treated as a proper sphere, as a shallow sphere, or as a plate, Fig. 5 and Refs. [1],[4],[15] and others. These limitations are a consequence either of the simplication made in the initial differential equations, as in the case of the sphere when it becomes a shallow sphere, or by the solution of the simplified system of differential equations, as in the case of the shallow sphere in which the completed solution is limited by the unity of the independent variable in the Kelvin function, thus:

$$\text{bei}(\chi) = \frac{e^{g_1(\chi)}}{(2\pi\chi)^{\frac{1}{2}}} \cos g_2(\chi)$$

$$\text{ber}(\chi) = \frac{e^{g_1(\chi)}}{(2\pi\chi)^{\frac{1}{2}}} \sin g_2(\chi)$$

$$\text{ker}(\chi) = \frac{e^{g_1(-\chi)}}{(2\chi/\pi)^{\frac{1}{2}}} \cos g_2(-\chi) \qquad (1.1)^*$$

$$\text{kei}(\chi) = \frac{e^{g_1(-\chi)}}{(2\chi/\pi)^{\frac{1}{2}}} \sin g_2(-\chi)$$

with

$$g_1(\chi) \simeq \frac{\chi}{\sqrt{2}} + \frac{1}{8\chi\sqrt{2}} - \frac{25}{384\chi^3\sqrt{2}} - \frac{13}{128\chi^4} - \cdots$$

$$g_2(\chi) \simeq \frac{\chi}{\sqrt{2}} - \frac{\pi}{8} - \frac{1}{8\chi\sqrt{2}} - \frac{1}{16\chi^2} - \frac{25}{384\chi^4\sqrt{2}} + \cdots$$

from Ref. [10], where $\chi = \gamma\sqrt{2}\alpha$; hence, if $\chi < 1$, the g_1 and g_2 series are not convergent. Besides the limitation in the solution due to the restraining in χ, it is normal procedure to use simplified expressions for g_1 and g_2, as can be seen in Appendix B, equations (B.17) and (B.18), or in Refs. [1] and [13]. If equations (1.1) are to be used when χ approaches or becomes less than unity, the plate solution is in some cases better than the shallow sphere solution; if (B.17) and (B.18) are to be used, when $\chi < 7$, as defined in Refs. [1] and [4], the plate solution is a more convenient approximation also.

The limit from which a shallow integration should be applied, instead of a sphere integration, is very difficult to define as a particular value to be applied in all cases, because the validity of the solution depends not only on the value of α, but also on the value of $2h/\rho$ for the geometry under study. A similar comment can be made as regards the plate integration to the shallow sphere integration.

---

*Numbers in brackets () indicate equations.

The convergence of the analytic solution depends not only on these geometrical considerations, but also on the loading, e.g. a high load bending situation will yield more inaccurate results than a uniform pressure situation.

A better convergence, depending on the value of χ and therefore, on the angle α, was found by Leekie and Penny, in Refs. [13] to [16], by using a variable substitution in the shallow sphere differential equation of f to $(\sin \alpha/\alpha)^{\frac{1}{2}}f$; the solution of the new equation must, accordingly, be multiplied by $(\alpha/\sin \alpha)^{\frac{1}{2}}$, Ref. [17].

1.1.3 Numerical Analysis

All the elastic calculations based on a finite difference technique in the present work have been done with the computer program, PVA1, used in several previous pieces of research work, e.g. Refs. [3], [7] to [9] in the discussion of [23] and [63], and first reported in Ref. [2].

This computer program uses the governing equations described in Appendix A, with four dependent variables (u, $\emptyset$, $d\emptyset/d\ell$ and F), and the meridional length (ℓ) as the independent variable.

The computer program was developed in order to study the elastic distribution of stresses, strains and displacements in a thin shell of revolution and therefore for structures containing one or more different geometries. A user's manual was written as a report by the C.E.G.B., Ref. [45].

The shell is assumed to be divided into at least two branches, but can contain up to four branches connected at the same part, which is called a junction. Each structure has at least one junction. The geometry within each branch can change, as long as it can be completely described by a formula of the type $a + b \cos \theta$, by a value for thickness, and, by a linear change in thickness, known as taper; the parts of the structure identified by the $a + b \cos \theta$ formula and by thickness-taper values are known as elements.

In the computer program each branch may be divided into no more than twenty elements, each having different values for the variables in $a + b \cos \theta$, or with different thickness, or linear changes in the thickness along the meridional length. Either the branches or the elements can be sub divided into equal lengths, so long as the number of steps within each branch does not exceed two hundred.

There are seven different methods of shell loading in this program:

(i) constant pressure within each branch;

(ii) constant axial load within each branch;

(iii) applied constant band forces along the meridian within each element in any branch;

(iv) applied meridional moment and radial force at the junction and at points on the meridian of any branch;

(v) a specified boundary condition at the end of each branch, as long as the boundary condition can be expressed in a linear form with the dependent variables;

(vi) constant axial body forces on the whole shell;

(vii) radial body forces, linear dependent on the radius vector (r) only.

In the present work, only internal pressures and axial loads from internal pressures, were considered, together with the membrane boundary condition expressed by the radial displacement and by the meridional moment equal to zero, thus:

$$u = \frac{r}{E} (\bar{\bar{\sigma}}_{\varphi} - \nu \bar{\bar{\sigma}}_{\ell}) \tag{1.2a}$$

$M_{\ell} = 0$ implies

$$\frac{d\emptyset}{d\ell} + \frac{\nu \sin \theta}{r} \emptyset = 0 \tag{1.2b}$$

Marcal introduced into the computer program the "O'Connell modification" which distributes the sharp corner forces, e.g. at cylinder-sphere intersections, over a prescribed meridional length from the junction along each branch. This modification was first reported in Ref. [8].

The numerical procedure used in the computer program is known as a predictor-corrector process and consists of guessing initial values for the four dependent variables at the junction and then using these as the starting values for a numerical integration procedure which calculates the values of the variables at each point along each branch. At the end of the branch the calculated values are compared with the values specified for the given boundary conditions. The initially guessed values of the dependent variables are then corrected by a boundary control technique using the values of the previous integration; this procedure is repeated until the specified accuracies of the integration and the boundary control are satisfied. For a more detailed description of the numerical process see Refs. [2] and [3].

1.2 Elastic-Plastic Theory

1.2.1 Introduction

As it is common procedure to allow a small amount of plastic flow to occur early in the life of a vessel, the problem of elastic-plastic deformation of vessels at once presents itself to the designer.

There have been some attempts to produce an algorithm capable of solving the problem of the elastic-plastic behaviour of shells. Firstly a "limit analysis" calculation was defined, and used by many authors, Refs. [4],[20],[31] to [40]. Later, more sophisticated methods were developed, with high speed computers in view. Mendelson, in 1959, Refs. [26] and [27], presented an algorithm for the solution of elastic-plastic deformation and Marcal in 1963, Refs. [21] and [28], presented

a new algorithm based on a "partial stiffness" method, more recently known as the "tangent modulus" method, Refs. [6],[29] and [30]. Since then new improved methods have been developed having in view a finite element type of analysis, Refs. [30] and [41]. The "tangent modulus" method has been applied to a wide variety of problems, e.g. Refs. [3], [6] to [9], [24],[29],[42] and [43]. A comprehensive description, and a comparison of Marcal's and Mendelson's methods may be seen in Ref. [6].

The computer program for elastic-plastic analysis used in this work includes Marcal's algorithm, and was developed from the elastic program, Section 1.1.3, described in more detail in Refs. [2] and [3].

Tests of the program's accuracy were made and good agreement with experimental results was arrived at, Refs. [3] and [5], when the geometry was within the limits of the thin shell theory. The case of a torispherical head showed reasonable agreement, but radial nozzles-on-sphere, however, produced far from accurate results with the program; not even with the use of the "thick curved bar" theory, where the ratio $2h/\rho$ is larger than .1, and which gives much better agreement than the simple thin shell theory, Refs. [3] and [9].

1.2.2 Numerical Analysis

The elastic-plastic calculations for thin shells of revolution were carried out using a computer program, PLINTH, developed from one of the elastic analyses described in Section 1.1.3, and modified in order to include Marcal's algorithm, described in Appendix C, and Refs. [3] to [6].

A user's manual has been written in the form of a report, Ref. [44].

Minor, but important, alterations have since been made, Ref. [3], which include a larger number of integration steps, from sixty-six, to two hundred, data for the material given in exponential form,

$\sigma = a(1 + b\bar{e}_p)^c$, and the output capable of being printed periodically at the increment required.

The larger number of integration steps improves convergence and allows the analysis of longer branches. For each type of geometry, there is an optimum number of integration steps as far as efficient convergence is concerned, but the present work was not, however, sufficiently extensive to arrive at a definite conclusion. The time of computation increases very sharply with the number of integration steps and with the development of the plastic area during the computation procedure.

The plastic stress-strain relation was modified as it was seen that the new relation fitted the experimental plastic stress-strain curve better. In Fig. 6 can be seen the plastic stress-strain curves for the material used by Cheung, Refs. [3] and [7], in Head A. The three curves are the experimental curve, the second degree polynomial form and the exponential form, of the elastic-plastic calculations.

The numerical procedure is the same as for the elastic case to the point where a convergent solution of the elastic problem to unit load is obtained.

Once the elastic solution has been found, the maximum von Mises stress is evaluated and used to scale the load in order to obtain the maximum von Mises stress equal to stress limit of elasticity.

The new value of the load is known as the elastic limit load of the particular shell.

Henceforward, the elastic-plastic calculation is carried out using the transition-region method with the Prandtl-Reuss stress-strain relationships, as in Marcal's algorithm, (see Appendix C), by increasing the load by a fraction of the first yield load. The integration is carried out, see Refs. [3] and [44] in order to obtain covergence to the

required accuracy. This procedure is repeated in accordance with the information of incremental procedure.

The printed output of the program can include stresses, strains (individual or plastic equivalent strains, or both), deflection and rotations, moments and forces, as well as the progress of yielding at each point of the shell.

CHAPTER 2

COLLAPSE AND SHAKEDOWN CONCEPTS

2.1 Introduction

The designer is faced with the fact that any structure is capable of failing and he must, therefore, attempt to make the likelihood of such a failure as remote as possible.

The safe operation of a pressure vessel depends on the stress-strain distribution under the relevant loading, the working temperature, the environment in which the vessel is going to be used, the material chosen, which must demonstrate economy and reliability in construction, and the total period during which the structure is meant to operate. It can, therefore, be seen that the designer is confronted most of the time with a combination of many varying parameters; the existing codes, Refs. [46] to [49], and [68], furthermore do not cover all possible circumstances affecting design. The latest codes, Ref. [46, division 2] and [68], present complex criteria for acceptable stress levels for defined geometries and loadings. Because it would be impossible to prescribe a code of safety covering all the vast number of possibilities, there is a tendency instead to give the basis for the criteria which the designer must apply to his particular problem in order to satisfy the code chosen by the client, Ref. [50].

As the designer, therefore, is called upon to do a work more fundamental in character, he must understand the mechanisms of failure, with their attendant variables, as well as the way they interact.

There have been attempts to classify the modes of failure, but to do so can become very difficult because of the combinations of the different modes, e.g. fatigue-creep, fatigue-corrosion.

Some more comprehensive classifications can be found in Refs. [3], [20], [50] and [51].

This thesis is concerned with elastic-plastic behaviour of pressure vessels and, therefore, with failures associated with stress and deformations. The object of this thesis is the better understanding of the collapse and shakedown mechanisms.

2.2 Shakedown

2.2.1 Basic Concepts

Any normally formed structure possesses residual stresses due to the manufacturing process, since all the processes, either mechanical or thermal, inevitably produce an effect on the material structure; because of this, careful precautions must be taken during the process of manufacture, Ref. [3], if the residual stresses are to be minimised.

If it is supposed that the residual stress distribution in a structure is known, and is defined by a function of stress $\sigma_{RE} = \sigma(P)$, where P is a point function (therefore, dependent on its location in the structure and on the properties of that structure), the stress distribution from the load may be found: $\sigma_L = \sigma(P)$.

When the two stress systems can be superimposed, such that the structure does not, at that time, yield anywhere within it, that is to say that is still elastic, then the structure has shaken-down for that particular loading.

It may be taken note that within the definition of shakedown and the theorems relating to it, the way in which the optimum residual stress may be obtained is not mentioned, Refs. [4], [53] to [55]; (N.B. In the general, non-technical sense of the word, "shakedown" implies a settling-down process whereas in the strictly technical sense, a cyclic process is not necessarily involved.) It is, however, always assumed that the structure is, in the beginning, free of residual stresses and that they are caused only by the unloading of the structure after some plastic deformation has occurred in the load process.

The material used and the structure into which it is incorporated have always formed an inherent part of the shakedown concept, and mechanism, as will be described later.

Consider two different structures:

(a) the simplest structure, which is an ideal tension test piece;

(b) a pressure vessel, which is the subject of this thesis.

In the case (a), when the tension load is increased up to the elastic limit (L_e, Fig. 7) and then relieved, it is most probable that no residual strain will appear, since creep has not been taken into account. If the loading has passed the elastic limit (L' or L", Fig. 7), and, therefore, plastic strain has developed, the level of stress will probably be much higher than the elastic limit (say σ' or σ'', Fig. 7). In the process of unloading, since the stress distribution is uniform, a non self-equilibrating system of residual stresses can be defined, the residual stress system is zero; theoretically speaking, the new limit of elasticity for this material will be σ' or σ'' (not including the effect of hysteresis), therefore the test piece has shaken down to a new value L' or L" bigger than L_e.

In reality, the process of shakedown implies an initial cyclic loading, Refs. [6], [56] to [62], of the structure since the material, with its inherent properties, presents different paths for loading and unloading, known as the hysteresis effect. Thus, when the load has arrived at L', Fig. 8, the cyclic process of zero to L', then back again to zero, will define the two paths, one of loading and the other for unloading; most materials have a tendency to settle down to a defined cycle, although there are exceptions, as can be found in Ref. [52], in which the strain history has its effect on plastic behaviour.

Materials which do settle down to a fixed cycle, often present either work-hardening or work-softening, Refs. [6], [58], [62] and [75].

The work-hardening* is shown in Fig. 9 for the case of overall load control, which is the usual method for work with pressure vessels, and it is characterised either by a decrease in strain amplitude or by an increase in stress amplitude, locally.

The work-softening* is shown in Fig. 10 for the case of overall load control; it is characterised either by an increase in strain amplitude or a decrease of stress amplitude, locally.

There are other metals which have neither work-softening nor work-hardening, but which do exhibit however the conformation shown in Fig. 8 after some cycles.

The cycles may stabilise anywhere between a few cycles or hundreds of cycles, Refs. [6], [60], [62] and [75].

In case (b) the problem is much more complicated, because:

(i) Some plastic strain may have occurred in the vessels once the load has been relieved; the part of the structure that remained elastic during the loading process will play a very important part in the stabilisation of the cyclic loading.

(ii) After some degree of plastic strain has occurred in the structure, assuming that it does occur, the residual stress will not be zero since the plastic work comes mainly from the bending action, introduced into the vessel due to the change in geometry, either in radii of curvature, or in thickness, or even because of a change in its material properties, Ref. [61].

There are many other problems connected with the shakedown mechanism, such as:

(a) The ability of the material to stabilise in a hysteresis cycle.

(b) Whether the material, being of a settle down type, will either work-harden or work-soften.

---

*A similar change in stiffness could also be caused by change in geometry.

(c) Whether the stress level for a shakedown load is in the region of: C1) Elastic instability, buckling;

C2) Creep-rupture;

C3) Fatigue-creep;

C4) Stress corrosion;

C5) Plastic instability, bursting;

C6) Collapse.

Since the designer has to prevent against all these types of failure, he must decide upon the load level that the vessel will take, or in other words, he has to design the vessel in order to prevent any of these possibilities becoming real.

The present work is, however, concerned only with shakedown and collapse and the rest of the thesis will concentrate on these topics.

2.2.2 The Mechanism of Shakedown

It has been seen in Section 2.2.1 that the decisive factors influencing the shakedown mechanism are that:

(a) The material has to have a settled cyclic behaviour.

(b) A defined residual stress system has to be well developed within the structure in a few cycles.

(c) The superimposition of the systems of stress, both residual and loading, must be within the bounds of elastic behaviour.

The material property has already been described in Section 2.2.1.

The stabilisation of a defined residual stress system, the material having been chosen from among those that settle, depends on the stress distribution in the structure due to the loading process. If it is assumed that the material has isotropic work hardening, then an incremental theory of plasticity can be used with any appropriate yield criterion, such as the von Mises or Tresca maximum shear stress. The implication of isotropic work hardening is that the yield surface expands

uniformly in a direction parallel to the octahedral plane. The Prandtl-Reuss incremental plasticity equations (C.1) have been used in all the elastic-plastic calculations in this work and are based on the assumption of isotropic work-hardening and on the von Mises yield criterion. Hence, this theory cannot be applied to describe the behaviour of a structure for a single cycle, Figs. 8 to 10, because of the Baushinger effect of the material. Since it is impossible by the use of the Prandtl-Reuss equation to describe a single cycle, it is assumed that the final state of stress and strain is better defined by the use of a settle cyclic curve, that can be obtained by using the methods described in Refs. [6] and [62] (the general path can be seen in Fig. 12) than by the use of a uniaxial tension test curve of the material.

This reasoning is found in Ref. [6]; intuitively it seems sensible and more appropriate, in determining the final stress-strain state of a structure that has been cycled, than the use of the stress-strain curve obtained from a simple tension test for the material.

Once the properties of the material have been specified for a theoretical elastic-plastic analysis, the influence of the structure's shape can be considered.

It is well established that the stress paths of the different points in a structure are dependent of the material used and the shape of the structure. It was found during the course of the present work that the structure which was most susceptible to the bending action normally had a stress path, in a biaxial stress space, moving around the von Mises ellipse and to a small extent toward the expanding work hardening ellipse. The reverse was true for structures with less susceptibility to bending action. It can therefore be concluded that this susceptibility to bending action is brought about, not only by a high stress concentration factor but also by the shape of the structure.

Let three different structures be considered, with the following assumptions being made:

(i) they follow the same elastic path in a biaxial stress space;

(ii) after yield has occurred at any point on the structure, the most highly stressed point in each follows the stress paths a,b,c, respectively, in Fig. 13 (the structures will be referred to from now on as 1, 2 and 3), as the load is increased;

(iii) deformations are negligible so that the stress paths in the unloading process can be taken as parallel to the initial elastic loading paths;

(iv) the materials are free of hysteresis, and are capable of stabilising;

(v) the extent of the expanding work hardening ellipse needed to double the load for first yield, anywhere in the structures, is the same for all three structures.

The points representing twice the load necessary to cause yield anywhere in the structures (1, 2 and 3) are marked in Fig. 13, as A, B and C, respectively, and the points that represent the residual stresses assuming no reverse yielding, are marked as A', B' and C' respectively.

Structure 1:

As long as the points representing the residual stresses of a structure from an unloading process do not violate the work-hardening ellipse derived from the loading process, it seems unlikely that a definition of an upper limit to shakedown for the expanding ellipse is possible for that structure.

Assuming the mechanism described in Ref. [24] (or Appendix E), and in Section 2.2.3, in which the ellipse for the elastic limit (yield surface) moves either in the direction of the elastic path, or in the

radial direction to the point on the stress path being considered, the structure has its shakedown limit near 2.(= L/Ly), but slightly below points A_C and A_T respectively.

Structure 2:

It is probable that this type of structure does have an upper limit to shakedown, but if this is so it is greater than 2.. For the other two criteria of the moving ellipse, Section 2.2.3, the values are both less than 2., with little difference between them.

Structure 3:

The upper limit of shakedown is less than 2., and the residual stress point will probably be in C'_R instead of C'. If this criterion is used, and a cyclic process is used between zero and twice the elastic load (Ly), then the structure will behave as shown in Fig. 11, but with the upper and lower stress limits equal in magnitude ($\pm \sigma$), but there will be an incremental collapse failure if the stabilisation behaviour cannot be defined. For the other two moving yield ellipse criteria, Section 2.2.3, the values of shakedown are well below 2. and are also very different from each other (points C_C and C_T, Fig. 13).

These conclusions were arrived at during the course of this work, when comparisons were made between the different pressure vessels analysed. In fact, the conclusions are much more complex because the elastic paths were not the same in each case, but the purpose here is to describe the influence of the geometrical characteristics of the structure in shakedown behaviour.

2.2.3 Shakedown Criteria

In Sections 2.2.1 and 2.2.2 the basic concept of, and variables connected with, the shakedown mechanism were described.

In this section the method of evolution of the shakedown values is described, assuming that elastic and elastic-plastic analyses have been

carried out and hence the stress distribution throughout the structure is known both at the elastic limit and at different load increment steps.

Leckie, Ref. [61], has derived a method based on Melan's theorem, Ref. [54], using the hypothesis of an elastic-perfectly plastic material, and an elastic analysis. This method is now well established, is often used in design to guard against shakedown, and has been used in this work (as well as in Refs. [12],[23],[24] and [63]). Macfarlane and Findlay, Ref. [12], have described a simple technique for shakedown calculation using Leckie's method in its simpler form with either the Tresca or the von Mises yield criteria.

This technique was used in Ref. [24] (or Appendix E), as well as in the present work, but only using the von Mises criterion in these cases.

Leckie's method has proved to be most helpful if work-hardening of the material is not included in the shakedown behaviour, and its application is much more economical than those described later in this section, since these methods are based on an elastic-plastic computation.

Prager, Refs. [64] and [65], presents a kinematic theory of plasticity allowing the yield surface to move laterally as well as to expand. This has been applied to shakedown behaviour of structures with work-hardening materials. Prager has defined the way in which the shift would be made, but in the present work, it is assumed that the yield ellipse moves in the direction either of the elastic path or of the radial vector of the point that represents the stress state of the particular load considered. The movement in these directions is made on the assumption that the principal direction of the stress tensor remains the same, and hence the axes of the initial ellipse and of the moving ellipse are parallel, and movement is made up to the point where the

nearest limit of the yield surface is on the point that represents the stress state of the particular load considered. In the case of the second movement the two surfaces, yield and work-hardening are tangential to each other. These movements of the yield surface, together with the unloading process described in Section 2.2.2, form the two initial criteria, referred to throughout this work as SPC and SPT.

A third criterion is used wherein the work-hardening surface reached during loading is taken as the limit for elastic unloading of the structure. This criterion may well be overambitious, as well as unconservative, but as far as the author is aware no theory has been developed that contradicts this assumption. This criterion will be referred to in this thesis as SPW.

Crisp, Ref. [57], uses the strain gauge readings from the experiments with the assumption of an elastic-perfectly plastic material, Prandtl-Reuss equations of incremental plasticity, and von Mises' criterion, in order to determine the post yield state of stress and the shakedown loads by assuming an elastic unloading.

2.3 Collapse

2.3.1 Basic Concepts and the Mechanism of Collapse

Consider a structure loaded such as to cause a stress state, at the most highly stressed point, just on the yield surface and therefore free of plastic strain, and assume the material to be either ductile or perfectly plastic, and the load increased to a fixed value: if the elastic-plastic deformation does not stop, the structure either collapses or bursts, hence this last load value is called a collapse load or bursting load, Ref. [20].

Collapse calculations have been reported in many papers, e.g. Refs. [3],[4],[7],[9],[20] and [24]; some experimental work has also been reported, e.g. Refs. [3],[7] and [57]. Sometimes the collapse load is referred to in the literature as the limit load.

The collapse concept assumes a monotonic increase in load.

Another type of collapse can take place in the case of cyclic load, but this is however recognised as a different kind of behaviour, that of incremental collapse. This behaviour assumes a process of yielding and reverse yielding, with geometrical changes in the structure's shape in each load cycle, Refs. [4],[20],[50],[66] and [67],

The principal variables as regards the collapse mechanism are: the structure's geometry and, therefore, the elastic stress and strain distribution; the material behaviour and its capacity to accommodate plastic strain; and in, if work-hardening is considered, the residual stresses in the structure, Ref. [4].

It can thus be seen that the larger the capability of the structure to sustain the plastic flow of a region in the plastic phase, the less likelihood there is of collapse. The growth of the plastic region is constrained mainly by the remaining elastic parts of the structure and, once the elastic regions are about to reach gross yielding, collapse is delayed only by the work-hardening of the material.

In Fig. 14, the effect of the material properties on the collapse load can be compared for two different structures with elastic-perfectly plastic material (curves a_1 and e_1) and structures with work-hardening material ($\sigma = 13.3\ (1 + 133\ \bar{e}_p)^{.269}$) (curves $\underline{a}$ and $\underline{e}$). It can, therefore, be readily concluded that material properties are of consequence in the collapse mechanism.

2.3.2 Collapse Criteria

It is critically important that the value of the collapse load is found, otherwise excessive deformation can be introduced into the structure during the testing process, especially since the value of the testing load is sometimes fixed as a fraction of the limit load. The ASME code, Section VIII, Division 2, Ref. [46] and BS3915, Ref. [68],

permit the use of limit analysis; the former specifies that the design loading must be less than two thirds of the limit load, although this carries with it further implications, as design stress is equal two thirds of the proof stress, Ref. [69].

Limit analysis has long been used in the plastic design of structures, and its theorems have been extended to the plastic design of pressure vessels, Ref. [50]. A relatively larger literature on the limit analysis of symmetrically loaded shells of revolution has been published, e.g. Refs. [31],[32],[38],[70] and [71], and some work has been reported on the asymmetric loading of shells of revolution, e.g. Ref. [72].

Limit analysis normally uses the Tresca criterion, and assumes a rigid-plastic material with a possible pattern of plastic deformation.

Since computer programs have become available for the analysis of the elastic-plastic behaviour of pressure vessels, attempts have been made to define some criteria in order to evaluate the collapse load from computational results, Refs. [3], [7] to [9] and [73].

Marcal and Turner, Ref. [8] have proposed the criterion of 1.5% maximum allowed strain. The load, therefore, that causes that percentage of strain is considered to be the collapse or limit load. This criterion will be hereafter referred as C15 ; it is probably unconservative if the material examined is elastic-perfectly plastic, but certainly depends on the structure itself.

Cheung and Turner, Ref. [7], have put forward two collapse criteria:

The first is based on the curves of individual strain, equivalent strain, and overall deflections, against load. This criterion is based on the intersection of the elastic curve with the tangent drawn to the point defined by a line of one third the elastic slope intersecting the considered curve. This criterion will generally be referred to as C3 in this work and, in particular as,

C3I for the curve of individual strain against load,

C3E for the curve of equivalent strain against load,

C3D for the curve of overall deflection against load.

The second criterion is based on the load necessary to cause 0.5% maximum strain on the outside surface. This criterion can be used with either the individual or the equivalent strain, and will be hereafter referred to as C5 and in particular as,

C5I for the individual strain,

C5E for the equivalent strain.

These two criteria, C3 and C5, are generally speaking conservative; perhaps the less conservative is C5 so long as elastic-perfectly plastic material is chosen for the computations. The C5 criterion is, of course, more conservative than C15I, because the internal and external maximum individual strains are not very different from each other, but do depend however on the structure's geometry; the C5 criterion is also convenient in the testing process since it can be used to control the collapse load.

Marcal and Turner, Ref. [7], and Crisp, Ref. [9], have proposed a criterion based on the growth of the plastic region. This criterion is probably better than those above mentioned, but is somewhat subjective in its nature, as it is difficult to define previously a reasonable spreading ratio of the local yield from which the collapse will spread quickly.

This criterion will be hereafter referred as BSLY.

Townley, Refs. [73] and [74], defines a collapse load by considering an equivalent strain of 1% as excessive deformation. This criterion is probably the most convenient since it lies between C5 and C15I, although for low stress concentration structures however it is certainly unconservative.

It can be appreciated on the basis of the above mentioned criteria that definition of a collapse mechanism applicable in all circumstances is a very difficult undertaking; it is here that the ability and experience of the designer is of primary importance.

From an extensive and detailed study of the elastic-plastic computer results, two new criteria are described.

The first is applied to geometries with neither concave, nor sharp corners, i.e. torispherical and hemispherical heads, and the second to geometries with concave corners either sharp or smooth, i.e. cylindrical nozzles-on-sphere geometries.

Collapse criterion for torispherical and hemispherical heads:

In the data used for the elastic-plastic computer program, the number of steps for the integration process is defined for each element, and the load increment is also defined. The computer program determines the yield load and its position on the vessel. The maximum equivalent strain is calculated for the outside surface, associated with its position. When the load was increased step by step during the original calculation, it was found that the position of the maximum equivalent strain on the outside surface changed its location, first from point to point, then over two or three points or even more. The jumping process of the maximum equivalent strain on the outside surface was first detected when the local yielded region across the thickness started to spread to membrane areas. Hence the load in which the jump begins to be large, can be defined as the collapse load.

This criterion will be hereafter referred as CMED.

This phenomenon is, like the Crisp criterion, Ref. [9], dependent on the integration step size, and the load increment selected, as well as on the analyst's knowledge of the subject. The load increment needed for a high stress concentration factor is about .15, but for a

medium stress concentration factor, of about 2. to 3., a value of about .05 or .075 is recommended. In case of a low stress concentration factor, a value lower than .05 is desirable, but of course when the stress concentration factor is near 1., then a much smaller value for the load increment has to be used with the scaling process to the load increment if this criterion is to be employed.

This phenomenon is better demonstrated in a computation with a work-hardening material, than one with an elastic-perfectly plastic, since the former allows a simpler computation, as well as the growth in plastic strain.

An application of this criterion, as well as the Crisp criterion, Ref. [9], can be seen in Fig. 15 for Head A from Cheung, Refs. [3] and [7], in Section 4, other particulars can be found.

Collapse criterion for internally pressurised cylindrical nozzles-on-sphere geometries:

This criterion was described from plotting the biaxial stresses obtained from the computer results. The computer program uses the von Mises criterion to define the yield surface. Plotting in the biaxial von Mises space the history path of both stresses (circumferential and meridional), for each particular point in the pressure vessel, gives Figs. 13, 16 and 17. The latter two figures are for radial nozzles-on-sphere geometries, and are obtained by plotting the computer program results for an elastic-plastic analysis. In Fig. 17 the stress paths for the cross-section containing the most highly stressed point of nozzle N5 (see Chapter 4) for both the elastic-perfectly plastic, and the work-hardening, cases can be seen. The stress paths for the internal point (i.e. the most highly stressed point in the structure) are marked by B1 and B2 on Fig. 17; B1 denotes the material treated as non-work-hardening and B2 the material treated as work-hardening.

The path B2 shows a clockwise movement around the ellipse as long as the local yield growth is smooth, but when the local yield begins to spread rapidly towards the membrane shell, the path begins to bend to anticlockwise. It is at this particular stage in the loading process that work-hardening becomes apparent in the highly stressed region. This criterion is based on the following observation:

Tracing from the centre of the yield ellipse a line tangential to the stress path, a point on the path is defined which corresponds to a defined pressure; this pressure is called the collapse pressure for the particular structure.

If the material is treated as non work-hardening the stress path shows similar behaviour to that of work-hardening material. The pressure at which reversal occurs is called the structure collapse pressure.

This criterion will be hereafter referred to as CSP.

This criterion is perhaps the simplest of those considered, but it requires more work than the others because of the necessary plotting.

CHAPTER 3

PRESENTATION AND DISCUSSION OF ELASTIC RESULTS

3.1 Introduction

In this chapter the results of elastic analysis using either an analytic integration or a finite difference computer program for symmetrically loaded shells of revolution are presented and, where possible, compared with published data. The effects due to welding are not taken into account in these calculations.

Analytic integration is explained in Appendix B, and is derived using the equations presented in Appendix A. The governing equations, and the type of analysis involved, are described by Turner, Refs. [1] and [76], using Love's shell theory Ref[77]. Many other works have been published using the same theory, e.g. Refs. [2] to [9], [13] to [16].

Once the simplifications for each particular geometry and loading have been introduced into the general governing equations for an analytic integration, (A.14) and (A.20), the calculated results are different for each particular situation and sometimes, for similar situations, the results are limited by the approximation, depending on whether a high bending situation, where θ is near $\pm \pi/2$, existed. Leckie and Penny, Refs. [13] to [16], have given an analytic solution that can be used for all values of θ.

The integration process used by Turner, Ref. [1], is used here, Appendix B, to evaluate the stress concentration factor for flush cylindrical nozzles-on-sphere geometries, as well as for spherical and hemispherical heads on cylinder geometries.

A computer program for the elastic-analysis of symmetrically loaded shells of revolution, developed by Pilgrim et al, Ref. [2], that uses the equations described in Appendix A, with a predictor-corrector process of integration and boundary value control,

e.g. Refs. [2] and [3], was used to determine some stress concentration factors for the two above-mentioned geometries, and also the stress distribution on some knuckles of cylindrical nozzles on spherical geometries, as well as for the tested radial nozzle on sphere, Fig. 37; the comparison for the latter geometry is made between experimental measurements and calculated strains.

3.2 Stress Concentration Factors

The stress concentration factor (SCF) of a pressure vessel is defined as the ratio between the maximum stress value in the structure and a membrane stress for the pressure vessel, i.e. nominal stress, hence:

$$SCF = \frac{\sigma_{max}}{\sigma_{memb.}} \qquad (3.1)$$

The stress values in (3.1) can be either individual stresses (circumferential or meridional) or equivalent stress values (either by the von Mises or Tresca criteria)

It is normal practice to say that the stress concentration factor is based on a yield criterion. The Tresca criterion is normally used when a limit analysis is involved, since its implications can be more easily set out than those for the von Mises criterion Ref. [32]. In the case of an elastic-plastic computation, using either the Marcal or Mendelson algorithms, the von Mises criterion is more convenient as its differential form is more suitable than that of the Tresca criterion. It therefore appears logical to use the Tresca criterion for (3.1) when a limit analysis is being undertaken, and von Mises criterion for (3.1) when an elastic-plastic computer program is being used.

For cases of nozzle geometries on spheresit is normal practice to define the stress concentration factor in terms of the membrane stress on the sphere, e.g. Refs. [16] and [78]; in the particular case of

internal pressure, the membrane stress, either individual or equivalent (Tresca or von Mises criteria), has always the same value; hence

$$\bar{\bar{\sigma}}_{s_{(\varphi \text{ or } 1)}} = \bar{\bar{\sigma}}_{s_{\text{Tresca}}} = \bar{\bar{\sigma}}_{s_{\text{von Mises}}} = \frac{pD}{4T}^{*}$$

therefore

$$\text{Tresca criterion:} \quad SCF = \frac{2\,\tau_{max}}{\bar{\bar{\sigma}}_s} \tag{3.2.1}$$

and

$$\text{von Mises} \quad : \quad SCF = \frac{\sigma_{e_{max}}}{\bar{\bar{\sigma}}_s} \tag{3.2.2}$$

For cases of hemispherical and spherical heads on cylindrical geometries, it is normal practice to define the SCF in terms of the membrane equivalent stress on the cylinder. If the Tresca criterion is used, e.g. Ref. [9], the membrane equivalent stress, for a pressure vessel, is equal to the membrane circumferential stress (= pd/2t); this SCF is defined by Crisp, Ref. [9], as the principal SCF. Using the von Mises criterion, the membrane equivalent stress is given by $\frac{\sqrt{3}}{2}\frac{pd}{2t}$, and Crisp, Ref. [9], refers to this SCF as the von Mises equivalent SCF.

Therefore

$$\text{Tresca criterion} : \quad SCF = \frac{2\,\tau_{max}}{\bar{\bar{\sigma}}_{\varphi_c}} \tag{3.3.1}$$

and

$$\text{von Mises criterion} : \quad SCF = \frac{\sigma_{e_{max}}}{\bar{\bar{\sigma}}_{e_c}} \tag{3.3.2}$$

Langer, Ref. [51], defines a stress index as the ratio of the maximum individual stress to the membrane circumferential stress on the cylinder, hence,

---

*$D = D_o$

$$\sigma_{index} = \frac{\sigma_{i_{max}}}{\bar{\bar{\sigma}}_{\varphi_c}} \quad , \; i = 1, \varphi \tag{3.3.3}$$

In the present work the inverse values of the SCF and stress index are used for spherical and hemispherical heads as these values were found to be more suitable for logarithmic plotting against acos (d/D_o). When referring to these values ($1/SCF$ or $1/\sigma_{index}$) the expressions "stress concentration ratio" and "stress index ratio" will be used.

3.2.1 Spherical and Hemispherical Heads on Cylindrical Pressure Vessels

In Figs. 4 and 5 the geometric variables for the spherical head and for the flat end are shown, respectively. It can clearly be seen that a spherical head may be defined by the following parameters:

$\frac{d}{D_o}$ = cylinder diameter/sphere diameter

$\frac{d}{t}$ = cylinder diameter/cylinder thickness

$\frac{t}{T}$ = cylinder thickness/sphere thickness

In the design of pressure vessels, an attempt is made to keep all component parts small, for economic reasons. This leads to an effort to equalise the membrane equivalent stresses on the different components. Hence, for the spherical head-on-cylinder geometry, this condition is given by

$$\bar{\bar{\sigma}}_{e_c} = \bar{\bar{\sigma}}_{e_s}$$

using the von Mises equivalent stress criterion. For internal pressure, the ratio of the membrane equivalent stress on the sphere to that on the cylinder, defines a variable $\bar{\bar{p}}_m$, that shows in which element the membrane yielding will occur first, hence,

$$\bar{\bar{p}}_m = \frac{\bar{\bar{\sigma}}_{e_s}}{\bar{\bar{\sigma}}_{e_c}} \tag{3.1}$$

This quantity can also be defined by the ratio of pressure to cause membrane yielding on the sphere, to that on the cylinder, hence

$$\bar{\bar{p}}_m = \frac{\bar{\bar{p}}_{ms}}{\bar{\bar{p}}_{mc}} \tag{3.2}$$

The values of $\bar{\bar{p}}_{ms}$ and $\bar{\bar{p}}_{mc}$, however, assuming the two components are made of the same material and have a limit of elasticity given by σ_y, are obtained from:

$$\bar{\bar{p}}_{ms} = 2\,\sigma_y\,\frac{2T}{D_o} \tag{3.3.1}$$

and

$$\bar{\bar{p}}_{mc} = \frac{2}{\sqrt{3}}\,\sigma_y\,\frac{2t}{d} \tag{3.3.2}$$

Therefore, from (3.2)

$$\bar{\bar{p}}_m = \sqrt{3}\,\frac{T}{t}\,\frac{d}{D_o} \tag{3.4}$$

For a given spherical head on a cylinder pressure vessel it can readily be decided which of the two membrane regions will yield first by using (3.4), since:

if $\bar{\bar{p}}_m = 1$, it will be most probable that both membrane regions will yield at the same pressure;

if $\bar{\bar{p}}_m < 1$, membrane yield will start on the sphere (head);

if $\bar{\bar{p}}_m > 1$, membrane yield will start on the cylinder (drum or body vessel).

The value of d/D gives the cosino of the angle (θ) of those points on the sphere which result from the intersection of the two mid-wall surfaces of the sphere and cylinder,

$$\frac{d}{D_o} = \cos\theta_o \tag{3.5}$$

The spherical head-on-cylinder geometries have two limiting cases: the hemispherical head for which $\theta = 0^{o}$, and the flat end with $\theta = \pm \pi/2$.

It is well known that for hemispherical heads on cylindrical geometries the mid-wall diameters of the sphere and the cylinder are equal (d = D) and therefore, from (3.4),

$$\bar{\bar{p}}_m = \sqrt{3}\,\frac{T}{t}$$

Hence, the value of unity for $\bar{\bar{p}}_m$ will be obtained for

$$\frac{t}{T} = \sqrt{3} \qquad (3.6)$$

Since it was realised that with hemispherical heads, the SCF, using the definition given by (3.3.2), diminishes with t/T increasing up to 1., and decreasing rapidly for t/T = 2., some extra calculations were made for t/T = 1.25, 1.5 and 1.75 (see (3.7)) and a graph drawn, Fig. 18, for stress concentration ratios (1/SCF) versus t/T; it was found that the maximum stress concentration ratio (or the minimum SCF) occurs for values of t/T between 1.5 and 1.75, and therefore the value given by (3.6) for t/T is a good approximation to the minimum SCF, Fig. 18.

The same reasoning could have been done for other geometrical situation but as it was not, no generalisation is possible.

The values of the geometrical parameters taken for the spherical heads were

$$\begin{aligned} &\theta_o(d/D) = 0^{o} \text{ to } 90^{o} \\ &d/T = 10,\ 20,\ 40,\ 80,\ 160,\ 400 \\ &t/T = .25,\ .5,\ 1.,\ 2.,\ 4. \end{aligned} \qquad (3.7)$$

Graphs and tables were drawn for the stress concentration ratio (1/SCF), using the definition (3.3.2), against the geometrical parameters $\theta_o(d/D)$, d/T and h/d, Figs. 19 to 25 and Tables HH1, HH2, SH1, SH2, FH1 to FH3 and TH1 to TH4, but in some tables other definitions were used for comparison with published results, Refs. [9] and [61].

In Figs. 19 to 22 , the stress concentration ratio was plotted against θ_o (d/D) with each curve for constant d/t (3.7); separate graphs were drawn for t/T = .25, .5 and 1, respectively, Figs. 19, 20 and 21, but in Fig. 22 the graphs for t/T = 2. and 4., have been included.

Some other graphs were drawn, Figs. 23 and 24, in order to obtain a final graph showing the maximum stress concentration ratio for all considered geometrical parameters, which may be seen in Fig. 25.

Each curve in Figs. 19 to 21 is made from three main approximations, the exponential integration (B.38), the approximation to Kelvin function integration (B.39) with (B.17), or the solid plate solution (B.34), but certain particular parts of the curves are from the elastic computer program (PVA1), e.g. values of θ_o(d/D) near $\pi/2$.

Let a particular curve be considered as an example, t/T = 1.0, Fig. 21, curve d/t = 10.:

This curve can be divided into three main parts, i.e. 0° to 20°, 20° to 60° and 60° to 90°. In the first interval (0° to 20°), either the exponential integration (B.38) or the Kelvin function approximation (B.17), as well as the values from the elastic computer program, give virtually the same values, e.g. hemispherical head, Table HH1. In the second interval (20° to 60°) in this particular case, the Kelvin function approximation (B.17) yields slightly higher values than the exponential integration (B.38) but, since they are very close to those obtained from the elastic computer program (PVA1), no table is given for comparison. In the third interval (60° to 90°), the true curve has been obtained using the elastic computer program, as both the solution from (B.38) and the solution using (B.17) considerably diverge, whereas the solution that uses an approximation to the Kelvin function (B.17) gives better values. The complete Kelvin function (1.1) would give better values than (B.17), but it is considered highly probable

that Leckie and Penny's solution, Refs. [13] to [16] would give a better approximation than (B.39). As expected, the solid plate solutions for values of $\theta_o(d/D)$ close to $\pi/2$ yield more accurate values than (B.39) with (B.17) solutions.

Generally speaking, all the curves in Figs. 19 to 22 can be divided into three parts but, for t/T = .25 and .50 in the second interval, the values obtained from the exponential solution (B.38) are slightly higher than the values from (B.39) which uses the approximation (B.17) to the Kelvin function; in the third interval the former solutions are better than the latter when compared with the results from the elastic computer program (PVA1). These conclusions may also be seen from Tables SH1 and SH2 for the spherical head case, and from Tables FH1 to FH3 for the flat end (solid plate) case.

In Figs. 19 and 20 some dotted lines are drawn which represent spherical heads with $2h/\rho$ larger than .1, and therefore outside the thin shell theory. If these curves are to be used the obtained values for SCF should be used very cautiously.

In the tables TH1 to TH4, values from Ref. [9] and from the analytic exponential integration (B.38) for the von Mises stress concentration ratio are presented. The purpose of these tables is to demonstrate the improvement gained by the inclusion of the knuckle on the spherical head. The comparison is made for torispherical [9], and spherical heads with equal d/D. From Ref. [9] the following equation can be written:

$$\frac{d}{D} = \frac{\frac{h}{d} - \frac{r}{d}}{(\frac{h}{d})^2 + .25 - \frac{r}{d}} \quad \text{with } h = \text{head height and } r = \text{knuckle radius} \qquad (3.8)$$

From (3.8) with defined r/d and h/d, the values of d/D can be determined and hence $\theta_o(d/D)$ from (3.5).

From Crisp, [9], the values of h/d = .15, .20, .25 and .4 and r/d = .06 and .10 were chosen for comparison. In Table TH1 the values of h/d for spherical heads are given for each h/d from [9]. The values of spherical h/d changes with r/d. In this table the values of r are quoted as percentage of vessel diameter, d. In Tables TH2 to TH4 different values of d/t have been considered, 20., 50. and 100., respectively.

3.2.2 Flush Cylindrical Nozzles on Spherical Pressure Vessels

For this type of geometry, two theoretical analyses, (Appendix B), were carried out, using either the exponential integration solution (B.36), or the solution by the Kelvin function's approximation (B.37) with (B.18); the elastic computer program was also used for comparison of its results with the values obtained from the above analyses. Comparisons can be done with values from Leckie [61] and [63]. Leckie has plotted curves for an average Tresca SCF (3.2.1) for constant values of t/T (.0, .25, .5, .1) against $\omega(= d/D_s\sqrt{D_s/2T})$, obtained from a cylinder sphere intersection analysis described in [14] to [16], with the assumption that the maximum stress occurs in the spherical portion (although in certain geometries of very thin nozzles the maximum stress probably lies in the cylinder portion), and that the cylinder can be treated as semi-infinite. Leckie also assumed that the pressure vessel could have a reinforcement pad (area replacement rule, Ref. [78]) away from the nozzle, but with a length such that the change in thickness in the sphere would not modify the stresses on the sphere close to the junction, and also that the highest stress point remained in the same position. Leckie and Penny have presented a discussion, Ref. [16] on pad size.

In the present work the same assumptions were made, except that the SCF is based on the maximum equivalent stress anywhere in the geometry; cases of cylinders thicker than the sphere are also considered. The "area replacement" rule and "pad size" were not studied, although some considerations regarding this can be seen in Section (3.4.1).

In Tables FN1 to FN4, values of SCF using either the (3.2.1) or (3.2.2) definitions, can be compared for values from analytic integration, either (B.36), or (B.37) with (B.18), from the elastic computer program, and from Ref. [61].

Graphs were plotted, Figs. 26 to 29, for the von Mises SCF (3.2.2) against $\omega (= d/\sqrt{2DT})$, together with values from the exponential integration analysis (B.36). Each graph is for constant t/T, and the cases t/T = 2. and 4. are plotted in the same Fig. 29. Figs. 26 to 28 are for t/T = .25, .5 and 1, respectively.

The geometrical parameters for cylindrical nozzle-on-sphere geometries, without considering any pad size, either on the cylinder or on the sphere, can readily be seen to be R/T, d/D and t/T, from Fig. 3. The parameter d/D has been substituted by ω in the graph, Figs. 26 to 29, as Leckie et al, have done. The geometrical parameter values considered are:

R/T = 400., 200., 100., 50., 20. and 10.

d/D = .0025 to .6

t/T = .25, .5, 1, 2. and 4.

Although the value of .6 for d/D may seem very high, Mershon has considered higher values, [79]; likewise although the minimum value of .0025 may well be too small (except for the case of R/T = 400 and t/T = .25), a value of 2.9 for the von Mises SCF is obtained, and hence it was decided to include this value in the graphs for $d/t \geqslant 10$ (although it should be $d/t \geqslant .20$).

In Figs. 26 to 29, two average curves for the von Mises Stress Concentration Factor can be seen for R/T = 10. to 400., and R/T = 10. to 100.. Because it was realised that errors as high as 40% and 30%, could occur respectively, in relation to these average curves, if it were to have been decided that a graph with only average curves were to be drawn, it was resolved instead not to present a unique graph like Leckie et al in Refs. [16], [61] and [63].

3.2.3 Discussion of Results

Firstly spherical heads are considered and the flush cylindrical nozzles on spherical geometries. This discussion is based on the above-mentioned tabulated values.

Hemispherical and Spherical Heads on Cylindrical Pressure Vessels

The results are tabulated separately for hemispherical, spherical, flat end (solid plate), and torispherical-spherical heads, for comparison between previously published data and the present calculations (which are described in Section 3.2.1), on Tables HH1-HH2, SH1-SH2, FH1-FH3 and TH1-TH4 respectively. (Note: The first letter of the title refers to the type of head, and the second to denote the fact that the table is for heads.)

Each geometry is considered separately and in the latter part of this section the torispherical-spherical heads comparison is made.

Hemispherical Heads on Cylindrical Pressure Vessels

From Table HH1, it can readily be seen that the analytic values, and Langer's values from Ref. [51], are in excellent agreement; it is relevant to note that the Tresca stress concentration ratios and stress index ratios are equal according to the elastic computer program.

From Table HH2, it may be concluded that the values obtained from Langer [51], Crisp [9] and by the analytic exponential integration, are independent of d/t and only change with t/T. The value from Crisp is very nearly the same as that obtained in the analytic solution.

Spherical Heads on Cylindrical Pressure Vessels

For these geometries, comparisons are only made for stress concentration ratios based on von Mises' criterion.

The values of d/D = .4 and .25 are chosen because for d/D > .4 the three solutions (exponential, approximation to Kelvin function, and elastic computer program) are in good agreement within ± 2%, while for d/D = .25 the divergence is greater than - 20%; naturally, these values depend to a large extent on the whole vessel, shown in Figs. 19 to 22.

From Tables SH1-2, it can be seen that the exponential solution yields results better than the approximation to Kelvin function for the case of thicker head than vessel, although the reverse is found to be true for a head and vessel of the same thickness. For thicker heads than vessels, the results from the exponential solution, when compared with those from the elastic computer program, are within - 10% to - 20%, Table SH1, and - 20% to - 30%, Table SH2, for d/D = .4 and .25, respectively. For similar comparisons for head-vessel of equal thickness, the results are within - 0% to - 10% and .5% to - 35% for d/D = .4 and .25, respectively. Comparing the results from the approximation to Kelvin functions solution with those from the elastic computer program, it is found that, for thicker heads than vessels the results are within - 10% to - 30% and - 30% to - 70% for d/D = .4 and .25, respectively, but for head-vessel of equal thickness the results are within - 7% to .5% and - 5% to - 20%, for d/D = .4 and .25 respectively.

Referring to Figs. 19-21, lines (b'b") mark the limit of good agreement between the analytic (Appendix B) and the numerical (computer program PVA1) integrations. On the right hand side of $\overline{b'b"}$ lines the analytic (either exponential or approximation to Kelvin function solutions) integrations may be applied instead of the elastic computer program, but on the left hand side of the $\overline{b'b"}$ line the former solutions

are in places much too conservative. In the same figures points A^i, i = ',","','V are marked; these points are of special consequence in that they denote the limits of application of the solid plate, as opposed to the spherical head, for an analytic solution (Appendix B) when the results are compared with those from the elastic computer program; point A' stands for d/t = 10, and so on, and A'V for d/t = 80.

Consider the following example:

Thicker head than vessel, t/T = .5, d/t = 20, (see Fig. 20, point A").

If acos (d/D) < $\theta_{A"}$, the cylinder-sphere solution (exponential, Appendix B), gives a better result than the solid plate solution, when compared with values from the elastic computer program (PVA1).

If acos (d/D > $\theta_{A"}$, the solid plate solution gives better results than any analytic solution considered in the present work when compared with the values from the elastic computer program (PVA1).

Flat Ends (Solid Plate) on Cylindrical Pressure Vessels

Referring to Figs. 19-22 and Tables FH1-3, it can be seen that the stress concentration ratios (either index, von Mises or Tresca) increase with the thickening of the head, as may be expected from Ref. [51]. For the considered geometrical parameter range (3.7), only nine geometries present stress concentration ratios higher than 1. The solid plate solutions for the von Mises stress concentration ratio are in very good agreement with values from the elastic computer program, but comparison of stress index ratios, from Langer [51], with the elastic computer program, show differences of up to 15%, which is an acceptable margin.

Comparison of Torispherical and Spherical Heads on Cylindrical Pressure Vessels of Equal d/D

Tables TH1-4 show that the presence of a knuckle raises the head, particularly for low h/d values and large r/d values. The knuckle inclusion gives an improvement as far as stress concentration is concerned although in certain conditions, taking the knuckle into account

does not bring the expected improvement, e.g. Table TH2, h/D = .25, .4, either 6% or 10% knuckle, and Table TH3-4, h/D = .4, either 6% or 10% knuckle; the improvement gained is less than 12% and certainly the cost will be higher with rather than without the knuckle.

The improvement for knuckles of 6% and 10% is within 0% to 30% and 0% to 45% respectively.

Thus once the values of d/D, d/t and t/T have been determined, it is a worthwhile exercise to study whether a geometry with a knuckle is a significantly better design with regard to economic factors.

Flush Cylindrical Nozzles on Spherical Pressure Vessels

A comparison is made between the values from the two analytic solutions (cylinder-sphere and cylinder-shallow sphere intersections) presented in Appendix B, and the elastic computer program for von Mises' Stress Concentration Factor, although values from Leckie, Ref. [61] are also compared with values from the computer program.

Tables FN1-4 are for R/T = 50. with t/T = .5, 1., and R/T = 100. with t/T = .5, 1. respectively.

Leckie's values [61], when compared with the results from the elastic computer program (PVA1), show that the former values are on average - 43% and + 5% different for nozzle-vessel thickness ratios (t/T) of .5 and 1. respectively; these results however are to be expected since Leckie assumes that the maximum Stress Concentration Factor lies on the sphere itself.

The results from the exponential and the approximation to Kelvin function solutions when compared to the results from the elastic computer program (PVA1), for nozzles thinner than sphere, are within - 11% to + 1% and 0% to 15% respectively, but for nozzle-vessel of the same thickness, the results are within - 12% to + 10%, with an exception of + 25%, and + 2% to + 30%, for exponential, and approximation to Kelvin

function, solutions (Appendix B) respectively. Generally speaking, the exponential solution yields lower values than the elastic computer program but the reverse is the case for the approximation to Kelvin function solution.

If one excludes the two following geometries from Tables FN1-4, d/D = .025, t/T = 1 with R/T = 50 and 100, the values obtained by the exponential solution lie within a range of ± 10% when compared to those from the elastic computer program, whereas values from the approximation to Kelvin function lie within 0% to 20%.

From the values obtained from Leckie [61], for a nozzle-vessel of the same thickness (t = T), it is very probable that Leckie's method will yield better results for von Mises' stress concentration factors than the methods based on the analytic integrations used here; however, a similar study using Leckie's method, Ref. [13], is recommended.

If the curves drawn in Figs. 26 to 28 are to be represented by a unique average curve from each graph, a very large degree of error would be entailed. For example, for t/T = .25, Fig. 26, the error would be within ± 25% and ± 45%, for the average curves of R/T = 10. to 100. and R/T = 10. to 400., respectively. The error for t/T = .5 and 1 would be within ± 20%, ± 35% and ± 20%, ± 30%, Figs. 27 and 28, respectively.

3.2.4 A Graph for Stress Concentration Ratios based on von Mises' Criterion in Spherical Heads on Cylindrical Pressure Vessels of t/T = .25, .5 and 1.

Results from the spherical head discussed in Section 3.2.3 can be considered reasonable and, because it was realised that a maximum stress concentration ratios graph could be obtained from Figs. 19-21, two intermediate graphs were drawn, Figs. 23 and 24, and then a final one drawn on the basis of these two, Fig. 25.

In Figs. 23 and 24 the maximum stress concentration ratios are shown for t/T = .25, .5 and t/T = .5, 1., respectively.

The final graph can be seen in Fig. 25 and shows the maximum stress concentration ratios for t/T = .25, .5 and 1; only cases of either d/t or D/t larger than or equal to 20 are there considered.

Three separate regions are defined in Fig. 25, the first for t/T = 1, in the region above line $\overline{324}$, the second for t/T = .5, bounded by line $\overline{123}$, and the third for t/T = .25, the region below line $\overline{124}$.

Hence, from this graph the designer can find out for a defined d/D and d/t, which value of t/T will give the lowest SCF if the geometry is of $2h/\rho \leqslant .1$ type.

3.3.1 The von Mises and Tresca SCF on some Knuckles of Cylindrical Nozzles on Spherical Pressure Vessels

The geometries in this section are also analysed by the elastic-plastic method, in Chapter 4. The geometries are divided into two series apart from the knuckle of cylindrical nozzles on spherical pressure vessel tested in the course of this work.

The first series is considered in order to study the effect of a change of geometry on the cylinder-sphere junctions; accordingly, the values of d/D_o and t/T are taken as constants and 2r/D (ratio of twice knuckle radius to sphere diameter) and thickness taper on the junction as variables. Details of the knuckle geometry are shown in Fig. 38. Other parameters are taken as

$$d/D_o = .2;\ t/T = .5;\ 2r/D_o = .0,\ .015, .045$$

The geometrical case of $2r/D_o = .0$ is treated using the fact that the forces at a "square corner" intersection can be distributed as bands of loading over a finite width of shell (equal say to the thickness of

the shell wall plus a fillet weld), rather than the point or line load of conventional shell theory, Refs. [2], [8] and [24]. The force is distributed over either the first step of integration or the first two steps in the elastic computer program.

For the other two geometries, the knuckle junction is treated by defining a small fillet of specified mean radius and taper. The taper details are shown in Fig. 38; these geometries are referred as C1, C2 and C3 for junction details of types A, B and F, Fig. 38, respectively, for $2r/D_o = .015$. The last junction detail, in this particular study, is for $2r/D_o = .045$ with type A knuckle, Fig. 38.

In the calculation of the knuckles of cylindrical nozzles on spherical geometry the "Winkler's curved beam" theory was used.

For each detail parameter, certain quantities are tabulated, Table 1, and the elastic von Mises SCF is given according to conventional shell theory, except for the case of a small local radius of curvature, when the Winkler type modification (Appendix D) is used. Values of Tresca SCF are also given, from the simple shell theory analysis and from Ref. [61].

The second series of knuckle of cylindrical nozzles-on-sphere geometries will be referred to as series N; they are for a given sphere, diameter D_o, thickness $T = .005\ D_o$, and with cylinder-knuckle-sphere of equal thickness ($t = T$, no taper). Various ratios of cylinder to sphere diameter $d/D_o = .05$ to .25 are used, with a constant knuckle radius $2r = .05\ D_o$. The stress and strain distributions are shown in Figs. 30 to 33 for the cases of $d/D_o = .05$ and .25, nozzles N1 and N5, respectively. Table 4, similar to Table 1, allows a comparison of the elastic SCF for series N, but in this case the Tresca and von Mises SCF's are calculated from the flush cylinder nozzle with simple shell theory and can be compared with values from Ref. [61], and to values from the

knuckle of cylindrical nozzles with Winkler's type approximation, respectively.

The knuckle of cylindrical nozzle-on-sphere geometry tested in the course of this work is shown in Fig. 37; the represented geometry is the best approximation to the real tested nozzle described in Section (5. 3.2). The geometrical parameters are: d/D_o = .112, D_o/t = 149, t/T = .5, $2r/D_o$ = .0134 and a type A cylinder-sphere junction, Fig. 38. In Table 7 the SCF values are derived either from the knuckle of cylindrical nozzle Winkler's approximation, or from flush cylinder nozzle simple shell theory. The values presented are based on the Tresca and von Mises criteria, from the elastic computer program, from the test, and from Ref. [61].

3.3.2 Discussion of Results

Series C (Table 1). Nozzles C5 and C6, those with band modification, present unrealistic stress concentration factors based on von Mises'criterion when compared with the Stress Concentration Factors from the simple shell theory for the flush nozzle; the reason for this, however, is possibly due to the size of the step involved, over which the point forces (sharp corner) are spread, although the lengths of the steps are those recommended in Ref. [8]; the unrealistic values abovementioned may be explained by comparing the C5 and C6 SCF values since, in the first, the spreading is over a smaller length (area) than the second, with the result that there is a worsening in the Stress Concentration Factor prediction. Unless great care is taken when applying this modification, the structure will be subjected to a large degree of deformation.

Other nozzles of this series, C1 to C3, show a negligible variation in the different details of connection, although C4 has a reduction of 30%, as could be expected for the larger knuckle radius. If a comparison is made with the von Mises stress concentration factor obtained

for a flush cylinder-on-sphere with the simple shell theory, it can be seen that the stress concentration factor values for nozzles C1 to C3 are lower by about 25%, but in the case of the C4 nozzle, by some 50%. The value from Ref. [61] is some 25% lower than the value from the flush nozzle simple shell theory, (K_1^*), but part of this difference can be justified by the fact that K_1^* is taken to be at any point in the structure in the present work, but in Ref. [61] is taken from the maximum stress concentration on the sphere; the rest of the difference is because Leckie's curves are averaged.

Series N (Table 4). The stress concentration factor values based on von Mises criterion for the knuckle nozzles are plotted in Fig. 39, together with the values from the flush nozzle simple shell theory, and from Ref. [61], Tresca SCF on sphere.

Comparing the von Mises Stress Concentration Factors, columns K_1 in Table 4, it may be observed that values from the knuckle nozzle "Winkler's curve beam" approximation, are 17% to 27% lower than those from the flush cylinder nozzle simple shell theory; however when the values of the Tresca Stress Concentration Factor, flush cylinder, and from Ref. [61] are compared, it can be seen that they have differences of - 7% to 2% from each other. This is brought about by the two different methods of calculation, since the maximum stress concentration is in this case on the sphere, and as well because Leckie's curves are averaged curves.

Tested Nozzle (Table 7). The strain distribution is shown in Figs. 34 and 35, based on the strain gauge readings and on the knuckle of cylinder nozzle "Winkler's curved beam" approximation elastic computer program results.

Comparing the stress concentration factor values K_1 (von Mises) from Winkler's approximation applied to the knuckle nozzle, with the test value, there is a + 11% difference but, when compared to the value

found using the flush nozzle simple shell theory, a - 23% difference is found. The good agreement between the test, and the knuckle nozzle Winkler's approximation, may well be described as unexpected since the knuckle radius used was too small, as can be realised from a study of Refs. [3] and [9].

The comparison with a stress concentration factor value based on Tresca's criterion shows a 40% reduction when the knuckle is introduced and a 46% reduction when the values from Ref. [61] are compared with the results from the elastic computer program, simple shell theory. The former reduction is due to the effect of knuckle radius, although the reduction may perhaps be too large for this; the latter reduction is due to the fact that in this case the high stress concentration region is definitely in the cylinder, though near the junction, and as well Leckie's curves are average curves, Ref. [61].

3.4 Stresses and Strains on some Knuckles of Cylindrical Nozzles on Spherical Pressure Vessels

From hereon in the present chapter, only the elastic computer program (PVA1) is referred to, and wherever possible its results are compared with experimental data obtained in the course of this work.

3.4.1 Stress and Strain Distribution on some Knuckles of Cylindrical Nozzles, Series N

As referred to in Sections 3.3, two main sets of elastic-plastic computations were undertaken on radial nozzles with closed ends subjected to internal pressure. In the second set, Series N, for a given sphere, diameter D, thickness T = D/200, cylinder-knuckle-sphere thickness t = T, with ratios of cylinder to sphere diameter from .05 to .25 were used with constant knuckle radius r = D/40. Graphs for the two extreme geometries, d/D = .05 and .25, were drawn in order to compare the

distribution of stresses and strains for both geometries.

The stress distributions can be seen in Figs. 30 and 31, for d/D = .05 and .25, respectively; the strain distributions are shown in Figs. 32 and 33.

From Figs. 30-33 the pad size may be approximately and intuitively visualised although further study of stress and strain distribution for a theoretical real structure is recommended.

As an example of, nozzle N1 (d/D = .05), it may be observed from a study of Figs. 30 and 32 that the thinning of the cylinder can being between 1.5" and 2.5" from the knuckle, though unnecessary in the sphere, since the SCF is less than 2.25; with nozzle N5, Figs. 31 and 33, (d/D = .25) the thinning must be done on the cylinder and sphere, since both stress concentration factors (in relation to the von Mises membrane stress on the sphere and on the cylindrical) are larger than 2.25. The thinning on the cylinder and on the sphere should probably begin at 12" to 15" from the cylinder-knuckle junction, and at about 42^{o} towards zero, respectively. It should be borne in mind that further stress and strain distributions ought to be calculated with the theoretical new shape in order to find out if there are any influences on the previous local stress concentration, and any major changes on the region near the thickness taper.

3.4.2.1 The Elastic Strain on the Test Knuckle Cylindrical Nozzle

The elastic strain distributions, from the elastic computer program, are plotted in Figs. 34 and 35, for 250 lb in^2 internal pressure, on the internal and external surfaces, respectively. In these figures, strain gauge readings for the same pressure on the test nozzle, Fig. 37 (see Section 5.3.2) are plotted for comparison.

On the internal surface, Fig. 34, the agreement is reasonable although gauge 90F, Fig. 37, circumferential and meridional, shows a

- 10% and + 40% disagreement, respectively, when the calculated strains are compared with the gauge reading; this is probably due to the asymmetry of the nozzle (see Section 5.3.2). Leaving aside these gauge readings (90f, Fig. 37) it can be stated that, on the internal surface, the reading and the calculated strains are within less than 15% disagreement.

On the external surface, Fig. 35, the problem of the asymmetric nozzle appears again, gauge 90C, however, there is in case another gauge pair (B in Fig. 37) that also presents a large disagreement. This disagreement with the gauges B probably takes place because of the welding fillet. Similar behaviour should be expected on the inside surface, gauges H, but gauges (outside) were fixed on the transition region (fillet to sphere) and gauges H well on the fillet. Continuing with the comparison, gauges 90C present on the circumferential and meridional directions, + 3% and - 25% disagreements, respectively, when the calculated strains are compared with strain gauge readings, and gauges B present on the circumferential and meridional directions, - 5% and - 40%, respectively, doing the comparison as before.

Leaving out this pair of gauge readings, B and 90C, the disagreement on the outside surface, can be said to be less than 18%.

From the analysis of the strains on the outside and inside surfaces, it may generally be stated that the elastic computer program with Winkler's modification gives a reasonable agreement if the geometry is properly defined and if other parameters, such as welding fillet-base material transition, do not wield too much influence.

3.4.2.2 Discussion of Results

The reliability of the elastic computer program (PVA1) has been tested before in many works, e.g. Refs. [2] and [3], and once more its

accuracy is within 10%, not considering welding fillet and asymmetry effects of the structure, and therefore within reasonable agreement.

Comparing the results from the gauges on the transition region (B, circumferential and meridional directions, see Fig. 37 for their positions, and Fig. 35 for the values) it can be seen, as could be expected, that the transition fillet-base material exerts more influence in the meri_dional direction than in the circumferential (- 40% and - 5% respectively). The difference in values is probably because a significant part of the area of the gauge for the meridional direction lies on the sphere (less than 50% of the total gauge area), whereas the circumferential gauge, although lying in a direction normal to the transition region, and which therefore registers the influence of this region, which influence can be expressed by Poisson's ratio, ν, has only a small area on the sphere. It is noteworthy to observe that the circumferential strains are overestimated by the computer program, with the exception of 90FC, in the circumferential direction, for which the circumferential strain is underestimated, and hence the influence of the weld-base transition region materials must be larger than - 5%.

The introduction of the knuckle with the Winkler's curve beam theory has improved the results and may be reliably used to study the "areareplacement rule" in order to find out which area and area-distribution is optimum.

CHAPTER 4

COMPUTED ELASTIC-PLASTIC BEHAVIOUR, COLLAPSE AND SHAKEDOWN OF SOME PRESSURE VESSEL COMPONENTS

4.1 Introduction

In this chapter the elastic-plastic results from the use of the PLINTH program for the elastic-plastic analysis of symmetrically loaded shells of revolution are presented, and compared with available data. For details of the computer program see Chapter 1, Refs. [3], [5] and [44].

In Chapter 3, two series of knuckle cylindrical nozzles on spherical pressure vessesl are defined, Tables 1 and 4, Series C and N, and the geometrical parameters for the tested knuckle nozzle are defined in Table 7. Besides these geometries the torispherical Head A from Ref. [3] is also analysed.

In these analyses the material was considered to be either of elastic-perfectly plastic or of work-hardening type.

Limit pressures are calculated, using some of the criteria described in Chapter 2 and, in this chapter, are compared with values from a limit analysis, Refs. [3], [33] or [63], whichever one is applicable to the geometry under consideration.

Values of shakedown pressure are calculated by using the criteria described in Chapter 2, and are compared with available data from Refs. [63] and [73], whichever is applicable to the geometry under consideration; however, the minimum value obtained by an application of Macfarlane and Findlay's method, [12] referred to in the present work as SEM (Section 2.2.3), an adaptation of Leckie's method [61], is made either at the cylinder-torus or the sphere-torus junctions since, as far as the writer is aware, this method cannot be applied to toroidal shells near $\theta = 90^{\circ}$, because of the discontinuity in the membrane stresses (Ref. [1], page 34).

The torispherical Head A, Refs. [3] and [7], and later, the knuckle cylinder nozzles, are treated in this chapter, but the tested knuckle radial nozzle results are only compared with values from strain gauge readings and other available data in Chapter 6.

4.2 Torispherical Head on Cylindrical Pressure Vessel

Cheung and Turner, [7] have compared limit pressures for two torispherical heads, using (a) an elastic-plastic computer program with and without work-hardening material, (b) limit analysis and, (c) static strain-gauge readings on a vessel with two torispherical heads pressurised beyond yield.

In the present work, the results for Head A, Refs. [3] and [7] are compared with values obtained from the elastic-plastic computer program, but using a better fitting than that used by Cheung and Turner to the material equivalent stress-plastic strain curve.

4.2.1 Comparison of Computed and Experimental Values

Cheung and Turner [7] used data regarding material behaviour in the computer program, that is, a fitted 0-2% stress-strain curve given by the second order polynomial expression

$$\sigma_e = 33.5 + 1336.9\ \bar{e}_p - 18159\ \bar{e}_p^2 \quad \text{(ksi)} \tag{4.1}$$

However it was realised, in the course of this work, that this expression was far from being a good representation of the equivalent stress-plastic strain curve of the material, since it would not give a good fitting where it was most necessary, at initial yielding and up to 1% equivalent plastic strain, Fig. 6. This is because it is in this range that local plastic flow takes place, and where the gross yield is much influenced by the local plastic flow history.

Because of this, a better fitting was attempted for the average tensile test stress-plastic strain curve for the material, by using the exponential approximation given by either

$$\sigma_e = 26.6 + 82.3\ \bar{e}_p^{\,.305} \tag{4.2}$$

or

$$\sigma_e = 27.2\ (1 + 6626\ \bar{e}_p)^{.132} \tag{4.3}$$

The computer program used for the evaluation of the constants in (4.2) and (4.3) indicated that (4.3) would provide the best fitting for the range 0-4.5% equivalent plastic strain. A comparison between the averaged tensile test stress-strain curve, the second order polynomial from (4.1), Ref. [3], and the exponential expression (4.3) for the material is shown in Fig. 6. The approximation (4.3) is unquestionably better than (4.1).

Computations were carried out using either (4.1) and (4.3). Some results are plotted in Figs. 40 and 41 in order to compare the improvement gained from the fitting used in the present work, (4.3) with that, (4.1), from Refs. [3] and [7].

The computed results from (4.3) were used in order to evaluate collapse pressure ratios (P_c^*), as well as shakedown pressure ratios (P_s^*), based on the different criteria described in Chapter 2. The SCF and collapse (K_3) and shakedown (K_2) pressure ratios to membrane yield pressure, may be seen in Tables 10-12, respectively, as well as the ratios of the lower and upper limit pressures, using limit analysis, to membrane yield pressure on the vessel body (cylinder), assuming a non-workhardening yield stress of 34.9 ksi (.2% strain, proof stress). All these values are based on von Mises' criterion, with the exception of the values from the limit analysis, in which the Tresca criterion is used, Ref. [3].

Some stress paths, including that of the most highly stressed point on Head A, Ref. [7], up to and beyond first yield, are plotted, Fig. 42, in terms of circumferential and meridional stress ratios for the inside, outside and mid-wall surfaces.

The maximum equivalent strain on the outside surface is plotted in Fig. 15, together with the point with which the particular value is associated. Head A is considered as two branches with the junction on the cylinder 2.5" from the knuckle-cylinder connection. The branch which contains the torispherical head is divided into 30, 50 and 120 elements on the cylinder, the knuckle and the sphere, respectively. It should be borne in mind that the numbering of the points on the shell begins at the junction.

4.2.2 Plastic Flow, Collapse and Shakedown

In Fig. 42, the stress paths for cross-sections A, B, C and D, the first two in the cylinder (vessel body), the third on the knuckle (this cross-section contains the most highly stressed point on the structure), and the fourth on the sphere, are plotted. Following the stress paths for A and B, those on the cylinder, it can be seen that Section B makes its elastic to plastic transition between 6 and 7 (numbers marked in Fig. 42), whereas A's lies between 7 and 8. Analysing the inside stress path of section C, it may be concluded that there is a change of curvature between 6 and 7, that is, where the plastic flow begins to spread into the membrane region of the cylinder. It is at this stage that the work-hardening of the material starts to make a major contribution to the plastic deformation. Another important point is that, in the sphere, the internal stress path shows a very high bending tendency, but when the yield begins to spread from outside to inside, in that region of the sphere, the bending tendency is greatly reduced. This mechanism is particularly important as far as shakedown,

with permitted work-hardening, is concerned, since if those points were left unanalysed, one might be led to conclude that no upper limit to shakedown could be found, or that P_s^* for shakedown was larger than 3., since the computations were made only up to that point. In fact, that is not the case, since as shown in Fig. 43, it is precisely because of the above-mentioned bending of the internal stress paths on that region of the sphere, that an upper limit to shakedown was found slightly less than 2.8. This situation is of particular interest, since, because the internal point on the cross-section E, Fig. 43, shows an elastic behaviour which is markedly non-linear, an upper limit of shakedown can be defined for this structure before plastic flow takes place at that point.

From Fig. 42, a collapse limit pressure can be estimated, since between 7 and 8 on the figure, the plastic flow moves from near B to A, that is a limit of between 2.2 and 2.4 for collapse pressure ratio (P_c^*). This value is probably the upper limit of collapse if no yield is permissible on the membrane region of the vessel body (cylinder).

If the collapse definition is straight away applied to calculate equivalent strains, then, by a careful analysis of the results, a graph of maximum equivalent strain on the outside surface can be drawn, Fig. 15, and, marking on the graph the corresponding points, it can be seen that for a non-work-hardening material, the position of the maximum equivalent strain on the outside surface starts at 106, moves to 105, 104 and finally to 102, and hence it is possible to define a collapse pressure ratio (ratio to first yield pressure) of between 1.9 and 2.1, perhaps 1.95, that is a value of .86 to K_3 in Table 11, line CMEO. The same analysis was made from the calculation using work-hardening material (4.3). The maximum equivalent strain, on the outside surface, is shown in Fig. 15, and it can

be seen that the collapse pressure ratio may be estimated at about 2.83, that is a value of 1.24 for K_3, Table 11.

4.2.3 Discussion of Results

The value of the stress concentration factor, based on the von Mises criterion, for Head A, with or without knuckle, can be seen in Table 10; a 40% improvement is obtained by the introduction of the knuckle.

Comparing the collapse pressure ratios (K_3), Table 11, obtained from the elastic-plastic computer program with test values, Ref. [7], it can be concluded that the values from the calculations with the second order polynomial expression, approximation to the material equivalent stress-plastic strain curve, (4.1), are within - 17% to - 28%; however the results using an elastic-perfectly plastic material are within - 19% to - 43%, and those obtained by using the exponential expression, (4.3), are within - 3% to - 15%, when compared to the values from the test results, Ref. [7]. The average test value in Table 11, when compared with the average calculated calues, in each column, differ by - 27%, -4% and - 32% from the computed values using (4.1) (the second order polynomial expression), (4.3) (the exponential expression), and the case of non-work-hardening materials, respectively. Without question, the exponential expression, (4.3), values give a better approximation than either the case of elastic-perfectly plastic material, or the second order polynomial expression, (4.1).

It should be pointed out that values K_3, either from the test results or from the calculation with the exponential expression, (4.3), are larger than the limit analysis upper limit.

From Table 11, one is led to conclude that values from a non-work-hardening calculation are more conservative than those from a work-hardening calculation, but they would,in fact, be reduced if a more realistic

equivalent to the idealised yield stress were to be used, for example, .2% proof stress rather than the linear limit of elasticity. In the case of Head A, the linear limit of elasticity is 27.2 ksi and the .2% proof stress is 34.9 ksi, and hence 26% larger than the former value.

It is very difficult to choose which criterion is more reasonable than the others but the most useful was found to be C5I, since it can be used in the testing of pressure vessle, and though it brings with it the uncertainty of where to attach the strain gauge, because of this, an elastic-plastic calculation using the best fitting curve for the equivalent stress-plastic strain curve should be used in order to decide the optimum place for attaching the gauge. The criterion CMEO yields a calculated value for collapse pressure ratio (K_3) 24% higher than the limit 1. of the criterion BSLY, but, since the maximum value from the test reading is 48% higher, it would seem to be applicable in this particular case, Head A; however, because of its unconservative characteristics, if it is to be applied, the designer has to take great care in making such a decision.

The C3 criteria are the most conservative in any calculation, as well as being shown by the test readings to be so, and therefore may be judged safely applicable.

The shakedown pressure ratios, K_2, may be compared in Table 12, from which it can be seen that the introduction of work-hardening (4.3) improves the K_2 values for either SPC or SPT when compared to values obtained from the elastic-plastic calculations, with non-work-hardening material, by 1%; however, if the work-hardening ellipse simply grows according to the load used, the shakedown pressure ratio K_2 will show an improvement of about 50% when compared with the non-work-hardening value. It should be recalled that the fitting curve is from a tensile test and not from a settled cyclic curve, since the latter type of curve was not available. The value obtained for SEM is larger than the

values from SPC and SPT, either work-hardening or elastic-perfectly plastic, although from [73] the K_2 value is some - 20% and 4% different from the values obtained in the present work, based on SPT for non-work-hardening and work-hardening, respectively.

From an examination of Tables 11 and 12, one is led to conclude that values from a non-work-hardening calculation are more conservative than those from a work-hardening calculation, but, in fact, such conservatism should be relaxed if a more realistic equivalent of the idealised stress is to be used, say, e.g. .2% proof stress rather than the linear limit of elasticity for the material.

4.3 Some Knuckle of Cylindrical Nozzles on Spherical Pressure Vessels

In Chapter 3, it is stated that elastic-plastic calculations had been carried out for some knuckle nozzles, Series C and N and the tested knuckle nozzle. These calculations were carried out using the elastic-plastic computer program described in Refs. [2] to [5], with the "Winkler's curve beam" modification on the meridional plane when $2h/\rho$ is larger than .1 (see also Chapter 1, Appendices A, C and D). The elastic-plastic calculations were carried out assuming a non-work-hardening, and a work-hardening curve, which latter is given by $\sigma = 13.3\ (1 + 133\ \bar{e}_p)^{.269}$; this was taken as representative of mild steel, ignoring the horizontal discontinuity at first yield.

Some graphs are plotted in order to facilitate comprehension of the plastic flow, and of the mechanisms of collapse and shakedown of the series of nozzles analysed, Figs. 14, 16, 17, 44 and 45.

Tables 1-9 are drawn up in order to compare the stress concentration factors (see Section 3.2), and the collapse and shakedown pressure ratios, from the elastic-plastic computer program using the different criteria described in Chapter 2 and the values from Refs. [33], [61] and [63], with either the von Mises or the Tresca criteria; Tables 7 to 9 for the test knuckle nozzles, however, are discussed in Chapter 6.

4.3.1 Plastic Flow, Collapse and Shakedown

The stress paths of the most highly stressed point in each of four nozzles, Series N, up to and beyond first yield are plotted in Fig. 16, in terms of circumferential and meridional stress ratios for the inside, outside and mid-wall surfaces.

For small values of SCF (case N1), the internal path turns anti-clockwise a very short distance around the ellipse for pressures of up to about 25% higher than first yield, and then clockwise for higher pressures (a_1, Fig. 16). A similar effect is noted for a rather higher SCF (case N2), for up to about 10% beyond first yield, and for even higher SCF values (cases N3 and N5), the stress path moves clockwise around the ellipse from the moment that first yield takes place (e.g. a_5, Fig. 16). The virtually stationary values of the stress ratios, for significant increases in pressure, only occur when the first region of stress concentration is yielding; however, when a second adjacent stress peak yields, the clockwise movement of the stress ratios begins as described above. In all the cases studied, first yield takes place on the inside surface, with the close second yielding on the outside, both cases being in bending mode.

The succeeding tendency of the stress ratios to move anti-clockwise (b_1 ... b_5, Fig. 16) appears at a pressure when the local plastic region begins to spread over a much greater area compared with the initial zone of small extent. This phenomenon is more marked for cases with small SCF (e.g. case N1 rather than case N5), as can be seen in Fig. 16. Another observation that can be made from Fig. 16 is that when the SCF is small, a larger degree of work-hardening is required in order to obtain a given level of non-dimensional loading, P/P_y. The locus $P/P_y = 2$. is shown chain-dotted in Fig. 16.

The fact that the stress ratio changes is of course well known, but here it can be understood quantitatively. The variation of such ratios increases with SCF, especially in the regions a_1 ... a_5, Fig.16.

This second change in the direction of the movement around the ellipse can most probably be considered as the beginning of collapse, since it is this re-distribution of stress which is caused by the rapid spreading of membrane yielding to areas of the sphere adjacent to the nozzle.

Another typical biaxial stress field is shown Fig. 17, for the cross-section containing the most highly stressed point of nozzle N5 for both the work-hardening and elastic-perfectly plastic cases. In both, the most highly stressed point follows a linear path, such as curve A, Fig. 17, to the point where the yield criterion is reached. If the material is considered as non-work-hardening, the stress path will be around the ellipse after yielding, and will be like curve B1, Fig. 17, or, if treated as work-hardening, along some line following the increasing size of the work-hardening ellipse, such as B2, Fig. 17.

Again, as with Head A, Section 4.2.2, Figs. 42 and 43, after yielding at any point in the structure, linearity of the stress path cannot be assumed. As the yielding is extended the direction of movement of the stress ratio for a point which is still elastic may change, sometimes reversing its original direction of movement, e.g. in Head A, an internal point between points D and E on Figs. 42 and 43, respectively. This non-linearity of the elastic region of the structure may be interpreted as the re-distribution of the elastic stresses caused by the yielding of adjacent parts of the structure.

As soon as the final anticlockwise movement begins on the stress path, the shakedown pressure obtained by using any of the criteria, SPC, SPT and SPW, with an elastic-plastic computation becomes higher

but unfortunately the collapse pressure, in terms of pressure ratio , grows smaller.

Here it is plain to see that the shakedown value can be limited by the collapse value, Ref. [80].

The values of the collapse (P_c^*, K_3 and K_3^*) and shakedown (P_s^*, K_2 and K_2^*) pressure ratios can be seen in Tables 2,5 and 8 and 3, 6 and 9, for nozzle series C, N and the tested nozzle , respectively.

The maximum individual strains for nozzle series N and C are plotted in Figs. 14, 44 and 45, respectively, in order to show that the maximum individual strain can start by being internal circumferential and end by becoming internal meridional, curves a, b and c, Fig.44, for an SCF larger than about 2.5; however, for a stress concentration factor less than about 2.5 they may end by becoming external meridional, curves d and c, Fig. 44, although when the band modification (the forces in a sharp corner spread over a small meridional length near the junction) is assumed for flush cylindrical nozzles, this behaviour may be different, see Fig. 45, curves e1 and e2 in which the initial behaviour is the same as described above, although the final behaviour for case C5 (spreading over a short meridional length) may end as internal circumferential as happens while the structure is still in the elastic range, with case C6 (spreading over a larger meridional length) becoming internal meridional and returning later to internal circumferential again.

4.3.2 Discussion of Results

Nozzle Series C

The minimum values of P_c^* were obtained by using the C3 criteria, but the maximum values were obtained by the C15 criteria applied to the maximum individual strain. Values obtained from the elastic-plastic computer program (cases C5 and C6) are generally unconservative except

for the C3 criteria. Comparing cases C1, C2, C3M and C3R, Table 2, one is led to conclude that minor changes in details of connection do not alter the values by more than 10%, although if band modification (cases C5 and C6) is used in the computer program, then the change can be larger than 35%.

Comparing case C1 with C4, it can be seen that the larger knuckles show a decrease in their collapse ratios (P_c^*), with a difference of about 25%, though the K_3 ratios have improved by the same amount, as might well be expected.

Comparing the pressure ratios K_3 and K_3^*, it can be seen that the low K_3 values (C1-C3) show no considerable difference; however, the band modification results show an increase of about 100%. Once again one is led to conclude that the use of this modification gives unconservative results, and hence the designer must exercise considerable caution when using it. The larger knuckle (C4) gives 18% and 30% improvements respectively, when the C5I and C15I criteria are used for K_3, compared with K_3^*, Ref. [63].

Generally speaking, the overall collapse factor, K_3, improves as SCF decreases; this fact is well known, Ref. [80].

The C15I criterion is probably very reasonable for an SCF larger than 3.5, and the C3 criteria are reasonable for an SCF of less than 2. The C5I criterion is reasonable for intermediate SCF values. These intervals cannot be accurately defined since a collapse criteria must be connected with the shape of the structure and environmental material properties.

Once again the values from the computer program, using the band modification, are unrealistic, with the exception of results obtained when the SEM criterion is used, Ref. [12].

Shakedown values derived from the elastic-plastic computer program results do not show any differences when either work-hardening or elastic-perfectly plastic materials are used, case C3, Table 3; this is because of the high SCF, 4.88 Table 1. Small differences in connection details (cases C1-C3) do not alter the P_s^* and K_2 values by more than 6%, although the larger knuckle (case C4, Table 3) when compared with case C1(same type of connection) do not show any considerable differences, either, for the SEM, SPC and SPT criteria; however case C4 shows an improvement of more than 14% if full work-hardening is considered (SPW).

The shakedown pressure ratios K_2, based on the SPT criterion, for cases C1-C3, are some 20% smaller when compared with those calculated using Leckie's (Tresca) value K_2^*, although the larger knuckle (case C4) shows an improvement of 18%. It is noteworthy that the SEM values for P_s^* are the same as Leckie's values.

Series N

The stress concentration factor and collapse and shakedown values for this series of radial nozzles are shown in Tables 4, 5 and 6, respectively.

The collapse pressure ratios (P_c^*) using the C3 criteria, with the results from the elastic-plastic computer program, are reasonable for cases N1 and N2, but conservative for cases N3 to N5, and in the overall range (N1 - N5) they are within $\pm$ 8% of an average value; the inclusion of work-hardening slightly improves the results.

The collapse pressure ratios based on the C5 criteria are within $\pm$ 10% of an average value, and are therefore slightly more sensitive to changes in geometry than the C3 criteria. The C5 criteria seem reasonable for all the cases N1 - N5.

The collapse criteria C15 give values within ± 16% of an average value, and therefore are more sensitive than the C5 and the C3 criteria to geometry changes. The C15 criteria, apart from the problem of the degree of strain (1.5%), are therefore much more subject to creeping than any of the other criteria, but are unconservative for a low SCF, cases N1 and N2, especially N1 with work-hardening (K_3 = 1.01, Table 5) although they are probably reasonable for cases N3 to N5.

The collapse criterion CSP gives values slightly lower than C5I. The CSP criterion is conservative for cases with a stress concentration factor larger than 2.5 (cases N3 - N5), but seems reasonable for cases N1 and N2, cases with a stress concentration factor lower than 2.5.

Referring to Table 6, the shakedown pressure ratios SEM show values equal to, or larger than, 2.if the SCF's are larger than 2.6; it should be borne in mind that these values are taken either on the sphere-torus or torus-cylinder intersections. For SCF values of 2.or less, the values obtained using the SEM criterion appear to be limited by the SCF value. When the shakedown criterion SPC is used, values within ± 2% of an average are obtained. The values from the SPT criterion slightly improve when values for work-hardening material, with ellipse moving toward the point considered on the stress path, are compared with values from an elastic-perfectly plastic material, although the former values are within ± 3% of an average value,while,in the latter, the value for N1 is some 11% smaller than the N5 value. The improvement gained with the application of SPT with work-hardening is some 22% for N1 and 3% for N5, in relation to the values obtained with the assumption of elastic-perfectly plastic material, N1R and N5R, respectively. The SPW criterion, which allows full work-hardening to be attained, is sensitive to changes in geometry or SCF values; the SPW values, Table 6, are within ± 19% of an average value. These values, when compared to the SPT values, show an improvement as the SCF values

grow, as expected. A point worthy of mention is that, for an SCF smaller than about 2.5, the SPW values (P_s^*) are probably larger than the SCF values, but for a SCF larger than 2.5 the SPW values are probably smaller than the SCF values, although this depends on the geometry.

The SPT criterion is suitable for any elastic-plastic calculation, giving unconservative values for a low SCF (less than 2), but more reasonable values for a large SCF (more than 2); however, SPW is always unconservative as far as the values for the collapse criteria used are concerned.

4.3.3 Comparison of K_2, K_2^*, K_3 and K_3^* Values for Nozzle Series N

In Fig. 46, the values of collapse pressure ratios K_3 (C5I and C15I) as well as the K_2 (SPT and SPW) values, and the SCF values based on von Mises' criterion for knuckle nozzles, are plotted against d/D_o (log scale), together with values based on the Tresca criterion for the SCF, and the K_2^* and K_3^* values, which last three are from Ref. [63] (flush nozzle).

The values from Ref. [63] show behaviour in which values for K_2^* are always smaller than those for K_3^*, and hence, in those cases, the design to prevent shakedown stops the structure collapsing.

The results obtained, for nozzle Series N, in the course of this work show, referring to Fig. 46, that:

(i) K_2 (SPW) is always larger than K_3 (C15I or C5I), and therefore full work-hardening will not be attained in any of the studied cases, since the collapse criterion must be satisfied,

(ii) for these particular structures, if d/D_o is less than .1 ($K_1 < 2.2$), the K_2 (SPW) value is limited by $K_2 = 1$.

(iii) the K_3 (C15I) values are larger than those for K_2 (SPT), for d/D_o larger than about .07 ($K_1 > 2$), hence, if minimum work-hardening is to

be attained in the cyclic settling down procedure, the structure must be designed against shakedown, although for d/D_o smaller than about .07, ($K_1 < 2$), the structure must be designed against collapse if the C15I criterion is used.

(iv) The K_3 (C5I) values are smaller than those for K_2 (SPT) for d/D_o smaller than about .2 ($K_1 < 3$), hence, the design must prevent collapse if the C5I criterion is used for collapse limiting; but for d/D_o larger than .2 ($K_1 > 3$), shakedown is the main criterion in design, if the SPT criterion is to be used.

In Fig. 46, the K_2 and K_3 values from the elastic-plastic computer program used for an elastic-perfectly plastic material are also plotted, and it can be seen that the difference between the values are minimal, with the values for K_2 (SPT) always slightly larger than or equal to, those for K_3 (C5I and C15I); hence the structure must be designed against collapse.

Considering the most suitable criteria for shakedown and collapse, the SPT (with or without work-hardening), and C5I criteria, respectively, may be chosen, as was done in Ref. [24], Appendix E; it may therefore be concluded from Fig. 46 that:

(a) If the SCF (von Mises') is larger than 3., the collapse pressure ratios K_3 are higher than the shakedown pressure ratios K_2;

(b) If the SCF (von Mises') is smaller than 3., the collapse pressure ratios K_3 are smaller than the shakedown pressure ratios K_2;

(c) If the SCF (von Mises') is smaller than about 2., that is, for case of d/D less than about .07, the shakedown pressure ratios, K_2 (SPT) are near 1., for those cases of work-hardening, but are rather lower (.87, case NIR) if work-hardening is neglected.

CHAPTER 5

DESCRIPTION OF MEASURING AND LOADING EQUIPMENT, TEST SPECIMENS AND TEST PROCEDURE

5.1 Introduction

The purpose of the tests carried out during the course of the present work was a better understanding of the mechanisms of shakedown since it was known that most of the materials commonly used in pressure vessel construction do either strain harden or soften in a cyclic process, Refs. [6] and [75]. This was known because of cyclic tests done under either stress or strain control. In reality, however, the load is usually the source of control, and hence the cyclic process will lie between neither - e and + e (strain control), nor - σ and + σ (stress control), but between either e_1 and e_2 or σ_1 and σ_2, with these limits changing with either the number of cycles, or the load limits, e.g. temperature changes. Cyclic behaviour is therefore difficult to comprehend and to define.

The cyclic loading for the tests was chosen between zero and a maximum.

Since one of the more commonly used materials for pressure vessel construction is mild steel, this material was chosen for the specimens. It is noteworthy to point out that mild steel is one of the few materials that perform cyclic strain softening for up to 10^3 cycles, Ref. [75].

In order to better understand the test procedure for shakedown study on the knuckle radial nozzle on a spherical pressure vessel, Fig.37, a test on a plate with a circular hole in the centre, Fig. 36, was carried out.

In the test of the circular plate with central hole, a Denison machine, and in the knuckle nozzle, an oil circuit, Fig. 47, were used for loading.

Strain measurements were made by using strain gauges with a Solartron Data logging system; the overall deflection was measured by means of a linear variable differential transformer (L.V.D.T.'s) displacement transducer.

5.2 Measuring and Loading Systems

5.2.1 Measuring Equipment

The strain gauges used in this work were made by the Tokyo Sokki Kenkyujo Co. Only one type was used, a wire with a 3 mm gauge length. They were made for registering up to 3% strain, and consisted of one element (Foil gauge, type FLA-3-11); because some of the gauges were to be attached to the inner surface of the cylinder, a quick drying adhesive was used. This was type CN, which dried in 1 min. There was one component only for this type of cement, which was supplied by the gauge manufacturer, and retained satisfactory properties at high-strains, Ref. [6]. The linearity of the gauges was not checked, because of economic reasons, but the manufacturer guaranteed linearity for up to 3% strain. The gauge factor was also not checked since the manufacturer guaranteed a constant value of 2.1 for a temperature range of $0^{\circ}C$ to $40^{\circ}C$ for the mild steel test object used by them, which was therefore of the same type of material as used for the specimens.

The internal strain gauges were coated with epoxy resin in order to prevent the oil from penetrating between the gauge and the pressure vessel surface. No water-proofing was necessary since a hydraulic oil (Shell, Tellus 27) with reasonably good insulating properties was used for pressurisation. The lead wires of the internal gauges were drawn through the cover flange in the cylinder by means of the sealing glands specially made for such a purpose by Conax Corp. (New York), Ref. [3]. The dummy strain gauges were attached to $\frac{1}{2}$", 1/4" and 1/8" thick mild steel plates, because of the different thicknesses of the specimen, Figs. 36 and 37.

A Solartron Data logging system was used for the measurement and recording of strain gauge resistance. This system allows up to 50 gauges to be scanned at a chosen rate per second, but this rate is limited by the recording method. Only 5 and 23 channels were used for the plate with central hole, and for the knuckle nozzle tests, respectively. The data logger contained fifty half-bridges and apex units; the out of balance bridge voltage could be recorded by means of a 14-column line printer, but only 8 columns were used and 2 channels per second chosen. Of the 23 channels used on the knuckle nozzle, one was for the deflection recording. Because the factor of the strain gauge was 2.1 for one active arm bridge, an excitation voltage of 1.9 volts was used, since direct readings of out of balance bridge voltages are approximately equal to the strain. The digital voltmeter had a resolution of 10μ V in the most sensitive range, and therefore gave a 10μ strain resolution. The absolute accuracy of the readings was $\pm$ 20 μV. Each set of readings was done by scanning the range of channels in use three times, which values were taken as average for the three values for each channel. If any of the values in each channel were out by 40 μV from the average values, then the reading for that particular channel was not used.

The overall deflection of the knuckle nozzle was measured on the cover flange on the cylinder by means of a linear variable differential transformer (L.V.D.T.'s) displacement transducer. The output from the transducer was measured by one of the channels on an S.E.Laboratories Ltd. Amplifier-Demodulator (S.E.905) with 3 kc/s 5V bridge excitation, which produced about 1 V D.C. output. The recording was taken using one of 23 channels of the data logger used in the knuckle nozzle test.

Internal pressure was measured with pressure gauges of Bourdon-tube type of 6" diameter, measuring up to 2000 lb in^{-2} in 100 lb in^{-2} divisions.

5.2.2 Loading Equipment

Plate with Central Hole, Fig. 36

The test with this plate was carried out in a tension and compression Denison machine (model T42B3), which provides variable load and speed. The procedure was to apply from 50 lb to each upper load limit, manually controlled, but with the exception of the first the cycles for each limit load were intended to all take about the same time, Section 5.4.1.

Knuckle Radial Nozzle on Sphere Pressure Vessel

Since the purpose of this test was not a fatigue but a shakedown investigation, few cycles of loading were to be applied, and so a manually controlled oil circuit was designed to satisfy the following requirements:

(i) variable load, and capability of maintaining any required pressure;

(ii) capability to begin and end each load cycle from and at zero. This requirement could not be satisfied unless the pump, at the end of each cycle, was turned off;

(iii) use of hydraulic oil with good insulating properties in order to prevent extra costs for the strain gauge insulation, and the potentially dangerous situation of bursting, if air were to have been used.

The oil circuit is shown in Fig. 47. The materials used in this circuit had been used by Blomfield, Refs. [6] and [60]. Pressure control was effected by means of a by-pass flow control relief value (1500 lb in^2). A relief valve set to the pump limit pressure was introduced between the pump and the tank. The pump was of a constant volume (2000 lb in^2) type. The internal pressure on the knuckle nozzle was measured directly from the pressure vessel.

5.3 Test Specimens

5.3.1 Plate with Central Hole

From a mild steel plate $\frac{1}{2}$" thick, the shape drawn in Fig. 36, with dimensions shown, was cut. The surface near the hole was finished in such a way as to facilitate strain gauge attachment. The positions of the gauges can be seen in Fig. 36. Gauges 1 and 3 were stuck on the inside of the hole, and therefore in an almost uniaxial state of stress. The results of the strain gauge readings are presented and discussed in Chapter 6.

The shape of the plate, Fig. 36, was chosen such as to have a small region of plasticity compared with the remaining elastic part, as this is the usual case with pressure vessels, but it was also desired that for higher levels of load the plasticity would spread on a large scale to other regions.

5.3.2 Knuckle of Cylindrical Nozzle on Spherical Pressure Vessel

Cheung, Ref. [3], tested tow knuckle radial nozzles on spherical geometries, the tests being of axial compression loading.

In order to carry out a test on a knuckle cylinder radial nozzle on a spherical geometry, it would have been necessary to obtain from outside the department the part for the sphere, since the other parts could be made in the departmental workshop. However, a spherical cap was available, which had been used in the thin cap experiment reported in Ref. [3]. It must be added that the size of the sphere was not ideal for a membrane region on the sphere adjacent to the junction region, Figs. 34 and 35, and had a high deformation towards the inside near the cylinder.

The original cylinder was cut off the sphere, as much as possible without damaging it and, because of the sphere's large deformation it was necessary to bring the shape back as near as possible to its original spherical form. Measurements were made on the inside and outside

surfaces in order to find the average radii of the least deformed region of the sphere. An inside 171/4" and outside 17½" radii were obtained. Two dies , female and male, were made from the largest available mild steel shaft, 10" diameter, with 17½" internal and 171/4" external radii, respectively. The dies were mounted on an Olsen Universal Testing Machine in order to apply a compression load. The sphere was placed centrally between the dies and left there for a period of time, the load having been increased; only at about 100,000 lb compression was the region near the hole on the sphere reshaped to a near smooth spherical surface. This structure with a near spherical shape was given heat treatment of 600°C lasting for three hours, in order to relieve the structure of residual stresses. No furnace with the needed dimensions was available that gave the 850°C required for the heat treatment of mild steel for a period of one hour. The structure proved to stay in its original shape, although, in its final form it did not have, as it did originally, a constant radius.

After all these processes the hole was enlarged to 4½" diameter in order to remove any welding deposits from the previous manufacturing process, Ref. [3].

A hot finish mild steel tube (B.S.3601) of 4½" outside diameter and 1/4" thickness was radially welded to the sphere; in the welding process mild steel filler rods (made by the British Oxygen Co.) complying to B.S.639(1952) were used. The welding preparation and final machining of the nozzle is shown in Fig. 37. This shape of knuckle was chosen in order to have a geometry as near as possible to the theoretical representation used in the computer program. In fact, current pressure vessel codes, Refs. [46], [47] and [68], specify minimum internal and external radii at the cylinder-sphere connections. Although that shape was more convenient for comparison with computed results, the maximum stress point would be some way from the welding zone.

Finally, another heat-treatment was applied to the finished structure, at 600°C, lasting for 2 hours, in order to relieve the structure from the welding and machining residual stresses.

New measurements of the internal and external surface radii were made in order to select a region of the sphere with a radius as near as possible constant; the variations of the average radii on the meridional plane were between 18" and 19". Fortunately, a relatively extensive region could be found with mean meridional radii of about $18\frac{1}{2}$" on the inside and $18\frac{3}{4}$" on the outside. The central meridional area of this region was prepared for the attachment of the strain gauges.

Another area, 90° away in the hoop direction, was also prepared for attaching some strain gauges, for comparison with readings from the corresponding gauges on the previous area.

The first strain gauges, therefore, on the chosen part of the structure, are referred to in Chapter 6 as follows:

X Y

where X stands for the position on the structure (A,B ... I, Fig. 37) and Y stands for measurement direction (M-meridional and C-circumferential); the strain gauges 90° away in the hoop direction are referred to as:

90 X Y

Only gauges on the positions C, E, F and I were chosen for comparison with those at 90°.

Position and direction of the strain gagues:

(i) A and I, about $4\frac{1}{4}$" along the mid-wall sphere surface in the axial plane from the knuckle sphere junction. The gauges were both meridional and circumferential, and external and internal respectively. A 90 IM gauge was attached for comparison.

(ii) D and E, about $2\frac{1}{2}$" from the knuckle-cylinder junction, the length being along the axial plane. Both gauges were circumferential only, and external and internal respectively. A 90 EC gauge was attached for comparison.

(iii) B on the outside surface just near the knuckle-sphere junction, about 1 mm away in the direction of the knuckle, meridional and circumferential.

(iv) C on the outside surface, near the knuckle-cylinder junction, about 1 mm away from the knuckle, meridional and circumferential. Gauges 90 C (M and C) were attached for comparison.

(v) F on the inside, on the knuckle-cylinder junction, meridional and circumferential; gauges 90 F for both directions were attached.

(vi) G on the inside, about 7 mm from the knuckle-cylinder junction on the knuckle (about halfway from the knuckle cylinder and sphere junctions), meridional and circumferential.

(vii) H on the inside, on the knuckle-sphere junction, meridional and circumferential.

5.4 Test Procedure

Before each test, the electrical system would be left on for 24 hours; it was never switched off either during each load test or between them.

The loading systems, Denison Machine and oil circuit, Fig. 47, would be switched on for at least one hour before the start of each day's testing.

5.4.1 Plate with Central Hole

This test was carried out in order to find out the general trend a shakedown experimental study would follow.

The procedure of this test was as follows:

(i) The test began by cycling in the elastic range from zero to a load that would give a maximum strain of about .05% on gauge 1 (the other gauges registered lower values), Fig. 36. In less than 10 cycles the initial and final values of the data logger would be about the same. Scanning of zero and at various load increments was done.

(ii) The load was increased in steps till a strain of .099% on gauge 1 was registered, Fig. 36, with the data logger being scanned at that load. The load was then left at its maximum for about 10 mins., during which no major changes in strain readings were recorded. The load was relieved in stages, with scanning carried out during this process.

(iii) Cycles from zero to the same maximum load as in (ii), and returning to zero, were done, with scanning at each load step. No major changes were recorded for 10 cycles.

(iv) The maximum load was increased by about 20% of the load in (ii). The load incrementally increased and decreased up to its maximum, with scanning of the data logger at each load step. The maximum load was then left at that level to allow creeping of the structure, and decreased when no major change on the data logger recording was seen during about 5 mins.

(v) Cycles from zero to the maximum load in (iv), returning to zero, were done, with scanning at each load step. When the width of the load-strain cycles was stable, the initial and final strain readings over 10 cycles were compared; if no major changes were found in the initial and final strain gauge readings over 10 cycles, the process was restarted as in (iv).

It was found for loads of between 1 and 2.36 x the load in (ii) the strain gauge readings would stabilise in width, and that initial-final readings would show no major change after 10 but before 20 cycles;

however, for loads larger than 2.5 x the load in (ii), the process of stabilisation of strain-gauge readings would require a higher number of cycles.

When stabilisation occurred within the first 20 cycles, the process was restarted from (iv), but when this did not happen, the process would be carried on for larger numbers of cycles.

5.4.2 Knuckle of Cylindrical Nozzle on Spherical Pressure Vessel

The procedure in this test was similar to that described in Section 5.4.1, i.e. the plate with central hole, but with these differences:

The elastic-plastic computer results were known and therefore for a chosen limit of linear elasticity of the material, an initial estimate of the pressure to first yield could be made, since

$$\sigma_y = 29.2 \text{ ksi} \quad \text{implies} \quad P_y = 250 \text{ lb in}^2$$

From hereon, the load in (i) (Section 5.4.1) was chosen as 200 lb in^2. The stabilisation of initial and final strain gauge values was again obtained after about 15 cycles.

The load increment up to 600 lb in^2 was selected as 100 lb in^2, since the divisions on the gauge pressure dial were of that amount. From 600 lb in^2 the load increment had to be taken at steps smaller than 100 lb in^2 since otherwise the deformation would be too large and less information would be available (see Chapter 6 for values of increments).

The number of cycles taken up by pressures smaller than 675 lb in^2 was about 20, but from thereon the number was chosen while the loading process was going on. In case of doubt about the correct interpretation of results the number of cycles would be increased.

The scanning of the data logger was generally done for the first five cycles, for the eight and tenth cycles, and later for each fifth or each tenth cycle, depending on the number of cycles already performed.

CHAPTER 6

ELASTIC-PLASTIC COMPUTED AND TEST RESULTS; DISCUSSION

6.1 Introduction

In Chapter 5, the measuring and loading equipment, the specimens and the test procedures, are described.

Very little experimental work on the shakedown behaviour of pressure vessels has been reported. As far as the author is aware, only Procter and Flinders, Ref. [59], have reported shakedown investigations on partial penetration welded nozzles in a spherical pressure vessel, and Findlay et al, Ref. [56], have reported limit-pressure and shakedown investigations on torispherical drum head pressure vessels; they have let creep take place in the first half-cycle of the cyclic process for each particular maximum load. In these works, there is a tendency to avoid the creeping of the material during a shakedown investigation; when creep does occur, the number of cycles has never exceeded 20, in Ref. [56], and 8, in Ref. [59]. It will be recalled that Findlay et al, Ref. [56], used mild steel. As mild steel is a work-softening material, Ref. [75], a stable value for the residual strains should not be expected, but rather a decrease, approaching zero, of the strain increment in each cycle compared to previous cycles. It is possible that only after 10^3 cycles, Ref. [75], would a stable residual strain be obtained. Of course the number of cycles needed for the stabilisation of residual strain in an overall load control test is dependent on the high strain level as well as on the membrane strain level, since the shakedown is dependent on the material and the shape of the structure.

In this chapter the result for each test is presented, analysed and discussed.

6.2 Plate with Central Hole

The plate geometry is shown in Fig. 36, as well as the positions of the strain gauges. A plot of the strain gauge readings against load can be seen in Figs. 48 to 51 for gauges 4-5, 2, 1 and 3 respectively.

As may naturally be expected, gauge 1 shows the highest strain value. The yield of the plate begins at about 24 klb for a strain of about .098%, which for a Young's modulus of about 29 ksi, gives an elastic limit of about 28.5 ksi. This value is probably low when compared with the value from a tensile test, but it must be borne in mind that about 15 cycles were accomplished in the elastic range for 20 klb, and 20 at about 24 klb, from which it may be concluded that the yield stress limit decreases as a consequence of the mild steel work-softening.

An examination of Fig. 48 reveals that the redistribution of stresses due to the cyclic process can in certain circumstances cause a reduction of strain, as well as an increase.

It can be seen from Figs. 48-51 that creep can stabilise during the first cycle, in about half to three-quarters of an hour (load cycles 64 klb and 68.7 klb); however when the cycle pressure begins, but with a stoppage for the purposes of scanning of about one minute in each load step, some creep can again take place, the occurrence of which can probably be accounted for by the biaxiality of the plastic deformation. This biaxiality effect begins to show itself at 64 klb, at which point gauge 3, Fig. 51, shows a slight reversal of straining. From the fact that this happens, an important point can be made.

Let gauges 1 and 2, Figs. 50 and 49 respectively, be assumed to be broken; one might therefore be led into error from Fig. 51, since one could say that the shakedown limit had not yet been reached. However, since gauges 1 and 2 did not break the following conclusion can be made:

If the cyclic strain measurements on a yielded region show a decrease in its equivalent value for one or more positions on the structure, and the other measurements do not reveal a reason for this, then some important point or points on the structure are not being examined in the measured locations and hence the interpretation of the results can be misleading.

In Figs. 49-51, it is shown that the maximum shakedown load lies between 57 klb and 64 klb. Taking the minimum value of 57 klb, a shakedown ratio (L/Ly) of 2.37, i.e. ellipse expanding by 18% is used in the cyclic shakedown process.

Analysing Fig. 50, gauge 1, in the last cyclic load process performed in the course of this test, an increase in the plastic strain is recorded up to the tenth cycle; after that the strain value starts to decrease because of a process of reverse yielding due to the biaxiality of the deformation, which process is demonstrated in Fig. 51. This phenomenon commences with the start of visible plastic flow in those regions marked with AA in Fig. 36. This was observed during the course of the test. An alternative explanation may be shown by means of the plastic flow of Sections BB, Fig. 36, as seen in Fig. 49 for gauge 2.

The strain gauge readings of position 1, Fig. 36, are tabulated for the 1st to 5th, 8th, 10th, 20th, 25th and 35th cycles in order to analyse quantitatively the cyclic settling-down of the structure:

(a) Up to 1.99 X first yield load, the settling process was reached in the first 10 cycles but, between 1.99 X and 2.37 X, the settling process was only reached in the first 20 cycles.

(b) For loads of about 2.66 X first yield load, the settle down process is certainly taking place, but a number of cycles greater than 25 will be necessary. In this stage reversal of straining was detected

in the region of gauges 3-5. (This should not be confused with reverse yielding but should rather be interpreted as an effect of the redistribution of stresses due to the cyclic process with the increase of local plastic flow towards gross yield in Sections BB, Fig. 36.).

(c) For the maximum cyclicly tested load (68.7 klb), reverse yield occurred after the 10th cycle, during which cycle a second type of creep behaviour manifested itself in the region of gauges 3-5. This load must be considered larger than that for an upper limit of shakedown since reverse yield is out of the question according to Melan's theorem, Ref. [54], although the strain reading had shown that the strain increment had a tendency to decrease, which is indicative of the settling down process.

From this analysis it is possible to draw three conclusions regarding shakedown behaviour:

(i) The shakedown in the early stages of straining of the structure is of a static character, since, within the first 20 cycles, shakedown can be defined. This shakedown is of local yield character, and is limited mainly by the location of the elastic regions of the structure.

(ii) When the local yield begins to grow, but is still controlled by the remaining elastic parts of the structure, it is possible to define a shakedown load for a number of cycles greater than 20. This type of shakedown may be defined as semi-static as this will only be possible if other parts of the structure can limit the local yield plastic growth.

(iii) When the yield is of gross type, then the reverse yielding can take place as a consequence of the biaxial character of the straining, and a load to settled-down behaviour can only be defined if the material is of the settling-down type; the strain gauge readings must therefore show a stabilisation tendency, and if this is so, it will be

possible to define a residual stress system which, together with the stress load system, will be within an expanded and settled ellipse of yield.

6.3 Knuckle of Cylindrical Nozzle on Spherical Pressure Vessel

This geometry, with its strain gauge positions, is described in Section 5.3.2 and is shown in Fig. 37.

The elastic results are presented and discussed in Section 3.4.2 and are shown in Figs. 34 and 35 for 250 lb.in^2 internal pressure.

The strain gauge readings and strain values from the elastic-plastic computer program are plotted against internal pressure values in Figs. 52 to 59. The overall axial deflection is plotted, in Fig. 60, against internal pressure, and also in Fig. 61, but there versus ratios of pressure to first yield pressure together with the overall deflection values from the elastic-plastic calculations.

Some of the readings from gauge FC, Fig. 37, which in fact gave the maximum strain readings, are shown in Table 14. Collapse and shake-down pressure ratios (P_c^*, P_s^*, K_3, K_2, K_3^* and K_2^*) can be seen in Tables 8 and 9 respectively.

The elastic-plastic calculations were carried out well before the tests were carried out, using data for a nominal equivalent stress-plastic strain curve of either 29.3 $(1 + 133\ \bar{e}_p^{.269})$ (ksi), which is not intended to represent either a settled cyclic, or a static, curve for the used mild steel from which the test specimens were constructed, for the work-hardening case, or 33.(ksi) proof stress for .2% strain for the non-work-hardening case, as representing mild steel material. However the equivalent stress-strain curves, either static or settled cyclic, were not known for the particular materials used in the construction. It should be noted that the sphere and the cylinder were made from different pieces of mild steel, and that the welding effect was not taken into account in the computations.

6.3.1 The Test Results

Figs. 52 to 57 show the effect of the structure being not quite symmetric, as pointed out in Section 5.3.2. The differences in length are larger in the meridional direction than in the circumferential, Fig. 57, which would appear to be logical because of the small radius used in the knuckle region.

The redistribution of strains, in those regions of the sphere and the cylinder away from the junction, which redistribution is due to the cyclic loading process, can be seen in Figs. 52 to 54.

Results for the cyclic process up to 500 lb in^2, internal pressure, are not presented in detail, as it was realised that, the strains values having settled down in less than 20 cycles, the structure is considered as having shaken-down.

It may be concluded from Fig. 60 that the structure has, in its overall behaviour, shaken-down for pressures of up to 815 lb in^2 due to the fact that the overall deflection indicates a settling down behaviour. Cycles at 900 lb in^2 were not performed because of over-deformation of the ring base of the sphere, Fig. 37. Since the von Mises stress concentration factor of about 2.92, Table 7, was obtained in relation to a membrane sphere, for some internal pressure less than 810 lb in^2, a behaviour similar to the test plate, (Section 6.2 and Fig. 50, at about 64 klb), was expected since, in the case of the plate the local yield starts to spread across Sections BB. However, in the vessel case the local yield which was expected to spread freely to the membrane areas of the sphere is limited by the fact that the sphere was clamped to its base ring. Hence the deformation of the membrane sphere was restricted; the straining of critical areas was not only controlled by the cylinder, still being elastic, Fig. 52, but by the sphere not being free to deform.

From Fig. 61 a comparison between the overall measured deflection and the calculated deflection can be made; for pressure ratios (P*) less than 1.5 the agreement is not as good as for pressure ratios larger than this figure. Once again the better approximation to the stress-strain curve of the material, the better will be the approximation obtained from the elastic-plastic computer program. Differences for pressure ratios higher than 2.2 can be accounted for by the fact that the computer program uses the initial geometry for the calculation.

(a) From Fig. 57, the movement of the internal stress path on a biaxial plane around the yield ellipse, described in Chapter 4, Section 4.3.1, may be visualised, since the meridional strain readings from gauges FM and 90 FM register a small initial increase with later a larger increase and then show a decrease in strain readings for higher loads. The initial increase can be identified with the first anticlockwise movement of small extent around the ellipse, as shown in Fig. 16. The second, larger, increase probably corresponds to the clockwise movement around the ellipse, of larger extent than the first anticlockwise movement, Fig. 16. The decrease in strain reading for higher loads can be identified with the last anticlockwise movement around the ellipse, Fig. 16 (see Section 4.3.1.).

(b) As shown in Figs. 55 and 58, gauges 90CC and CC, respectively, register a reversal of straining (see Section 6.2, (b)) for 675 lb in^2 internal pressure, due to the redistribution of stresses in the local yielded region caused by the cyclic loading process. This behaviour is probably different in origin from that described in Section 6.2 (b) because in this case there is a cross-sectional effect at the local yielded region, whereas in the case of the plate it is due to the start of gross yielding in Sections BB, Fig. 36, and which is therefore not as localised.

(c) Fig. 58 shows the strain reading from gauge CC; this registers a reverse yielding at 715 lb in^2 internal pressure, although none of the strain readings demonstrated the incremental behaviour shown for the test plate in Figs. 49 and 50; it was therefore concluded that a point, or points, of importance, on the structure had not been considered for strain measurement readings, since Fig. 53 shows that yielding in some areas of the sphere has probably been reached. This line of reasoning concurs with that in Section 6.2 for gauge 3 on the test plate, Fig. 36, for 64 klb. Accordingly, since the strain gauge readings have shown a settling down behaviour for a number of cycles larger than 20, and because no membrane yielding has been reached, it may be concluded that a settling-down behaviour has been attained. This is probably different of shakedown behaviour because reverse yielding has been recorded.

The same reasoning can be applied to loading cycles of 770 and 815 lb in^2 internal pressure; no last stage as in the test plate for 68.7 klb, was obtained, probably because of the deformation restraint or because no cyclic loading was possible at 900 lb in^2 internal pressure since the sealing on the base ring of the sphere, Fig. 37, had broken, due to excessive twist deformation on the ring.

The conclusions reached here are more complicated than in the case of the test plate in which the strain gauges, 1 and 3, Fig. 36, gave readings of near uni-axial strain by virtue of their position; in the present case, however, the situation is that of biaxial straining.

From Table 14 for gauge FC, the following conclusions may be arrived at:

(i) Up to 675 lb in^2 internal pressure, a near stable behaviour is obtained within the first 20 cycles, hence this is a static shakedown, as in Section 6.2 (i).

(ii) At about 715 lb in^2 internal pressure, a near stable behaviour is obtained for a number of cycles larger than 20, hence this is a semi-static shakedown, as in Section 6.2 (ii).

(iii) For internal pressures larger than 770 lb in^2, there is a tendency to settle down, but more than 50 cycles are necessary. Gross yield on the sphere, Figs. 53 and 54, is obtained, and hence this is a gross yield settle down behaviour, although controlled by the nozzle, which is still in the elastic range, Fig. 52. This type of settle down, although dependent on the ability of the material to settle down, does not show the large incremental straining as in the case of the test plate, Figs. 50 and 51, due either to the restraint deformation by the base ring of the sphere, Fig. 37, or the possibility that incremental straining was not detected, or both.

Comparing the test values registered by all the gauges, (see (b)), with the particular values registered by gauge FC, which gave the maximum reading, (see (i)), for static shakedown, that is settle down within the first 20 cycles, it can be seen that values 675 lb in^2 are obtained, but in (b) a reversal of yielding was recorded. It therefore seems logical to take the limit for static shakedown as an average value of 600 lb in^2 and 675 lb in^2 internal pressure. Hence 637 lb in^2 internal pressure will be taken hereafter on the static shakedown limit for this particular structure.

6.3.2 Comparison of the Results from the Test and the Elastic-Plastic Computer Program

In Figs. 52 to 59 and 61 the strain and deflection curves, respectively, from the elastic-plastic calculation with work-hardening and elastic-perfectly plastic materials information, are plotted and demonstrate that the general agreement is reasonable.

Collapse and shakedown pressure ratios (P_c^*, P_s^*, K_2 and K_3) are listed in Tables 8 and 9, respectively; the values were obtained by the application of the criteria described in Sections 2.3.2 and 2.2.3 respectively.

Collapse Pressure Ratios

The collapse pressure ratios (P_c^*, K_3 and K_3^*) can be compared in Table 8.

The collapse pressure ratios, P_c^*, from the elastic-plastic calculation with work-hardening and elastic-perfectly plastic materials are within - 10% to 20%, and $\pm$ 20% respectively, compared with values obtained from the strain gauge reading curves.

It is particularly noteworthy to see the good agreement between the values for the C5I criterion, especially for the elastic-perfectly plastic material (σ_y = 33 ksi, .2% proof stress), and the 5% difference for the work-hardening case, when compared with the values from the test. The values for the C15I criteria present a difference of - 15% for the elastic-perfectly plastic, and - 7% for the work-hardening, cases when compared with the values from the test.

The C3I criterion yields values with very good agreement, but the C3 criteria are, once again, comparatively conservative.

The CSP criterion, from the test results, cannot be precisely defined, as can be seen from Fig. 57, but can be taken as lying between 2.45 and 2.6 (XP_y). Taking the average value, 2.52, it may be concluded that the values obtained using the elastic-plastic computer program with work-hardening and elastic-perfectly plastic materials are about 15% and 20% smaller, respectively, than the average values from the test.

The collapse pressure ratios to the membrane yield pressure, K_3, were obtained by using the C5I and C15I criteria; K_3^* was obtained from Ref. [63] and was based on the Tresca criterion with limit analysis from Ref. [33].

The K_3^* value is in any case smaller than K_3, and is also smaller than K_3 from the test readings, by 10% for the C5I, and 28% for the C15I criteria, when compared with values from the test data.

The K_3 value obtained using the C5I and C15I criteria, when compared with the results from the computer calculations, are smaller than the values from the strain gauge readings by 4%, 17% and 8%, 22% for the work-hardening and elastic-perfectly plastic material cases respectively, for the C5I, C15I, criteria.

Shakedown Pressure Ratios

Value P_s^* from Ref. [63] is equal to the value obtained by the application of criterion SEM, from Ref. [12], to the case of the cylinder and sphere junction with the knuckle (see Section 2.2.3).

The P_s^* value from the use of the SPC and SPT criteria for the work-hardening case are about 6% lower than the SEM value, but for the elastic-perfectly plastic case, the shakedown value is some 15% less.

The application of criterion SPW, hence allowing the yield ellipse to expand with work-hardening from the loading process, gives two values for the shakedown pressure ratios, lower and upper limits. This geometry was the first that the author came across with such shakedown behaviour. The reason for this is the small amount of work-hardening used up to a relatively large load (2.5 of first yield pressure). The lower limit is defined before the last anticlockwise movement around the ellipse has begun, but just before the turning point on the stress path where the structure would have shaken down again, up to about 2.45 X first yield pressure, from which the structure would not, from a theoretical point

of view, shakedown again for the work-hardening used. In the loading process it should be recalled that this particular geometry was not a realistic structure since the membrane deformation on the sphere was restrained by the ring and plate base, Fig. 37; this is probably the reason for the small amount of work-hardening used in the loading process.

The lower limit is some 3.5% higher than the limit of 2, from the hypothesis of the moving ellipse of yield, but is some 10% higher than the values obtained from the application of the SPC and SPT criteria.

The upper limit is some 22% higher than the limit 2., of the moving ellipse of yield criteria, but is about 30% higher than the values obtained using the SPC and SPT criteria.

The upper limit, P_s^*, obtained for the SPW criterion with the computer results is some 6% larger than the average value obtained from the test data for the static shakedown (Section 6.3.1, last paragraph), but the computed lower limit is some 10% lower than the test knuckle (static shakedown).

The shakedown pressure ratios to the membrane yield pressure, K_2, obtained from the calculations with the SPT criterion are smaller than K_2^*, from Ref. [63], but with the SPW criterion are larger than K_2^*. The differences are about 7% and 18% for the SPT criterion with work-hardening and elastic-perfectly plastic cases respectively, and almost the same for the lower limit of the SPW criterion, but about 18% higher for the upper limit.

It is particularly noteworthy that the K_2 values obtained from the experimental criterion, of settling down in the first 20 cycles (Section 6.3.1, last paragraph), gives an upper limit close to the upper limit obtained from the calculation with SPW criterion, in which work-hardening is permitted. The difference is about 4%.

Since from the test results an average value of 2.31, for P_s^*, was obtained it can be said that the settled down yield surface has expanded by at least 16% and hence at least about 16% of work-hardening was used for the experimental static shakedown behaviour. The reasoning is by no means correct, since the stress path has a movement around a settled ellipse of yield, as with an elastic-perfectly plastic material, the shakedown limit being $2.(XP_y)$, the values are in most of the cases below 2., but it defines a lower limit for expansion of a settled yield ellipse. Using the same reasoning, for the results from the computer program, work-hardening case, it can be realised that a 22% expansion is obtained with the upper bound ($P_s^* = 2.45$, Table 9) from the SPW criterion, but in fact the computer results show a 30% expansion. For the lower bound ($P_s^* = 2.07$, Table 9), a 3.5% expansion is obtained using that line of reasoning, but in fact the computer results show an 11% expansion.

It should be noted that from the test plate readings an 18% expansion of the settled down yield surface was obtained, which compared with 16% for the test discussed in this section. This allows an approximation of the permissible work-hardening of a settled ellipse of yield, for mild steel, of 17%. Of course the value cannot be accepted as definitive for mild steel; a more extensive study is necessary.

If the 17% expansion of the settled down yield ellipse is introduced in the SPT criterion, a value of 2.18 for P_s^* is obtained, which improves the shakedown pressure ratio, P_s^*, by 15% when compared with the simple value for SPT (moving the yield ellipse) criterion. The shakedown pressure ratio to membrane yield pressure, hence, has a value of .68, which is 14% less than the value from the test results. These values, 2.18 and .68, have not been included in Table 9, since the figure of 17% for the expansion, as understood by the author, is not intended as an exact value, as above mentioned.

6.3.3 Comparison of Collapse and Shakedown Pressure Ratios (K_3 and K_2)

A final conclusion is arrived at in Chapter 7, but here some interim comments are made.

From the calculations, once again, as in the Series N nozzles in Chapter 4, Fig. 46, the upper limit of K_2 (SPW) is larger than K_3 (C5I, C15I), but from the experiment the opposite situation is found for the C15I value, and the same situation (i.e. larger) for the C5I criterion.

If the C5I criterion is chosen as the criterion to design against collapse, then, in this case the design will be limited by the shakedown criterion if SPT or the lower limit for SPW are used, but the opposite is true for the upper limit for the SPW criterion.

The C5I criterion seems sensible and reliable, but C15I although it appears, in the theoretical calculations, safe, in the experiment it is unreliable as far as a static shakedown is concerned. This C15I criterion shows a marked creep deformation, hence precautions during design against creep should be considered by the designer.

If the C3I criterion is used in the design to help prevent collapse, it is possible that no precautions against shakedown need to be considered, unless an elastic-perfectly plastic case is being studied.

CHAPTER 7

CONCLUSIONS AND RECOMMENDATIONS FOR FUTURE WORK

7.1 Conclusions

7.1.1 Elastic Results

Heads:

For hemispherical heads the stress concentration factor depends solely on the cylinder-sphere thickness ratio. For this geometry, the minimum stress concentration factor, based on the von Mises criterion, is found when the thickness ratio (t/T) is between 1.5 and 1.75, Fig. 18. A similar line of reasoning can be made for other spherical heads.

The approximation to the Kelvin functions (Appendix B) gives for spherical heads(caps) with $\theta_o(d/D)$,(3.5), near $\pi/2$, a better approximation than the exponential solution (Appendix B), for cylinder-sphere thickness ratios equal to or larger than 1., but a poor approximation for t/T equal to or less than .5. There are values for t/T between .5 and 1., for which both solutions give the same results. A comparison with the solutions obtained for the solid plate (Appendix B) indicates that even the best of the above-mentioned solutions should not be used for some values of $\theta_o(d/D)$ near $\pi/2$; values of $\theta_o(d/D)$ from which the plate yields to better solutions than the other two (Appendix B) are defined in Figs. 19-21, for t/T = .25, .5 and 1., respectively, and are associated with points marked on these figures by A^i ($i = ', '', ''', ^{IV}$) for some values of d/t (= 10., 20., 40., 80., respectively). In the text (Section 3.2.3), the value of θ_o is represented by $\theta_A i$. This paragraph can be shown schematically, thus:

$$\theta_o(d/D)[\text{plate solution}] > \theta_A i > \theta_o(d/D)\begin{cases} t/T \leq .5, \text{ exponential solution} \\ t/T \geq 1., \text{ approximation to Kelvin function solution} \end{cases}$$

($.5 < t/T < 1.$ was not considered in this study)

These conclusions were arrived at by comparing the results obtained from the exponential, the approximation to the Kelvin function, and solid plate solutions (Appendix B), with the results from the elastic computer program (PVA1) used in the course of this work, for stress concentration factors based on von Mises' criterion.

When a knuckle is introduced into a spherical head, for it to become a torispherical head, the improvement gained for the stress concentration factors based on von Mises' criterion is not as large as might be expected for some geometries of h/d larger than .25 (torispherical); however, research into the question of whether or not a geometry with a knuckle is a significantly better design with regard to economic factors, is recommended.

Nozzles:

Flush Cylindrical Nozzles:

For the geometries considered in this work, it is concluded that Leckie's method, Refs [13] to [16] would yield better results for the maximum stress concentration factors, for all geometries, based on von Mises' criterion, than the solutions presented in Appendix B (exponential solution (B.36.2)and approximation to Kelvin function solution (B.37.2) with (B.18)), the elastic computer program results being used as the basis for the comparison.

The presentation of a single graph with averaged curves for each value of the cylinder-sphere thickness ratio (t/T), would cause considerable errors, so accordingly, the author has preferred to present graphs for single values of t/T, for the stress concentration factors based on the von Mises criterion.

Series C Nozzles:

The band O'Connell modification (which allows the forces at a "square corner" intersection to be distributed as bands of loading over a finite width of shell, equal say to the thickness of the shell wall plus a fillet weld, rather than the point or line load of conventional shell theory) will give unrealistic values unless an optimum size of band width is selected.

Small differences in the detailed junction geometry of a continuous nozzle-sphere do not significantly alter the elastic stress concentration factor, although large knuckle radii do give lower values.

Test Knuckle Nozzle

The stress concentration factor based on the von Mises criterion, from the elastic computer program, is 11% larger than the value obtained from the test, which indicates that the computer program gave a reasonable approximation, especially in view of the fact that the knuckle radius was small. This agreement is perhaps as good as it is only because of the described irregularities of the geometry.

The strains predicted by the elastic computer program at the most differ by 18% from the strain readings Figs. 34 and 35, hence these results are not so good as those obtained for the stress concentration factor; the weld effect is not considered in the 18%.

7.1.2 Elastic-Plastic Results

The elastic-plastic strains predicted by the elastic-plastic computer program are, in both cases, for elastic-perfectly plastic and for work-hardening materials (nominal curves, Section 6.3), in reasonable agreement with the test nozzle results; the work-hardening (either (static or cyclic settled work softening) curves were, however, not known for the mild steel used, and the proof stress was obtained for a .2% strain from the nominal curve used in this case.

It is particularly important to use a proper representation of the material behaviour in the computer program, if the elastic-plastic behaviour of the structure is to be correctly predicted, as can be seen from the results for head A, Ref. [7].

Intuitively, it would seem proper to use a static equivalent stress-plastic strain curve for a study of collapse, since a static elastic-plastic deformation is involved in the collapse behaviour; however, for a cyclic elastic-plastic deformation study, an equivalent stress-plastic strain settled cyclic curve will probably give a better prediction for the shakedown behaviour, as may be concluded from a study of Section (6.3.2) Some other comments will be made on the shakedown behaviour from the elastic-plastic computer program in Section 7.1.4.

7.1.3 Collapse Criteria

One of the initial ideas was the intention of presenting, from the computed results, and comparing them with some available experimental data, a collapse criterion that would satisfy any of the geometries studied in the course of this work; however this was found to be impossible (in the following paragraphs the assumption that K_3 cannot be larger than 1. is made throughout), as:

(a) The C3 criterion has safe characteristics for the whole range of geometries studied, except that for a geometry with elastic stress concentration factors (von Mises' criterion) higher than about 2.2, the collapse pressure ratios are very conservative ($K_3 \ll 1$).

(b) The C5 criteria have safe characteristics for geometries with stress concentration factors (von Mises') larger than about 1.75; however, for cases with stress concentration factors lower than about that value, these criteria have unconservative($K_3 > 1$) characteristics.

(c) The C15 criteria not only gives highly unconservative ($K_3 > 1$) collapse pressure ratios for stress concentration factors (von Mises') lower than about 2., but also has the defect that design against creep, even at room temperature, must be considered.

(d) The BSLY criterion, although giving reasonable results for collapse pressure ratios, for head geometries, is a subjective criterion.

(e) The CMEO criterion, for head geometries, being a direct application of the definition of collapse, gives unconservative ($K_3 > 1$) values.

(f) The CSP criterion, for nozzle geometries, gives reasonable values for stress concentration factors larger than about 1.75, but brings with it the necessity of plotting stress paths.

From the foregoing paragraphs, it may be concluded that the C5I criterion is very useful for stress concentration factors (von Mises') larger than about 1.75, since it can be used in the course of the pressure vessel test under consideration, although the correct positions for fixing the strain gauge must be known beforehand. For cases of stress concentration factors (von Mises') lower than about 1.75, the C3I or C3D criterion is probably more suitable.

7.1.4 Shakedown Criteria

Conclusions regarding shakedown behaviour were reached with greater difficulty than those for collapse, since the static and cyclic settled equivalent stress-strain curves were not known, and because a cyclic process is involved, which cannot be described by the incremental theory of plasticity used here for the elastic-plastic computations.

There are two main questions to be answered in any theoretical shakedown study:

(i) which curve should the elastic-plastic computer program be fitted with?

(ii) which shakedown criterion for permissible elastic unloading should be used?

There are, of course, other questions e.g. the effect of change in geometry, which stress path should be followed in the unloading process, and many others, which will influence the shakedown behaviour of the structure.

Since a cyclic process is involved in shakedown behaviour, it seems logical that the elastic-plastic computer program used in the course of the present work should be fitted with a curve such that:

(a) if the material is of settled cyclic work-hardening type, a settled cyclic equivalent stress-strain curve should probably be used; however a static curve would give conservative results;

(b) if the material cyclically neither work-hardens nor work-softens, the only possible approximation to a work-hardening case is the static equivalent stress-strain curve;

(c) if the material is of settled cyclic work-softening type, a settled cyclic curve is probably better than a static curve, although the latter will probably give unconservative results.

It is, therefore, highly probable that the elastic-plastic computer program should be fitted with a settled cyclic equivalent stress-strain curve for a study of shakedown.

Once the elastic-plastic results are available from a computer program, the other main question is which shakedown criterion is more

suitable for consideration as permitting elastic unloading of the structure?

The SPW criterion (full expansion of the ellipse of yield with the loading process) is probably too ambitious, as may be concluded from the shape of some available stress-strain curves obtained (in previous works) in the process of defining a settled cyclic equivalent stress-strain curve; however, in any structure, the stress limits on a cyclic process are not $\pm \sigma$, but some values σ_1 and σ_2 in which σ_1 is probably larger than $-\sigma$ and $\sigma_2 = \sigma$, although σ_1 and σ_2 change with the cyclic process until stable values are obtained and hence the cyclic strain amplitude will be smaller in the structure than in the test piece, and the reversal of yielding will either be of small extent or probably zero; the results obtained, therefore, from the application of the SPW criterion are probably not conservative, unless there is zero reverse yielding.

The SPT criterion (moving the ellipse of yield towards the stress state reached) is very reasonable, although, from inspection of some available data, it is highly probable that the ellipse of yield defined from the settled cyclic equivalent stress-strain curve will expand by an unknown amount depending on the strain level; it seems probable from these considerations, as well as from the test results, that this criterion (SPT), with defined expansion for the settled cyclic ellipse of yield, is so far the most correct shakedown criterion described. Unfortunately the author is not in a position to present the reader with any values derived from the use of this criterion, although an estimated value was used, in Chapter 6 (17% for mild steel), for the expansion of the ellipse of yield used in the calculation.

The SPC criterion is nearly the same as the SPT, except that the movement of the ellipse of yield is in the direction defined by the linear elastic path. The SPC criterion gives slightly lower values than the SPT.

If an elastic-perfectly plastic material is under study, the results are conservative or unconservative depending on the level of the chosen proof stress; however the shakedown pressure ratios (P_s^* and K_2) are underestimated for the cases of low stress concentration factors (von Mises'), when compared to values from the SPT criterion (non-expansion of the yield ellipse).

7.1.5 Final Conclusions

Small differences in the detailed geometry of continuous nozzle-sphere connections do not significantly alter the elastic stress concentration factors, or the shakedown and collapse loads of the vessel, despite the junction being at the region of highest stress in the vessel. The agreement obtained between the elastic-plastic computer program and experimental strain results makes possible elastic-plastic shell theory calculations with some assurance that the results can be applied usefully to real vessels even if only the nominal details of the shape of the junction are known.

In a shakedown behaviour study which takes into account the effect of the settled cyclic behaviour of the material (i.e. work-hardening according to a settled cyclic behaviour, which may be harder or softer than the static curve), the assumption of a moving ellipse must be made. Because the real size of the moving ellipe is not initially known, the ellipse that should be used is the settled ellipse of yield (i.e. the settled value of first yield).

In the collapse pressure ratio calculations, a unique value was not found, at least not for .5% and 1.5% level of strains.

From the various collapse criteria examined for incipient collapse, the C5I criterion (.5% maximum outside the strain), and either the C3I or C3D criteria, were chosen as suitable for geometries with elastic stress concentration factors (von Mises') larger than about 2., and lower than about 2., respectively.

A comparison of collapse pressure ratios K_3 (based on the C5I, C3I and C3D criteria), with shakedown pressure ratios K_2 (based on the SPT criterion, moving the ellipse of yield), leads to the conclusion that for elastic stress concentration factors (von Mises') below about 2.5, incipient collapse occurs before shakedown. The broad trends of previous calculations based on elastic stress distributions, and on the limit load concept, are confirmed, although the elastic-plastic computations show rather lower collapse loads for nozzles with low stress concentration factors if work-hardening is neglected.

It was realised that the settling down process of the structure deformation could be divided into three main, not mutually inclusive, types, making the assumption that time has been allowed to let the structure to creep in the first half cycle:

(a) Static shakedown, which depends only on the local yield, but is generally limited by the disposition of the remaining elastic parts of the structure. The cyclic settling down process can be arrived at in a few cycles (up to 20 for the case of mild steel).

(b) Semi-static shakedown, which is an intermediate gross yield stiation in which the cyclic settling down process not only depends on the ability of the material to settle down, but also on the remaining elastic parts of the structure. In this situation reversal of

straining can appear due to the redistribution of stresses and strains, which is a result of the cyclic loading process; the number of cycles needed to settle down, however, will be larger than for a static shakedown.

(c) When a gross yield situation has been reached on a large scale in the structure, the cyclic settling down process depends solely on the ability of the material to settle down, although reverse yielding and large incremental straining can appear as a consequence of the biaxiality of the plastic deformation, in the early cycles.

7.2 Recommendations for Future Work

Since the results of the elastic-plastic computer program gave reasonable agreement with the test results, the study of the "area replacement rule" can be made from a general point of view, since small differences in the connection details (nozzle-sphere) do not show a significant effect on the elastic stress concentration factor, and on the incipient collapse behaviour.

The differences between the calculated and the test values become greater for higher loads, hence it seems logical to attribute this increase in the difference to the change in geometry during the load process; it is, therefore, recommended that the necessary alterations to allow for the effect of geometry changes due to the loading process, in the calculations, be introduced into the computer program.

One of the first stages in a shakedown and collapse behaviour study, using an elastic-plastic computer program,is to obtain the settled cyclic and the static equivalent stress-strain curves for the material under consideration for construction of a pressure vessel. In the particular case of a shakedown calculation, it is necessary to assess the possible expansion of a settled cyclic ellipse of yield for different levels of strain. Once these curves are known,

elastic-plastic calculations should be carried out and their results compared with those found from tests with carefully constructed pressure vessel components.

After careful consideration, the author feels that it would be worthwhile to include finite-element techniques in future pressure vessel research, especially for sphere-nozzle junctions or other discontinuity regions.

REFERENCES

1. Turner, C.E. "Introduction to Plates and Shells Theory". Longmans, London, 1965.

2. Pilgrim, W.R., Cheung, J.S.T. and Marcal, P.V. "Computer Program for Elastic Analysis of Pressure Vessels". C.E.G.B. Research and Development Dept., RD/C/N/22, June 1965.

3. Cheung, J.S.T. Ph.D.Thesis. "The Elastic-Plastic Behaviour of some Axisymmetric Pressure Vessel Heads and Nozzles". University of London, 1969.

4. Gill, S.S. "The Stress Analysis of Pressure Vessels and Pressure Vessel Components". Pergamon Press, London, 1970.

5. Marcal, P.V. and Pilgrim, W.R. "A Stiffness Method for Elastic-Plastic Shells of Revolution". C.E.G.B., Research and Development Dept., RD/C/N/37, August, 1966.

6. Blomfield, J.A. Ph.D.Thesis. "The Elastic-Plastic Behaviour of Pipe Bends subjected to Cyclic Loading". University of London, 1970.

7. Cheung, J.S.T. and Turner, C.E. "Elastic-Plastic Behaviour of Pressure Vessel Heads". First Int.Conf. on Pressure Vessels Technology, Delft, The Netherlands, October, 1969, pp.597-611, American Soc.Mech.Eng.(ASME).

8. Marcal, P.V. and Turner, C.E. "Elastic-Plastic Behaviour of Flush Nozzles in Spherical Pressure Vessels". J.Mech.Eng. Sci., Vol.9, No.3, 1967, pp.182-189.

9. Crisp, R.J. "A Computer Survey of the Behaviour of Torispherical Drum Heads under Internal Pressure Loading", Part I. The Elastic Analysis, Part II. The Elastic-Plastic Analysis", Nuclear Eng. and Design, Vol.11, 1970, pp.457-494.

10. Watson, G.N. "A Treatise on the Theory of Bessel Functions". Cambridge University Press, 1966.

11. Ford, H. "Advanced Mechanics of Materials". Longmans, 1969.

12. Macfarlane, W.A. and Findlay, G.E. "A Simple Technique for Calculating Shakedown Loads in Pressure Vessels". Proc.Inst.Mech.Eng., Vol.186, 4/72, 1972, pp.45-52.

13. Leckie, F.A. "Localised Loads Applied to Spherical Shells". J.Mech.Eng.Sci., Vol.3, No.2, 1961, pp.111-118.

14. Leckie, F.A. and Penny, R.K. "Critical Study of the Solutions for the Asymmetric Bending of Spherical Shells". Welding Res.Council, Sept. 1963, Bull.90, pp.1-7.

15. Penny, R.K. and Leckie, F.A. "Solution for the Stresses at Nozzles in Pressure Vessels". Welding Res.Council, Bull.90, Sept.1963, pp.8-18.

16. Leckie, F.A. and Penny, R.K. "Stress Concentration Factors for the Stresses at Nozzle Intersections in Pressure Vessels". Welding Res.Council, Bull.90, Sept.1963, pp.19-26.

17. Flügge, W. "Stresses in Shells". Springer-Verlag, 1960.

18. Timoshenko, S.P. and Woinowsky-Krieger, S. "Theory of Plates and Shells". McGraw-Hill Book Co.Inc., London, 1959.

19. Novozhilov, V.V. "Thin Shell Theory". P. Noordhoff, The Netherlands, 1964.

20. Bickell, M.B. and Ruiz,C. "Pressure Vessel Design and Analysis". Macmillan, London, 1967.

21. Marcal, R.V. and Turner, C.E. "Numerical Analysis of Elastic-Plastic Behaviour of Axisymmetrically Loaded Shells of Revolution". J.Mech.Eng.Sci., Vol.5, No.3, Sept.1963, pp.232-237.

22. Hopkins, N.G. and Prager, W. "The Load Carrying Capacities of Circular Plates". J.Mech.Phys.Solidis, Vol.2, 1953, pp.1-13.

23. Fox, J.D., Kraus,H. and Penny, R.K. "Shakedown of Pressure Vessels with Ellipsoidal Heads". Proc.Inst.Mech.Eng., Vol.186, 1972, pp.431-437.

24. Sampayo, V.M. and Turner, C.E. "Computed Elastic-Plastic Behaviour and Shakedown of some Radial Nozzle-on-Sphere Geometries". Second Int.Conf. on Pressure Vessel Technology, The Am.Soc.Mech.Eng., Oct.1973, pp.331-341.

25. O'Connell, J.M. and Chubb, E.J. "Improved Methods of Calculating Stresses at the Intersections of a Cylindrical Nozzle and Spherical Vessels". Appl.Mech.Convn. Proc.Inst.Mech.Eng., Vol.178, 1963-64 (PT3J), p.224-230

26. Mendelson, A. and Manson, S.S. "Practical Solution of Plastic Deformation Problems in the Elastic-Plastic Range". NASA TR-28, 1959.

27. Mendelson, A., Hirschberg, M.H. and Manson, S.S. "A General Approach to the Practical Solution of Creep Problems". J.Basic Eng., Trans.A.S.M.E.(D), Vol.81, No.4, 1959, pp.585-598.

28. Marcal, P.V. "The Elastic-Plastic Straining of some Shells of Revolution with special reference to Expansion Bellows". Ph.D.Thesis, University of London, 1963.

29. Marcal, P.V. "Comparative Study of Numerical Methods of Elastic-Plastic Analysis". AIAA, J.V.6,No.1, 1968, p.127 - 128.

30. Zienkiewicz, O.C., Valliappan, S. and King, I.P. "Elasto-Plastic Solutions of Engineering Problems "Initial Stress", Finite Element Approach". Int.J.Numerical Methods in Engineering, Vol.1, No.1, 1969, pp.75-100.

31. Hodge, Jr. P.G. "Limit Analysis of Rotationally Symmetric Plates and Shells". Prentice-Hall,Inc., 1963.

32. Hodge, Jr. P.G. "The Mises Yield Condition for Rotationally Symmetric Shells". Quart.Appl.Math., Vol.XVIII, 1961, No.4, pp.305-311.

33. Cloud, R.L. "The Limit Pressure of Radial Nozzles in Spherical Shells". Nuc.Str.Engng.1, 1965, pp.403-413.

34. Gill, S.S. "The Limit Pressure for a Flush Cylindrical Nozzle in a Spherical Pressure Vessel". Int.J.Mech.Sci., 1964, Vol.6, pp.105-115.

35. Allman, D.J. and Gill, S.S. "The Effect of change of Geometry on the Limit Pressure of a Flush Nozzle in a Spherical Pressure Vessel", in Engineering Plasticity (Heyman and Leckie, eds.) Cambridge University Press, London, 1968, pp.1-20.

36. Dinno, K.S. and Gill, S.S. "Limit Pressure for a Protruding Cylindrical Nozzle in a Spherical Pressure Vessel". J.Mech.Eng.Sci., Vol.7, No.3, 1965, pp.259-270.

37. Gill, S.S. and Leckie, F.A. "The Effect of Geometry Change on the Application of Limit Analysis to the Design of Pressure Vessel Nozzles". Int.J.Mech.Sci., Vol.10, 1968, pp.989-993.

38. Drucker, D.C. and Shield, R.T. "Limit Analysis of Symmetrically Loaded Thin Shells of Revolution". J.Appl.Mech., Trans.A.S.M.E., March 1959, pp.61-68.

39. Marcal, P.V. and Turner, C.E. "Elastic Solution in the Limit Analysis of Shells of Revolution with Special Reference to Expansion Bellows". J.Mech.Eng.Sci., Vol.3, No.3, 1961, pp.252-257.

40. Hodge, Jr. P.G. "Limit Analysis with Multiple Load Paramter". Int.J.Solids Struct., Vol.6, 1970, pp.661-675.

41. Argyris, J.H. "Elasto-Plastic Displacement Analysis of Three-Dimensional Continua". J.Roy.Aero.Soc., Vol.69, Tech.Note, Sept.1965, pp.633-636.

42. Spera, D.A. "A Numerical Analysis of Elastic-Plastic Thin Shells of Revolution Containing Discontinuities". A.I.A.A., Vol.1, Nov.1963, pp.2583-3589.

43. Tuba, I.S. "A Method of Elastic-Plastic Plane Stress and Strain Analysis". J.Strain Analysis, Vol.1, No.2, 1966, P.115-120.

44. Pilgrim, N.R. and Marcal, P.V. "Computer Program for Plastic Analysis of Pressure Vessels - Users Manual". C.E.G.B. Rep.No.RD/C/N/38, Oct.1965

45. Pilgrim, N.R. and Marcal, P.V. "Computer Program for Elastic Analysis of Pressure Vessels - Users Manual". C.E.G.B. Rep.No.RD/C/N/36, Oct.1965.

46. ASME Section VIII (1968). Division 1, Pressure Vessels: Division 2, Alternative Rules for Pressure Vessels.

47. B.S.1515. Fusion Welded Pressure Vessels: Part 1, Carbon and Ferritic Alloy Steels, 1965; Part 2, Austentis Stainless Steel, 1968.

48. B.S.1500. Fusion Welded Pressure Vessels: Part 1, Carbon and Low Alloy Steel, 1958.

49. German Unfired Pressure Vessel Code (AD-specification 1967, English Translation).

50. Nichols, R.W. "Pressure Vessels Engineering Technology". Elsevier, London, 1971.

51. Langer, B.F. "P.V.R.C. Interpretation Report of Pressure Vessels Research". Welding Research Council, Bull.101, Apr.1964.

52. Budiansky, B. and Sanders, Jr. J.L. "On the Best First Order Linear Shell Theory". Progress in Applied Mechanics Macmillan, 1963.

53. Findlay, G.E. and Spence, J. "Applying the Shakedown Concept to Pressure Vessel Design". The Engineer, 12 July 1968, pp.63-65.

54. Symonds, P.S. "Shakedown on Continuous Media". J.Appl.Mech. Trans.ASME, Vol.73, March 1951, pp.85-89.

55. Koiter, W.T. "A New General Theorem on Shakedown of Elastic-Plastic Structures". Proc. of Ro.Neth.Acad.Sci., 1956, B.59, pp.24-34.

56. Findlay, G.E., Moffat, D.G. and Stanley, P. "Torispherical Drum-heads: A Limit-Pressure and Shakedown Investigations". J.Strain Anal., Vol.6, No.3, 1971, pp.147-166.

57. Crisp. R.J. "Calculation of Post-Yield Stresses and Shakedown Loads from Strain Gauge Readings". J.Brit.Nuc.Energy Soc., Vol.8 (2), 1969, pp.116-122.

58. Taylor, T.E. "Shakedown Loads for Pressure Vessels of Strain Hardening Materials". J.Mech.Eng.Sci., Vol11, No.3, 1969, pp.340-342.

59. Procter, E. and Flinders, R.F. "Shakedown Investigations on Partial Penetration Welded Nozzles in a Spherical Shell". Nuc.Eng. and Design, Vol.8, 1968, pp.174-185.

60. Blomfield, J.A. and Jackson, P.B.M. "Fatigue Tests on some Cupro-Nickel Pipe Bends and a Comparison of some Failure-Prediction Methods". 1st Int.Conf. on Pressure Vessels Technology, Part II, Paper 95, p.1221-1231, Delft, Netherlands, Oct.1969, Pg. by ASME.

61. Leckie, F.A. "Shakedown Pressures for Flush Cylinder-Sphere Shell Intersections". J.Mech.Eng.Sci., Vol.7, No.4, 1965, pp.367-371.

62. Landgraf, R.N., Morrow, J. and Endo, T. "Determination of the Cyclic Stress-Strain Curve". J. of Materials (ASTM) Vol.4, No.1, March 1969, pp.176-188.

63. Leckie, F.A. and Payne, D.J. "Some Observations on the Design of Spherical Pressure Vessels with Flush Cylindrical Nozzles". Proc.Inst.Mech.Eng., 1965-66, V.180,pp.497-512.

64. Prager, W. "A New Method of Analysing Stresses and Strains in Work Hardening Plastic Solids". J.Appl.Mech.(ASME) Vol.23, Dec.1956, pp.493-496.

65. Prager, W. "Introduction to Plasticity". Addison-Wesley, 1959.

66. Parkes, E.W. "Incremental Collapse due to Thermal Stress". Aircraft Eng., Nov.1956, pp.395-396.

67. Edmunds, H.G. and Beer, F.J. "Notes on Incremental Collapse in Pressure Vessels". J.Mech.Eng.Sci., Vol.3, No.3 1961, pp.187 - 199.

68. B.S.3915. Carbon and Low Alloy Steel Pressure Vessels for Nuclear Reactors.

69. Poynor, J.F. "A Review of Current Pressure Vessel Codes". Sept. 1970.

70. Robinson, M. and Gill, S.S. "The Effect of Finite Changes of Geometry on the Rigid-Plastic Limit Pressure of Flush Nozzles in Spherical Pressure Vessels". Int.J.Mech.Sci., Pergamon Press, 1969, Vol.11, pp.253-267.

71. Corn, M.D, and Gill, S.S. "The Effect of Change of Geometry on the Rigid-Plastic Limit Load of Cylinders". Inst.J.Mech.Sci., Pergamon Press, 1968, Vol.10, pp.355-368.

72. Palusamy, S. and Lind, N.C. "Limit Analysis of Non-symmetrically Loaded Spherical Shells". J.Appl.Mech., Trans.ASME, June 1972, pp.422-430.

73. Townley, C.H.A., Findlay, G.E., Goodman, H.M. and Stanley, P. "Elastic-Plastic Computations as a Basis for Design Charts for Torispherical Pressure Vessel End". Proc.Inst.Mech.Eng., 1970-71, Vol.185, pp.63-71.

74. Townley, C.H.A. "The Design of Pressure Vessels Details". Engineer, London, 1968, Vol.227, pp.438-445.

75. Blatherwick, A.A. and Lazan, B.J. "The Effect of Changing Cyclic Modulus on Bending Fatigue Strength". Proc.ASTM, Vol.56, 1956, pp.1012-1037.

76. Turner, C.E. "Study of the Symmetrical Elastic Loading of some Shells of Revolution, with special reference to Toroidal Elements". J.Mech.Eng.Sci., Vol.1, No.2, 1959, pp.113-129.

77. Love, A.E.H., "A Treatise on the Mathematical Theory of Elasticity". Cambridge University Press, Cambridge, 1906.

78. Rose, R.T. "New Design Method for Pressure Vessel Nozzles". The Engineer, July 20, 1962, pp.90-93.

79. Mershon, J.L. "PVRC Research on Reinforcement of Openings on Pressure Vessels". Welding Res.Council, Bull.77, May 1962.

80. Panel E/-/3/2/2. "SBN:580 05570 1", approved by the Pressure Vessels Standards Committee E/-/3, published under the authority of the Executive Board on 27 June 1969.

81. Drucker, D.C. "Limit Analysis of Cylindrical Shells under Axially Symmetric Loading". Proc. of 1st Midwestern Conf. in Solid Mechanics, 1954, pp.158-163.

APPENDIX A

FUNDAMENTAL EQUATIONS FOR ELASTIC SYMMETRICALLY LOADED SHELLS OF REVOLUTION

The notation used in Figs. 1 and 2 is the same as used in the following equations and, with minor changes, in references [1,2,3].

A.1 Equilibrium Equations

Referring to Fig. 1, the equations of equilibrium are:

A.1.1 Axial equilibrium

$$\frac{d(wr)}{d\ell} - 2\,h\,r\,Y - p\,r\sin\theta = 0 \tag{A.1}$$

A.1.2 Radial equilibrium

$$\frac{d(Fr)}{d\ell} - N_{\varphi} + pr\cos\theta + 2\,h\,r\,X = 0 \tag{A.2}$$

A.1.3 Moment balance

Because of the axisymmetry of loading it will only be necessary to consider the meridional balance,

$$\frac{d(M_{\ell}r)}{d\ell} - Fr\cos\theta - M_{\varphi}\sin\theta + Wr\sin\theta = 0 \tag{A.3}$$

A.1.4 The meridional stress resultant N_{ℓ} is given by

$$N_{\ell} = W\cos\theta + F\sin\theta \tag{A.4}$$

A.2 Displacement , rotation and strain relationships

Referring to Fig. 2, the relationship between the displacements, rotation and strains, are given by:

A.2.1 Mid-wall strains

$$\bar{e}_{\ell} = \frac{1}{\sin\theta}\,\frac{du}{d\ell} + \phi\cot\theta \tag{A.5}$$

$$\bar{e}_{\varphi} = \frac{u}{r} \tag{A.6}$$

A.2.2 Strains at any position through the thickness, with the assumption that plane sections remain plane, are given by

$$e_{\ell} = \bar{e}_{\ell} + z\,\frac{d\phi}{d\ell} \tag{A.7}$$

$$e_{\varphi} = \bar{e}_{\varphi} + z\,\frac{\sin\theta}{r}\,\phi \tag{A.8}$$

A.2.3 The axial displacement is related to the radial displacement and rotation through the following equation, again referring to Fig. 2a

$$\frac{dv}{d\ell} = \emptyset \sin\theta + \bar{e}_{\ell} \cos\theta \qquad (A.9)$$

From (A.5) it is possible to write a similar equation for the radial displacement

$$\frac{du}{d\ell} = -\emptyset \cos\theta + \bar{e}_{\ell} \sin\theta \qquad (A.5.1)$$

A.3 Elastic stress-strain law

Hookean material will be considered, therefore

$$e_i = \frac{1}{E}(\sigma_i - \nu\,\sigma_i) \;, \quad i,j = \ell,\varphi \qquad (A.10)$$

A.4 Other relations

It is usual to have as dependent variables either $\emptyset$ and F, or functions of them, in an analytic solution, and $\emptyset$, $\frac{d\emptyset}{d\ell}$, u and F in a numerical solution, hence it is necessary to eliminate stress and moment resultants from some of the above equations.

In order to proceed using these dependent variables, it will be necessary to know the relationships between the latter variables and the former dependent variables. These relationships are as follows:

Denoting the thickness of the shell by 2h:

A.4.1 Stress resultants

$$N_i = \int_{-h}^{+h} \sigma_i \, dz, \quad i = \ell,\varphi$$

or

$$N_i = \frac{2\,E\,h}{1-\nu^2}(\bar{e}_i + \nu\bar{e}_j), \quad i,j = \ell,\varphi \qquad (A.11)$$

A.4.2 Moment resultants

$$M_i = \int_{-h}^{+h} \sigma_i \, z \, dz \;, \quad i = \ell,\varphi$$

or

$$M_{\ell} = D\left(\frac{d\emptyset}{d\ell} + \frac{\nu \sin\theta}{r}\emptyset\right) \qquad (A.12.1)$$

and

$$M_{\varphi} = D\left(\frac{\sin\theta}{r}\,\phi + \nu\,\frac{d\phi}{d\ell}\right) \tag{A.12.2}$$

where $D = 2\,E\,h^3/3(1-\nu^2)$

The derivative of M_{ℓ} is required in the solution of (A.3), hence, from (A.12.1)

$$\frac{dM_{\ell}}{d\ell} = \frac{2\,E\,h^2}{1-\nu^2}\left(\frac{d\phi}{d\ell} + \nu\,\frac{\sin\theta}{r}\,\phi\right)\beta + D\left[\frac{d^2\phi}{d\ell^2} + \nu\left(\frac{\sin\theta}{r}\,\frac{d\phi}{d\ell} - \frac{\sin^2\theta}{r^2}\,\phi + \frac{1}{r}\,\phi\,\frac{d(\sin\theta)}{d\ell}\right)\right] \tag{A.13}$$

where β, which is equal to $\frac{dh}{d\ell}$, is the taper.

A.5 The equations used in a numerical integration or in an analytic integration are different forms of the above equations, e.g. (A.11), with $i = \varphi$ and $j = \ell$, is substituted into (A.2) giving

$$\frac{d}{d\ell}(Fr) + pr\cos\theta - \frac{2\,E\,h}{1-\nu^2}\,(\bar{e}_{\varphi} + \nu\,\bar{e}_{\ell}) + 2hr\,X = 0 \tag{A.21}$$

(A.1) is generally used as an integral form

$$Wr = V + \int (pr\sin\theta + 2\,h\,r\,Y)\,d\ell \tag{A.1.1}$$

Using (A.11), with $i = \ell$ and $j = \varphi$, and substituting into (A.4), the following equation is obtained

$$\frac{2\,E\,h}{1-\nu^2}\,(\bar{e}_{\ell} + \nu\,\bar{e}_{\varphi}) = W\cos\theta + F\sin\theta \tag{A.4.1}$$

Replacing the values of M_{ℓ}, M_{φ} and $\frac{dM_{\ell}}{d\ell}$, respectively, from (A.12.1) (A.12.2) and (A.13) into (A.3), the following equation is obtained

$$\frac{d^2\phi}{d\ell^2} + \left[\frac{2\,Eh^2}{D(1-\nu^2)}\beta + \frac{\sin\theta}{r}\right]\frac{d\phi}{d\ell} + \left[\frac{2\,\nu\,Eh^2}{D(1-\nu^2)}\,\frac{\sin\theta}{r}\,\beta + \frac{\nu}{r}\cos\theta\,\frac{d\theta}{d\ell} - \frac{\sin^2\theta}{r^2}\right]\phi - \frac{F}{D}\cos\theta + \frac{W}{D}\sin\theta = 0 \tag{A.14}$$

A.6 As far as an analytic solution is concerned, a better equation than (A.5.1) can be derived for use in conjunction with (A.14). Considering the case X, Y and β equal to zero and using the definition of N_i, $i = \ell,\varphi$ from [1]

$$\bar{\sigma}_i = \frac{N_i}{2h}, \quad i = \ell,\varphi \tag{A.15}$$

Substituting the value of σ_i, $i = \ell,\varphi$ into (A.10) for $i,j = \ell,\varphi$, gives

$$\bar{e}_i = \frac{1}{2\,hE}\ (N_i - \nu\, N_j), \quad i,j = \ell,\varphi \tag{A.16}$$

Taking the values of N_φ and N_ℓ, respectively, from (A.2) and (A.4) and replacing them into (A.16) for $i = \varphi$ and $j = \ell$, and then multiplying by r and differentiating in relation to ℓ, these can be written

$$\frac{d(r\,\bar{e}_\varphi)}{d\ell} = \frac{1}{2hE}\left[\frac{d}{d\ell}\left(r\,\frac{d(Fr)}{d\ell}\right) - \nu(Fr)\,\sin\theta\right] + \cos\theta\,\frac{d(pr^2)}{d\ell}$$

$$+ \sin\theta\,(-\,pr^2 + \nu\,V + \nu\int pr\,\sin\theta\,d\ell)\frac{d\theta}{d\ell} \tag{A.17}$$

Substituting $i = \ell$, $j = \varphi$ into (A.16), and using N_ℓ and N_φ from (A.4) and (A.2), respectively, the following equation is obtained

$$\bar{e}_\ell = \frac{1}{2hE}\left[-\,\nu\,\frac{d(Fr)}{d\ell} + F\,\sin\theta + \cos\theta\left(\frac{1}{r}\int pr\,\sin\theta\,d\ell - \nu\,pr + \frac{V}{r}\right)\right] \tag{A.18}$$

Taking the value of u from (A.6) and replacing into (A.5.1) gives

$$\emptyset\,\cot\theta = -\,\frac{1}{\sin\theta}\,\frac{d(r\bar{e}_\varphi)}{d\ell} + \bar{e}_\ell \tag{A.19}$$

Again, taking the values of $\bar{e}_{\ell}$ and $\frac{d(r\bar{e}_{\varphi})}{d\ell}$, respectively, from (A.18) and (A.17) and substituting them into (A.19), gives

$$\frac{1}{\sin\theta}\ \frac{d}{d\ell}\left[r\,\frac{d(Fr)}{d\ell} - \nu\,(Fr)\,\sin\theta \right] + \nu\,\frac{d(Fr)}{d\ell} - F\,\sin\theta + 2Eh\,\emptyset\,\cot\theta$$

$$= \cos\theta\left(-\frac{1}{\sin\theta}\,\frac{d(pr^2)}{d\ell} + \frac{1}{r}\int pr\,\sin\theta\,d\ell + \frac{V}{r}\right)$$

$$+ \left(pr^2 - \nu V - \nu\int pr\,\sin\theta\,d\ell\right)\frac{d\theta}{d\ell} \qquad \text{(A.20)}$$

The equation (A.14), with the assumptions already made for (A.20), forms with this latter equation the system of differential equations used to solve analytically the problems of stress distribution in pressure loaded shells of revolution in this thesis and many other works.

APPENDIX B

CYLINDER-SPHERE INTERSECTIONS FOR INTERNALLY PRESSURISED HEADS AND NOZZLES

Referring to Figs. 3, 4 and 5 it can be seen that for each particular type of geometry the following relationships may be applied:

- Sphere:
$$R = D_o/2$$
$$r = R \cos\theta$$
$$d\ell = -R\, d\theta \qquad \text{(B.1)}$$
$$\beta = 0$$
$$2h = T$$

- Cylinder:
$$d\ell = dx$$
$$r = d/2$$
$$\theta = 0^o \qquad \text{(B.2)}$$
$$\beta = o$$
$$2h = t$$

- Plate:
$$\theta = \pi/2 \text{ or } \alpha = 0$$
$$d\ell = dr \qquad \text{(B.3)}$$
$$2h = T$$
$$\beta = 0$$

It will be assumed, hereafter, that X and Y are zero and that the pressure is constant, i.e. X = 0, Y = 0; p = (constant).

Certain of the equations to be found in Appendix A, referring to the particular geometry, either sphere or cylinder, under consideration, give rise to the following relationships:

B.1.1 - Sphere

Substituting (B.1) into (A.14) and using (A.1), the following result is obtained:

$$\frac{d^2\phi}{d\theta^2} - \tan\theta\,\frac{d\phi}{d\theta} - (\nu + \tan^2\theta)\phi - \frac{D_o}{2D}(Fr) = -\frac{D_o}{2D}\tan\theta\,(V + \tfrac{1}{2}pr^2) \qquad \text{(B.4)}$$

Likewise, introducing the conditions of (B.1) into (A.20)

$$\frac{d^2(Fr)}{d\theta^2} - \tan\theta \frac{d(Fr)}{d\theta} - (\tan^2\theta - \nu)(Fr) + \frac{TED_o}{2}\phi$$

$$= -\frac{3}{4} p D_o^2 \cos\theta \sin\theta + (1 + \nu) \tan\theta \left\{\tfrac{1}{2} pr^2 + V\right\} \qquad (B.5)$$

(B.4) and (B.5) form the system of differential equations which will be used to solve the analytical problem of stress distribution in a spherical shell.

This system is similar to that in Ref. [1], page 110, except that the right hand side has been altered to take the load condition into account. (B.4) and (B.5) are, also, similar to the system presented in Ref. [4], page 23, except that they use a different system of axes, and definitions concerning the directions of the stress and moment resultants.

The right hand side of equations (B.4) and (B.5) gives the particular integral which corresponds to the membrane solutions for the type of loading under consideration, Refs. [1] and [4].

A complete solution to the problem will consist of the solution resulting from the application of the homogeneous system, known as the edge bending solution, plus the particular integrals from the above system, which is dependent on the loading of the shell.

Using the following relationships,

$$Fr = \frac{\omega}{\cos^{\frac{1}{2}}\theta} \qquad (B.6.1)$$

and

$$\phi = \frac{\varepsilon}{\cos^{\frac{1}{2}}\theta} \qquad (B.6.2)$$

similar to those used in Ref. [1], and substituting them into (B.4) and (B.5), the following system of equations is obtained for the edge bending conditions:

$$\frac{d^2\epsilon}{d\theta^2} - \epsilon[\frac{3}{4}\tan^2\theta + (\nu - \tfrac{1}{2})] + \frac{D_o}{2D}\omega = 0 \qquad \text{(B.7.1)}$$

$$\frac{d^2\omega}{d\theta^2} - \omega[\frac{3}{4}\tan^2\theta - (\nu + \tfrac{1}{2})] - \frac{TED_o}{2}\epsilon = 0 \qquad \text{(B.7.2)}$$

The system of differential equations is the same as that in Ref. [1], page 111.

Since the terms in ϵ and ω, in (B.7.1) and (B.7.2) respectively, are minute compared with the terms in $\frac{d^2\epsilon}{d\theta^2}$ and $\frac{d^2\omega}{d\theta^2}$ in the same equation, the former terms will henceforth be neglected. Once the solution of the simplified system has been arrived at it will become apparent that the terms of the second derivatives are of the order of λ^2, with λ a constant for each particular geometry and material, in relation to the single functions ϵ and ω respectively. It should be noted that the larger the value of λ, the better will be the approximation to the solution.

It should also be noted, as regards the solution of the simplified system from (B.7.1) and (B.7.2) that, when the comparison was made between the values of terms ϵ and ω and those of $\frac{d^2\epsilon}{d\theta^2}$ and $\frac{d^2\omega}{d\theta^2}$, actual values of the coefficients of ϵ and ω in (B.7.1) and (B.7.2) respectively, were not given; in fact when θ is near $\pm \pi/2$ the values of these coefficients may be larger than λ and, if this is the case these terms cannot therefore be regarded as negligible in comparison with the second derivatives.

Taking (B.7.1) and (B.7.2), and neglecting the terms in ϵ and ω, respectively, gives

$$\frac{d^2\epsilon}{d\theta^2} + \frac{D_o}{2D}\omega = 0 \qquad \text{(B.8.1)}$$

and

$$\frac{d^2\omega}{d\theta^2} - \frac{TED_o}{2}\epsilon = 0 \qquad \text{(B.8.2)}$$

Eliminating ϵ between them, the following result is obtained:

$$\frac{d^4\omega}{d\theta^4} + 4\lambda^4\omega = 0 \qquad (B.9)$$

where

$$4\lambda^4 = \frac{TED_o^2}{4D}$$

or, recalling that $D = ET^3/12(1 - \nu^2)$,

$$\lambda = \sqrt[4]{3(1 - \nu^2)}\sqrt{\frac{D_o}{2T}} \qquad (B.10)$$

The solution of (B.9) is well known, [1], i.e.

$$\omega = e^{\lambda\theta}(C_1 \cos \lambda\theta + C_2 \sin \lambda\theta)$$

$$+ e^{-\lambda\theta}(C_3 \cos \lambda\theta + C_4 \sin \lambda\theta) \qquad (B.11)$$

where C_1, C_2, C_3 and C_4 are constants of integration, determined by the boundary conditions.

From the foregoing assumptions, and from (B.10) it can be stated that the higher the value of $D_o/2T$ and the greater the difference between θ and $\pm \pi/2$ the better will be the approximation given by the solution of (B.8.1) and (B.8.2).

The validity of solution (B.11) for the system (B.7) is inter-dependent on R/T and θ, hence it will be difficult to define the applicability limits of such a solution.

B.1.2 Shallow Spherical Shells

In the theory of shallow shells, the independent variable is taken as the complementary angle of θ; only the case of θ being near to $+ \pi/2$ is considered here.

Let α be the independent variable, defined by

$$\alpha = \pi/2 - \theta \qquad (B.12.1)$$

as used in [1].

Since θ is near $+ \pi/2$, α must be a small angle, hence

$$\tan \theta \simeq 1/\alpha \qquad (B.12.2)$$

Substituting (B.12) into the homogeneous system of differential equations formed by (B.4) and (B.5), the following relationships are, respectively, obtained:

$$\frac{d^2\emptyset}{d\alpha^2} + \frac{1}{\alpha}\frac{d\emptyset}{d\alpha} - \left(\frac{1}{\alpha} + \nu\right)\emptyset - \frac{D_o}{2D}(Fr) = 0 \qquad (B.13.1)$$

$$\frac{d^2(Fr)}{d\alpha} + \frac{1}{\alpha}\frac{d(Fr)}{d\alpha} - \left(\frac{1}{\alpha} - \nu\right)(Fr) + \frac{TED_o}{2}\emptyset = 0 \qquad (B.13.2)$$

Substituting the value of $\emptyset$ from (B.13.2) into (B.13.1) gives:

$$\left(\frac{d^2}{d\alpha^2} + \frac{1}{\alpha}\frac{d}{d\alpha} - \frac{1}{\alpha^2}\right)\left(\frac{d^2}{d\alpha^2} + \frac{1}{\alpha}\frac{d}{d\alpha} - \frac{1}{\alpha^2}\right)(Fr) + 4\gamma^4(Fr) = 0 \qquad (B.14)$$

where $4\gamma^4 = 4\lambda^4 - \nu^2$ (recalling $4\lambda^4 = TED_o^2/4D$).

(B.14) is identical to the corresponding equation in [1], page 117, hence it will have the same solution:

$$Fr = C_1\,ber'\chi + C_2\,bei'\chi + C_3\,ker'\chi + C_4\,kei'\chi \qquad (B.15)$$

where ber, bei, ker and kei are known as Kelvin functions, and χ is defined by:

$$\chi = \gamma\sqrt{2}\,\alpha \qquad (B.16)$$

Since the Kelvin function will be required, an approximated expression is given here:

$$ber\,\chi = \frac{1}{\sqrt{2\pi\chi}}\,e^{\chi/\sqrt{2}}\cos\left(\chi/\sqrt{2} - \pi/8\right)$$

$$ber'\chi = \frac{1}{\sqrt{2\pi\chi}}\,e^{\chi/\sqrt{2}}\cos\left(\chi/\sqrt{2} + \pi/8\right) \qquad B.17)$$

$$bei\chi = \frac{1}{\sqrt{2\pi\chi}}\,e^{\chi/\sqrt{2}}\sin\left(\chi/\sqrt{2} - \pi/8\right)$$

$$bei'\chi = \frac{1}{\sqrt{2\pi\chi}}\,e^{\chi/\sqrt{2}}\sin\left(\chi/\sqrt{2} + \pi/8\right)$$

and

$$\ker \chi = +\sqrt{\pi/2\chi}\; e^{-\chi/\sqrt{2}} \cos(\chi/\sqrt{2} + \pi/8)$$

$$\ker' \chi = -\sqrt{\pi/2\chi}\; e^{-\chi/\sqrt{2}} \cos(\chi/\sqrt{2} - \pi/8)$$

$$\mathrm{kei}\chi = -\sqrt{\pi/2\chi}\; 3^{-\chi/\sqrt{2}} \sin(\chi/\sqrt{2} + \pi/8) \qquad \text{(B.18)}$$

$$\mathrm{kei}' \chi = +\sqrt{\pi/2\chi}\; e^{-\chi/\sqrt{2}} \sin(\chi/\sqrt{2} - \pi/8)$$

as used in [1].

These equations make an adequate approximation to the Kelvin functions as long as χ is bigger than 7 ($\chi > 7$) Refs. [1] and [4], which is common for most practical shell problems.

The solution for Fr, given by (B.15), of the differential equation (B.14), is an approximated one as the function $\tan\theta$ was substituted for by an approximate value, $1/\alpha$. In connection with this solution, it should be noted that, once (B.17) and (B.18) are used as approximated functions to Kelvin function, the solution Fr (B.15), will also be limited to values of θ close to $+\pi/2$.

If the complete expression for the Kelvin function, (1.1), are to be used, then the solution validity will be limited by values of χ near to and less than 1, unless some artifice is used as by Leckie Ref. [13].

B.1.3 Solid Plate

Since the Kelvin functions are limited by the condition that χ may not be smaller than unity, Ref. [10], and as it has already been stated that (B.17) and (B.18) are good approximations of $\chi > 7$, the solid plate solutions must be known if either a flat, or almost flat, head is to be studied using an analytic solution, otherwise a numerical solution will have to be used.

The solid plate end is the limit of a spherical head when d/D_o tends to zero, see Fig. 5.

Introducing (B.3) into the homogeneous system from (A.14) and (A.20), Appendix A, the following results are respectively obtained:

$$\frac{d}{dr}\left[\frac{1}{r}\frac{d}{dr}(r\,\emptyset)\right] + \frac{W}{D} = 0 \qquad (B.19)$$

and

$$\frac{d}{dr}\left[\frac{d(rF)}{dr} + F\right] = 0 \qquad (B.20)$$

These two equations form the system of differential equations that will be used to solve the analytical problem of stress distribution in a solid plate.

This homogeneous system of differential equations, together with data concerning the particular boundary conditions, will be used to obtain the edge bending solution of a solid plate.

Since (B.19) and (B.20) are independent of each other as far as integration is concerned, the expressions for F and for $\emptyset$ from these equations are obtained by a straightforward integration, giving respectively:

$$\emptyset = A'r + \frac{A''}{r} \qquad (B.21.1)$$

and

$$F = B' + \frac{B''}{r} \qquad (B.21.2)$$

Therefore, these two expressions can be used to obtain the edge bending solution for an almost flat head as can be seen from (B.3).

B.1.4 Cylinder

The geometry of a cylinder with constant thickness, $2h = t$, and closed end, is now considered: substituting (B.2) into (A.14) and (A.20) there will be obtained respectively:

$$\frac{d^2\emptyset}{dx^2} - \frac{F}{D} = 0 \qquad (B.22.1)$$

and

$$\frac{d^2}{4}\frac{d^2F}{dx^2} + Et\phi = 0 \qquad (B.22.2)$$

where D, for a cylinder of thickness t, is given by

$$D = Et^3/12(1 - \nu^2)$$

From the fact that the system of differential equations formed by (B.22.1) and (B.22.2), which will later be used to solve the problem of a pressurised cylinder intersecting a spherical shell, already have a homogeneous form, the membrane solution for F and ϕ are both zero; this does not however mean that the membrane stresses and strains are zero.

Taking the value of ϕ from (B.22.2) and substituting it into (B.22.1), gives

$$\frac{d^4F}{dx^4} + 4k^4F = 0 \qquad (B.23)$$

where

$$4k^4 = \frac{48(1 - \nu^2)}{d^2 t^2} \qquad (B.24)$$

The differential equation is identical to the corresponding equation in Ref. [1], page 103, hence the corresponding solution can be written as:

$$F = e^{kx}(A_1 \cos kx + A_2 \sin kx) + e^{-kx}(A_3 \cos kx + A_4 \sin kx) \qquad (B.25)$$

where A_1, A_2, A_3 and A_4 are the constants of integration, depending either upon the edge bending or the boundary conditions.

B.2 Formulae of N_φ, N_ℓ, M_ℓ, M_φ, u and ϕ as functions of (B.11), (B.15), (B.21) and (B.25) respectively for sphere, shallow sphere, solid plate and cylinder

Referring to Figs. 3, 4 and 5, and denoting by superscript = either the membrane values concerned or the particular integral of the differential systems,((B.4) and (B.5)) for the spheres, (B.13) for the

shallow sphere, ((B.19) and (B.20)) for the solid plate and (B.22) for the cylinder, the following results are obtained:

B.2.1 Sphere

Considering the junction geometry (see Figs. 3 and 4) and the axial equilibrium for $\alpha_o = \text{acos}\ (d/D_o)$, $\bar{\bar{W}}$ will be given by

$$\bar{\bar{W}}(\theta = \alpha_o) = \frac{pD_o}{4} \cos \alpha_o;$$

accordingly the constant of integration from (A.1), will be V = 0, hence

$$\bar{\bar{W}} = \frac{pD_o}{4} \cos \theta \qquad \text{(B.26)}$$

Substituting the well known membrane value of $\bar{\bar{N}}_\varphi$ $(= \frac{pD_o}{4})$ for the sphere, into (A.2) and integrating together with conditions (B.1), the following is obtained:

$$\bar{\bar{F}} = \frac{1}{4} pD_o \sin \theta + \bar{\bar{F}}_1 / \cos \theta \qquad \text{(B.27.1)}$$

where $\bar{\bar{F}}_1$ is the constant of integration.

Replacing the values of $\bar{\bar{W}}$ and $\bar{\bar{F}}$ from (B.26) and (B.27.1), respectively, with the membrane value of $\bar{\bar{N}}_\ell$ $(=pD_o/4)$ into (A.4), it can be seen that $\bar{\bar{F}}_1 = 0$, hence

$$\bar{\bar{F}} = \frac{1}{4} pD_o \sin \theta \qquad \text{(B.27.2)}$$

Substituting (B.27.2) and (B.26) into (B.5), the following result is obtained:

$$\bar{\bar{\emptyset}} = 0$$

Substituting into (A.10) with $i = \varphi$ and $j = \ell$, the membrane stress values $(\bar{\bar{\sigma}}_i,\ i = \ell, \varphi)$, a formula for $\bar{\bar{e}}_\varphi$ will be obtained which, when substituted into (A.6) will give

$$\bar{\bar{u}} = \frac{pD_o^2}{8ET} (1 - \nu) \cos \theta \qquad \text{(B.28)}$$

Once the membrane values are known, it will be possible to derive the complete solution (membrane + bending) for the sphere:

the solution for Fr will be obtained from (B.27.2) and (B.6.1):

$$Fr = \frac{\omega}{\cos^{\frac{1}{2}}\theta} + \frac{1}{8} p D_o^2 \cos\theta \sin\theta \qquad (B.29.1)$$

Introducing (B.26.1) into (A.2) with (B.1) gives

$$N_\varphi = -\frac{1}{R}\frac{d}{d\theta}\left(\frac{\omega}{\cos^{\frac{1}{2}}\theta}\right) + \frac{1}{4} p D_o \qquad (B.29.2)$$

Substituting (B.29.1), (B.26) and (B.1) into (A.4), the following result is obtained:

$$N_\ell = \frac{\omega \sin\theta}{R\cos^{3/2}\theta} + \frac{1}{4} p D_o \qquad (B.29.3)$$

Using (A.16) for $i = \varphi$, $j = \ell$ and replacing with (B.29.2) and (B.29.3) the values of N_φ and N_ℓ, respectively, the value of $\bar{e}_\varphi$ will be found which, substituted into (A.6) with (B.1), will give

$$u = \frac{D_o \cos\theta}{2 T E}\left[-\frac{1+2\nu}{D_o}\frac{\sin\theta}{\cos^{3/2}\theta}\omega - \frac{2}{D_o\cos^{\frac{1}{2}}\theta}\frac{d\omega}{d\theta} + \frac{p D_o}{4}(1-\nu)\right] \qquad (B.29.4)$$

Recalling that equations (B.8.1) and (B.8.2) apply only to the bending solutions and that $\bar{\bar{\phi}} = 0$ for a sphere, determining ϵ from (B.8.2) and substituting into (B.6.2), the solution for ϕ is given by

$$\phi = -\frac{2}{T E D_o \cos^{\frac{1}{2}}\theta}\frac{d^2\omega}{d\theta^2} \qquad (B.29.5)$$

Using the previous equations, the bending moments are given from (A.12.1) and (A.12.2) respectively for meridional and circumferential moments,

$$M_\ell = \frac{1}{4\lambda^4}\left[\frac{1-2\nu}{2}\frac{\sin\theta}{\cos^{3/2}\theta}\frac{d^2\omega}{d\theta^2} + \frac{1}{\cos^{\frac{1}{2}}\theta}\frac{d^3\omega}{d\theta^3}\right] \qquad (B.29.6)$$

and

$$M_{\varphi} = \frac{1}{4\lambda^4}\left[\frac{2-\nu}{2}\frac{\sin\theta}{\cos^{3/2}\theta}\frac{d^2\omega}{d\theta^2} - \frac{\nu}{\cos^{\frac{1}{2}}\theta}\frac{d^3\omega}{d\theta^2}\right] \qquad (B.29.7)$$

Once determined, the constants in (B.11), which will be defined by the boundary conditions, equation (B.26) together with (A.5) to (A.8), (A.15) and (B.11) form the solution of the sphere problem, as long as the geometry lies within the original definitions, Section (B.1.1).

B.2.2 Shallow Spherical Shell

Both the membrane solution and the particular integral are the same as for the sphere, and so will not be here presented.

The edge bending value of F is given by (B.16), but the subscript b will be used here, otherwise it can be confused with the complete solution for the radial force, hence:

$$F_b r = C_1\,\mathrm{ber}'\chi + C_2\,\mathrm{bei}'\chi + C_3\,\mathrm{ker}'\chi + C_4\,\mathrm{ker}'\chi$$

Therefore, using (B.27.2), the complete solution for Fr is:

$$Fr = C_1\,\mathrm{ber}'\chi + C_2\,\mathrm{bei}'\chi + C_3\,\mathrm{ker}'\chi + C_4\,\mathrm{ker}'\chi + \frac{1}{8}pD_o^2\sin\theta\cos\theta \qquad (B.30.1)$$

Substituting Fr and (B.1) into (A.2), gives

$$N_{\varphi} = \frac{2}{D_o}\frac{d}{d\theta}(F_b r) + \frac{pD_o}{4} \qquad (B.30.2)$$

and replacing the value of $\bar{\bar{W}}$ from (B.26) with (B.30.1) into (A.4), the following result is obtained

$$N_{\ell} = \frac{2\sin\theta}{D_o\cos\theta}(F_b r) + \frac{pD_o}{4} \qquad (B.30.3)$$

Taking $\bar{e}_{\varphi}$ from (A.16) for $i = \varphi$ and $j = \ell$, N_{φ} and N_{ℓ} from (B.30.2) and (B.30.3), and substituting into (A.6) gives:

$$u = \frac{D_o\cos\theta}{2\,T\,E}\left[-\frac{2}{D_o}\frac{d}{d\theta}(F_b r) - \frac{2\nu}{D_o}\frac{\sin\theta}{\cos\theta}(F_b r) + (1-\nu)\frac{pD_o}{4}\right] \qquad (B.30.4)$$

Noting that (B.13.1) and (B.13.2) apply only for the edge bending solution and that $\bar{\emptyset} = 0$ for the shallow spherical shell, the following equation is obtained from (B.13.2):

$$\emptyset = -\frac{2}{TED_o}\left[\frac{d^2}{d\alpha^2}(F_b r) + \frac{1}{\alpha}\frac{d}{d\alpha}(F_b r) - (\frac{1}{\alpha^2} - \nu)(F_b r)\right] \qquad (B.30.5)$$

From equation (A.12.1) with (B.12) it is found for the meridional moment

$$M_\ell = \frac{2D}{D_o}(\frac{d\emptyset}{d\alpha} + \frac{\nu}{\alpha}\emptyset)$$

but using (B.13),

$$M_\ell = -\frac{1}{4\lambda^4}\left[\frac{d^3}{d\alpha^3}(F_b r) + \frac{1+\nu}{\alpha}\frac{d^2}{d\alpha^2}(F_b r) + (\frac{\nu-2}{\alpha^2} + \nu)\frac{d}{d\alpha}(F_b r) + (\frac{2-\nu}{\alpha^2} + \frac{\nu^2}{\alpha})(F_b r)\right] \qquad (B.30.6)$$

With the above-mentioned conditions, but this time using (A.12.2) instead of (A.12.1), the circumferential moment will be given by

$$M_\varphi = \frac{2D}{D_o}(\frac{1}{\alpha}\emptyset + \nu\frac{d\emptyset}{d\alpha})$$

hence,

$$M_\varphi = -\frac{1}{4\lambda^4}\left[\nu\frac{d^3(F_b r)}{d\alpha^3} + \frac{1+\nu}{\alpha}\frac{d^2(F_b r)}{d\alpha^2} + (\frac{1-2\nu}{\alpha^2} - \nu^2)\frac{d(F_b r)}{d\alpha} + (\frac{2\nu-1}{\alpha^3} + \frac{\nu}{\alpha})(F_b r)\right] \qquad (B.30.7)$$

Equations (B.30) together with (A.5) to (A.8), (A.10) and (A.15) form the solution of the problem for the shallow sphere as long as the geometry is within the conditions of approximation and once the constants in (B.16) are known from boundary conditions.

B.2.3 Solid Plate

Since (B.20) is the complete equation, it is obvious that the membrane value for the radial force, $\bar{\bar{F}}$, is zero and, hence, from substituting (B.3) into (A.4) the following result is obtained:

$$\bar{\bar{N}}_r = 0$$

a value to be expected since the pressure is normal to the mid-wall.

Introducing (B.3) into (A.1) and integrating, the following equation is obtained:

$$\bar{\bar{W}}r = \tfrac{1}{2} pr^2 + V$$

where V is a constant of integration. Since the plate is solid, and because the axial equilibrium at $r = r_o$ is given by $2\pi r_o \bar{\bar{W}} = \pi r_o^2 p$, it can be seen that $V = 0$, hence:

$$\bar{\bar{W}} = \tfrac{1}{2} pr \qquad (B.31)$$

Substituting $\bar{\bar{F}}$ and (B.3) into (A.2), the following result is obtained:

$$\bar{\bar{N}}_\varphi = 0$$

the expected value.

From (B.19) can be deduced that $\bar{\bar{\emptyset}}$ is not zero, since the vertical equilibrium has to be satisfied.

Substituting (B.31) into (B.19) and integrating the membrane solution for $\emptyset$ there obtained

$$\bar{\bar{\emptyset}} = -\frac{1}{16D} pr^3 \qquad (B.32)$$

Bearing in mind that it is a solid plate that is being considered, the edge bending solutions for $\emptyset$ and F given by (B.21) have an infinite value for $r = 0$, hence the constants of integration A" and B", respectively, must be zero. Those equations can, therefore, be written as follows:

$$\emptyset = A'r \tag{B.33.1}$$

and

$$F = B' \tag{B.33.2}$$

The complete solution for the solid plate will be given by the following equations:

since $\bar{\bar{F}} = 0$, from (B.33.2)

$$F = B' \tag{B.34.1}$$

Substituting (B.34.1) and (B.3) into (A.2)

$$N_{\varphi} = B' \tag{B.34.2}$$

and (B.3) with (B.34.1) into (A.4)

$$N_{\ell} = B' \tag{B.34.3}$$

Substituting (B.3) and the values of N_{ℓ} and N_{φ} into (A.16) for $i = \varphi$ and $j = \ell$, a value of $\bar{e}_{\varphi}$ is obtained which, substituted into (A.6), gives:

$$u = \frac{r}{TE}(1 - \nu)B'' \tag{B.34.4}$$

Adding (B.32) and (B.33.1) the solution for $\emptyset$ is given by

$$\emptyset = -\frac{1}{16D} pr^3 + A'r \tag{B.34.5}$$

Substituting $\emptyset$ and (B.3) into (A.12), the moment resultants are given by:

$$M_r = -\frac{pr^2}{16}(3 + \nu) + A'D(1 + \nu) \tag{B.34.6}$$

and

$$M_{\varphi} = -\frac{pr^2}{16}(1 + 3\nu) + A'D(1 + \nu) \tag{B.34.7}$$

These equations (B.34) together with (B.3), (A.5) to (A.8), (A.10) and (A.15) form the solution of a solid plate with pressure normal to its mid-wall surface; the constant of integration will be determined from the boundary conditions.

B.2.4 Cylinder

Referring to Figs. 3 and 4 and observing that axial equilibrium has to be satisfied at the junction, the following equation can be written:

$$\bar{\bar{W}}(x = 0) = \frac{pd}{4}$$

which is equivalent to (B.26) when $\theta = \alpha_o$.

The constant of integration from (A.1) will, therefore, be V = 0, thus:

$$\bar{\bar{W}} = \frac{pd}{4} \qquad \text{(B.34.1)}$$

Substituting the well known value of $\bar{\bar{N}}_\varphi$ $(= \frac{pd}{2})$ for the pressurised cylinder, and (B.2) into (A.2) and integrating, gives:

$$\bar{\bar{F}} = \bar{\bar{F}}_1$$

where $\bar{\bar{F}}_1$ is the constant of integration.

Taking (A.3) with the values of $\bar{\bar{W}}$ and $\bar{\bar{F}}$ substituted, as well as (B.2), and since the membrane definition implies zero bending moment, the following result is obtained:

$$\bar{\bar{F}}_1 = 0$$

and hence,

$$\bar{\bar{F}} = 0 \qquad \text{(B.34.2)}$$

Substituting $\bar{\bar{F}}$ into (B.22.2) gives

$$\bar{\bar{\emptyset}} = 0 \qquad \text{(B.34.3)}$$

These two latter equations have already been pointed out, in Section (B.1.4).

The value of $\bar{\bar{e}}_\varphi$ is obtained by substituting the membrane stress values ($\bar{\bar{\sigma}}_i$, $i = \ell, \varphi$) into (A.10), with $i = \varphi$ and $j = \ell$. Once $\bar{\bar{e}}_\varphi$ is known, it can be put into (A.6) giving

$$\bar{\bar{u}} = \frac{pd^2}{8\,Et}(2 - \nu) \qquad \text{(B.34.4)}$$

Since the membrane solutions are known, the complete solution (bending + membrane) for the cylinder can now be presented.

Recalling (B.25) and (B.34.2) the radial force will be given by

$$F = e^{kx}(A_1 \cos k\,x + A_2 \sin kx) + e^{-kx}(A_3 \cos kx + A_4 \sin kx) \tag{B.35.1}$$

Substituting (B.2) into (A.2) and using $\bar{\bar{N}}_\varphi = pd/2$,

$$N_\varphi = \frac{d}{2}\frac{dF}{dx} + p\,\frac{d}{2} \tag{B.35.2}$$

Replacing (B.2) and (B.34.1) into (A.4) gives

$$N_\ell = \frac{pd}{4} \tag{B.35.3}$$

Substituting the values of N_φ and N_ℓ into (A.16) for $i = \varphi$ and $j = \ell$, a value of $\bar{e}_\varphi$ will be obtained, which, substituted into (A.6), gives for u:

$$u = \frac{d^2}{4Et}\left(\frac{dF}{dx} + p - \frac{\nu}{2}p\right) \tag{B.35.4}$$

Similarly, recalling (B.22.2) gives

$$\emptyset = -\frac{d^2}{4Et}\frac{d^2F}{dx^2} \tag{B.35.5}$$

Replacing $\emptyset$ and (B.2) into (A.12), the moment resultants will be given by:

$$M_\ell = -\frac{1}{4k^4}\,\frac{d^3F}{dx^3} \tag{B.35.6}$$

and

$$M_\varphi = \nu\, M_\ell \tag{B.35.7}$$

Having been determined, the constants of integration in (B.35.1) which are obtained from the boundary conditions, equations (B.35) together with (A.5) to (A.8), (A.10) and (A.15), form the solution to the problem of the pressurised cylindrical shell, as long as the geometry is within the conditions of approximation.

B.3 Constants of Integration

Since the ends away from the junction are considered to have membrane conditions, the edge bending solution at the connection (cylinder-sphere intersection) has to diminish away from the junction or at some distance from the junction which increases nearer to the end with membrane conditions. Therefore in (B.11), (B.15) and (B.25), for the sphere, shallow sphere and cylinder, respectively, only the terms that die away when the independent variable takes values different from the junction value should be taken, e.g. for the cylinder in a flush nozzle, Fig. 3, where $x = 0$ at the junction and x is positive only the terms that contain e^{-kx} should be considered, unless on the other end of the cylinder ($x = \ell$, where ℓ is equal to cylinder length), some conditions other than membrane conditions were applied.
The same reasoning can be applied to the sphere and shallow sphere with the intention of finding out which terms should be applied to the particular geometry.

B.3.1 Flush Nozzle

Let the flush nozzle, Fig. 3, be considered as a whole.

B.3.1.1 Cylinder-Sphere Geometry

Cylinder - x is positive and increasing, therefore, from (B.25), the edge value of F may be written as

$$F = e^{-kx}(A_3 \cos kx + A_4 \sin kx) \qquad (B.36.1)$$

Sphere - θ is negative and increasing, hence, from (B.11), the value of ω for the edge bending condition may be calculated by

$$\omega = e^{-\lambda\theta}(C_3 \cos \lambda\theta + C_4 \sin \lambda\theta) \qquad (B.36.2)$$

Hence, from equations (B.36), it can be seen that only four constants of integration need to be determined from the boundary conditions.

B.3.1.2 Cylinder-Shallow Sphere Geometry

As it has been pointed out before in this appendix, when d/2R has a small value, which corresponds to α near zero, the solution for the shallow sphere should be applied, particularly in cases of high bending conditions at the junction, Refs. [1] and [4].

Because the shallow sphere has been studied only for θ near + $\pi/2$ and therefore θ positive, the cylinder has to be taken in an opposite sense to that of Fig. 3, hence, x is negative and decreasing.

Cylinder - x is negative and decreasing, so as a consequence of (B.25):

$$F = e^{kx}(A_1 \cos kx + A_2 \sin kx) \qquad (B.37.1)$$

Shallow sphere - α positive and increasing, therefore the same conditions are found to χ (B.16); from (B.17) and (B.18), it can be seen that for the shallow sphere, equations (B.18) should be taken. These are an approximation to the ker and kei functions, hence for the edge bending conditions the solution (B.16) should be taken as

$$F_b r = C_3 \text{ ker}'\chi + C_4 \text{ kei}'\chi \qquad (B.37.2)$$

B.3.2 Spherical Head

Referring to Fig. 4, it can be seen that the cylinder has x negative and the sphere has θ negative, but if the shallow sphere solution is to be applied, then because θ was taken near + $\pi/2$, the reverse situation will be found, just because of the same reason as that for the cylinder-shallow sphere geometry, and therefore x and χ are positive.

B.3.2.1 Cylinder-Sphere Geometry

Cylinder - x is negative and decreasing, hence the same situation will apply to the cylinder as to the cylinder-shallow sphere geometry, Section B.3.1.2, and so (B.37.1) should be applied.

Sphere - θ is negative and decreasing, therefore the terms in $e^{\lambda\theta}$ of (B.10) should be applied, hence

$$\omega = e^{\lambda\theta}(C_1 \cos \lambda\theta + C_2 \sin \lambda\theta) \qquad (B.38)$$

B.3.2.2 Cylinder-Shallow Sphere Geometry

Cylinder - x is positive and increasing, so in consequence, it is the same case as for the cylinder of the cylinder-sphere geometry of a flush nozzle, and therefore (B.36.1) can be applied.

Shallow sphere - from Section B.3.2, α is positive and decreasing, therefore equation (B.17) which is an approximation to ber and bei functions, should be applied, hence, from (B.16), the solution for $F_b r$, to the edge bending conditions can be written as follows:

$$F_b r = C_1 \text{ ber}'\chi + C_2 \text{ bei}'\chi \qquad (B.39)$$

B.3.2.2 Cylinder-Solid Plate Geometry

The cylinder has the same solution as in section B.3.2.2 but the solid plate case does not have damping consideration.

—— (B.10), (B.15) and (B.22) having been reduced to their simplest forms, and because of the membrane conditions far from the junction, it may be seen that each particular intersection case will only need four boundary conditions at the connection, since only four constants of integration are necessary in order to solve the problem completely.

B.4 Boundary Conditions for Cylinder-Sphere Intersections

Referring to Figs. 3 to 5 can be seen that the boundary conditions for cylinder-sphere intersections for nozzles, Fig. 3, and heads, Figs. 4 and 5, can be of displacement and rotation type and as well as of forces and moment type.

In order to obtain geometric continuity at the junction, the radial displacement and the rotation there should be equal for the cylinder and sphere. Using the subscripts c for the cylinder and s for the sphere or plate, these conditions are as follows:

$$u_c = u_s \tag{B.40.1}$$

and

$$\phi_c = \phi_s \tag{B.40.2}$$

In order to satisfy the equilibrium at the junction the radial force and meridional bending moment have to be in equilibrium, therefore:

$$F_c = F_s \tag{B.40.3}$$

and

$$M_{\ell_c} = M_{\ell_s} \tag{B.40.5}$$

because no extra loads have been considered other than the internal pressure.

Equations (B.40) are four boundary conditions that can be used in order to evaluate the four constants of integration, (A_3,A_4,C_3,C_4), (A_1,A_2,C_3,C_4), (A_1,A_2,C_1,C_2), (A_3,A_4,C_1,C_2) and (A_3,A_4,A',B') respectively, the first two for the flush cylinder and the last three for the spherical head. Hence, it can be seen that a system of linear equations has been formed having dimensions [4 x 4] and its solution gives the four constants of integration, and hence the complete solution can be found.

APPENDIX C

MARCAL'S METHOD FOR ELASTIC-PLASTIC ANALYSIS OF SYMMETRICALLY LOADED SHELLS OF REVOLUTION

Marcal's method has been known as the "stiffness method" Ref. [3], [5] and [6], but presently it is called the "tangent modulus method", [6], and it has been employed in investigations into small elastic-plastic deformations in pressure vessels, e.g. in Refs. [7], [8], [9]. This method uses the von Mises' criterion and the Prandtl-Reuss. equations of plasticity.

C.1 Partial Stiffness

Using the Prandtl-Reuss equations in order to write the elastic-plastic stress-strain increment relationships, the following equation may be obtained:

$$\delta e_i = \frac{3}{2}\frac{\sigma_i'}{\sigma_e}\delta \bar{e}_p + \frac{1}{E}(\delta\sigma_i - \nu\delta\sigma_j),\ i,j = \ell,\varphi \qquad (C.1)$$

Denoting the slope of the equivalent stress to equivalent plastic strain curve by H', and differentiating the von Mises yield criterion, the following equation is obtained:

$$2\sigma_e H'\,\delta\bar{e}_p = 3\sigma_\ell'\,\delta\sigma_\ell + 3\sigma_\varphi'\,\delta\sigma_\varphi \qquad (C.2)$$

Defining a one-column matrix of individual stresses and equivalent plastic strain increments, $\{\delta\sigma_\ell\ \delta\sigma_\varphi\ \delta\bar{e}_p\}$, the equations (C.1), for $(i = \ell,\ j = \varphi)$ and $(i = \varphi,\ j = \ell)$, together with (C.2), may be written in a matrix form, thus:

$$\begin{bmatrix} \frac{1}{E} & -\frac{\nu}{E} & \frac{3}{2}\frac{\sigma_\ell'}{\sigma_e} \\ -\frac{\nu}{E} & \frac{1}{E} & \frac{3}{2}\frac{\sigma_\varphi'}{\sigma_e} \\ \frac{3}{2}\frac{\sigma_\ell'}{\sigma_e} & \frac{3}{2}\frac{\sigma_\varphi'}{\sigma_e} & -H' \end{bmatrix} \begin{bmatrix} \delta\sigma_\ell \\ \delta\sigma_\varphi \\ \delta\bar{e}_p \end{bmatrix} = \begin{bmatrix} \delta e_\ell \\ \delta e_\varphi \\ 0 \end{bmatrix} \qquad (C.3)$$

Since this system of equations is linear, it can be inverted thereby giving the increments of the individual stress, and the equivalent plastic strain to the individual strain increments. These increments can also be written in a partial differential form:

$$\delta\sigma_i = \frac{\partial\sigma_i}{\partial e_i}\delta e_i + \frac{\partial\sigma_i}{\partial e_j}\delta e_j, \quad i,j = \ell,\varphi \tag{C.4.1}$$

and

$$\delta\bar{e}_p = \frac{\partial\bar{e}_p}{\partial e_\ell}\delta e_\ell + \frac{\partial\bar{e}_p}{\partial e_\varphi}\delta e_\varphi \tag{C.4.2}$$

because $\sigma_i = \sigma_i(e_i,e_j)$, $\bar{e}_p = \bar{e}_p(e_i,e_j)$, $(i,j = \ell,\varphi)$ and $e_i = e_i(\ell,z,L)$.

Marcal and Pilgrim [5] call the partial derivatives in (C.4.1) "partial stiffnesses"; these may be determined by inverting the matrix in (C.3). In the same way, the partial derivatives of the equivalent plastic strain in respect of each individual strain can be found.

C.2 Stiffness Coefficients

Considering the stress and moment resultants, $(N_i,M_i,i = \ell,\varphi)$, the following equations may be written:

$$\delta N_i = \frac{\partial N_i}{\partial e_i}\delta e_i + \frac{\partial N_i}{\partial e_j}\delta e_j, \quad i,j = \ell,\varphi \tag{C.5.1}$$

and

$$\delta M_i = \frac{\partial M_i}{\partial e_i}\delta e_i + \frac{\partial M_i}{\partial e_j}\delta e_j, \quad i,j = \ell,\varphi \tag{C.5.2}$$

Another form of equations (A.7) and (A.8), may be written thus:

$$e_i = \bar{e}_i + z\phi_i, \quad i = \ell,\varphi \tag{C.6}$$

where ϕ_i denotes the in-plane curvature change; therefore comparing (C.6) with (A.7) and (A.8),

$$\phi_\ell = \frac{d\phi}{d\ell} \tag{C.7}$$

and

$$\phi_\varphi = \frac{\sin\theta}{r}\,\phi$$

The total increment of the individual strain is given by the sum of the increments of the mid-wall strain, $\bar{e}_i$, and of the strain increments from the increment of curvature change, $\delta\emptyset_i$, hence using (C.6), the total increment is given by:

$$\delta e_i = \delta\bar{e}_i + z\,\delta\emptyset_i \,, \quad i = \ell,\varphi \tag{C.8}$$

Differentiating the integral form of (A.11) and (A.12) in respect to the individual strains, and substituting (C.4.1), the following results are obtained:

$$\delta N_i = \int_{-h/2}^{h/2} \delta\sigma_i \, dz \quad \text{with } i = \ell,\varphi \tag{C.9}$$

and

$$\delta M_i = \int_{-h/2}^{h/2} \delta\sigma_i \, z dz \quad \text{with } i = \ell,\varphi \tag{C.10}$$

Replacing (C.8) for $i = \ell,\varphi$, with (C.7) into (C.4.1), the increments of the individual stresses in relation to the increment of the mid-wall strain, and, to the strains from the increment of the curvature change, are given by

$$\delta\sigma_i = \frac{\partial\sigma_i}{\partial e_i}(\delta\bar{e}_i + z\,\delta\emptyset_i) + \frac{\partial\sigma_i}{\partial e_j}(\delta\bar{e}_j + z\delta\emptyset_j), \; i,j = \ell,\varphi \tag{C.11}$$

Using (C.11) either for ($i = \ell$, $j = \varphi$) or ($i = \varphi$, $j = \ell$), and substituting into (C.9) and (C.10) with either $i = \ell$ or $i = \varphi$ respectively, the values of the partial derivatives of the stress and moment resultants are given by:

$$\frac{\partial N_i}{\partial\bar{e}_j} = \int_{-h/2}^{h/2} \frac{\partial\sigma_i}{\partial e_j} dz \,, \; i,j = \ell,\varphi \tag{C.12.1}$$

$$\frac{\partial N_i}{\partial\emptyset_j} = \int_{-h/2}^{h/2} \frac{\partial\sigma_i}{\partial e_j} z dz, \quad i,j = \ell,\varphi \tag{C.12.2}$$

and

$$\frac{\partial M_i}{\partial \bar{e}_j} = \int_{-h/2}^{h/2} \frac{\partial \sigma_i}{\partial e_j} \, z dz \quad , \quad i,j = \ell,\varphi \tag{C.13.1}$$

$$\frac{\partial M_i}{\partial \bar{\varphi}_j} = \int_{-h/2}^{h/2} \frac{\partial \sigma_i}{\partial e_j} \, z^2 dz \quad , \quad i,j = \ell,\varphi \tag{C.13.2}$$

The partial derivatives on the left hand side of (C.12) and (C.13) are known as the "stiffness coefficients", Refs. [4] and [5], and are expressed as an integral form of the partial stiffnesses.

C.4 Transition Elements

Once the load which causes first yield at any point in the shell has been obtained from an elastic analysis, then, using the equations explained in Appendix A, together with von Mises yield criterion, the procedure consists of adding fractional increments to the first yield load. All the other elements, therefore, except the most stressed, will undergo, during the incremental loading, an elastic deformation and, at a certain stage in the increment action, the deformation will become elasto-plastic. Such elements are collectively known as the "transition region", Refs. [5], [8] and [9]. Hence, those elements that yield during a particular increment will have a partial stiffness form in two parts, one elastic and the other elasto-plastic.

The elastic partial stiffnesses are easily obtained from the generalised Hooke's law of elasticity, thus:

$$\frac{\partial \sigma_i}{\partial e_i} = \frac{E}{1 - \nu^2} \quad , \quad i = \ell,\varphi \tag{C.14}$$

and

$$\frac{\partial \sigma_i}{\partial e_j} = \frac{\nu E}{1 - \nu^2} \quad , \; i \neq j, \; i,j = \ell,\varphi$$

In the transition elements, the strains caused by the next successive increment are estimated by making them equal to the previous load increment and then scaling them to the elastic limit.

In order to determine these values, the yield stresses of the transition elements must be known; when they are, the partial stiffnesses can be calculated, by assuming elastic-plastic behaviour. The mix partial stiffness at the transition element is given by

$$\left.\frac{\partial \sigma_i}{\partial e_j}\right|_{mix} = m \left.\frac{\partial \sigma_i}{\partial \sigma_j}\right|_{elastic} + (1 - m) \left.\frac{\partial \sigma_i}{\partial e_j}\right|_{plastic} \qquad (C.15)$$

where m is the scaling factor.

Usually, the initial value of m is a rough estimate, and the strain values produced by the subsequent calculation should be compared with the previous estimated values. This process is repeated until a value of strain considered to be within an assumed error, as compared with the value of the previous iteration, is reached.

Once the transition elements have passed the elastic yield limit, the calculation is made using the stiffness coefficients derived in Section C.3, and the partial stiffnesses, Section C.2.

C.5 Method of Solution

Once the elastic analysis has been performed using the thin shell equation, Appendix A, the first yield load having been found (von Mises criterion), the solution of the problem is obtained by making use of the incremental form of the thin shell equations, in which the von Mises criterion is employed with the partial stiffness or mix partial stiffness, using the stiffness coefficient explained previously in this appendix, and each time incrementing the load.

The numerical solution is obtained by using a step-by-step predictor-corrector integration method with Newton-Rophson boundary control.

These methods are used as demonstrated in Refs. [3], [5] and [6], in that they are the most suitable for a finite difference solution for the elastic-plastic analysis of thin shells.

APPENDIX D

A NON-LINEAR STRAIN DISTRIBUTION THROUGH THE THICKNESS OF SYMMETRICALLY LOADED SHELLS OF REVOLUTION

The assumptions made are the same as those for thin shell theory, except that the strain distribution through the wall thickness is appraised in the same way as "Winkler's theory of curved beams", Ref. [11], p.249, but applied here to symmetrically loaded shells of revolution in that region which has ratios of thickness to meridional radius larger than 0.1. This approximation, although inconsistent with a thin shell theory, gives better results than either this theory, Refs. [3] and [9], or the "O'Connell modification" (or the band modification) Ref. [8], and Chapters 3 and 4 of this thesis.

The general case is considered first, then the assumptions concerning ratios of thickness to radius of curvature are introduced.

Referring to Fig. 2, the angles θ before and after deformation are, respectively

$$\theta \quad \text{and} \quad \theta - \phi$$

where ϕ is the angle through which the mid-wall surface of the shell at the corresponding point θ has rotated; the radial radius r for any point on the cross-section θ, is therefore, $r + z \cos \theta$.

The mid-wall radial radius r, after deformation, becomes $r + u$, $r + z \cos \theta$ becomes $r + u + z \cos (\theta - \phi)$, and the meridional radius b becomes $b + \delta b$, hence the mid-wall strain and the strain at any point in the thickness, respectively, may be written thus:

Hoop strain,

$$\bar{e}_{\varphi} = \frac{u}{r} \tag{D.1.1}$$

$$e_{\varphi} = \frac{\bar{e}_{\varphi} + \frac{z}{r} \phi \sin \theta}{1 + \frac{z}{r} \cos \theta} \tag{D.1.2}$$

Meridional strain,

$$\bar{e}_{\ell} = \frac{1}{\sin \theta} \frac{du}{d\ell} + \emptyset \cot \theta \qquad (D.2.1)$$

$$e_{\ell} = \frac{\bar{e}_{\ell} + z \frac{d\emptyset}{d\ell}}{1 + \frac{z}{b}} \qquad (D.2.2)$$

Defining a variable U_i, $i = \ell, \varphi$ such that

$$U_i = C_i \, h, \quad i = \ell, \varphi \qquad (D.3.1)$$

with

$$C_{\ell} = \frac{1}{b} \qquad (D.3.2)$$

and

$$C_{\varphi} = \frac{\cos \theta}{r} \qquad (D.3.3)$$

and defining a function $f(U_i)$ by

$$f(U_i) = 2 U_i - \ell n \left(\frac{1 + U_i}{1 - U_i} \right) \qquad (D.4.1)$$

or, limiting U_i to a value of less than unity, $(U_i < 1)$, the function $f(U_i)$ can be written in a series form by

$$f(U_i) = - \sum_{n=1}^{\infty} \frac{2 U_i^{2n+1}}{2n + 1} \qquad (D.4.2)$$

Because the values of the following integrals are required for the calculation of the stress and moment resultants, as functions of $\bar{e}_{\ell}$, $\bar{e}_{\varphi}$ and $\emptyset$, they are presented here, but without the use of the index i:

$$\int_{-h}^{+h} \frac{dz}{1 + Cz} = \frac{1}{C} [2U - f(U)] \qquad (D.5.1)$$

$$\int_{-h}^{h} \frac{z dz}{1 + Cz} = \frac{1}{C^2} f(U) \qquad (D.5.2)$$

$$\int_{-h}^{h} \frac{z^2 dz}{1 + Cz} = - \frac{1}{C^3} f(U) \qquad (D.5.3)$$

Integrating e_i, $i = \ell,\varphi$, with respect to z,

$$\int_{-h}^{h} e_i dz = \bar{e}_i \left[\frac{1}{C_i} (2U_i - f(U_i) \right] + \emptyset_i \frac{1}{C_i^2} f(U_i) \qquad (D.6.1)$$

and $e_i z$, $i = \ell,\varphi$, with respect to z,

$$\int_{-h}^{h} e_i z dz = \bar{e}_i \frac{1}{C_i^2} f(U_i) - \emptyset_i \frac{1}{C_i^3} f(U_i) \qquad (D.6.2)$$

where $\emptyset_i$, $i = \ell,\varphi$, is given by

$$\emptyset_\ell = \frac{d\emptyset}{d\ell} \qquad (D.7.1)$$

$$\emptyset_\varphi = \frac{\sin \theta}{r} \emptyset \qquad (D.7.2)$$

as used in Appendix C, (C.7).

The stress resultants are given by

$$N_i = \int_{-h}^{+h} \sigma_i \, dz \quad , \quad i = \ell,\varphi$$

and the moment resultants by

$$M_i = \int_{-h}^{+h} \sigma_i \, z dz, \quad i = \ell,\varphi$$

However, from the generalised Hooke's law

$$\sigma_i = \frac{E}{1 - \nu^2} (e_i + \nu e_j), \; i,j = \ell,\varphi$$

therefore, using (D.6), the following expressions can be deduced for N_i and M_i, $i = \ell,\varphi$, respectively:

$$N_i = \frac{E}{1-\nu^2}\left[\bar{e}_i \frac{1}{C_i}[2U_i - f(U_i)] + \phi_i \frac{1}{C_i^2} f(U_i) + \nu\left(\bar{e}_j \frac{1}{C_j}[2U_j - f(U_j)] + \phi_j \frac{1}{C_j^2} f(U_j)\right)\right] \tag{D.8.1}$$

and

$$M_i = \frac{E}{1-\nu^2}\left[\bar{e}_i \frac{1}{C_i^2} f(U_i) - \phi_i \frac{1}{C_i^3} f(U_i) + \nu\left(\bar{e}_j \frac{1}{C_j^2} f(U_j) - \phi_j \frac{1}{C_j^3} f(U_j)\right)\right] \tag{D.8.2}$$

with $i,j = \ell,\varphi$.

If the assumptions of $U_i \ll 1$ for $i = \ell$ and $i = \varphi$, the linear strain distribution assumption, are made, (D.8.1) and (D.8.2) accordingly generate equations (A.11) and (A.12).

Since geometries possessing small radii of curvature are the knuckle regions in either radial nozzles or heads, the following assumptions are made, as in Ref. [3]:

$$\frac{\cos\theta}{r} h \ll 1 \tag{D.9.1}$$

and

$$\frac{h}{b} < 1 \tag{D.9.2}$$

When θ is near to $\pi/2$, near the axis of symmetry, condition (D.9.1) is not satisfied and the following expressions should not therefore be applied, e.g. cone part near the vortex.

The radial radius is assumed to be of the form

$$r = a + b\cos\theta$$

where a and b are constants for each particular shell element as in the computer programs used in this work, and hence b is the meridional radius of the shell element.

Introducing (D.4.2) and conditions (D.9) into (D.8.1), with, respectively, $i = \ell$, $j = \varphi$ and $i = \varphi$, $j = \ell$, the following equations are obtained:

$$N_\ell = \frac{E}{1 - \nu^2}\left[2h(\bar{e}_\ell + \nu\bar{e}_\varphi) + 2b\sum_{n=1}^{\infty}\frac{(\frac{h}{b})^{2n+1}}{2n+1}\left(\bar{e}_\ell - b\frac{d\emptyset}{d\ell}\right)\right] \qquad (D.10.1)$$

and

$$N_\varphi = \frac{E}{1 - \nu^2}\left[2h\,(\bar{e}_\varphi + \nu\bar{e}_\ell) + 2\nu b\sum_{n=1}^{\infty}\frac{(\frac{h}{b})^{2n+1}}{2n+1}\left(\bar{e}_\ell - b\frac{d\emptyset}{d\ell}\right)\right] \qquad (D.10.2)$$

Using the same procedure as with the equations of (D.10), but now with (D.8.2), the following expressions are obtained for M_ℓ and M_φ, respectively:

$$M_\ell = \frac{E}{1 - \nu^2}\left[\frac{2h^3}{3}\left(\frac{d\emptyset}{d\ell} + \nu\frac{\sin\theta}{r}\,\emptyset\right)\right. \qquad (D.11.1)$$

$$\left. - 2b^2\left(\frac{1}{3}\left(\frac{h}{b}\right)^3\bar{e}_\ell + \sum_{n=2}^{\infty}\frac{(\frac{h}{b})^{2n+1}}{2n+1}\left[\bar{e}_\ell - b\frac{d\emptyset}{d\ell}\right]\right)\right]$$

and

$$M_\varphi = \frac{E}{1 - \nu^2}\left[\frac{2h^3}{3}\left(\frac{\sin\theta}{r}\,\emptyset + \nu\frac{d\emptyset}{d\ell}\right)\right. \qquad (D.11.1)$$

$$\left. - 2\nu b^2\left(\frac{1}{3}\left(\frac{h}{b}\right)^3\bar{e}_\ell + \sum_{n=2}^{\infty}\frac{(\frac{h}{b})^{2n+1}}{2n+1}\left[\bar{e}_\ell - b\frac{d\emptyset}{d\ell}\right]\right)\right]$$

Comparing (D.10) with (A.11), and (D.11) with (A.12), it can be seen that the new values of N_ℓ, N_φ, M_ℓ and M_φ receive further contributions from $\bar{e}_\ell$ and $\frac{d\emptyset}{d\ell}$.

The derivative of M_ℓ in respect to ℓ is necessary in equation (A.3),

$$\frac{dM_\ell}{d\ell} = \frac{2Eb^3}{1-\nu^2}\left[\sum_{n=1}^{\infty} \frac{(\frac{h}{b})^{2n+1}}{2n+1}\right]\frac{d^2\phi}{d\ell^2}$$

$$+ \frac{2Eb^3}{1-\nu^2}\left[\frac{1}{3}(\frac{h}{b})^3 \frac{\nu \sin\theta}{r} + \frac{1}{b}\sum_{n=1}^{\infty}(\frac{h}{b})^{2n}\beta\right]\frac{d\phi}{d\ell}$$

$$+ \frac{2Eb^3}{1-\nu^2}\left[\frac{1}{3}(\frac{h}{b})^3\left(\frac{\nu}{r}\frac{d(\sin\theta)}{d\ell} - \nu\frac{\sin^2\theta}{r^2}\right) + \nu\frac{h^2}{b^3}\frac{\sin\theta}{r}\beta\right]\phi$$

$$- \frac{2Eb^3}{1-\nu^2}\left[\frac{1}{b^2}\beta\sum_{n=1}^{\infty}(\frac{h}{b})^{2n}\bar{e}_\ell + \frac{1}{b}\sum_{n=1}^{\infty}\frac{(\frac{h}{b})^{2n+1}}{2n+1}\frac{d\bar{e}_\ell}{d\ell}\right]$$

From (A.3), substituting M_ℓ, M_φ, $\frac{dM_\ell}{d\ell}$ and $f(\frac{h}{b})$ from (D.4.2), and using $f'(\frac{h}{b})$ as the derivation of f in respect to $\frac{h}{b}$, the following expression is obtained:

$$\frac{d^2\theta}{d\ell^2} = \left[\left(\frac{1}{3}\frac{(\frac{h}{b})^3}{f(\frac{h}{b})} + 1\right)\frac{\nu\sin\theta}{r} - \frac{1}{b}\frac{f'(\frac{h}{b})}{f(\frac{h}{b})}\beta - \frac{\sin\theta}{r}\right]\frac{d\phi}{d\ell}$$

$$+ \left[\frac{1}{3}\frac{(\frac{h}{b})^3}{f(\frac{h}{b})}\left(\frac{\nu}{r}\cos\theta\frac{d\theta}{d\ell} - \frac{\sin^2\theta}{r^2}\right) + \frac{\nu h^2}{b^3}\frac{\sin\theta}{r}\beta\frac{1}{f(\frac{h}{b})}\right]\phi$$

$$+ \left[-\frac{\nu}{b}\frac{\sin\theta}{r} + \frac{1}{b}\frac{\sin\theta}{r} + \frac{1}{b^2}\beta\frac{f'(\frac{h}{b})}{f(\frac{h}{b})}\right]\bar{e}_\ell$$

$$+ \frac{1}{b}\frac{d\bar{e}_\ell}{d\ell} - \frac{1-\nu^2}{2E}\frac{1}{b^3}F\cos\theta + \frac{1-\nu^2}{2E}\frac{1}{b^3}\frac{1}{f(\frac{h}{b})}W\sin\theta \qquad (D.13)$$

Substituting N_φ from (D.10.2) into (A.2) the following equation is obtained for the derivation of F in respect to ℓ:

$$\frac{dF}{d\ell} = -\frac{\sin\theta}{r} - p\cos\theta + \frac{2Eh}{1-\nu^2}\frac{1}{r}(\bar{e}_\varphi + \nu\bar{e}_\ell) - 2hX$$

$$-\frac{2Eh}{1-\nu^2}\ \frac{1}{r}\ f(\frac{h}{b})\left(\bar{e}_\ell - b\frac{d\emptyset}{d\ell}\right) \qquad (D.14)$$

Comparing (D.14) and (D.13), with (A.2.1) and (A.14), respectively, it can be seen that an extra contribution from $\bar{e}_\ell$ and $\frac{d\emptyset}{d\ell}$ is obtained for the former equations due to the assumption of a non-linear strain distribution. (D.14) and (D.13) will, therefore, replace (A.2.1) and (A.14) in a numerical analysis, when the $2h/\rho < .1$ assumption of the meridional plane of thin shell theory is not fulfilled as regards the linear strain distribution through the thickness. The same applies to (D.10) and (D.11), in relation to (A.11) and (A.12) respectively.

When an elastic-plastic analysis is carried out using the method described in Appendix C, the procedure is exactly the same, except that the incremental form of the equations is used.

For more details of this modification see Ref. [3].

I–24

Computed Elastic-Plastic Behaviour and Shakedown of Some Radial Nozzle-on-Sphere Geometries

V. M. SAMPAYO and C. E. TURNER
Imperial College
London, England

ABSTRACT

Elastic-plastic computations are described for cylindrical nozzle-on-sphere junctions. Various geometrical details of the junction are examined to ensure that results for shakedown and collapse are not greatly affected by such differences of detail. Brief comparison is made of computed plastic strain and previously determined experimental results on a head, to verify the general reasonableness of the results. The effect of work hardening is studied with particular reference to the assumption of how the range of stress available for shakedown can best be represented, and how incipient collapse best defined. A range of nozzle to sphere diameters is then studied. The results show that the details of geometry have little effect on shakedown or collapse. It is concluded that the most realistic model for work hardening implies a translation rather than expansion of the yield surface and that, except for cases with low stress concentration, the effect of work hardening on shakedown and collapse is small, and that for such low stress concentrations, incipient collapse may precede shakedown.

NOMENCLATURE

d mean diameter of cylindrical nozzle

D mean diameter of spherical vessel

k_1 stress concentration factor; ratio of maximum von Mises equivalent stress to membrane equivalent stress (SCF)

k_1^* stress concentration factor; ratio of maximum shear stress to membrane shear stress. The * notation also applies to k_2 and k_3

k_2 ratio of shakedown pressure to membrane yield stress ($= P_s^x/k_1$)

k_3 ratio of collapse pressure to membrane yield stress ($= P_c^x/k_1$)

P internal pressure

P_y pressure for first yield anywhere in the vessel

P_c^x ratio of collapse pressure to first yield pressure

P_s^x ratio of shakedown pressure to first yield pressure

r radius of toroidal knuckle

t thickness of cylindrical nozzle

T thickness of spherical vessel

σ_m^x ratio of meridional stress to yield or proof stress

σ_c^x ratio of circumferential stress to yield or proof stress

w nozzle parameter (Ref. 20) $d/\sqrt{2DT}$

ABBREVIATIONS (FOR FURTHER DETAILS SEE TEXT)

In connection with shakedown based on: –

SEM elastic calculations by the method of Macfarlane and Findlay (Ref. 7)

SEL elastic calculations from Leckie (Ref. 20)

SPC elastic-plastic computations with the ellipse of yielding moving along the path of the elastic stress ratios

SPT elastic plastic computations with the ellipse of yielding moving along the radius to the actual stress point considered

SPW elastic plastic computations with the ellipse of yielding increasing in size with work hardening.

Note: Case SPT is used for values of k_2 Tables 3 and 6.

In connection with incipient collapse: Intersection of the elastic line with the tangent drawn to a particular point on a given curve defined by: –

C3I a line of one third the elastic slope intersecting an individual strain curve

C3E a line of one third the elastic slope intersecting an equivalent strain curve

C3D a line of one third the elastic slope intersecting the overal deflection curve

based on the pressure to cause: –

C5I 0.5 percent individual maximum strain on the outside surface

C5E 0.5 percent equivalent maximum strain on the outside surface

Note: Criterion C5I is used for values of k_3 Tables 2 and 4.

INTRODUCTION

The practice of allowing a small amount of plastic flow to occur early in the life of a vessel is well established. The amount of plastic flow is restricted by the need to avoid one or more of three possible modes of behavior; plasticity sufficiently gross in either magnitude or extent to lead to bursting or plastic collapse of a major feature of the vessel; cumulative increments of small scale plasticity leading to incremental collapse or "ratcheting"; alternating plastic flow leading to low cycle fatigue. Other modes of failure such as thermal and conventional high cycle fatigue, creep, corrosion and brittle fracture have to be guarded against, of course, but these are outside the scope of the present paper. In considering the extent of plastic flow permissible, it is convenient to distinguish three loosely defined regions of a vessel; general shell or membrane regions, extensive features of well defined geometry, such as end closures, and local features often with a geometry only defined nominally, such as nozzle details or reinforcing rings. Collapse of a vessel shell or head, or small scale plasticity leading to either incremental collapse or fatigue in a region of stress concentration are the primary features to be avoided. The former might occur on a single overload and the latter from a few thousand repeated loadings to design pressure.

Although in thick walled vessels, and even in certain cases of thin walled vessels such as gas pipe lines and some containment vessels made of very rapidly work hardening material [1] the main shell is deliberately taken beyond yield, for most vessels and materials the attainment of general yield in the shell or head is an obvious design point often limiting in itself or at least providing a "stake point" from which to proceed carefully. At such a point the membrane regions of a vessel are protected from bursting by work hardening. Where collapse may set in from bending action, subsequent changes in geometry may delay the onset of complete collapse. The normal method of predicting general yield is to assess the collapse level by limit analysis using the original shape [2], [3] to determine upper and lower bounds of load in between which collapse of the component must occur, in the absence of work hardening or changes in geometry. The effect of changes in geometry in increasing the limit pressure of some nozzles has also been studied [4].

A great advantage of this method is that the real pattern of plastic flow leading to collapse need not be considered so that estimates of the lower bounds can be made from elastic solutions and of the upper bound from any plausible (but not necessarily correct) deformation pattern that can be envisaged.

Incremental collapse or low cycle fatigue are in principle cycle dependent and must be so treated if a limited life design is proposed. For many purposes an assurance of avoidance of these problems is preferred since some small degree of conservatism gives a certain latitute for the acceptability of unknowns in the anticipated service experience of the vessel. In these circumstances the concept of shakedown [5] or the settlement of a component to entirely elastic behavior after some initial excursion into the plastic region, has become an accepted criterion. Although the principle is clear in allowing material to experience only a cycle of stress between tensile and compressive yield and thereby remain entirely elastic, the concept becomes blurred when details of the process are considered. Predictions can again be based on an extension of elastic solutions [6], [7], thus avoiding the complexities of plastic analysis but some doubt exists on how far such solutions might be affected by work hardening, and the detail of the analysis used to determine the elastic stress concentration factors.

The object of the present paper is to extend the study of these two modes of behavior, collapse and shakedown, by means of an elastic-plastic computer program. Earlier work [8], [9], [10], [11] has shown the general feasibility of such studies and confirmed their reasonableness in the broadest terms but it must be clear that only continued experimentation and service experience can finally confirm the correctness or otherwise of the predictions. Whereas confidence in prediction of elastic shell theory, whether applied by numerical or algebraic analysis, has been established against much carefully controlled experimental work [for example, 12] and its limitations gener-

ally appreciated, there is far less evidence against which to judge the results of detailed elastic-plastic computations, and any divergences noted between calculation and experiment may be attributed either to inherent weaknesses in the computations per se or to differences in the assumed and real modes of plastic deformation. It is thus necessary to attempt to establish confidence in the computational method, by detailed comparisons where available, and thus infer the general reasonableness of the more widespread predictions which are the object of the present study.

OUTLINE OF THE METHODS USED

The computer program used is a development of that described Ref. 13, which was itself used for some of the studies already referenced [8], [9], [10]. Conventional small displacement shell theory is assumed expressed in terms of circumferential and meridional bending and direct stress resultants. The von Mises yield criterion is assumed with the Prandtl-Reuss equations for incremental plastic flow, allowing either non-work hardening or work hardening behavior to be expressed. The program is restricted to axial symmetry, and original geometry. Each element of a shell structure is divided into numbered steps convenient for the application of a Rünge-Kutta forward integration method starting from a junction. The whole solution is first worked elastically, scaled to first yield, and then extended in increments such as 0.1 of first yield load.

The developments from Ref. 13 include a "thick curved bar" theory for treating knuckles of small radius of curvature [14], [15]. This approximation allows an elastic stress pattern to develop, non linear across the thickness (as in Winkler's theory for curved bars), but still ignores shear and through thickness deformations. The original program included elements tapering in thickness and a previous modification [8] allowed the forces at a "square corner" intersection to be distributed as bands of loading over a finite width of shell (equal say to the thickness of the shell wall plus a filet weld) rather than the point or line load of conventional shell theory. Thus three representations of a nozzle junction can be made; a simple intersection as is conventional shell theory, a distributed band load and a small filet of specified mean radius and taper. It is not to be expected that simple shell theory can predict reasonable local stresses and strains at a discontinuity in shape and it was pointed out Ref. 8 that a realistic collapse behavior for such discontinuities could not be obtained without recourse to the band load model. To the extent that the "thick curved bar" treatment is adequate, the curved and tapered corner can be fitted to a specified real curved junction or used as an arbitrary approximation to a nominal or unspecified corner detail. One of the objects of the present study was to determine the extent to which such variations in assumed geometry of detail affected predictions of collapse or shakedown of adjacent regions.

A second improvement of the program is the better representation or work hardening and departure from linearity at a proof stress, appropriate to materials without a distinct yield point, either by an exponential or power formula of the type $\bar{\sigma} = a\,(1 + b\,\bar{e}_p)^c$ where $\bar{\sigma}$, $\bar{e}_p$ are the von Mises equivalent stress and equivalent plastic strain and a, b, c are constants over some range of a stress strain curve. Several such representations can be joined together where a particular stress and strain curve is closely known.

COMPARISON BETWEEN SOME COMPUTED AND EXPERIMENTAL RESULTS

The general validity of the computed values of plastic strain and deflection were shown Ref. 10, in which comparison was made with strain gage measurements on the tori-spherical head of a stainless steel test vessel. As remarked Ref. 10, the degree of detail agreement achieved was not as close as for elastic analyses, where Ref. 12 and much previous work suggested differences from shell theory might be of the order of 12 percent for reasons of departure from the nominal geometry of the vessel. Fig. 1 shows the improved agreement, now to within about 10 percent in pressure, based on experimental values of first yield pressure, or within 5 percent based on first yield calculated from tensile test data. This latter close agreement reflects the better representation of proof stress now possible with the better description of the stress-strain curve. Values of the pressure for insipient collapse as defined Ref. 10 (by backward extrapolation of the tangent from the point defined by a line giving 1/3 of the initial elastic slope) are marked on Fig. 1. It should be recalled that the stainless steel used showed a rapid work hardening with no distinct yield point and clearly the previous "best fit" available, which matched stresses of around 2 percent strain with an under estimate of stress for smaller plastic strains and an over estimate of the proof stress, was not in fact a very good compromise. There is a similar improvement in all the other detailed stress-strain-displacement records re-studied from these tests, leading to the belief that the computed results are more numerically realistic than previously realised, at least for smooth shell regions of a vessel. In the absence of a corresponding detailed study of strain distributions in a specified nozzle shape (in which matters such as the difference in stress-strain behavior of the parent shell and weld metal might

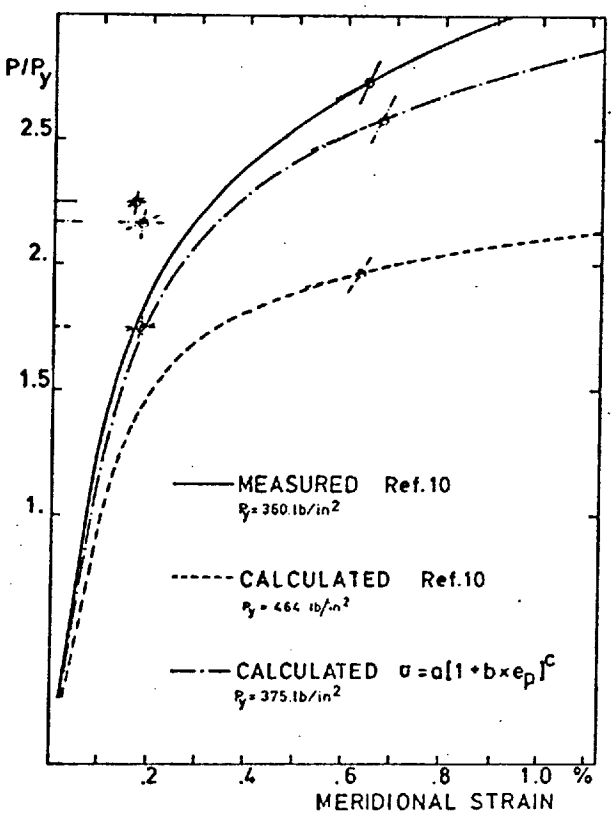

FIG. 1 COMPARISON OF EXPERIMENTAL AND COMPUTED ELASTIC-PLASTIC STRAINS ON A PRESSURE VESSEL HEAD

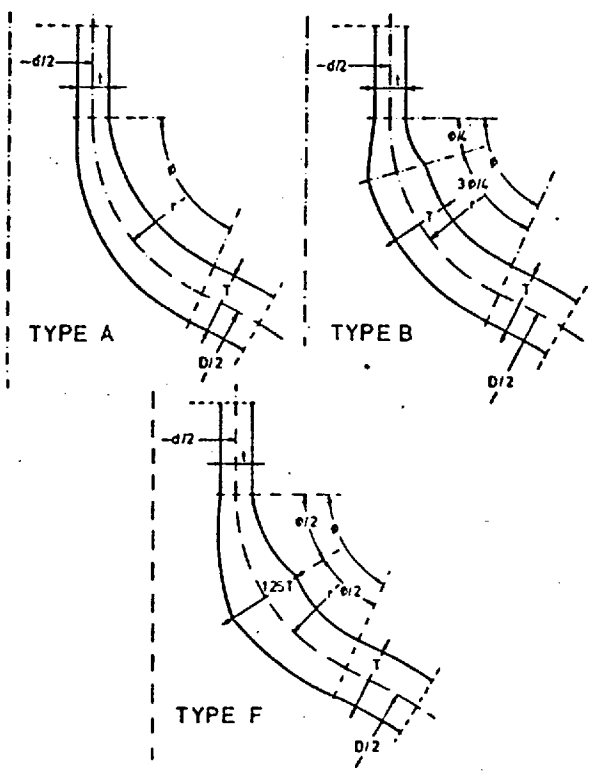

FIG. 2 DETAILS OF NOZZLE JUNCTION AS USED FOR COMPUTATIONS OF NOZZLES TYPE C

also be relevant) some uncertainty must of course remain over the accuracy of the present program for such regions.

COMPUTATION ON SOME NOZZLE GEOMETRIES

Two main sets of elastic-plastic computations have been conducted on radial nozzles with closed ends subjected to internal pressure. In the first set, Series C, a nozzle of thickness t, diameter d, set in a sphere $D = 5d$, thickness $T = 2t = D/100$ has been examined for various junction details (Fig. 2). For each detail certain quantities are tabulated, Table 1. The elastic stress concentration factor (SCF) based on von Mises equivalent stress is given according to conventional shell theory, except when the local radius of curvature is small when the Winkler type modification already described is used [14, 15]. The SCF is quoted as the ratio of local stress to the membrane meridional or hoop stress in the sphere. Since these equal the von Mises equivalent stress this ratio also equals the ratio of membrane yield pressure in the sphere to first yield pressure anywhere in the structure.

Table 1. Nozzle details: Series C. $w = 1.41$

Geometry Parameters and SCF for $d/D = .2$; $T/D = .01$; $t/T = .5$			
Ref.	$2r/d$	Taper Type	k_1
C1	.015	A	4.91
C2	.015	B	4.96
C3	.015	F	4.88
C4	.045	A	3.21
Value from Ref. 20: $k_1^* = 4.3$			

Table 2. Nondimensional collapse pressures, P_c^x and k_3: Series C

Ref.		Collapse Criteria					k_3
		C3I	C3E	C3D	C5I	C5E	
C1		1.83	1.84	2.31	2.31	2.13	.47
C2		1.89	1.92	2.45	2.33	2.17	.47
C3	M	1.93	2.06	2.37	2.31	2.18	.47
	R	1.9	1.87	–	2.28	2.12	.47
C4		1.49	1.55	1.64	1.88	1.76	.59
Value from Ref. 20: $P_c^x = 2.15$ $k_3^* = .5$							

Values of the incipient collapse pressure are given, Table 2, according to the three definitions used in Ref. 10. Two of these are based arbitrarily on the intersection of the elastic line with a backward tangent drawn to the loading curve at a certain point. The loading curve used is firstly overall deflection v load, or secondly, maximum

strain ν load and in either case the point at which the tangent is constructed is defined by the intersection of the loading curve with a straight line drawn from the origin with a slope one third of the elastic line, Fig. 1. The third criterion is the value of load obtained for a maximum strain of 0.5 percent on the outside surface. A feature of this last criterion is that it can be measured during a test of a vessel, although there may be a problem of where to take measurements since the point of maximum strain can change its location along the vessel wall as plasticity spreads. The last two criteria can be based either on individual circumferential or meridional strain – this is clearly simpler for experimental work – or more logically on a von Mises equivalent strain basis. Both values are tabulated, Table 2.

Values of the shakedown pressure are given according to several criteria described below, Table 3. Some typical dimensionless pressure-maximum strain curves are shown Fig. 3 for a work hardening curve $\sigma = 13.3\,(1 + 133\,\bar{e}_p)^{0.269}$ representative of mild steel ignoring the horizontal discontinuity at first yield.

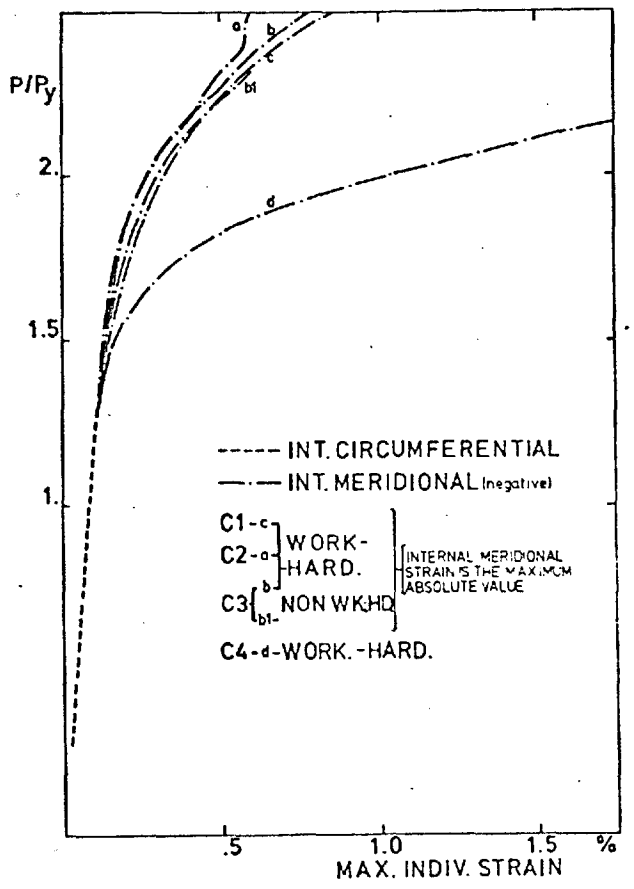

FIG. 3 COMPOSITE CURVES OF MAXIMUM COMPUTED STRAIN AGAINST PRESSURE FOR SEVERAL NOZZLE JUNCTION DETAILS

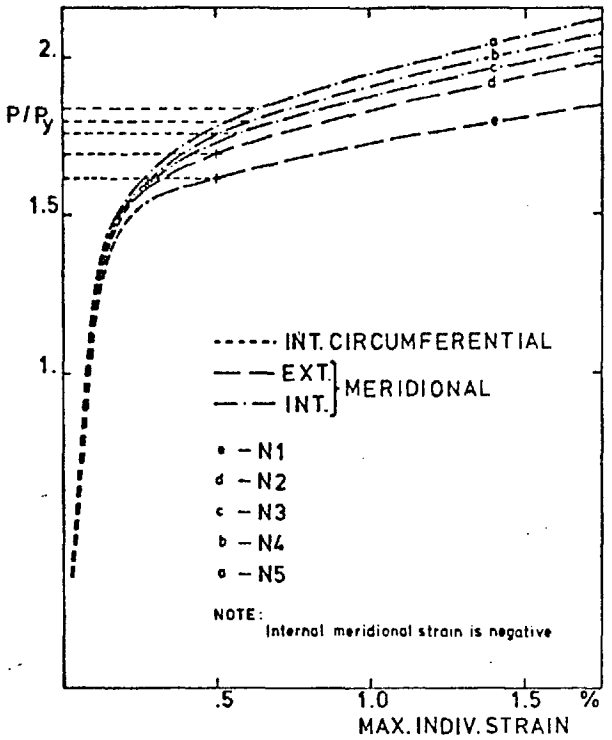

FIG. 4 COMPOSITE CURVES OF MAXIMUM COMPUTED STRAIN AGAINST PRESSURE FOR A SERIES OF NOZZLE TO SPHERE DIAMETER RATIOS

A second set of similar results, Series N, is shown in Tables 5, 6 and 7 for a given sphere, diameter D, thickness $T = D/200$, cylinder thickness $t = T$. Various ratios of sphere to cylinder diameter D/d from 20 to 4 were used with constant knuckle radius $r = D/40$. The variation of maximum strain with nozzle diameter ratio is shown Fig. 4 as a series of composite curves against load.

Elastic – perfectly plastic material has also been considered for the cases C3, N1 and N5, to show the effect of lack of work hardening. The variation of maximum strain with the two different materials is shown (Figs. 3 & 5) and the values for P_c^x, P_s^x are tabulated in the corresponding Tables 5 and 6.

PLASTIC FLOW, WORK HARDENING, SHAKEDOWN AND COLLAPSE

For the most highly stressed point in each of four nozzles, series N, the stress path up to and beyond first yield has been plotted, Fig. 6, in terms of circumferential and meridional stress ratios, for inside, outside and mid-wall surfaces.

For small values of SCF (Case N1) the internal path moves anticlockwise around the ellipse to a very small extent (not visible to the scale of Fig. 6) for pressures up to some 25 percent above first yield and then moves clock-

wise for higher pressures (a_1 Fig. 6). For rather higher SCF (case N2) the same effect is noted up to about 10 percent above first yield. For yet higher SCF. (cases N3, N5) the stress path moves clockwise around the ellipse from the instant of first yield (e.g. a_5 Fig. 6). The near stationary value of the stress ratios for appreciable increase of pressure occurs when only the first region of stress concentration is yielding but when a second adjacent stress peak yields, the clockwise movement of the stress ratios begins as just described. In all the cases studied, first yield is on an inside face, with the second nearby yielding on the outside face, both clearly in bending modes.

The next tendency for the stress ratios to move anti clockwise (Fig. 6, $b_1 \ldots b_5$) appears at a pressure when the region of plasticity begins to spread greatly compared with initial zone of small extent. This tendency is more marked for the cases with small SCF (e.g. case 1 rather than case 5) as can be seen in Fig. 6.

Another observation that can be made from Fig. 6 is that when the SCF is small, a larger degree of work-hardening will be necessary to obtain a given level of nondimensional loading P/P_Y. The locus $P/P_Y = 2$ is shown chain dotted in Fig. 6.

The fact that the stress ratio changes, is of course well known, but can here be followed quantitatively. The variation of such ratios increases with SCF especially in the regions $a_1 \ldots . a_5$, Fig. 6.

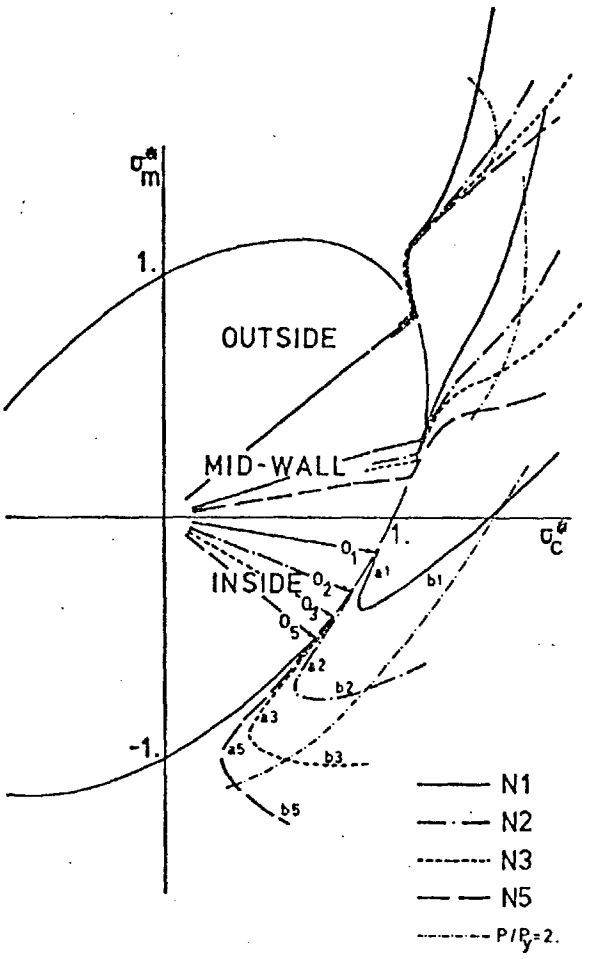

FIG. 6 ELASTIC-PLASTIC STRESS PATHS FOR A SERIES OF NOZZLES BEYOND FIRST YIELD IN A WORK HARDENING MATERIAL

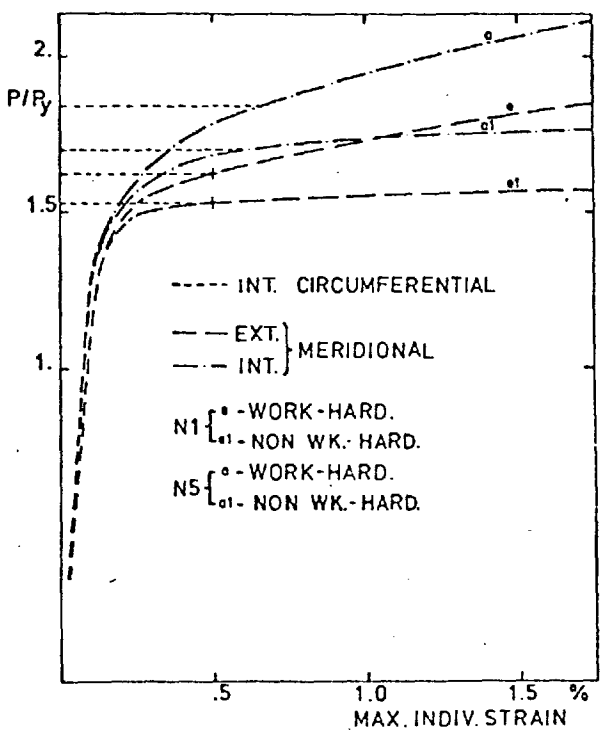

FIG. 5 THE EFFECT OF WORK HARDENING ON THE COMPUTED VALUES OF MAXIMUM STRAIN IN TWO NOZZLES

Probably this second change in the direction of the movement around the ellipse can be considered as the beginning of collapse, since it is the rapid spreading of membrane yield to areas of the sphere adjacent to the nozzle which is causing this re-distribution of stress.

Another typical biaxial stress field is shown Fig. 7, for the cross section that contains the most highly stressed point of nozzle N5 for both work hardening and elastic-perfectly plastic cases. In both, the most highly stressed point follows a linear path, such as curve A, Fig. 7 until the yield criterion is reached. If the material is treated as non-workhardening, the stress path after yielding will be around the ellipse and will be such as curve B1, Fig. 7, or if workhardening, along some line following the increasing size of the workhardening ellipse, such as B2, Fig. 7.

After yielding, anywhere in the structure, the linearity of a stress path cannot be assumed. As the yielding be-

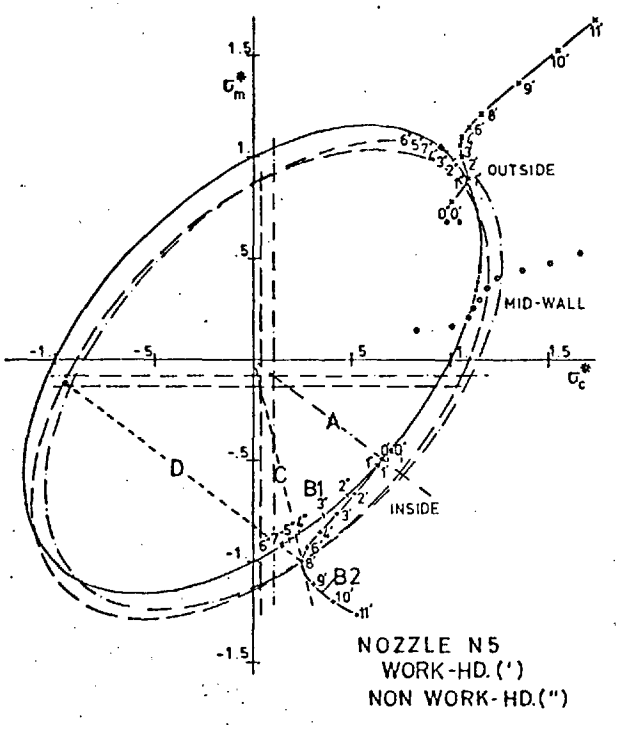

FIG. 7 THE EFFECT OF WORK HARDENING ON THE ELASTIC-PLASTIC STRESS PATHS FOR A NOZZLE BEYOND FIRST YIELD

comes more extensive the direction of movement of the stress ratio for a point which is still elastic may change, sometimes reversing an original direction of movement. This non-linearity of the elastic region of the structure may be interpreted as the re-distributing the elastic stresses caused by yielding of adjacent points of the structure.

For the case shown, Fig. 7, the change in stress ratio leads to a reduction of the highest pressure for shakedown because the length of the unloading path available decreases from twice *A* to some lesser value, path *D*.

If workhardening is included a question arises on what unloading path should be permitted. It is generally recognised that reversal of stress causes a reduction in the yield stress in the reversed direction of flow such that ultimately a settled cyclic yield stress curve may be defined [16]. Such a curve usually lies above the curve for original loading of a material in the soft condition but may in fact lie below that (i.e. work softening) obtained from an initially hardened material, even if the hardening is by thermal rather than mechanical treatment [17].

The number of cycles to reach this settled state is in most cases not large in relation to the number of cycles to cause low cycle fatigue, but even if only 50 or 80, is perhaps rather more than normally envisaged for shakedown to occur. If known, however, the settled cyclic curve would appear to be the rational one at which to aim, although the development of it under biaxial stresses, some components of which may not completely reverse under repeated (one way) pressurisation, has not been well documented as far as the authors are aware.

In the present work the calculations of shakedown have therefore been based on one of three assumptions. The first is that the work hardening ellipse simply grows according to the load used. As just explained, if that law is taken to represent a conventional uniaxial stress-strain curve then the stress range of twice the workhardened yield stress available between yielding in one direction and the other will be an over statement of the real situation and the calculation unconservative in most cases. If the curve is fitted to (or here simply taken to represent) a settled cyclic curve rather than an original uniaxial one then the stress ranges implied may be realistic. In the second and third cases alternative assumptions akin to Prager's "sliding pin" model [18] are used, to allow the ellipse of yielding to remain at its original size but translate with axes kept parallel (initial principal direction remain the same). In the second case the translation is along *A*, Fig. 7, the elastic path to first yield, until the ellipse passes through the stress point for the increment (such as increment 8, on curve B2, Fig. 7) being considered. This second case has proved sometimes to be unrealistic for the cases when the stress ratio moves round the ellipse to a point remote from the extension of *A* at the particular load considered. In the third case the translation of the ellipse is along the radius *C* to the stress point for the increment in question, Fig. 7. The second is slightly more conservative in the cases presented but the third seems more reasonable intuitively. It may be noted that for some of the cases studied the point of which the structure first yields does not remain the critical point for shakedown or for collapse, particularly for cases with small SCF. Thus the development of the plastic zone has to be watched carefully on both inner and outer faces if the worst condition is to be monitored.

DISCUSSION OF RESULTS

The values of SCF, Table 1, based on equivalent stresses show a negligible variation for the different connection details, but a reduction of some 30 percent as can be expected for the larger knuckle radius, case C4. If a comparison is made with the meridional SCF obtained supposing a flush cylinder on sphere, (20), it can be seen that the values of SCF for C1 to C3 nozzles are higher by about 15 percent, but the case C4 nozzle is lower by some 25 percent. It may be noted that the calculated SCF based on equivalent stresses for a flush nozzle is substantially higher at 6.5. The values of non-dimensional collapse pressures are compared, Table 2, for the various nozzle

details, Series C, and the several collapse criteria adopted, firstly as a ratio to first yield pressure. For a given nozzle detail, the criteria differ by ±15 percent. In general the maximum value of collapse is given by the C5I or C3D criteria. The difference between nozzles C1 to C3 and nozzles C4 again reflects the differences between the values of knuckle radius – the larger radius gives collapse pressure ratios some 25 percent lower. The overall collapse factor (i.e. ratio to membrane yield, not to first yield) is shown in the final column, k_3 Table 2. It increases, of course, as SCF decreases, and is here based on method C5I.

Comparison of the collapse ratios P_c^x, Table 2, with the value of a limit pressure obtained from Ref. 20 shows a variation of about ±10 percent for nozzles C1 to C3 according to the criterion used, with present values some 25 percent lower for the case of nozzle C4. It will be recalled that, for all cases except C3R, a work hardening material has been assumed. Comparing C3M (work hardening) with C3R (nonwork hardening) an increase of collapse pressure of only some 2-3 percent is found by the inclusion of work hardening. Values of k_3 for nozzles C_1–C_3, here inclusive of work hardening fall 5 percent below the nonwork hardening value from Ref. 20.

The shakedown ratios P_c^x for nozzles C_1 to C_3, Table 3, are very close to the value 2 that can be obtained from Ref. 20. Case C1 gives values slightly smaller (5 percent) than the other two cases perhaps because the highest stressed region on nozzles C2 and C3 is smaller than on nozzle C1. The values of shakedown for nozzle C4, for methods SPC and SPT (where the ellipse of yielding translates but does not expand) are again smaller than C1 but by only 1-2 percent, i.e. some 9 percent below the value of 2 from Ref. 20.

For all nozzles, method SPW (allowing the ellipse of yielding to expand uniformly to accommodate work hardening) gives the highest values for shakedown but still within the region ±4 percent of the value 2 except for nozzle *D* where the effects of lower SCF and the SPW model of work hardening combine to give a value in excess of 2.28. The final column, Table 3, expresses the factor k_2 for shakedown in relation to membrane yield rather than first yield, based on method SPT. Despite work hardening, k_2 is some 20 percent less than k^x [Ref. 20] for C_1 to C_3.

In summary, the different connection details make negligible effect on stress concentration, shakedown or collapse (i.e. less than 5 percent). A larger knuckle radius reduces SCF, reduces collapse and affects shakedown according to the model used for work hardening. Work hardening itself has surprisingly little effect (e.g. 5 percent) on incipient collapse as defined here or on shakedown with any but the least conservative (expanding ellipse) model for cases with low SCF.

The results of the calculations for series N having various ratios of nozzle to sphere diameter, are shown Table 4, dimensions and SCF, and Table 5, collapse. If the values of SCF are plotted against diameter ratio, all the five points for the series N nozzles fall on a straight line, (not shown). The SCF value, Table 4, can be compared with the values obtained from Ref. 20 treating the nozzles of serial N as flush cylinders on sphere of equal thickness. The present results are some 20-30 percent lower.

The values of collapse for all nozzles N1 to N5, Table 5, are within a margin of ±10 percent of an average value. Comparing Table 4 with Table 5 it can be seen that the collapse value as here defined, increases with SCF value, as is well known, the nozzles (e.g. N5, N4) with SCF higher by a factor of about 2 having collapse pressures some 10 percent higher. The values of collapse for criteria C3I, C3E, C3D are smaller than the values of C5I and C5E by about 10-15 percent. The effect of non-workhardening (N1R and N5R) or work hardening (N1M and N5M) is again not more than 5 percent. The greatest plastic strain is internal for N3-N5 (high SCF) but external for N1 and N2 (low SCF).

For all the cases studied, C5I gives the highest value for incipient collapse, and from Fig. 5 it is seen that for nonwork hardening materials this pressure is near actual collapse. The nonhardening results fall 10 percent below

Table 3. Nondimensional shakedown pressures, P_s^x and k_2: Series C

Ref.		Shakedown Criteria				
		SEM	SPC	SPT	SPW	k_2
C1		1.98	1.86	1.87	1.96	.38
C2		1.96	2.	2.	2.09	.4
C3	M	2.	1.97	1.97	2.09	.4
	R	2.	****	1.97	****	.4
C4		2.	1.81	1.85	>2.28	.59

Value from Ref. 20: $P_s^x = 2.$ $k_2^x = .5$

Table 4. Nozzle details: Series N. $w = 10\ d/D$

Ref.	Geometry Parameters and SCF for $T/D = .005$; $2r/D = .05$; $t/T = 1$			
	d/D	Torus Angle	k_1	k_1^*
N1	.05	84°5	1.79	2.2
N2	.10	81°8	2.18	3.1
N3	.15	79°0	2.63	3.9
N4	.20	76°2	3.08	4.7
N5	.25	73°4	3.55	5.4

Ref. 20 for low SCF (N1R) and equal to it for high SCF (N5R). Inclusion of work hardening gives results for 3 percent below (N1) to 8 percent above (N5) Ref. 20 but the rising slopes of curves *a* and *e* Fig. 5, and for nozzles C Fig. 3, suggest that denoting collapse by a larger strain of 1 or 1.5 percent (as Ref. 8) to give P_c^x some 10 percent higher might be acceptable for the degree of work hardening used here.

Table 5. Nondimensional collapse pressures, P_c^x and k_3: Series N

Ref.		Collapse Criteria						
		C3I	C3E	C3D	C5I	C5E	k_3	k_3^*
N1	M	1.42	1.44	1.41	1.62	1.56	.91	.94
	R	1.39	1.4	1.37	1.52	1.5	.85	.94
N2		1.44	1.44	1.47	1.69	1.6	.78	.77
N3		1.48	1.48	1.52	1.76	1.64	.67	.63
N4		1.48	1.48	1.57	1.80	1.67	.58	.54
N5	M	1.5	1.49	1.6	1.84	1.7	.52	.48
	R	1.49	1.49	1.57	1.7	1.63	.48	.48

Table 6. Nondimensional shakedown pressures, P_s^x and k_2: Series N

Ref.		Shakedown Criteria					
		SEM	SPC	SPT	SPW	k_2	k_2^*
N1	M	1.78	1.8	1.9	1.96	1.06	.79
	R	1.78	***	1.56	***	.87	.79
N2		1.97	1.74	1.83	2.25	.84	.65
N3		2.	1.76	1.84	2.45	.7	.52
N4		2.	1.74	1.83	>2.2	.59	.43
N5	M	2.	1.77	1.82	2.88	.51	.38
	R	2.	***	1.76	***	.5	.38

In Table 6, the values of shakedown for nozzle N1 to N5 are compared by the different criteria used, as explained earlier in the paper. The minimum value obtained by an application of Macfarlane and Findlay [7] graphical adaptation of Leckie's method [6], is taken at the cylinder-torus or sphere-torus junctions because, as far as the authors are aware, this method cannot be applied to toroidal shells near $\theta = 90°$, because of the discontinuity in the membrane stresses [Ref. 19, page 34]. The highest stressed points are in fact in the knuckle near the sphere junction, so for the cases N1 to N5 the minimum value obtained here is at sphere-torus junction. For elastic type calculations, cf P_s^x, (methods SEL, SEM) the values of shakedown increase with the SCF from 1.74 (low SCF) up to 2 (high SCF). The values of SPW also increase, and lie some 10-30 percent above these values, increasingly so as the SCF increases. The more conservative, and probably more realistic critera SPT or SPC are within 5 percent of each other for values of SCF thus showing no trend with nozzle/sphere diameter ratio.

Because for elastic perfectly plastic material the ellipse of yielding stays at its initial position, comparison of the effect of work hardening is made against the SPT criterion, Table 6. For N1, the neglect of work hardening reduces shakedown by 15 percent. For N5, there is a decrease of about 3 percent. Thus the neglect of work hardening may allow a signiciant underestimation of shakedown for low SCF ($\triangleq$ 2.0) but not for high SCF ($\triangleq$ 3.5). It thus appears that the little effect of diameter ratio on shakedown by method SPT is a consequence of a greater effect of work hardening on nozzles with low SCF (such as N1) offsetting the lower shakedown found for these lower SCF cases if work hardening is ignored. The results, inclusive of work hardening, fall some 30 percent above Ref. 20 when expressed as the ratio k_2 to membrane yield.

All values of shakedown and smaller than the values of a limit pressure, [Ref. 20]. Comparing the values here, Fig. 8, the shakedown ratios P_s^x (SPT) are larger than the collapse rations P_c^x (C5I) except for values of d/D greater

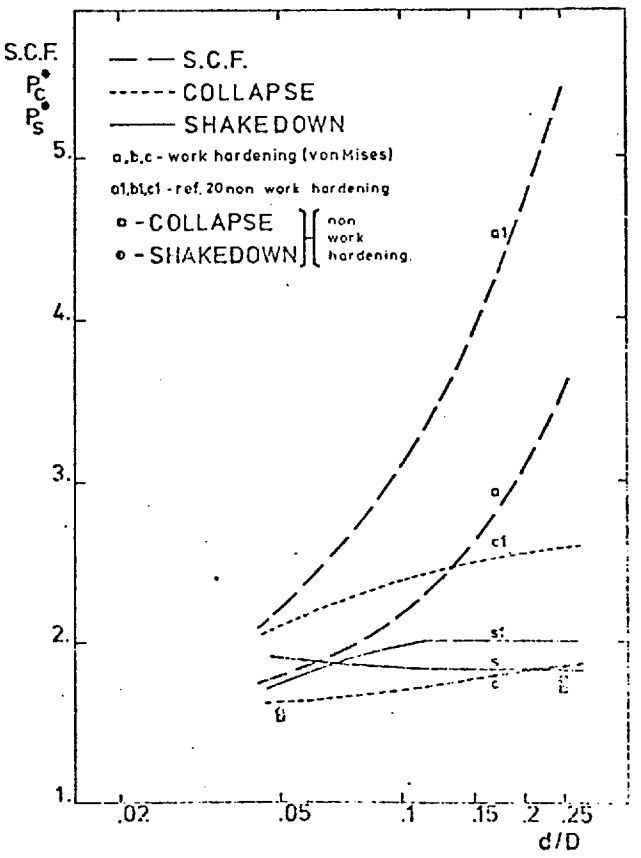

FIG. 8 ELASTIC STRESS CONCENTRATION FACTORS, SHAKEDOWN AND COLLAPSE RATIOS FOR A SERIES OF NOZZLE TO SPHERE DIAMETER RATIOS

than 0.22 (high SCF). The two non-hardening cases (N1R, N5R) also show shakedown ratios marginally above incipient collapse.

Summarizing all the cases so far computed;

(i) for a high SCF (> 3.5) the shakedown ratio is near 2, for work hardening or elastic-perfectly plastic material. It is considered that C5I is the best criterion for incipient collapse. These collapse pressures are higher than shakedown.

(ii) for the intermediate SCF (2.5 to 3.5) a shakedown ratio near 1.85 is obtained for work hardening material or rather lower (about 1.75) for the one case (N5) of non-work hardening in this regime. The collapse and shakedown pressure ratios are not markedly different.

(iii) for low SCF (< 2.5; N1 and N2) shakedown is between 1.85 and 2.0 if work hardening is included but substantially lower (1.56 for N1) if work hardening is neglected. Criterion C5I is again considered most suitable for incipient collapse. This collapse is always less than the shakedown value.

CONCLUSIONS

Small differences in the detailed geometry of continuous nozzle-sphere connections do not alter significantly the elastic SCF or the shakedown and collapse loads of the vessel despite the junction being the region of highest stress in the vessel. Comparison with previously published plastic strains now shows good agreement between experimental and computed values. Thus it is possible to perform elastic-plastic shell theory computations with some assurance that the results can be applied usefully to real vessels even if only the nominal details of the shape of the junctions are known.

For computations including the effect of work hardening an assumption must be made on the movement of the ellipse of yielding. Translation towards the stress state reached, without expansion unless a steady state cyclic stress strain curve is known, appears most reasonable. This then shows a significant effect of work hardening on values of shakedown or collapse pressure only for the cases of low SCF although the values of plastic strain are smaller than if work hardening is neglected. For a more than twofold increase in SCF the ratio to first yield, P_s^x, does not vary greatly while P_c^x increases by 40 percent, but the ratios k_2 and k_3 to membrane yield increase twofold for the hardening used here, as the SCF is halved. In such computations a unique collapse load is not found, at least for small strains, but rather a gradual change from elastic to plastic behavior. Of the various arbitrary criteria examined for incipient collapse that based on reaching 0.5 percent individual (i.e. hoop or meridional) strain at the most highly strained point on the outside surface seems not too conservative. It is also amenable to easy use in experimental work. Further examination of this criterion for experimental results would be useful.

For the particular equal thickness nozzle-sphere geometries reported here the shakedown load did not vary greatly with nozzle-sphere diameter ratio, due to the opposing effects of geometry and work hardening, with results 30 percent above previous estimates. For values of SCF below about 2.5, incipient collapse occurs before shakedown. The broad trends of previous calculations based on elastic stress distributions and limit load concepts are confirmed, although the elastic plastic computations show rather lower collapse loads for nozzles with low SCF if work hardening is neglected. Now that the effects of detailed alterations in geometry, the criteria used for incipient collapse and of assumptions on work hardening behavior have been assessed, results for other component configurations and load systems can be calculated with some confidence.

ACKNOWLEDGEMENTS

One of the authors (V.M.S.) would like to thank the Calouste Gulbenkian Foundation and the University of Lorenco Marques for support during the work reported here. Both the authors would like to thank Dr. J. A. Blomfield, late of Imperial College now with the Central Electricity Generating Board, Dr. L. C. Laming Imperial College and Mr. J. F. Poynor, Babcock and Wilcox Ltd. for their advice and help and interest in this project.

REFERENCES

[1] Duffy, A. R., "Studies of Hydrostatic Test Loads and Defect Behaviour". Symposium on Line Pipe Research, American Gas Association Report Catalogue No. L30,000, March 1966, pp. 139-160.

[2] Hodge, P. G., *"Limit Analysis of Rotationally Symmetric Plates and Shells"*. Prentice-Hall, London, 1963.

[3] Cloud, R. L., *"Limit Pressure of Radial Nozzles in Spherical Shells"*. Nuclear Structural Engineering, Vol. 1, No. 4, April 1965, pp. 403-413.

[4] Allman, D. J., Gill, S. S., *"The Effect of Change of Geometry on the Limit Pressure of a Flush Nozzle in a Spherical Pressure Vessel."* Engineering Plasticity (Heyman and Leckie, eds.), Cambridge University Press, London, 1968, pp. 1-20.

[5] Findlay, G. E., Spence, J., "Applying the Shakedown Concept to Pressure Vessels Design". *The Engineer*, July 1968, pp. 63-65.

[6] Leckie, F. A., "Shakedown Pressures for Flush Cylinder-Sphere Shell Intersections". *Journal Mechanical Engineering Science*. Vol. 7, No. 4, 1965, pp. 367-371.

[7] Macfarlane, W. A. and Findlay, G. E., "A Simple Tech-

nique for Calculating Shakedown Loads in Pressure Vessels". *Proceedings of the Institution of Mechanical Engineers,* Vol. 185, 1972, pp. 45-52.

[8] Marcal, P. V. and Turner, C. E., "Elastic-Plastic Behaviour of Flush Nozzles in Spherical Pressure Vessels". *Journal Mechanical Engineering Science,* Vol. 9, No. 3, 1967, pp. 182-189.

[9] Blomfield, J. A. and Jackson, P. B. M., "Fatigue Tests on some Cupro-Nickel Pipe Bends and a Comparison of Some Failure Prediction Methods." *First International Conference on Pressure Vessels Technology,* Delft, The Netherlands, October 1969, pp. 1221-1231. American Soc. Mech. Eng.

[10] Cheung, J. S. T. and Turner, C. E., "Elastic-Plastic Behaviour of Pressure Vessel Heads". *First International Conference on Pressure Vessels Technology,* Delft, The Netherlands, October 1969, pp. 597-611. American Soc. Mech. Eng.

[11] Spere, D. A., "Analysis of Elastic-Plastic Shells of Revolution Containing Discontinuities". *American Institute of Aeronautics and Astronautics Journal,* Vol. 1, No. 11, 1963, pp. 2583-2589.

[12] Johns, R. H., Morgan, W. C., and Spere, D. A., "Analysis of Stress at Several Junctions in Pressurised Shells". *American Institute of Aeronautics and Astronautics Journal,* Vol. 1, No. 2, 1963, pp. 455-457.

[13] Marcal, P. V. and Pilgrim, W. R., "A Stiffness Method for Elastic-Plastic Shells of Revolution". *Journal Strain Analysis,* Vol. 1, No. 4, 1966, pp. 339-350.

[14] Cheung, J. S. T., Ph.D. Thesis, *"The Elastic-Plastic Behaviour of some Axisymmetric Pressure Vessel Heads and Nozzles",* University of London, 1969.

[15] Crisp, R. J., *"A Computer Survey of the Behaviour of Torispherical Drum Heads under Internal Pressure Loading".* Nuclear Engineering and Design, Vol. 11, 1970, Parts I and II, pp. 457-476.

[16] Benham, P. P., *"Fatigue of Metals Caused by a Relatively Few Cycles of High Load or Strain Amplitude".* Metallurgical Review, The Institution of Metals, Vol. 3, No. 11, 1958, pp. 203-234.

[17] Mackenzie, C. T. and Benham, P. P., "Push-Pull Low Endurance Fatigue of En25 and En32B Steels at 20°C and 450°C". *Proceedings, Institution of Mechanical Engineers,* Vol. 180, Pt. 1, No. 30, pp. 709-726.

[18] Prager, N., "A New Method of Analysing Stresses and Strains in Work Hardening Plastic Solids". *Journal of Applied Mechanics,* December 1956, pp. 493-496.

[19] Turner, C. E., *"Introduction to Plates and Shells Theory".* Longmans, London, 1965.

[20] Leckie, F. A. and Payne, D. E., "Some Observations on the Design of Spherical Pressure Vessels with Flush Cylindrical Nozzles". *Proceedings of the Institution of Mechanical Engineers,* Vol. 180, Pt. 1, No. 20, 1965-66, pp. 497-501.

TABLE HH1

ELASTIC STRESS CONCENTRATION AND INDEX RATIOS FOR SOME HEMISPHERICAL HEADS ON CYLINDRICAL PRESSURE VESSELS

d/t = 10					
t/T	Langer*	Analytically**	PVA 1 Program		
	(a)	(b)	(a)	(b)	(c)
.5	.961	.962	.977	.972	.977
1.0	.971	.968	.972	.969	.972
2.0	.900	.807	.904	.795	.904

(a),(b),(c) see Section 3.2.1

(a) Stress index ratio
(b) von Mises criterion
(c) Tresca criterion
* Ref. [51]
** Either using approximation to Kelvin functions or exponential solutions (Appendix B)

TABLE HH2

ELASTIC STRESS CONCENTRATION AND INDEX RATIOS FOR A RANGE OF HEMISPHERICAL HEADS ON CYLINDRICAL PRESSURE VESSELS

$10 \leqslant d/t \leqslant 300.$			
t/T	Langer*	Crisp***	Analytically**
	(a)	(b)	(b)
.5	.961	....	.962
1.0	.971	.967	.968
2.0	.900	....	.807

*,**, (a),(b),(c) see Table HH1. *** Ref.[9] $20 \leqslant d/t \leqslant 100$.

TABLE FH1

ELASTIC STRESS CONCENTRATION AND INDEX RATIOS FOR SOME FLAT ENDS ON CYLINDRICAL PRESSURE VESSELS

t/T = .25					
d/t	Langer*	Analytically**	PVA1 Program		
	(a)	(b)	(a)	(b)	(c)
10.	.52	.47	.47	.46	.47
20.	.41	.39	.40	.39	.40
40.	.26	.27	.24	.27	.24
80.	.15	.15	.13	.15	.13

(a),(b),(c),* see Table HH1
** Solid plate solution (Appendix B)

TABLE FH2

ELASTIC STRESS CONCENTRATION AND INDEX RATIOS FOR SOME FLAT ENDS ON CYLINDRICAL PRESSURE VESSELS

t/T = .50					
d/t	Langer*	Analytically**	PVA1 Program		
	(a)	(b)	(a)	(b)	(c)
10.	.44	.37	.37	.36	.37
20.	.25	.22	.22	.21	.22
40.	.12	.11	.10	.11	.10

(a),(b),(c),* see Table HH1
** See Table FH1

TABLE FH3

ELASTIC STRESS CONCENTRATION AND INDEX RATIOS FOR SOME FLAT ENDS ON CYLINDRICAL PRESSURE VESSELS

t/T = 1.0					
d/t	Langer*	Analytically**	PVA1 Program		
	(a)	(b)	(a)	(b)	(c)
10.	.26	.26	.27	.26	.27
20.	.14	.14	.14	.13	.14

(a),(b),(c),* see Table HH1
** See Table FH1

TABLE SH1

ELASTIC STRESS CONCENTRATION AND INDEX RATIOS FOR SOME SPHERICAL HEADS ON CYLINDRICAL PRESSURE VESSELS

$d/D_o = .40$						
t/T	d/T	PVA1 Program			Analytically	
		(a)	(c)	(b)	Exponent. (b)	AP.Kelvin* (b)
1.0	10.	.386	.386	.369	.338	.344
	20.	.266	.266	.242	.240	.248
.5	10.	.435	.435	.425	.354	.330
	20.	.291	.291	.277	.258	.249
.25	10.	.503	.503	.492	.417	.333
	20.	.408	.408	.394	.336	.296

(a),(b),(c) see Table HH1
*Approximation to Kelvin functions (Appendix B)

TABLE SH2

ELASTIC STRESS CONCENTRATION AND INDEX RATIOS FOR SOME SPHERICAL HEADS ON CYLINDRICAL PRESSURE VESSELS

$d/D_o = .25$						
t/T	d/t	PAV1 Program			Analytically	
		(a)	(c)	(b)	Exponent. (b)	AP.Kelvin* (b)
1.0	10.	.326	.326	.311	.190	.242
	20.	.202	.202	.184	.157	.174
.5	10.	.402	.402	.392	.264	.223
	20.	.250	.250	.239	.190	.173
.25	10.	.491	.491	.479	.338	.170
	20.	.399	.399	.384	.272	.194

(a),(b),(c) see Table HH1. *see Table SH1

TABLE TH1

COMPARISON OF THE HEIGHT RATIO FOR TORISPHERICAL AND SPHERICAL HEADS WITH EQUAL d/D_o

Torispherical h/d	Spherical without knuckle of			
	$\frac{r}{d}$ = 6%		$\frac{r}{d}$ = 10%	
	h/d	θ_o *	h/d	θ_o *
.15	.111	64.9°	.074	73.1°
.20	.170	52.5°	.142	58.2°
.25	.227	41.2°	.207	45.1°
.40	.391	13.7°	.386	14.6°

* θ_o = acos (d/D)

TABLE TH2

COMPARISON OF ELASTIC STRESS CONCENTRATION RATIOS FOR TORISPHERICAL AND SPHERICAL HEADS ON CYLINDRICAL PRESSURE VESSELS OF EQUAL THICKNESS, AND THE SAME DIAMETER RATIO: d/t = 20

(1) h/d	Torispherical (1) with knuckle of		Spherical * without knuckle of	
	6%	10%	6%	10%
.15	.297	.259	.255	.206**
.20	.408	.400	.359	.309
.25	.532	.537	.480	.434
.40	.954	.954	.954	.953

(1) from Ref. [9]
*Value from analytic solution (Appendix B)
** Value from the elastic computer program

TABLE TH3

COMPARISON OF ELASTIC STRESS CONCENTRATION RATIOS FOR TORISPHERICAL AND SPHERICAL HEADS ON CYLINDRICAL PRESSURE VESSELS OF EQUAL THICKNESS, AND THE SAME DIAMETER RATIO: d/t = 50

(1) h/d	Torispherical[(1)] with knuckle of		Spherical * without knuckle of	
	6%	10%	6%	10%
.15	.205	.183	.160	.119
.20	.289	.303	.231	.198
.25	.381	.410	.318	.284
.40	.865	.876	.829	.806

(1),*, see Table TH2

TABLE TH4

COMPARISON OF ELASTIC STRESS CONCENTRATION RATIOS FOR TORISPHERICAL AND SPHERICAL HEADS ON CYLINDRICAL PRESSURE VESSELS OF EQUAL THICKNESS, AND THE SAME DIAMETER RATIO: d/t = 100

(1) h/d	Torispherical[(1)] with knuckle of		Spherical * without knuckle of	
	6%	10%	6%	10%
.15	.161	.149	.113	.083
.20	.227	.257	.163	.138
.25	.298	.345	.227	.202
.40	.713	.736	.666	.656

(1),* see Table TH2

TABLE FN1

ELASTIC STRESS CONCENTRATION FACTORS FOR SOME FLUSH CYLINDRICAL NOZZLES ON SPHERICAL PRESSURE VESSELS

Ref.	R/T = 50. ; t/T = .50				
d/D_o	Leckie*	PVA1 Program		Analytically	
	(1)	(1)	(2)	(2)**	(2)***
.025	1.8	2.96	2.60	2.30	2.85
.05	2.1	3.50	3.09	3.00	3.42
.10	2.7	4.76	4.30	4.35	4.63
.25	4.6	8.24	7.58	7.58	7.72
.50	7.	11.98	10.95	10.97	11.05

* Ref.[63]
**Exponential Solution (Appendix B)
***Approximation to Kelvin function solution (Appendix B)
(1) Tresca criterion
(2) von Mises criterion

TABLE FN2

ELASTIC STRESS CONCENTRATION FACTORS FOR SOME FLUSH CYLINDRICAL NOZZLES ON SPHERICAL PRESSURE VESSELS

Ref.	R/T = 50. ; t/T = 1.0				
d/D_o	Leckie*	PVA1 Program		Analytically	
	(1)	(1)	(2)	(2)**	(2)***
.025	1.8	1.68	1.38	1.72	1.81
.05	2.	1.78	1.61	1.77	2.00
.10	2.6	2.58	2.27	2.16	2.41
.25	4.4	4.13	3.59	3.57	3.68
.50	6.6	5.92	5.12	5.12	5.24

*,**,***,(1),(2) see Table FN1

TABLE FN3

ELASTIC STRESS CONCENTRATION FACTORS FOR SOME FLUSH CYLINDRICAL NOZZLES ON SPHERICAL PRESSURE VESSELS

Ref.	R/T = 100. ; t/T = .50				
d/D_o	Leckie*	PVA1 Program		Analytically	
	(1)	(1)	(2)	(2)**	(2)***
.025	1.85	3.26	2.87	2.72	3.21
.05	2.3	4.20	3.77	3.78	4.14
.10	3.2	6.22	5.74	5.81	6.01
.25	5.7	11.44	10.72	10.71	11.01
.50	8.7	17.00	15.81	15.68	15.70

*,**,***,(1),(2) see Table FN1

TABLE FN4

ELASTIC STRESS CONCENTRATION FACTORS FOR SOME FLUSH CYLINDRICAL NOZZLES ON SPHERICAL PRESSURE VESSELS

Ref.	R/T = 100. ; t/T = 1.0				
d/D_o	Leckie*	PVA1 Program		Analytically	
	(1)	(1)	(2)	(2)**	(2)***
.025	1.85	2.03	1.94	1.70	1.89
.05	2.2	2.38	2.15	2.00	2.28
.1	3.1	3.19	2.77	2.71	2.95
.25	5.4	5.54	4.85	4.80	4.98
.50	8.15	8.13	7.16	7.08	7.19

*,**,***,(1),(2) see Table FN1

TABLE 1

NOZZLE DETAILS: SERIES C. $\omega = 1.41$

Geometry Parameters and S.C.F. for $d/D_o = .2$; $T/D = .01$; $t/T = .5$			
Ref.	2r/D	Taper Type	K_1
C1	.015	A	4.91
C2	.015	B	4.96
C3	.015	F	4.88
C4	.045	A	3.21
C5	.0	Band Modification 1 step	1.75
C6	.0	Band Modification 2 steps	1.34
Value from Ref.[61]: Flush nozzle simple shell theory		Tresca $K_1^* = 4.3$ von Mises $K_1 = 6.5$ Tresca $K_1^* = 5.8$	

TABLE 2

NON-DIMENSIONAL COLLAPSE PRESSURES, P_c^* and K_3: SERIES C

Ref.	Collapse Criteria								K_3	
	C3I	C3E	C3D	C5I	C5E	C15I	C15E	C.S.P.	C5I	C15I
C1	1.83	1.84	2.31	2.31	2.13	> 2.5	> 2.45	> 2.5	.47	> .51
C2	1.89	1.92	2.45	2.33	2.17	> 2.7	> 2.62	2.15	.47	> .54
$C3^M_R$	1.93	2.06	2.37	2.31	2.18	> 2.5	> 2.49	2.3	.47	> .51
	1.9	1.87	-	2.28	2.12	> 2.28	> 2.28	> 2.28	.47	> .47
C4	1.49	1.55	1.64	1.88	1.76	2.12	2.03	2.05	.59	.66
C5	1.29	1.29	-	1.48	1.41	~1.7	1.62	> 1.675	.85	.91
C6	1.23	1.26	1.26	1.42	1.37	1.72	1.54	1.52	1.06	1.28
Value from Ref. [63] : $P_c^* = 2.15$; $K_3^* = .5$										

TABLE 3

NON DIMENSIONAL SHAKEDOWN PRESSURES, P_s^* and K_2: SERIES C

Ref.	Shakedown Criteria				K_2	
	SEM	SPC	SPT	SPW	SPT	SPW
C1	1.98	1.83	1.87	1.96	.38	.4
C2	1.96	2.	2.	2.09	.4	.42
C3 M	2.	1.97	1.97	2.09	.4	.43
C3 R	2.	***	1.97	***	.4	-
C4	2.	1.81	1.85	> 2.28	.59	> .71
C5	1.69	1.62	> 1.675	> 1.675	> .96	> .96
C6	1.1	1.54	1.59	1.64	1.18	1.22
Values from Ref. [63]: $P_s^* = 2.$; $K_2^* = .5$						

TABLE 4

NOZZLE DETAILS: SERIES N. $\omega = 10\ d/D$

Geometry Parameters and S.C.F. for $T/D_o = .005$; $t/T = 1.$						
Ref.	d/D	Torus Angle	K_1		K_1^* $(2r/D_o = .0)$	
			$2r/D_o = .05$	$2r/D = .0$	Ref. 63	Anywhere in the stru.
N1	.05	$84^{\circ}.5$	1.79	2.15	2.2	2.38
N2	.10	$81^{\circ}.8$	2.18	2.77	3.1	3.19
N3	.15	$79^{\circ}.0$	2.63	3.4	3.9	3.85
N4	.20	$76^{\circ}.2$	3.08	4.1	4.7	4.65
N5	.25	$73^{\circ}.4$	3.55	4.85	5.4	5.50

TABLE 5

NON-DIMENSIONAL COLLAPSE PRESSURES. P_c^* and K_3: SERIES N

		Collapse Criteria								K_3		K_3^*
		C3I	C3E	CED	C5I	C5E	C15I	C15E	CSP	C5I	C15I	
N1	M	1.42	1.44	1.41	1.62	1.56	1.81	1.72	1.62	.91	1.01	.94
	R	1.39	1.4	1.37	1.52	1.5	1.53	1.54	1.58	.85	.86	.94
N2		1.44	1.44	1.47	1.69	1.6	1.95	1.8	1.67	.78	.89	.77
N3		1.48	1.48	1.52	1.76	1.69	1.98	1.88	1.71	.67	.75	.63
N4		1.48	1.48	1.57	1.80	1.67	2.01	1.93	1.76	.58	.66	.54
N5	M	1.5	1.49	1.6	1.84	1.7	2.07	1.97	1.83	.52	.58	.48
	R	1.49	1.49	1.57	1.7	1.63	1.76	1.76	1.68	.48	.5	.48

TABLE 6

NON-DIMENSIONAL SHAKEDOWN PRESSURES, P_s^* and K_2: SERIES N

Ref.	Shakedown Criteria				K_2		K_2^*
	SEM	SPC	SPT	SPW	SPT	SPW	
N1 M	1.78	1.8	1.9	1.96	1.06	1.09	.79
N1 R	1.78	****	1.56	****	.87	-	.79
N2	1.97	1.74	1.83	2.25	.84	1.03	.65
N3	2.	1.76	1.84	2.45	.7	.93	.52
N4	2.	1.74	1.83	>2.2	.59	>.72	.43
N5 M	2.	1.77	1.82	2.88	.51	.81	.38
N5 R	2.	****	1.76	****	.5	-	.38

TABLE 7

TEST NOZZLE DETAILS: ω = .97

Geometry Parameter and S.C.F. d/D_o = .112 ; D_o/T = 149 ; t/T = .5				
$2r/D_o$	K_1		K_1^*	
	Computed	Test	Computed	Ref. [63]
.0134	3.2	2.92	3.62	-
.0	5.5	-	6.0	3.2

TABLE 8

NON-DIMENSIONAL COLLAPSE PRESSURES, P_c^* and K_3: TEST NOZZLE

Ref.	Collapse Criteria								K_3	
	C3I	C3E	C3D	C5I	C5E	C15I	C15E	CSP	C5I	C15I
M	1.77	1.76	2.09	2.24	2.05	2.43	2.39	2.15	.69	.74
R	1.76	1.75	2.07	2.12	1.94	2.21	2.18	1.95	.66	.69
Test	1.78	-	1.75	2.13	-	2.6	-	~2.52	.73	.89
Value from Ref. [63]: K_3^* = .64; P_c^* = 2.05										

TABLE 9

NON-DIMENSIONAL SHAKEDOWN PRESSURES, P_s^* and K_2: TEST NOZZLE

Ref.	Shakedown Criteria				K_2	
	SEM	SPC	SPT	SPW	SPT	SPW
M	2.	1.88	1.89	2.07(1) 2.45(2)	.59	.64(1) .76(2)
R	2.	-	1.69	-	.52	-
Value from the Test(3) : $P_3^* \leqslant 2.31$; $K_2 \leqslant .79$						
Value from Ref. [63] : $K_2^* = .63$; $P_s^* = 2.$						

(1) Lower limit

(2) Upper limit

(3) Based on the static shakedown (less than 20 cycles)

TABLE 10

HEAD A (REF. [7]) DETAILS

Geometry parameter and S.C.F. d/D_o = .578 ; d/t = 74 ; h/D_o = .245	
r/d	von Mises S.C.F.
.245	2.28
.0	3.7

TABLE 11

NON-DIMENSIONAL COLLAPSE PRESSURES, K_3: HEAD A (Ref. [7])

		Calculated		
Ref.	Test*	Work-Hardening		Non-Work-Hard
		$\sigma = a_1 + b_1 \bar{e}_p + c\bar{e}_p^2$	$\sigma = a(1. + b\bar{e}_p)^c$	
C3I	* .98	* .77	.95	* .74
C3E	-	-	.97	-
C3D	* 1.0	* .83	-	* .81
C5I	* 1.48	* 1.06	1.26	* .84
C5E	-	-	1.24	.80
C15I	**1.34	-	1.33	-
C15E	-	-	1.34	.87
BSLY	-	-	.99	.79
CMEO	-	-	1.24	.86
Limit Analysis*				
Lower Bound = .81			Upper Bound = .91	

* Value from Ref. [7]
**1% Maximum strain

TABLE 12

NON-DIMENSIONAL SHAKEDOWN PRESSURE, P_s^* and K_2

HEAD A (REF. [7])

Ref.	SEM	SPC	SPT	SPW	K_2		
					SPT	SEM	SPW
W.H.	2.	1.94	1.96	2.79	.861	.88	1.22
Non W.H.		-	1.85	-	.811		-
Value from Ref. [73] : K_2 = .828							

TABLE 13

STRAIN GAUGE READINGS FROM POSITION 1 ON THE TEST PLATE: GAUGE 1

(1) L/L_y	L	Cycle Number 1	2	3	4	5	8	10	20	25	35
1	0-24	.00* ** .099 .002***	.002 .10 .003	.003 .101 .003	.003 .101 .003	.002 .101 .003	.003 .101 .003	.004 .102 .003	.003 .101 .003	— —	— —
-1.58	0-38	.010 .225 .075	.075 .226 .075	.075 .225 .076	.076 .226 .077	.077 .226 .076	.076 .226 .077	.076 .226 .076	.077 .226 .077	— —	— —
-1.79	0-43	.076 .480 .310	.310 .490 .317	.317 .495 .322	.322 .497 .325	.325 .498 .326	.326 .508 .327	.326 .508 .326	.327 .508 .326	— —	— —
-1.99	0-47.6	.326 .812 .586	.579 .814 .582	.582 .816 .586	.586 .817 .589	.589 .819 .592	.593 .821 .594	.594 .820 .595	.595 .820 .594	— —	— —
-2.16	0-52	.594 1.138 .856	.853 1.143 .858	.857 1.146 .862	.862 1.148 .866	.866 1.149 .870	.872 1.151 .876	.877 1.151 .876	.877 1.152 .878	— —	— —
-2.37	0-57	.878 1.460 1.139	1.131 1.461 1.190	1.185 1.463 1.180	1.180 1.465 1.175	1.175 1.466 1.162	1.156 1.467 1.156	1.154 1.468 1.154	1.153 1.470 1.153	— —	— —
2.66	0-64	1.152 1.958 1.602	1.643 2.190 1.868	1.866 2.302 1.977	1.976 2.415 2.092	2.088 2.405 2.102	2.190 2.517 2.200	2.225 2.552 2.239	2.275 2.593 2.276	2.297 2.620 2.298	— —
-2.86	0-68.7	2.299 3.180 2.727	2.707 3.240 2.902	2.902 3.300 2.993	2.968 3.332 3.027	3.028 3.348 3.051	3.056 3.372 3.078	3.085 3.387 3.093	2.921 3.173 2.918	2.723 2.944 2.717	2.673 2.876 2.667

* Initial
** Maximum } (%)
*** Final

(1) L_y — 24 klb

TABLE 14

INTERNAL CIRCUMFERENTIAL STRAIN GAUGE READINGS FROM POSITION F ON THE TEST NOZZLE: GAUGE FC

(1) P/P_y	Cycle Number									
	1	2	3	5	8	10	20	30	40	50
1.82	* .018 ** .278 *** .120	.120 .279 .120	.120 .280 .121	.121 .281 .121	.122 .280 .122	.121 .281 .120	.120 .280 .121	--	--	--
2.18	.120 .597 .398	.420 6.18 .421	.421 .620 .423	.422 .621 .422	.424 .624 .425	.428 .629 .429	.430 .630 .429	--	--	--
2.45	.427 1.297 1.070	1.068 1.322 1.100	1.096 1.332 1.104	1.106 1.340 1.110	1.114 1.347 1.119	1.129 1.352 1.131	1.132 1.359 1.132	--	--	--
2.60	1.132 1.880 1.649	1.647 1.886 1.659	1.670 1.904 1.676	1.686 1.910 1.688	1.688 1.917 1.690	1.693 1.922 1.693	1.704 1.928 1.703	1.706 1.930 1.706	1.709 1.932 1.708	1.710 1.934 1.709
2.8	1.729 2.608 2.446	2.439 2.685 2.446	2.446 2.690 2.450	2.454 2.695 2.457	2.463 2.701 2.467	2.469 2.705 2.474	2.484 2.721 2.484	2.497 2.736 2.498	2.523 2.760 2.526	2.539 2.776 2.539
2.96	2.541 3.612 3.362	3.366 3.623 3.378	3.378 3.626 3.381	3.385 3.632 3.385	3.398 3.641 3.399	3.410 3.648 3.425	3.417 3.666 3.416	3.423 3.673 3.424	--	--

* Initial
** Maximum
*** Final

(1) P_y - 275 lb in^2

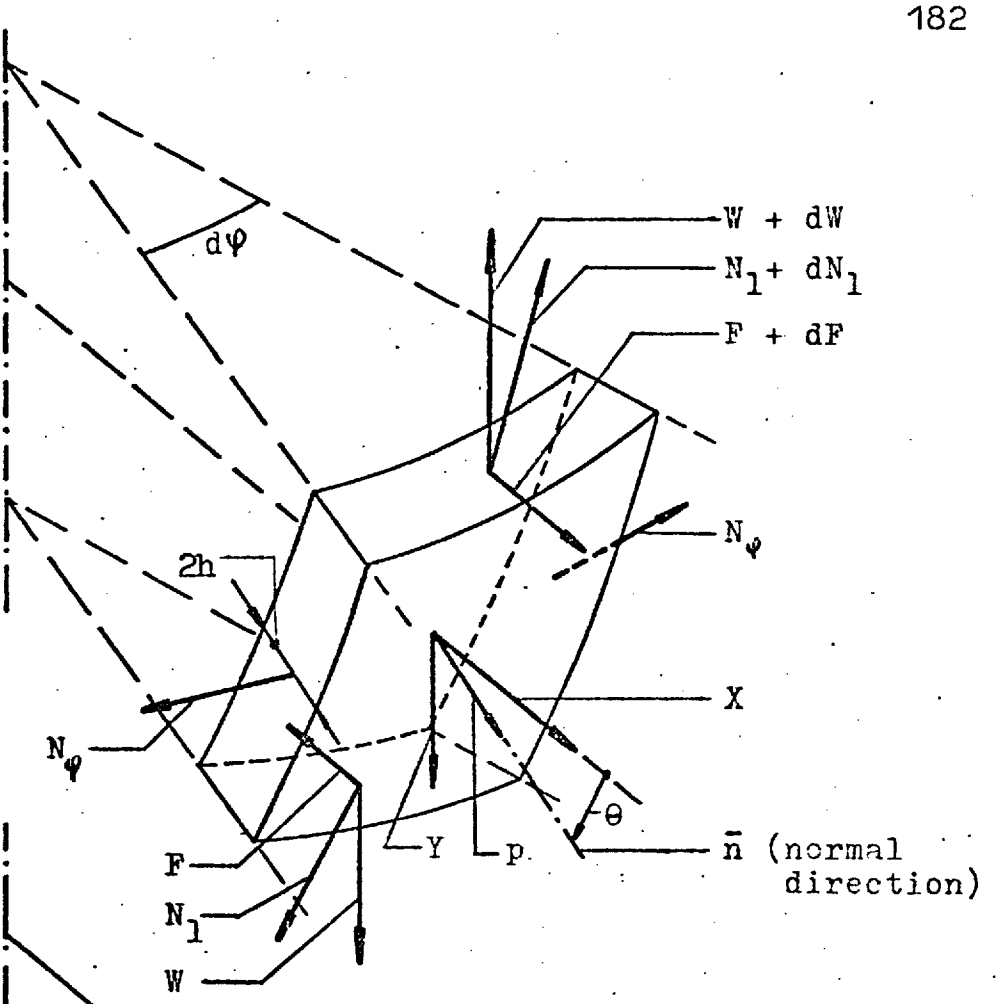

FIG. 1a

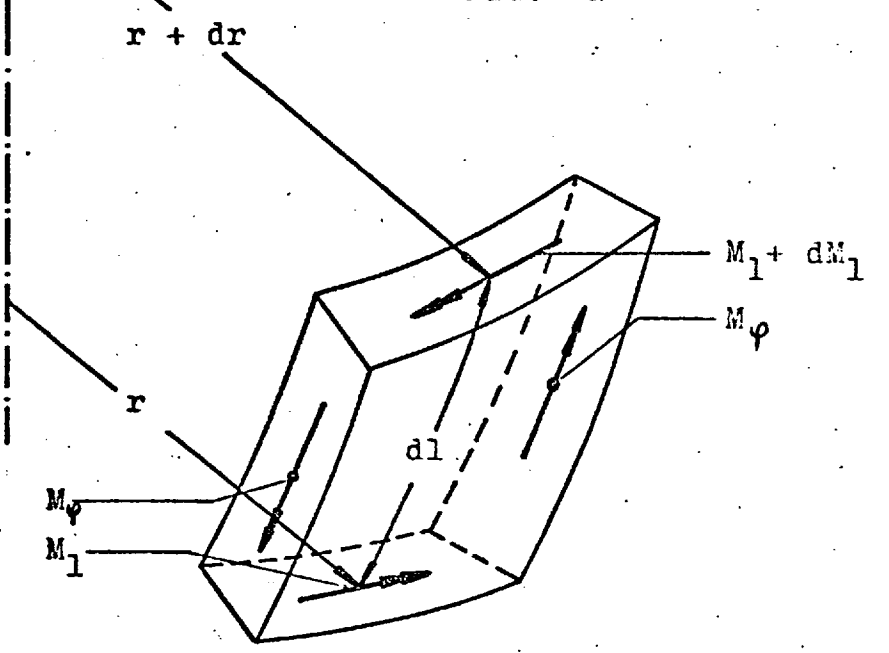

FIG. 1b

FORCES AND MOMENTS ON AN ELEMENT OF SYMMETRICALLY LOADED SHELL OF REVOLUTION

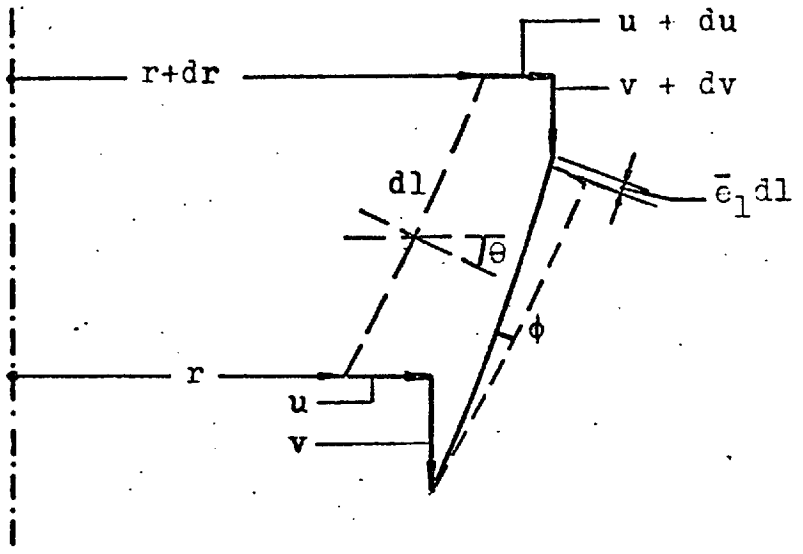

FIG. 2a

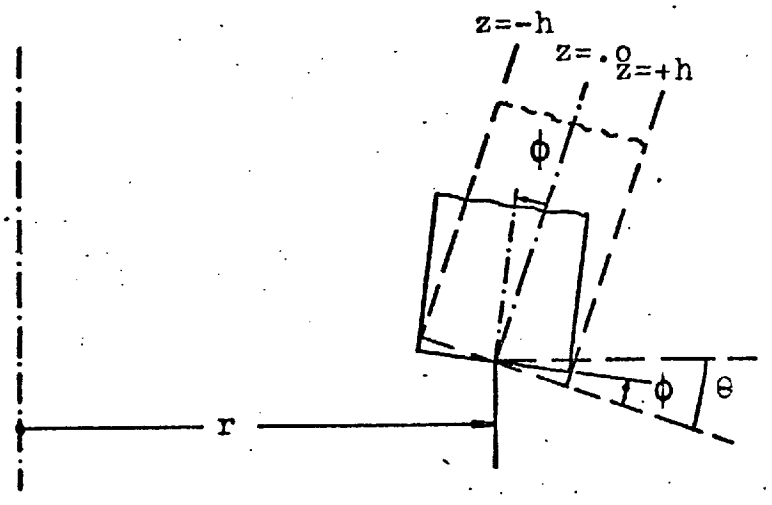

FIG. 2b

GEOMETRY OF DEFORMATION FOR SYMMETRICALLY LOADED SHELL OF REVOLUTION

---- Original position

—— final position

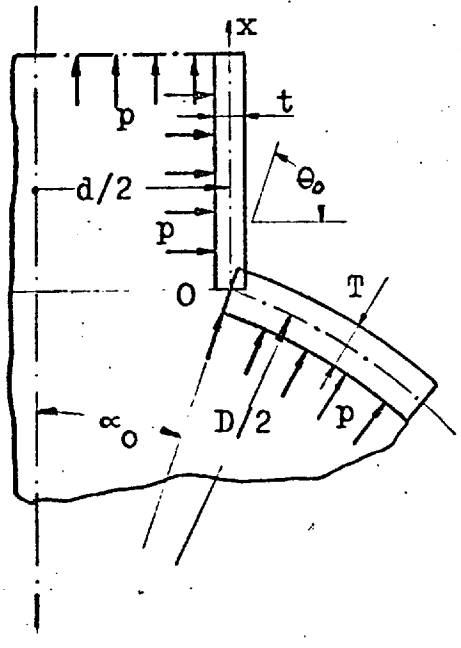

Fig.3 Flush radial nozzle in sphere

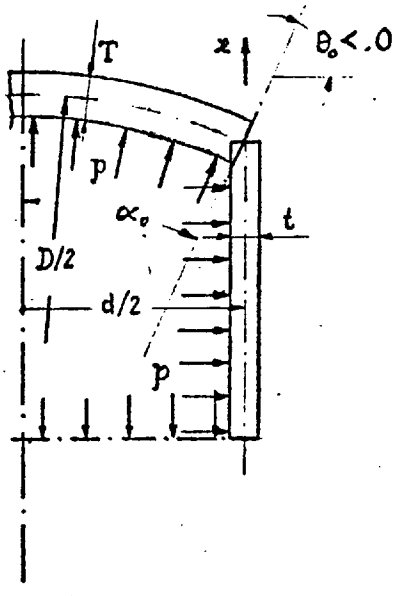

Fig.4 Spherical head in cylinder

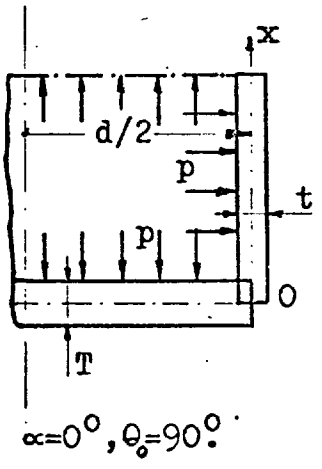

$\alpha=0^o, \Theta_o=90^o$

Fig.5 Flat end in cylinder

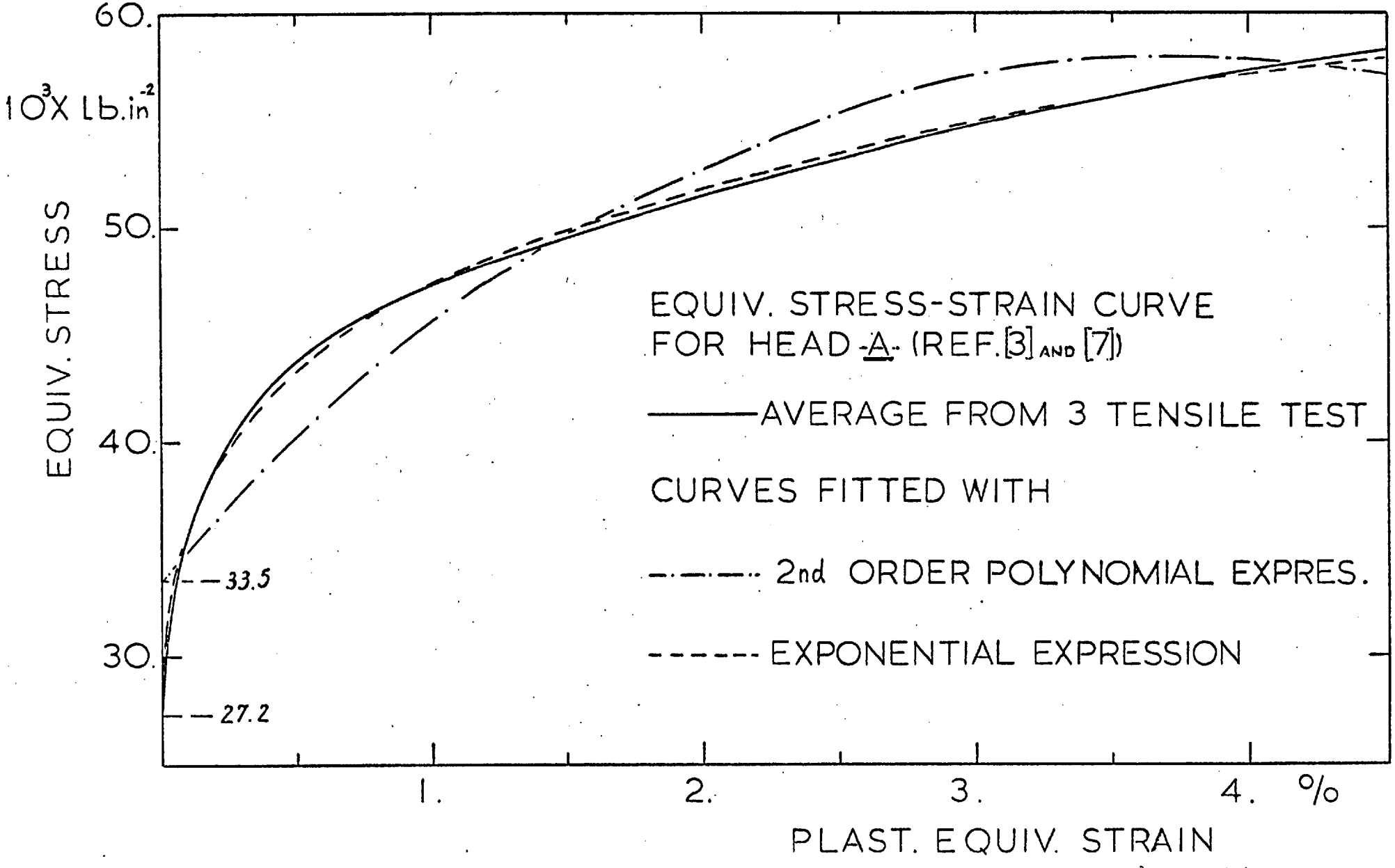

FIG. 6 STRESS-STRAINCURVE HEAD A MATERIAL

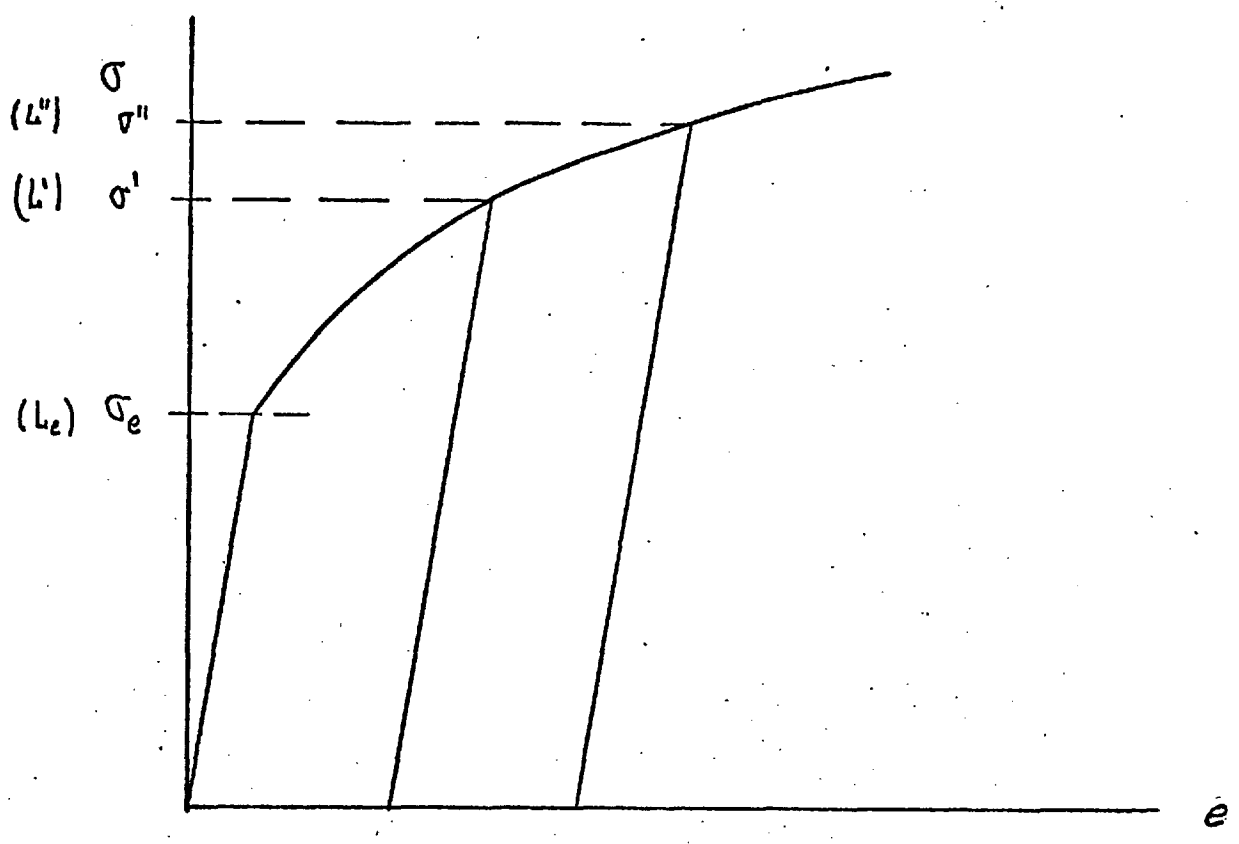

FIG.7

STRESS–STRAIN CURVE FOR AN IDEAL TENSION TEST PIECE

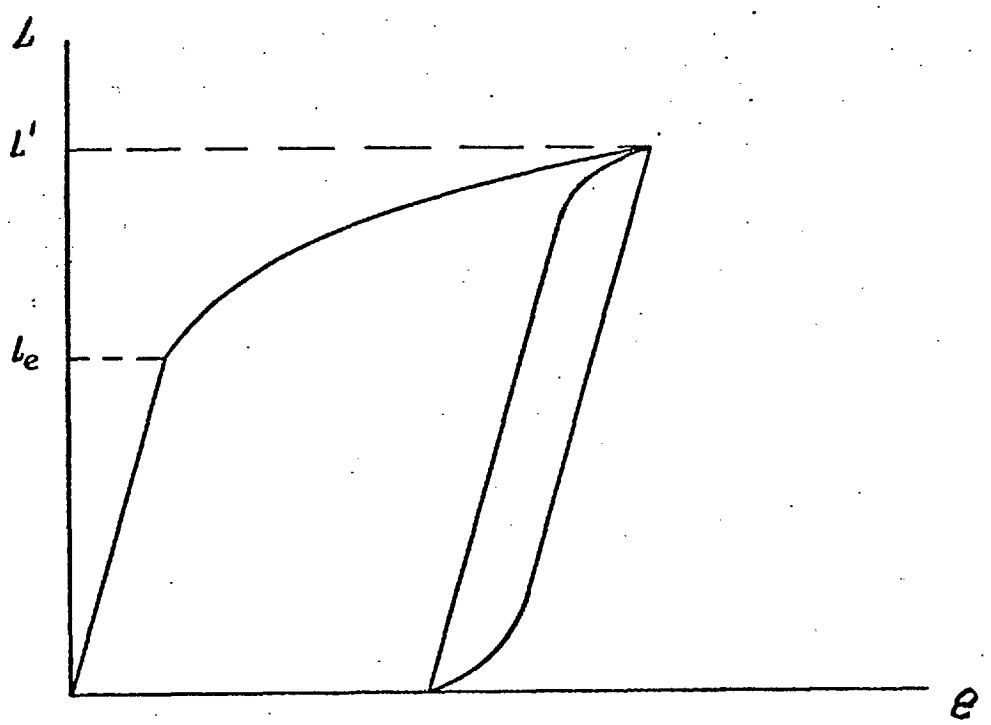

FIG.8

LOADING AND UNLOADING PATHS FOR STRUCTURES WITH STABLE MATERIAL
(Hysteresis Loop)

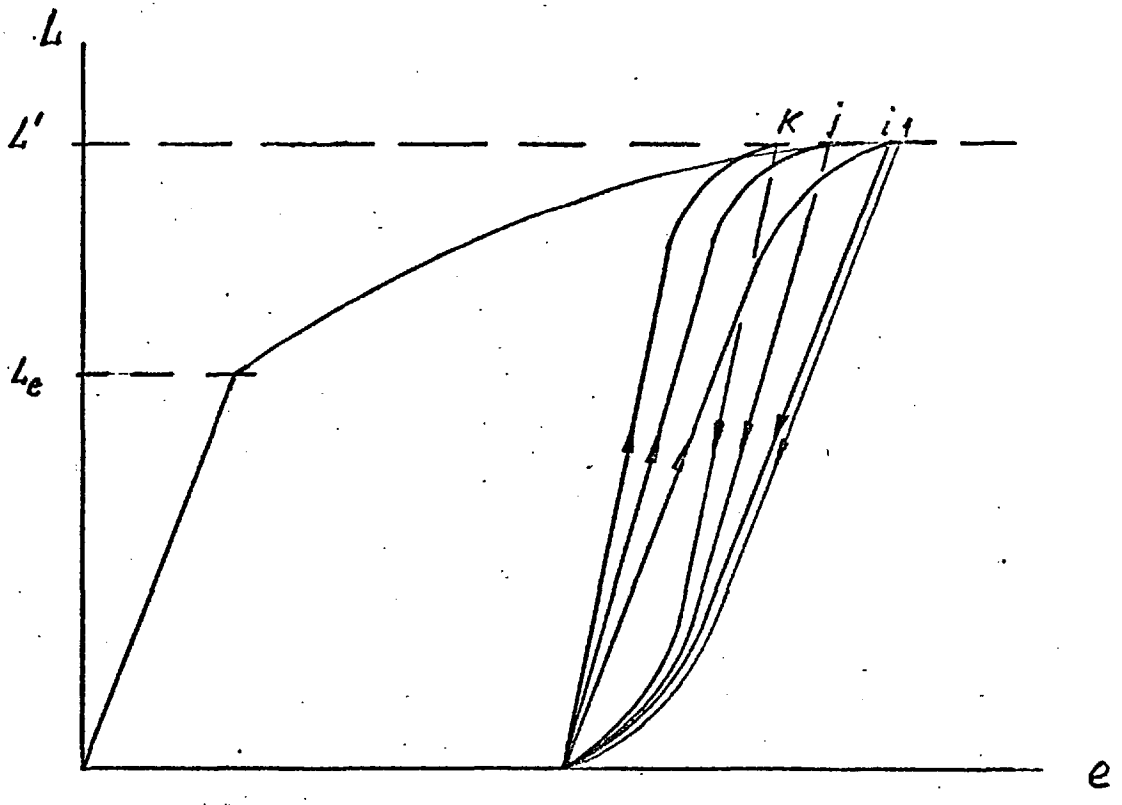

FIG.9

THE EFFECT OF OVERALL LOAD-CONTROLLED CYCLIC WORK-HARDENING ON STRAINS ADJACENT TO THE YIELDED REGION

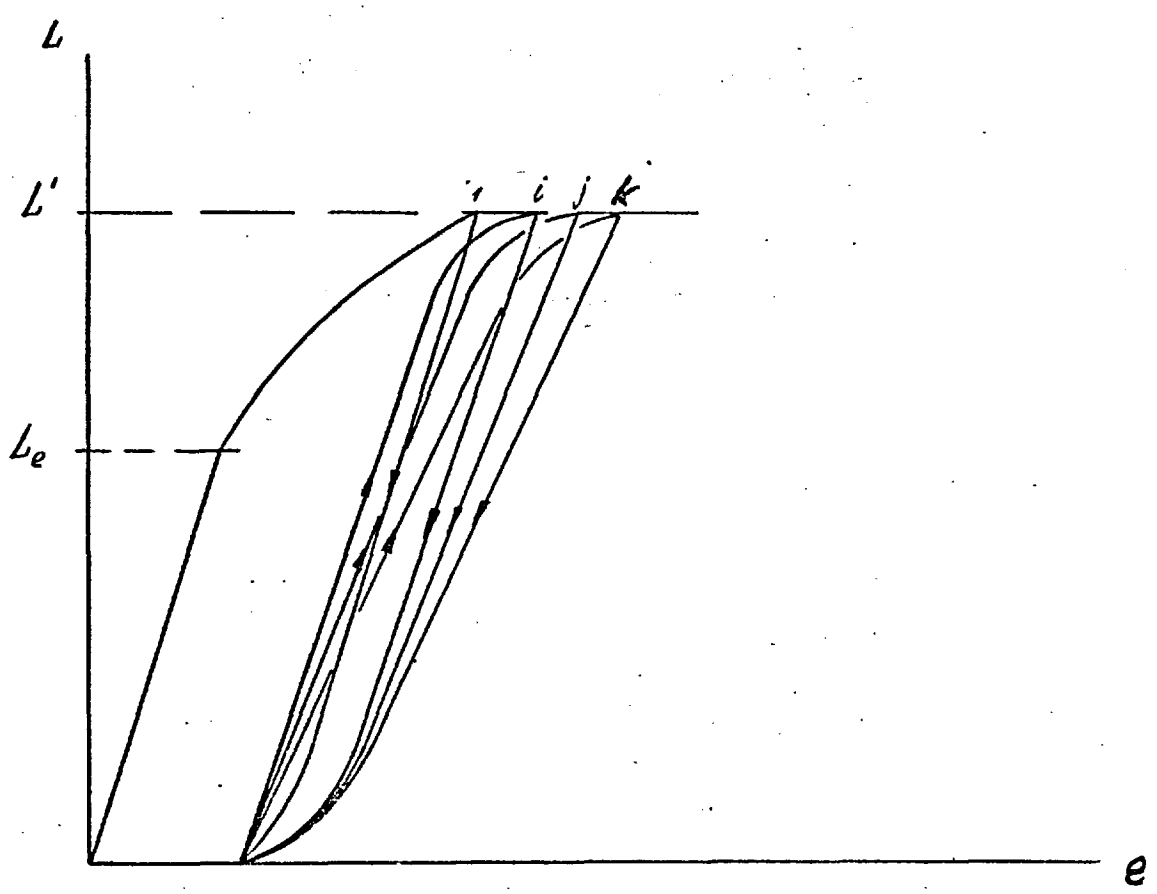

FIG.10

THE EFFECT OF OVERALL LOAD-CONTROLLED CYCLIC WORK-SOFTENING ON STRAINS ADJACENT TO THE YIELDED REGION

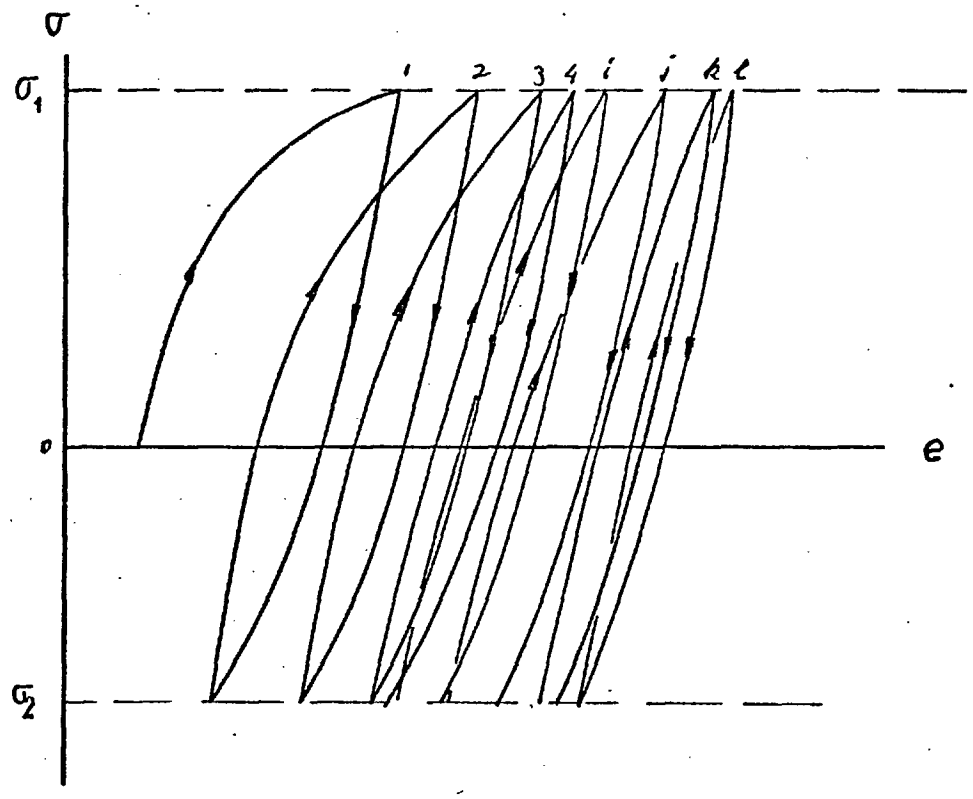

FIG. 11

STRESS-CONTROLLED TEST WITH CYCLIC STRAIN ACCUMULATION

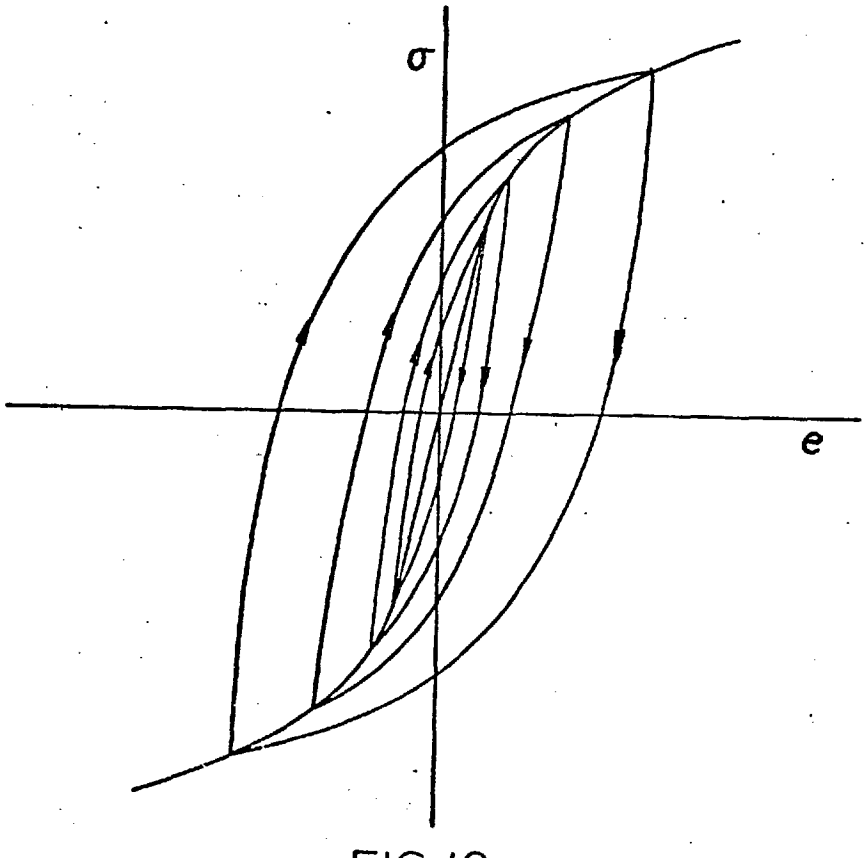

FIG. 12

CONSTRUCTION OF SETTLED CYCLIC STRESS-STRAIN CURVE

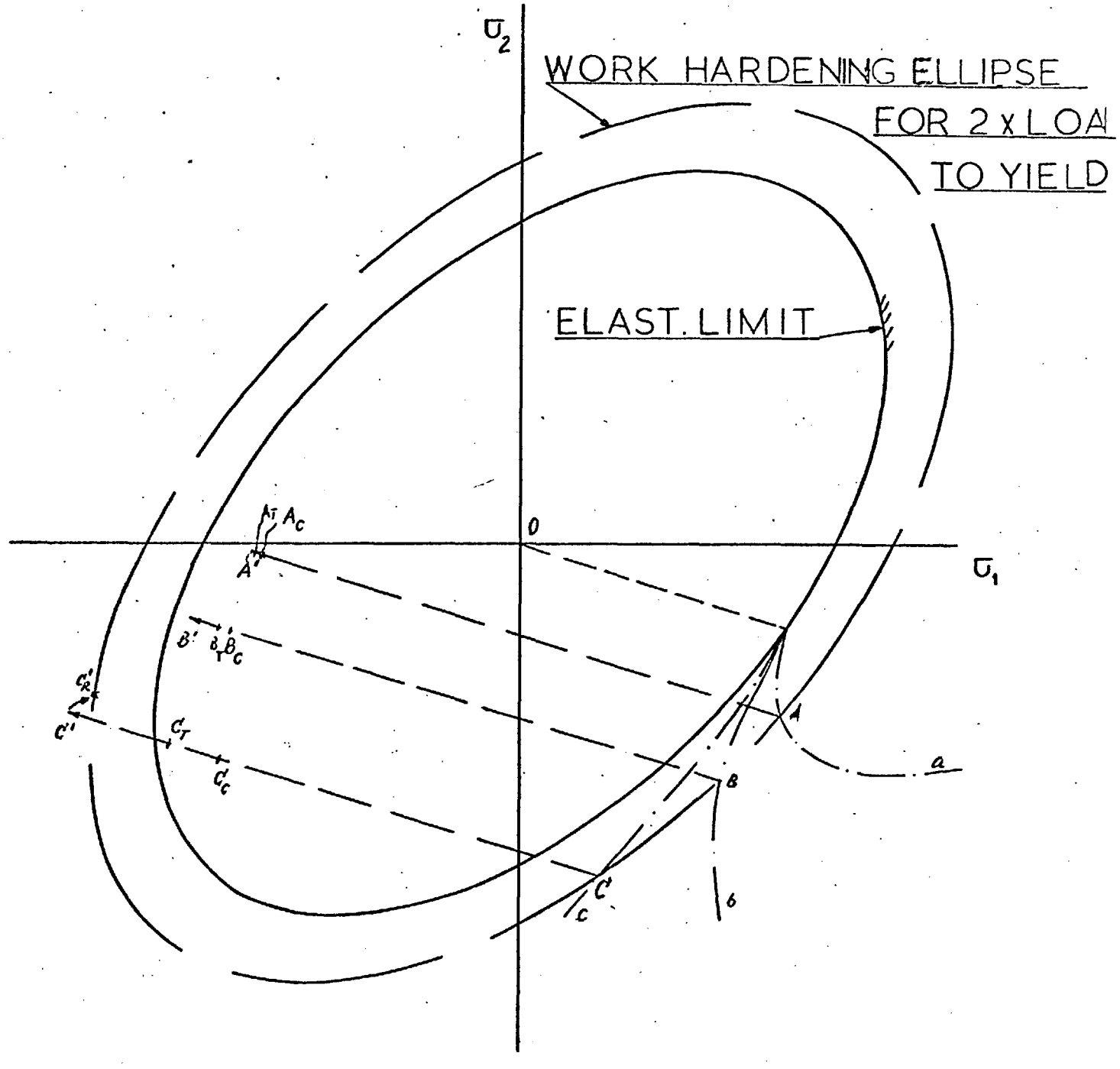

FIG. 13

ELASTIC-PLASTIC STRESS PATHS FOR THREE DIFFERENT STRUCTURES LOADED BEYOND FIRST YIELD IN A WORK HARDENING MATERIAL

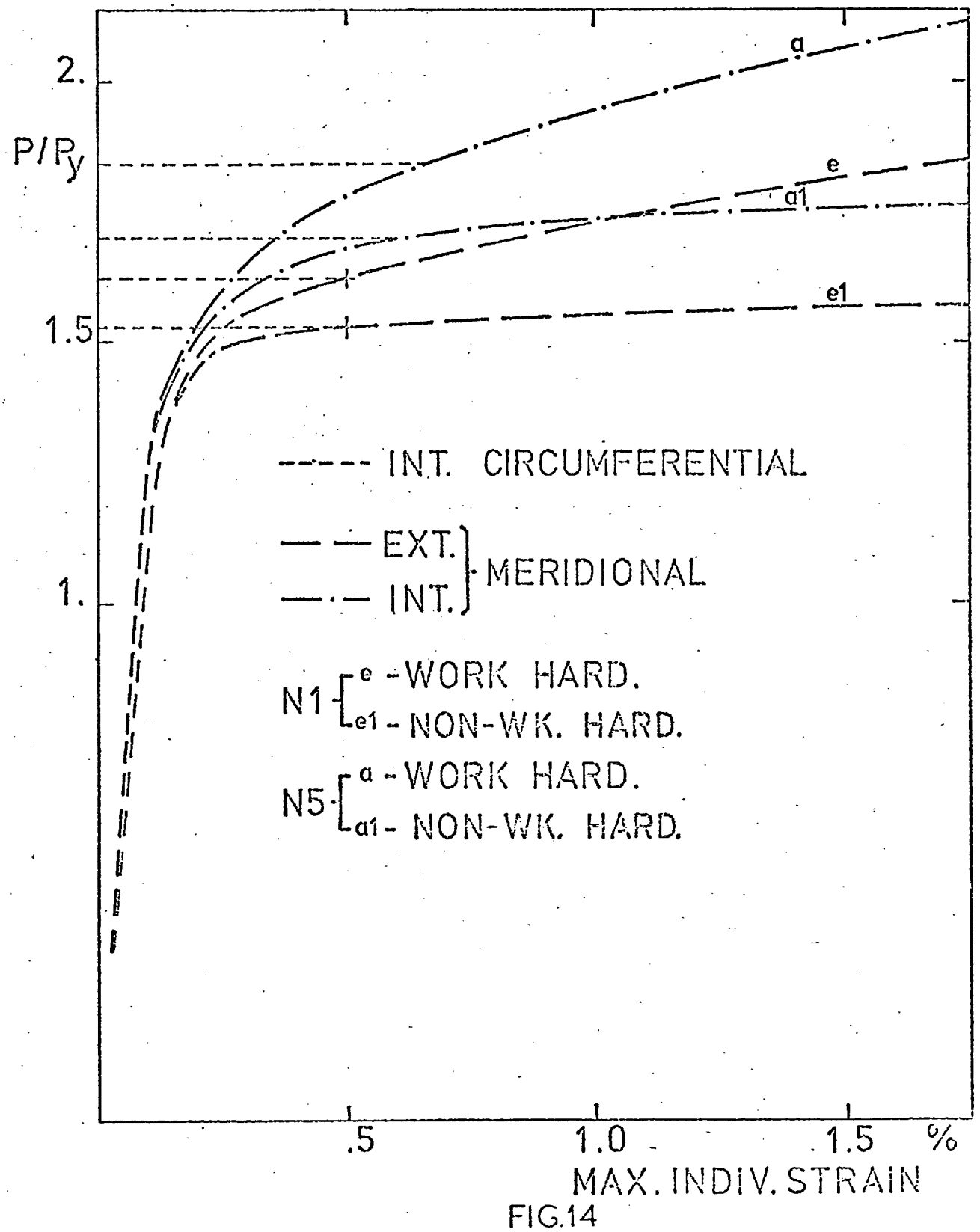

FIG.14

THE EFFECT OF WORK HARDENING ON THE COMPUTED VALUES OF MAXIMUM STRAIN IN TWO NOZZLES

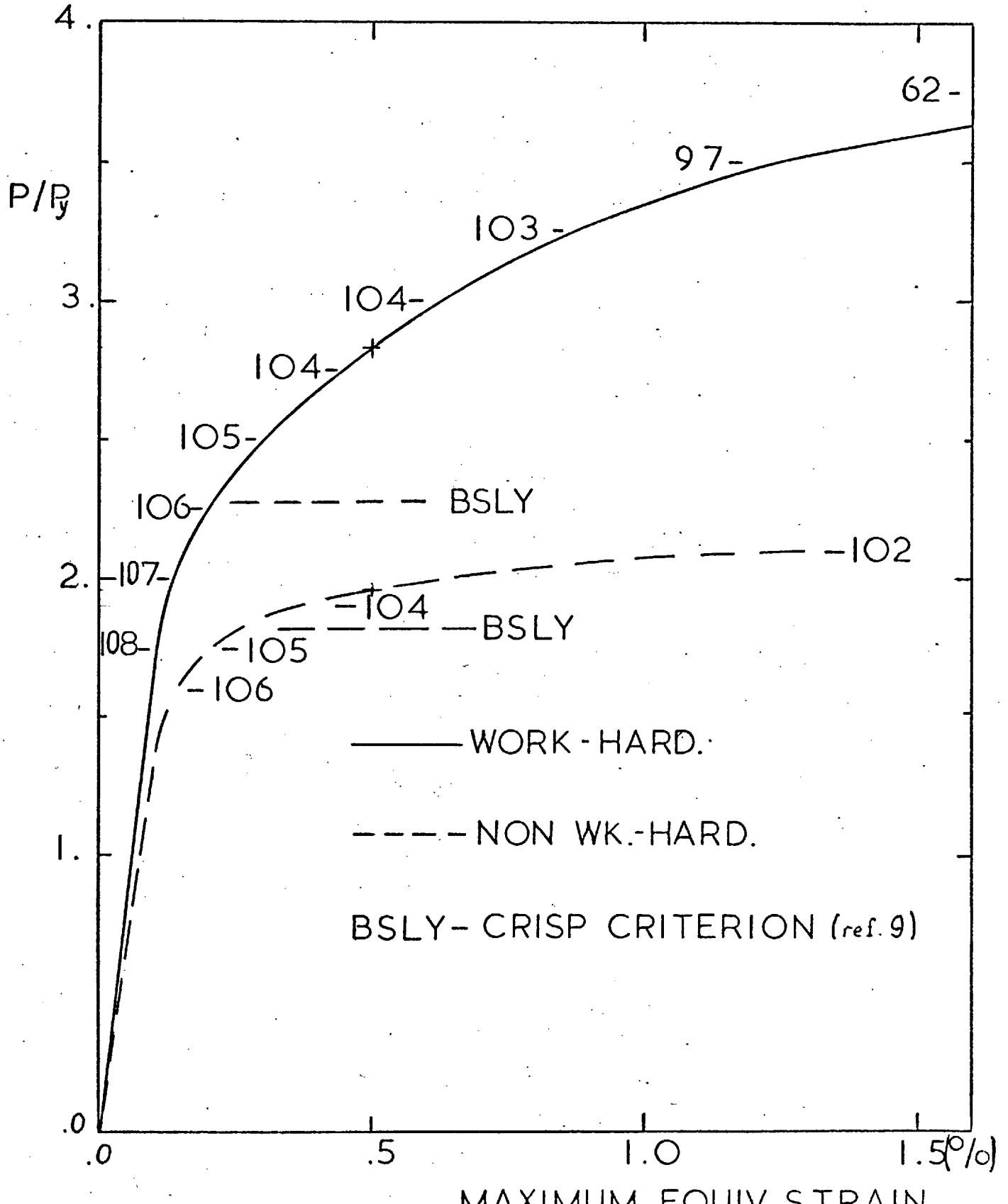

FIG.15

. MAXIMUM EQUIVALENT STRAIN ON THE OUTSIDE SURFACE OF HEAD A (Ref. [7])

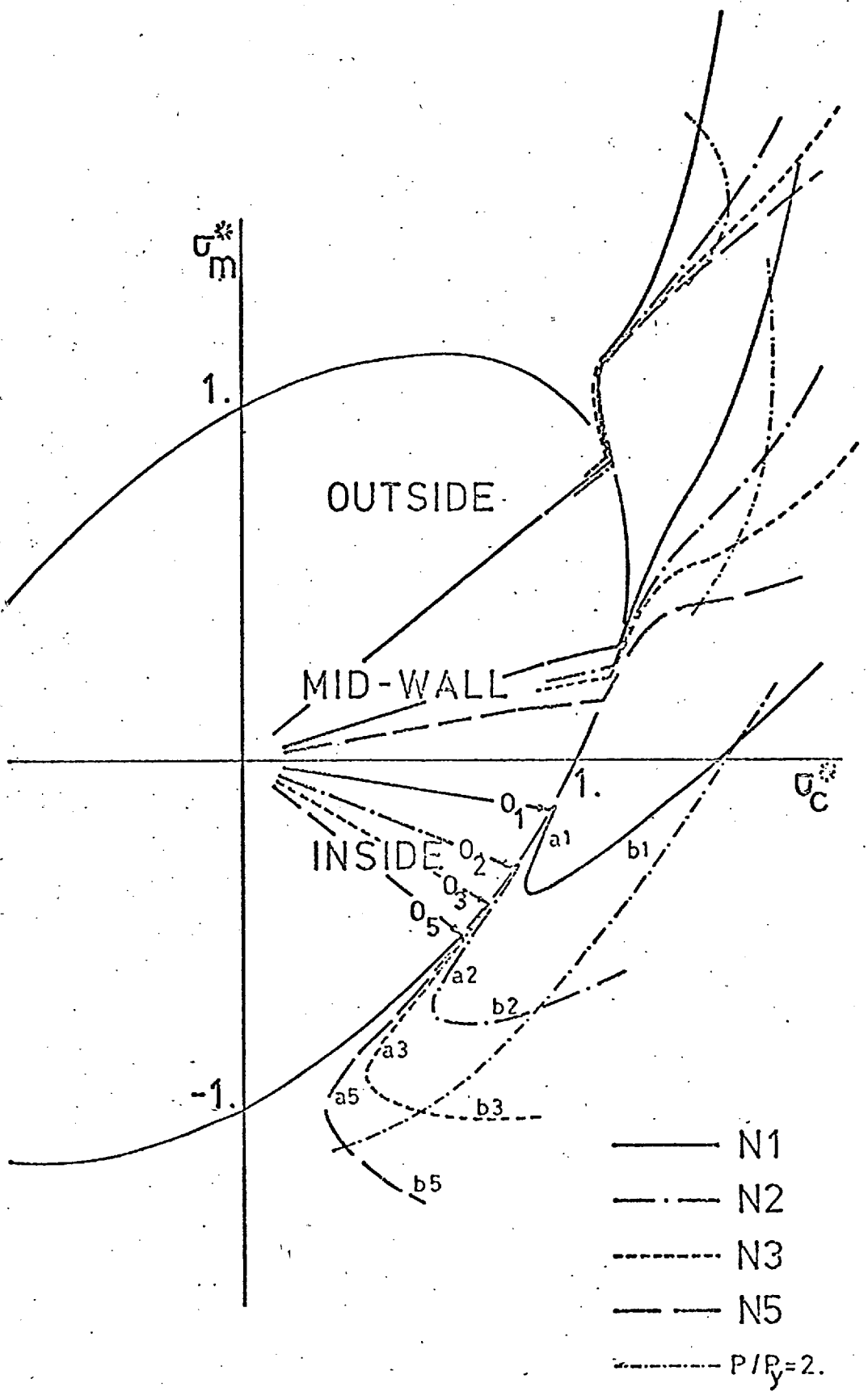

FIG.16

ELASTIC-PLASTIC STRESS PATH FOR A SERIES OF NOZZLES LOADED BEYOND FIRST YIELD ON A WORK HARDENING MATERIAL

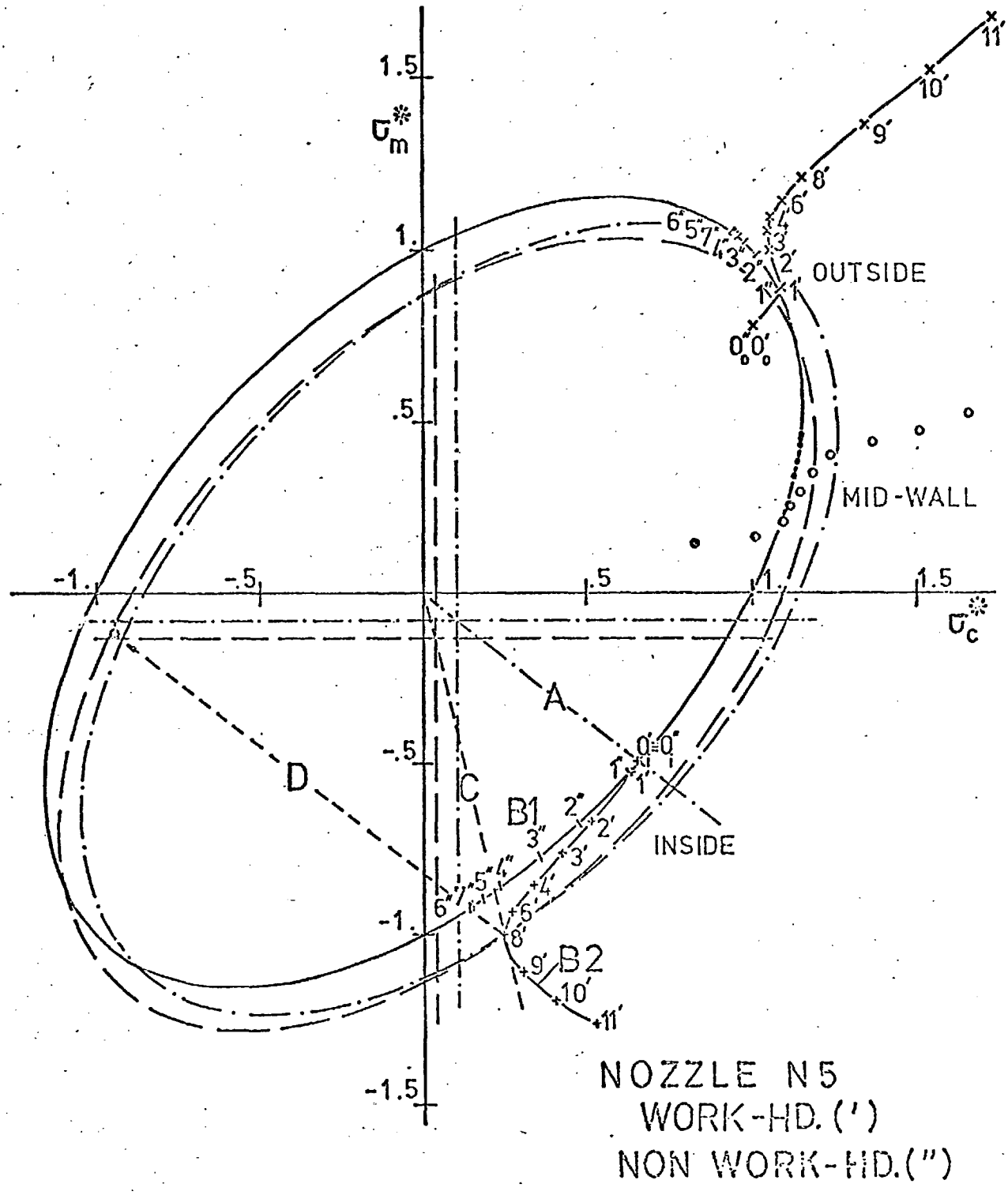

FIG.17

THE EFFECT OF WORK HARDENING ON THE ELASTIC-PLASTIC STRESS PATH FOR A NOZZLE LOADED BEYOND FIRST YIELD

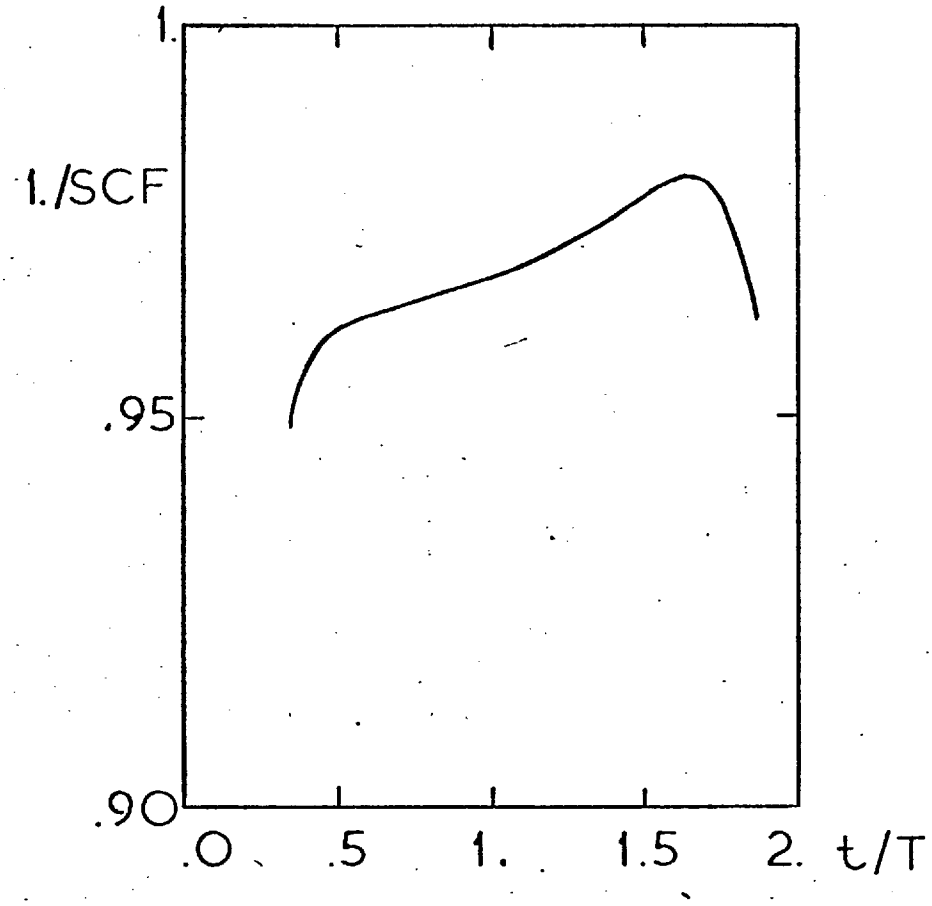

FIG.18

MAXIMUM STRESS CONCENTRATION RATIO FOR HEMISPHERICAL HEADS OF DIFFERENT CYLINDER-SPHERE THICKNESS RATIOS (t/T)

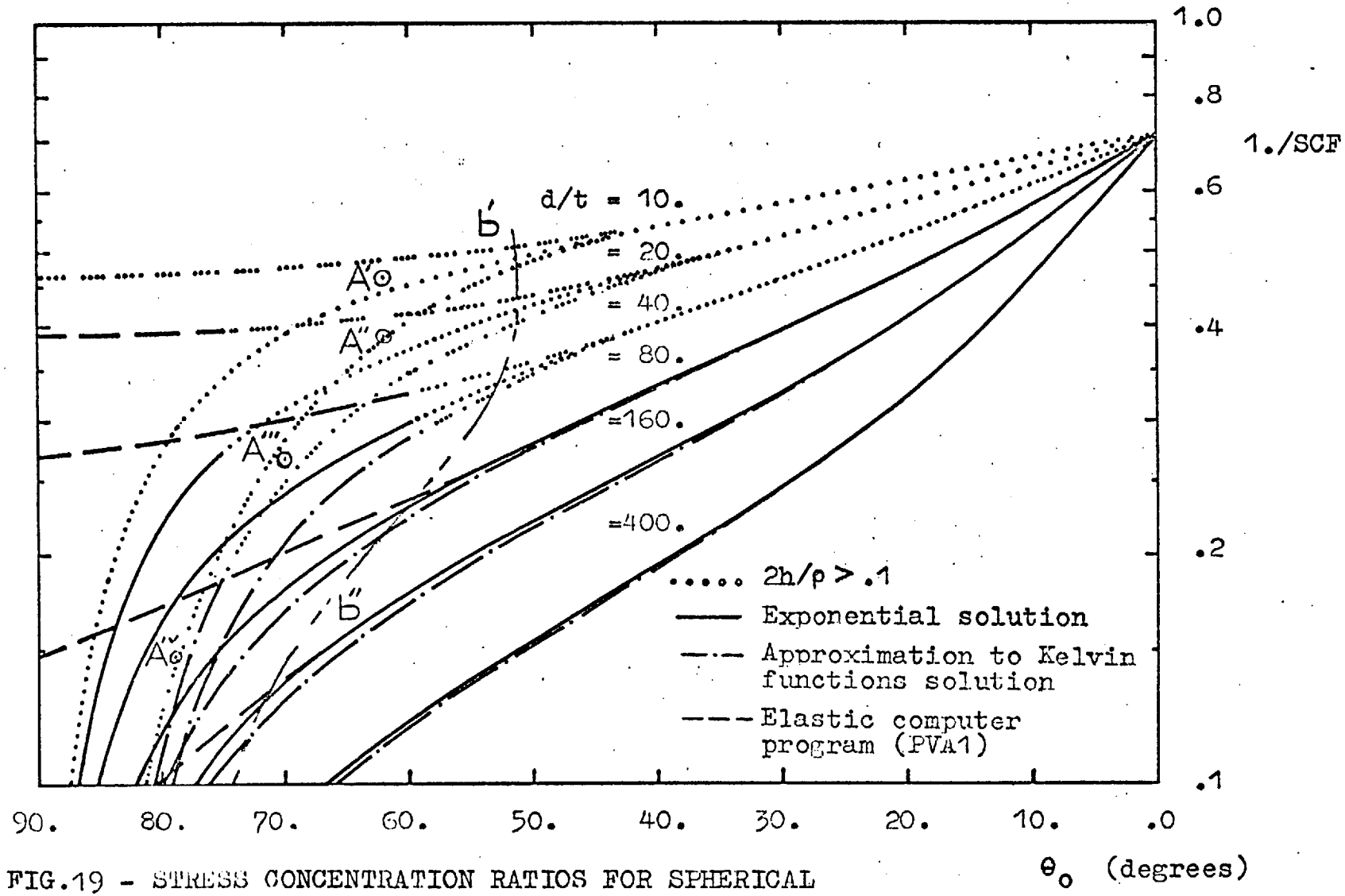

FIG.19 - STRESS CONCENTRATION RATIOS FOR SPHERICAL HEADS ON CYLINDRICAL PRESSURE VESSELS WITH t/T = .25

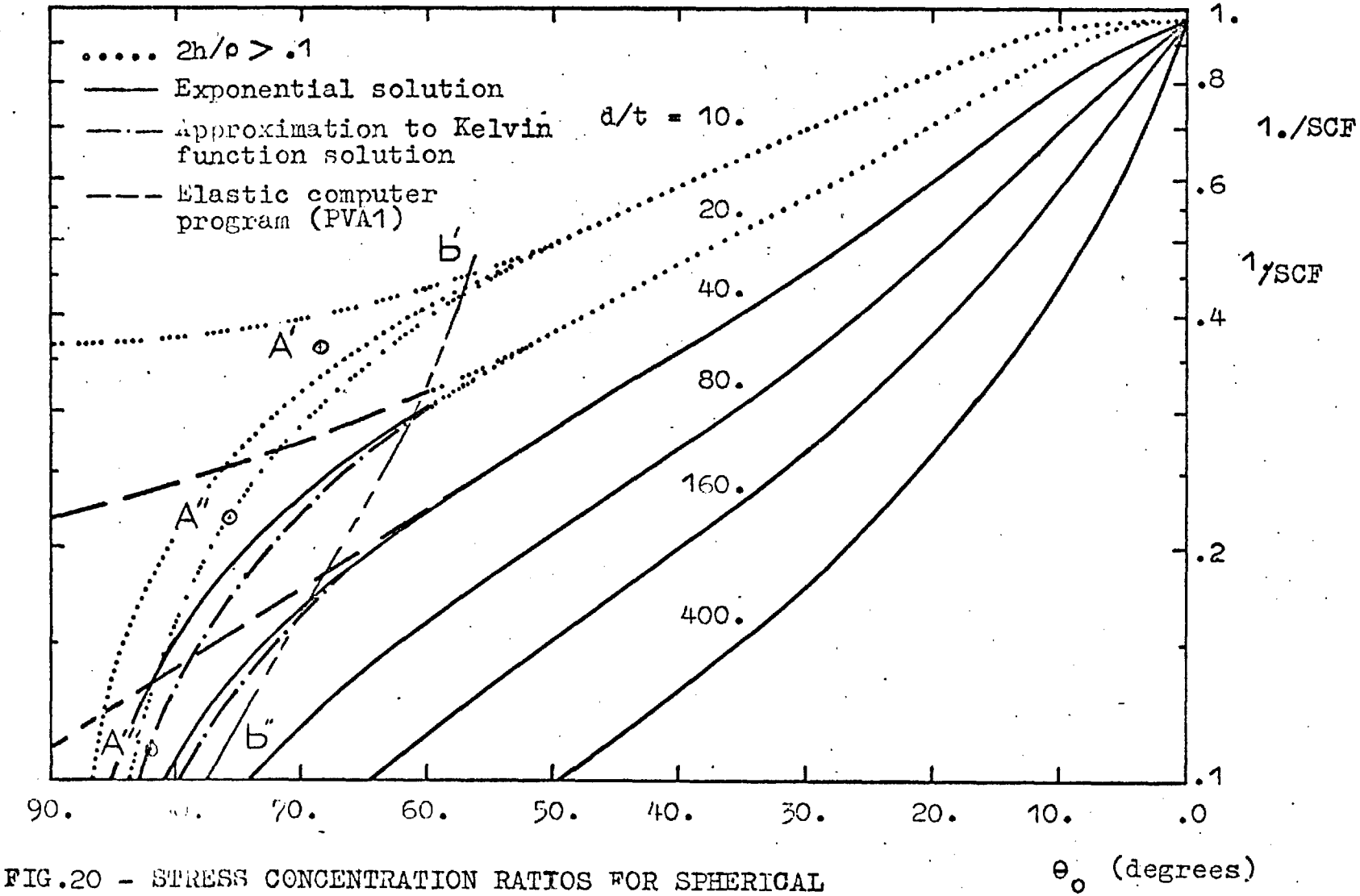

FIG.20 - STRESS CONCENTRATION RATIOS FOR SPHERICAL HEADS ON CYLINDRICAL PRESSURE VESSELS WITH t/T = .50

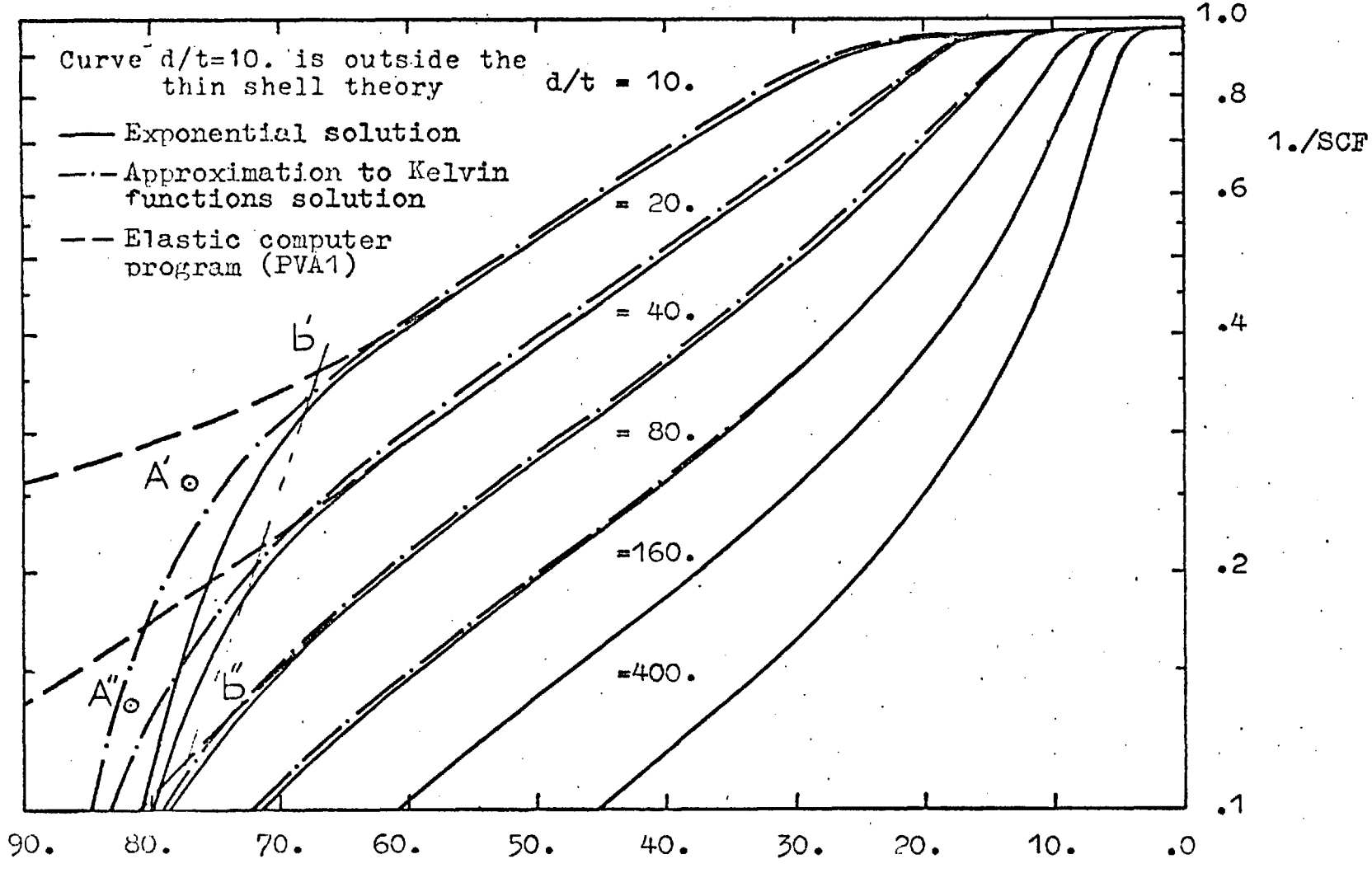

FIG.21 - STRESS CONCENTRATION RATIOS FOR SPHERICAL HEADS ON CYLINDRICAL PRESSURE VESSELS WITH t/T =1.0

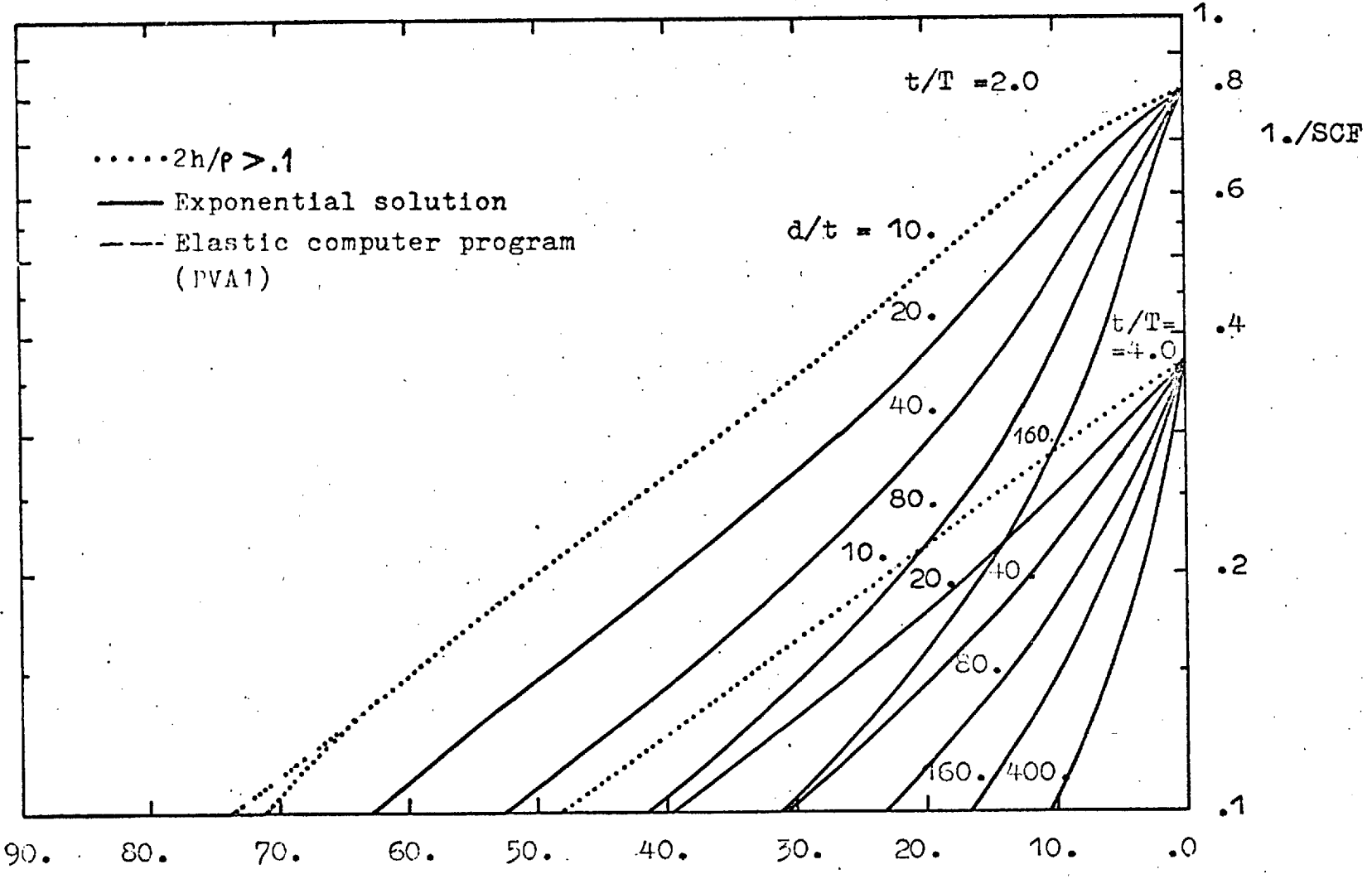

FIG.22 - STRESS CONCENTRATION RATIOS FOR SPHERICAL HEADS ON CYLINDRICAL PRESSURE VESSELS WITH t/T =2.0 AND 4.0

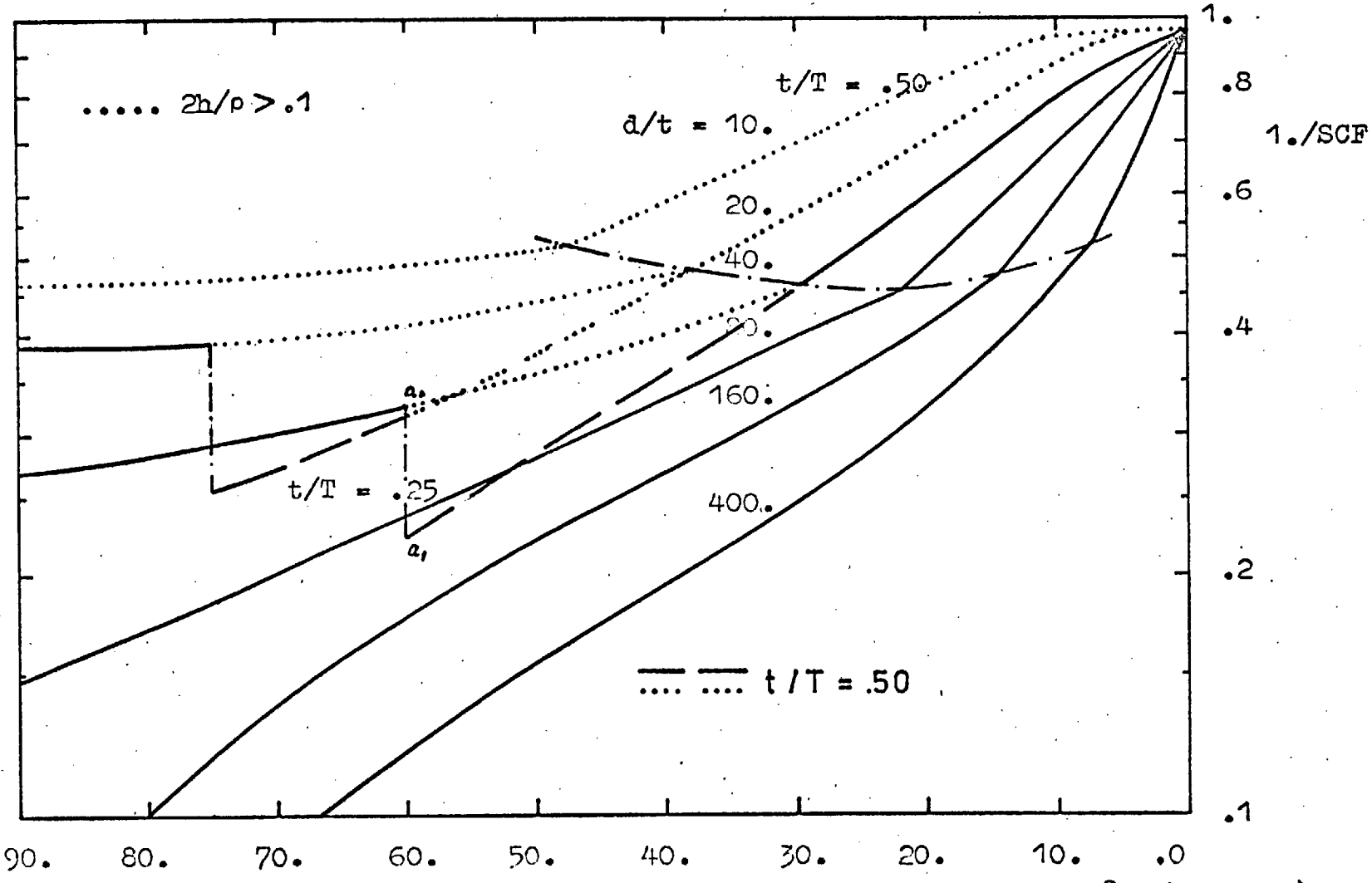

FIG.23 - MAXIMUM STRESS CONCENTRATION RATIOS FOR SPHERICAL HEADS ON CYLINDRICAL PRESSURE VESSELS OF t/T = .25 AND .50

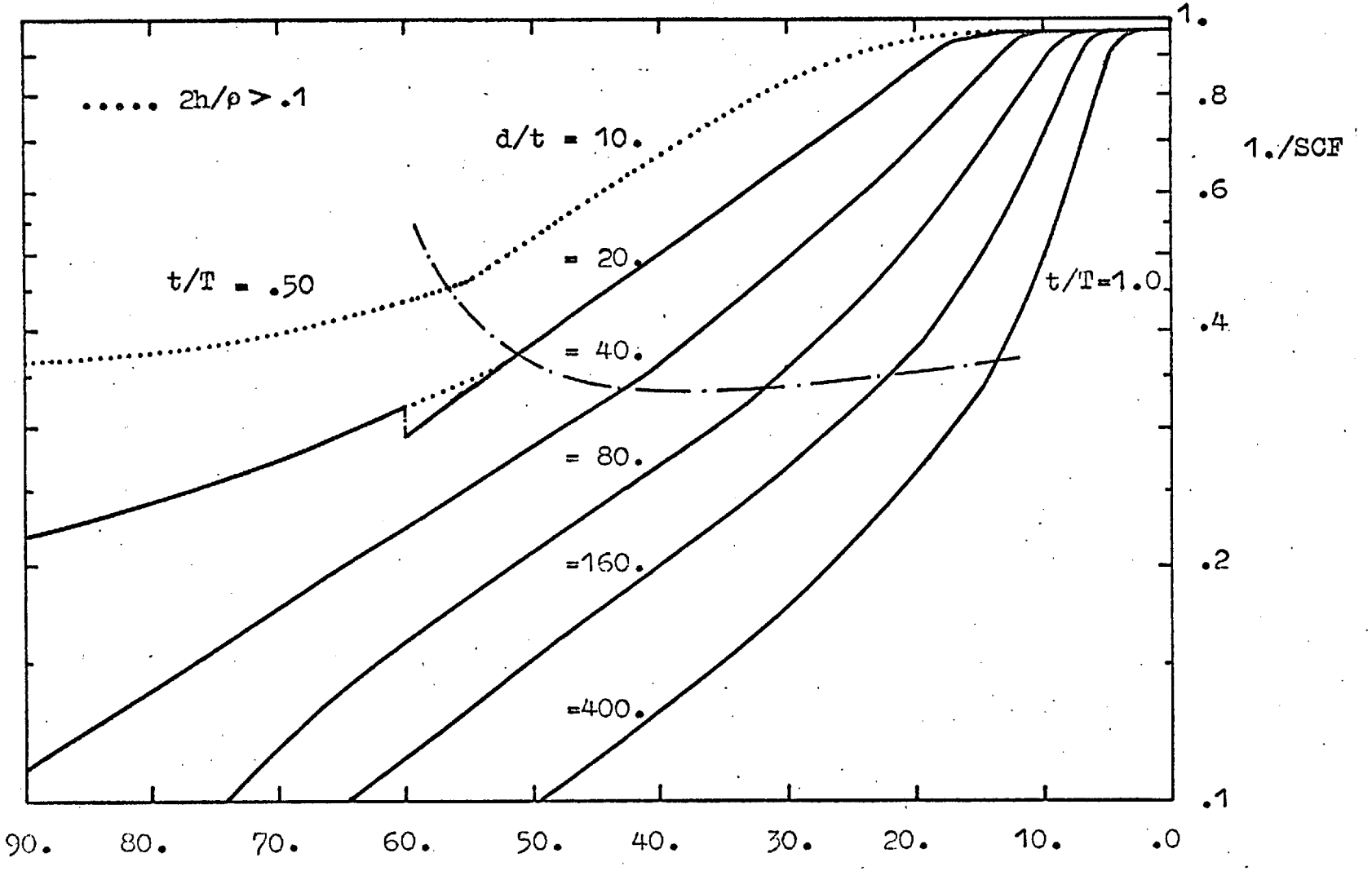

FIG.24 - MAXIMUM STRESS CONCENTRATION RATIOS FOR SPHERICAL HEADS ON CYLINDRICAL PRESSURE VESSELS OF t/T = .50 AND 1.0

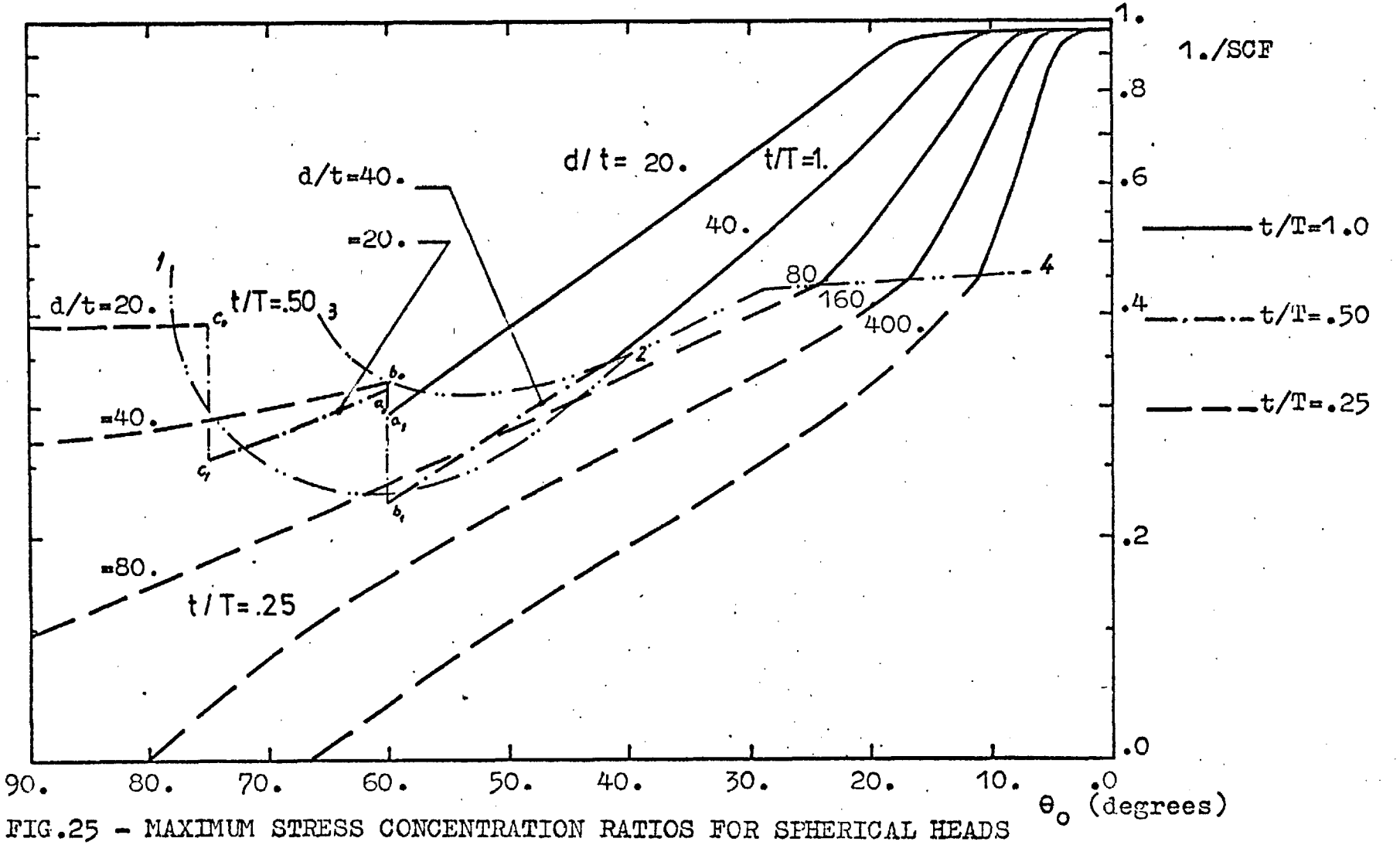

FIG.25 - MAXIMUM STRESS CONCENTRATION RATIOS FOR SPHERICAL HEADS ON CYLINDRICAL PRESSURE VESSELS OF t/T = .25, .50 AND 1.0

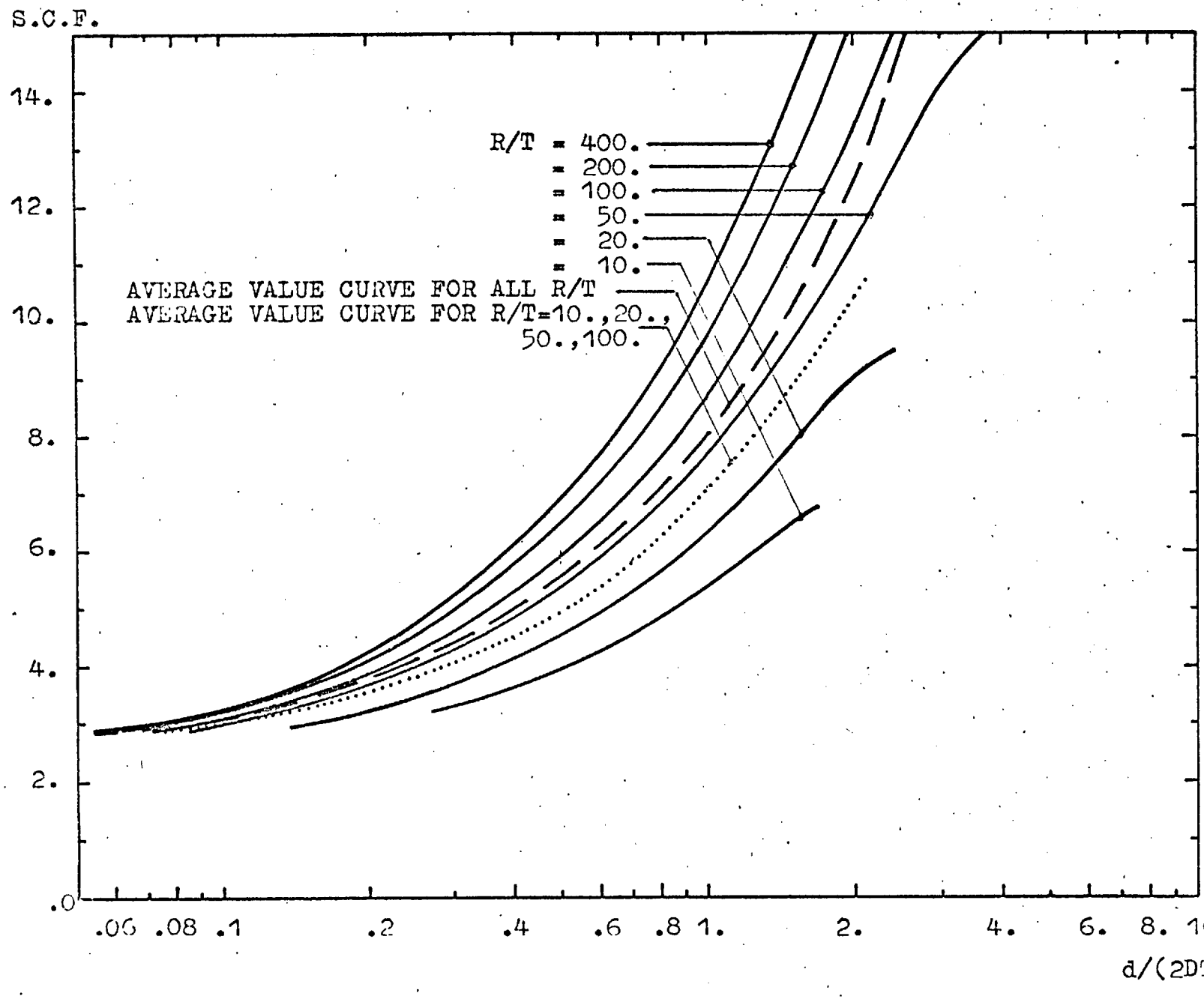

FIG.26 - ELASTIC STRESS CONCENTRATION FACTORS FOR FLUSH CYLINDRICAL NOZZLES ON SPHERICAL PRESSURE VESSELS (t/T = .25)

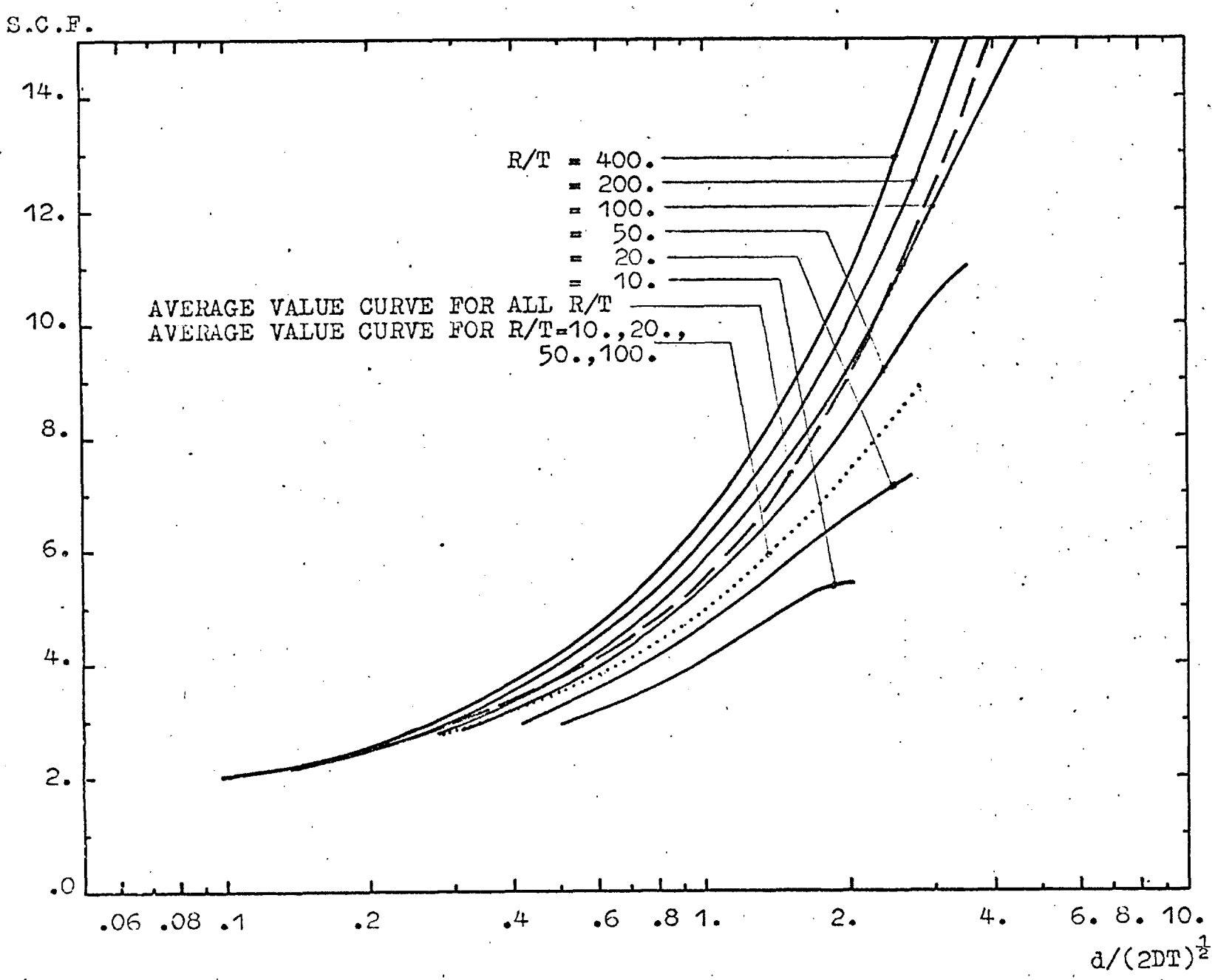

FIG.27 - ELASTIS STRESS CONCENTRATION FACTORS FOR FLUSH CYLINDRICAL NOZZLES ON SPHERICAL PRESSURE VESSELS (t/T = .50)

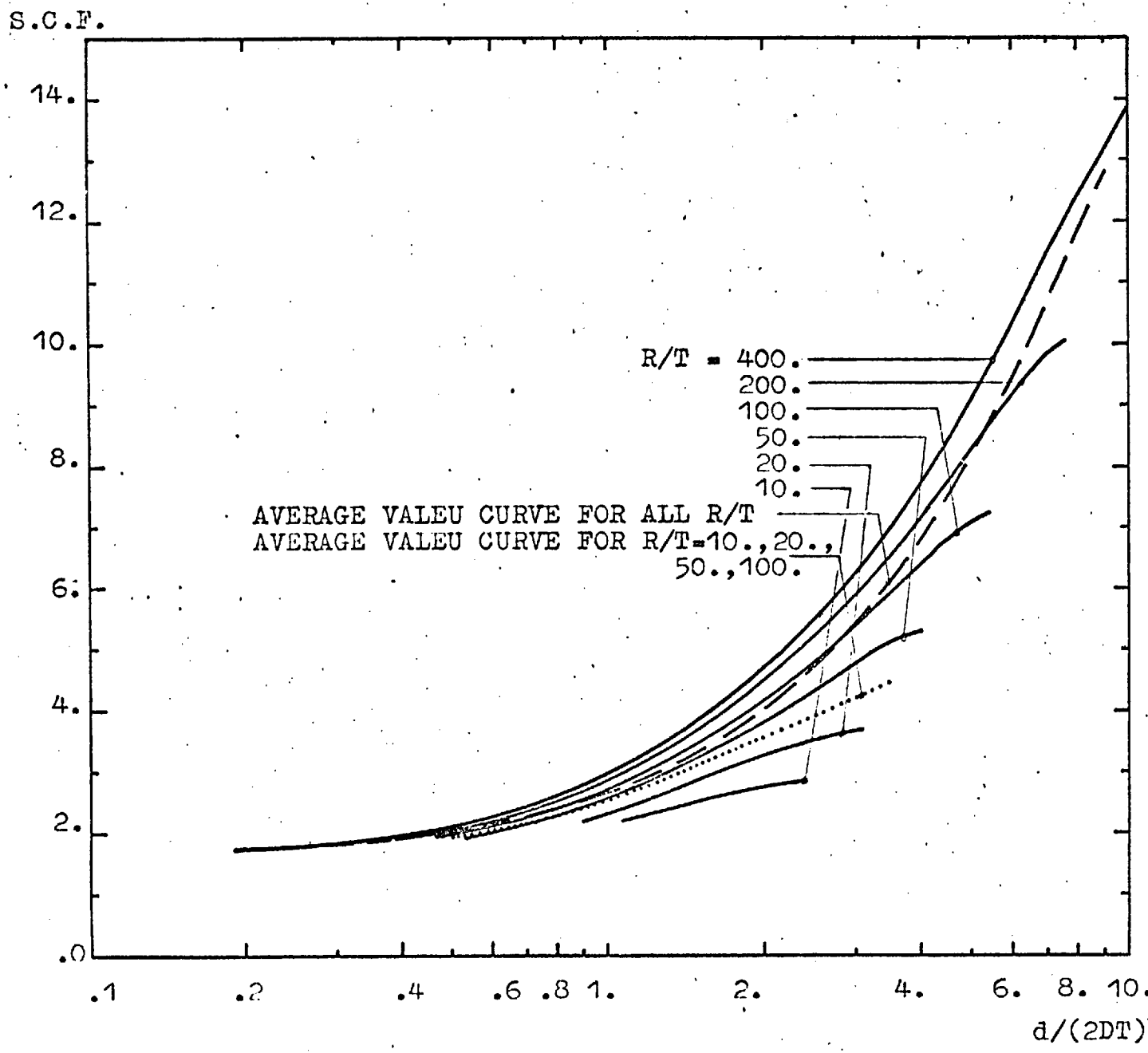

FIG.28 - ELASTIC STRESS CONCENTRATION FACTORS FOR FLUSH CYLINDRICAL NOZZLES ON SPHERICAL PRESSURE VESSELS (t/T = 1.0)

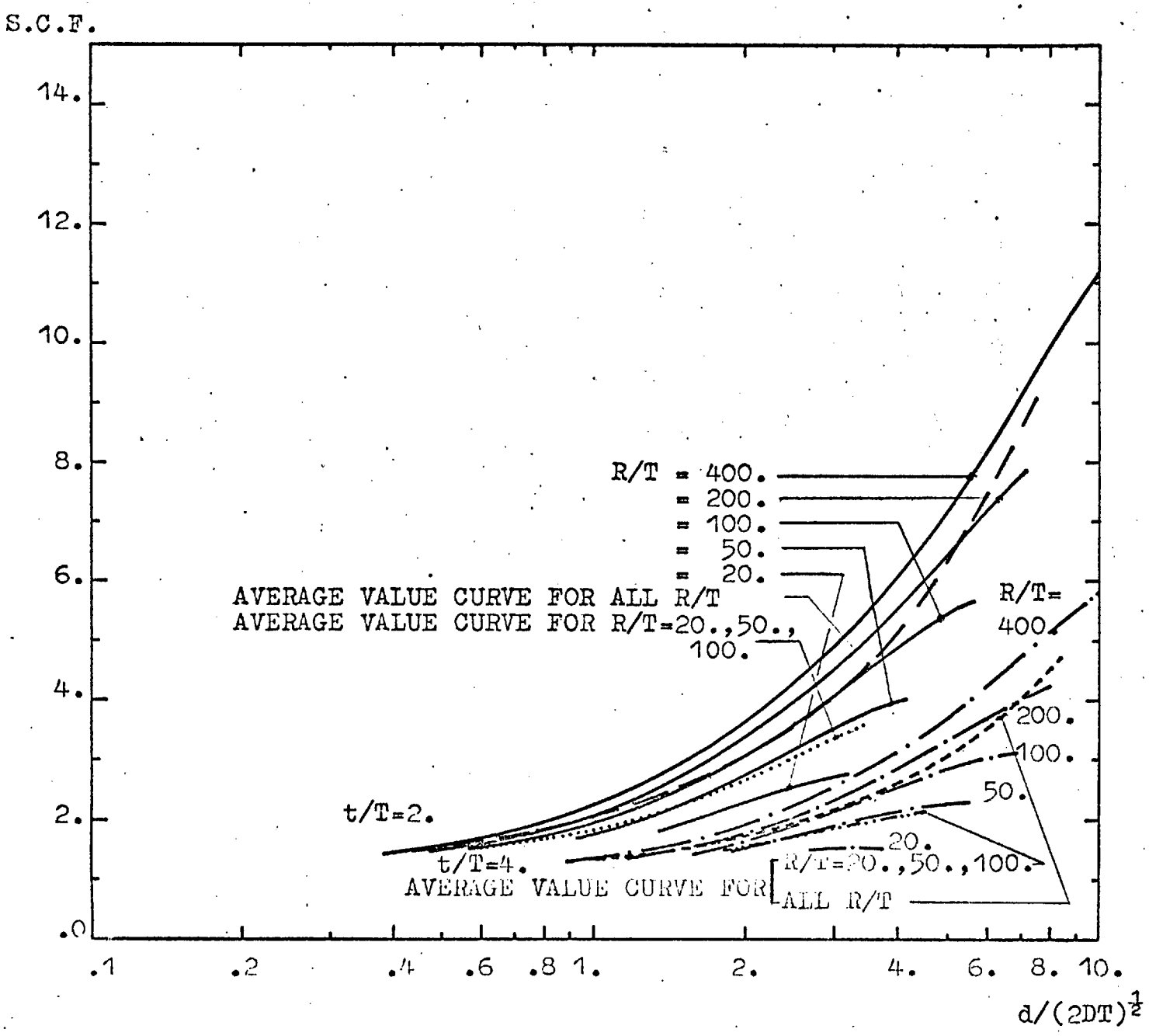

FIG.29 - ELASTIC STRESS CONCENTRATION FACTORS FOR FLUSH CYLINDRICAL NOZZLES ON SPHERICAL PRESSURE VESSELS (t/T=2.0 AND 4.0)

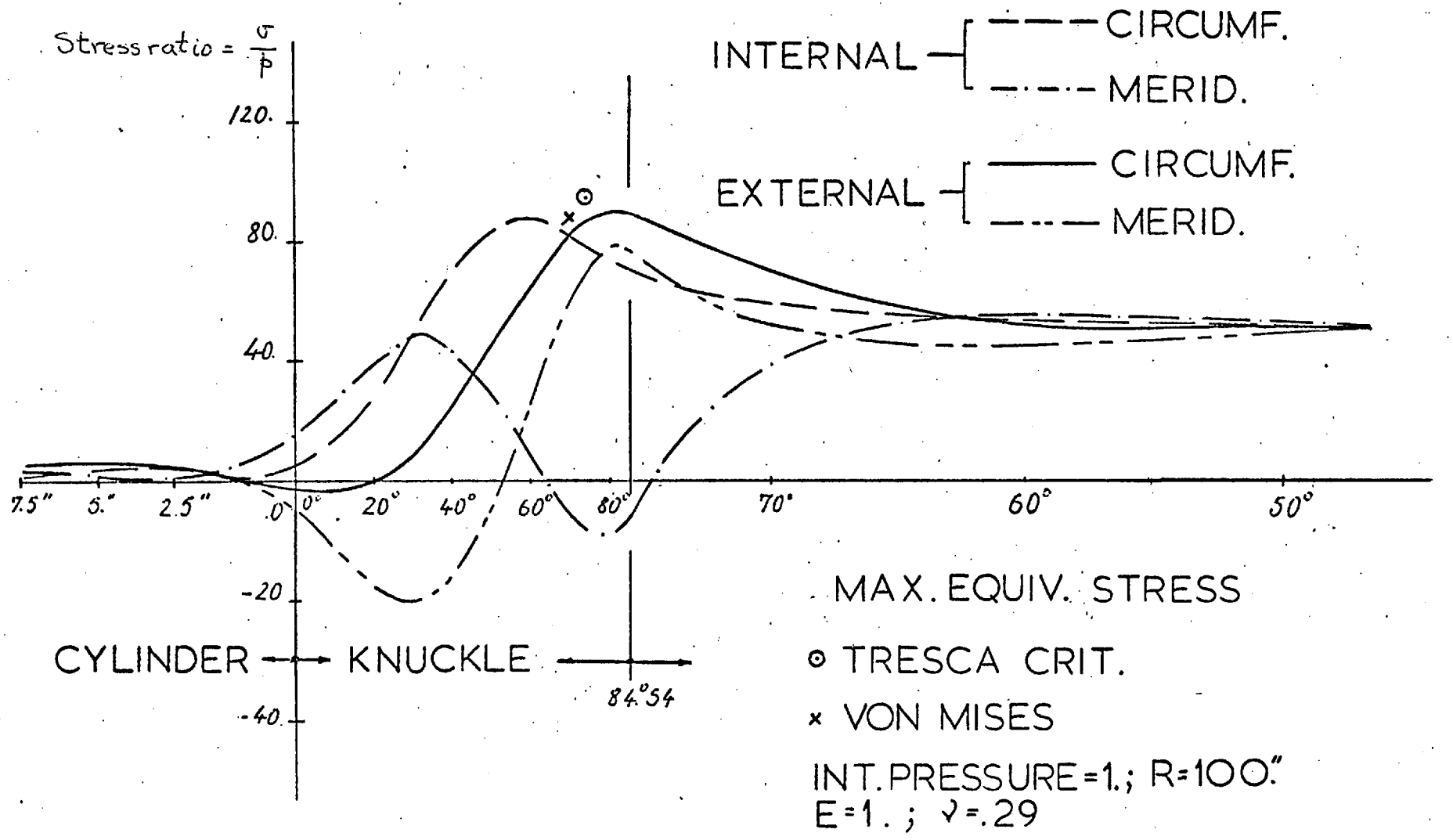

FIG.30 - STRESS DISTRIBUTION ON NOZZLE N1

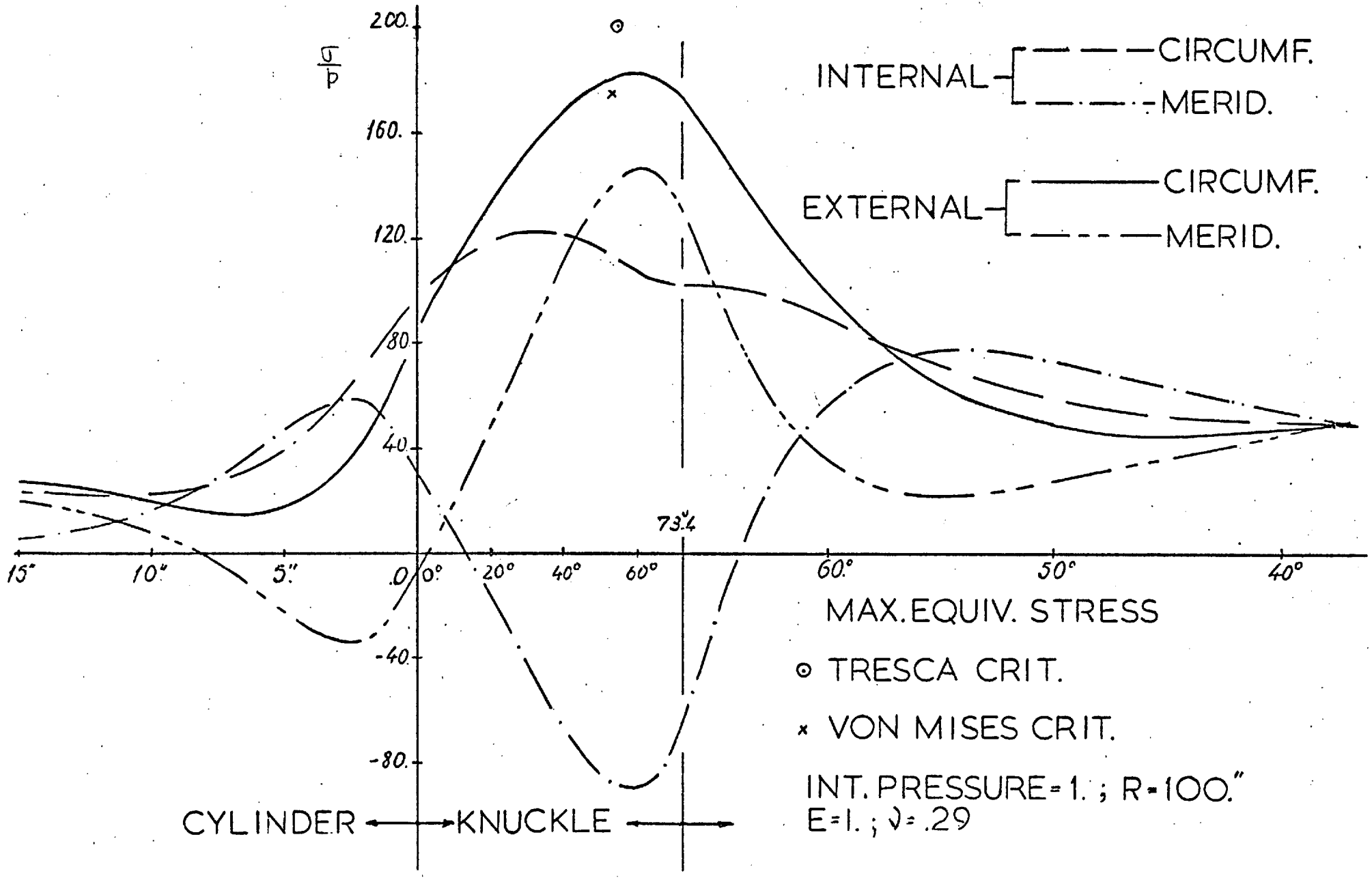

FIG. 31- STRESS DISTRIBUTION ON NOZZLE N5

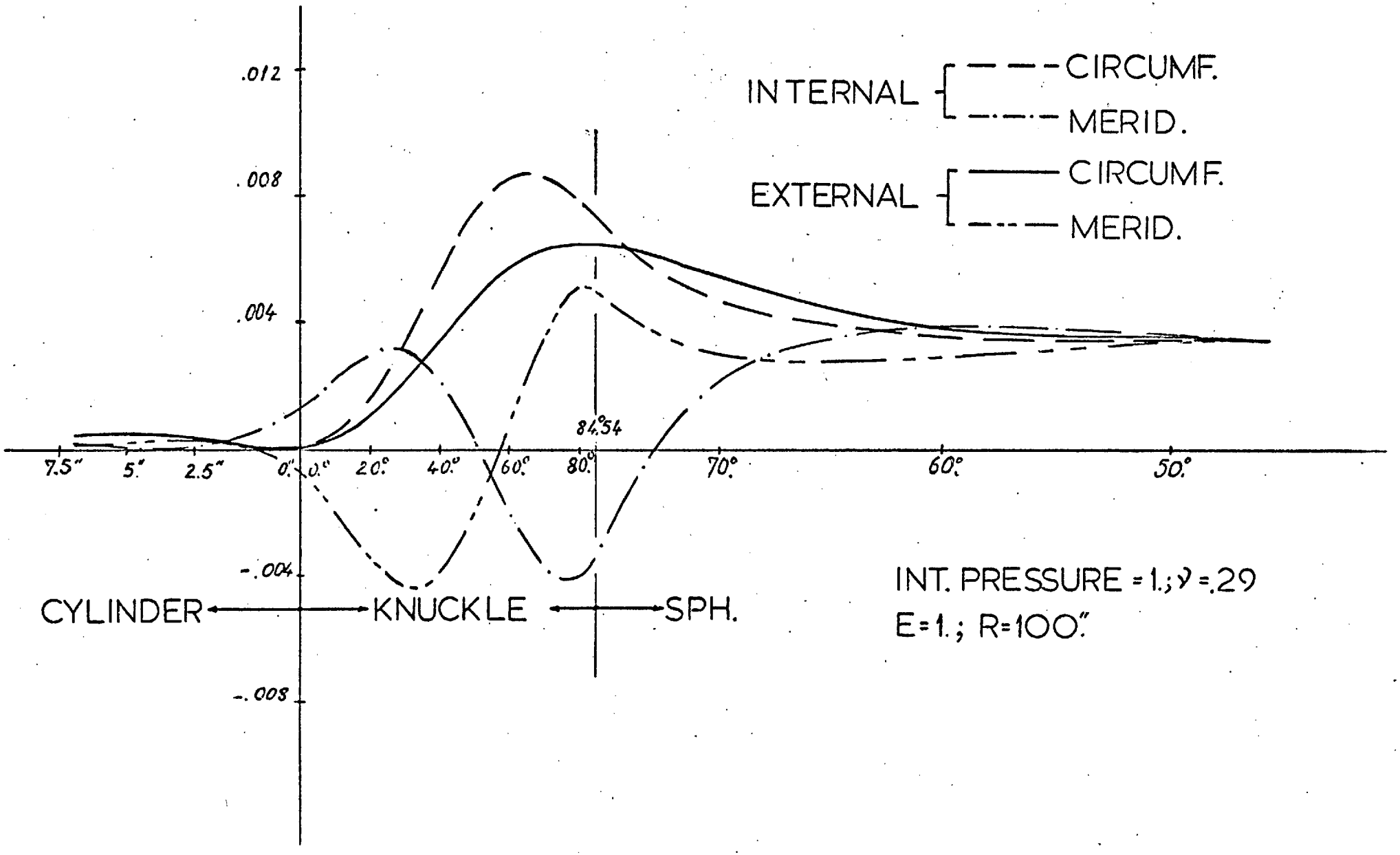

FIG.32 - STRAIN DISTRIBUTION ON NOZZLE N1

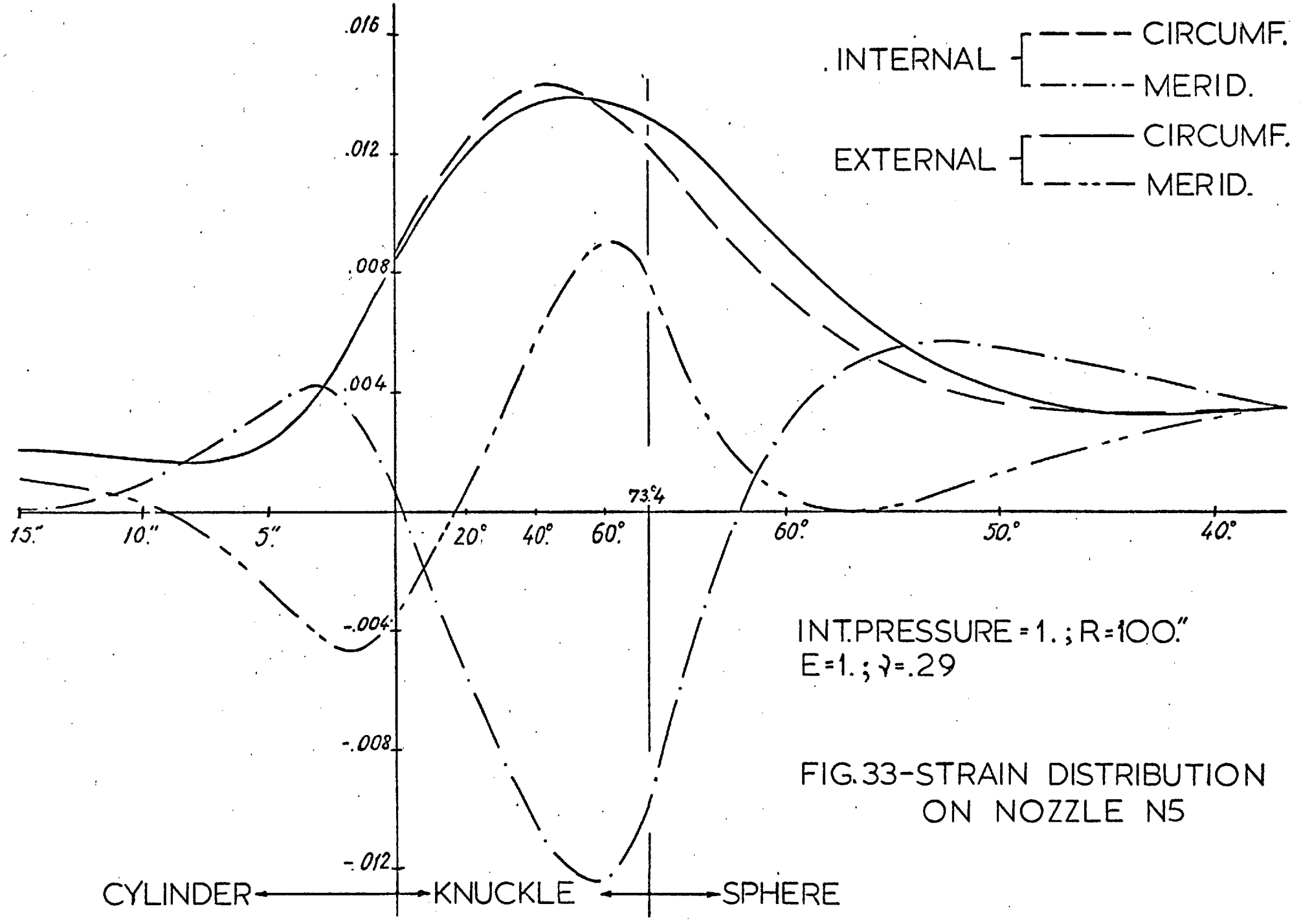

INT.PRESSURE = 1. ; R = 100."
E = 1. ; ν = .29

FIG. 33 - STRAIN DISTRIBUTION ON NOZZLE N5

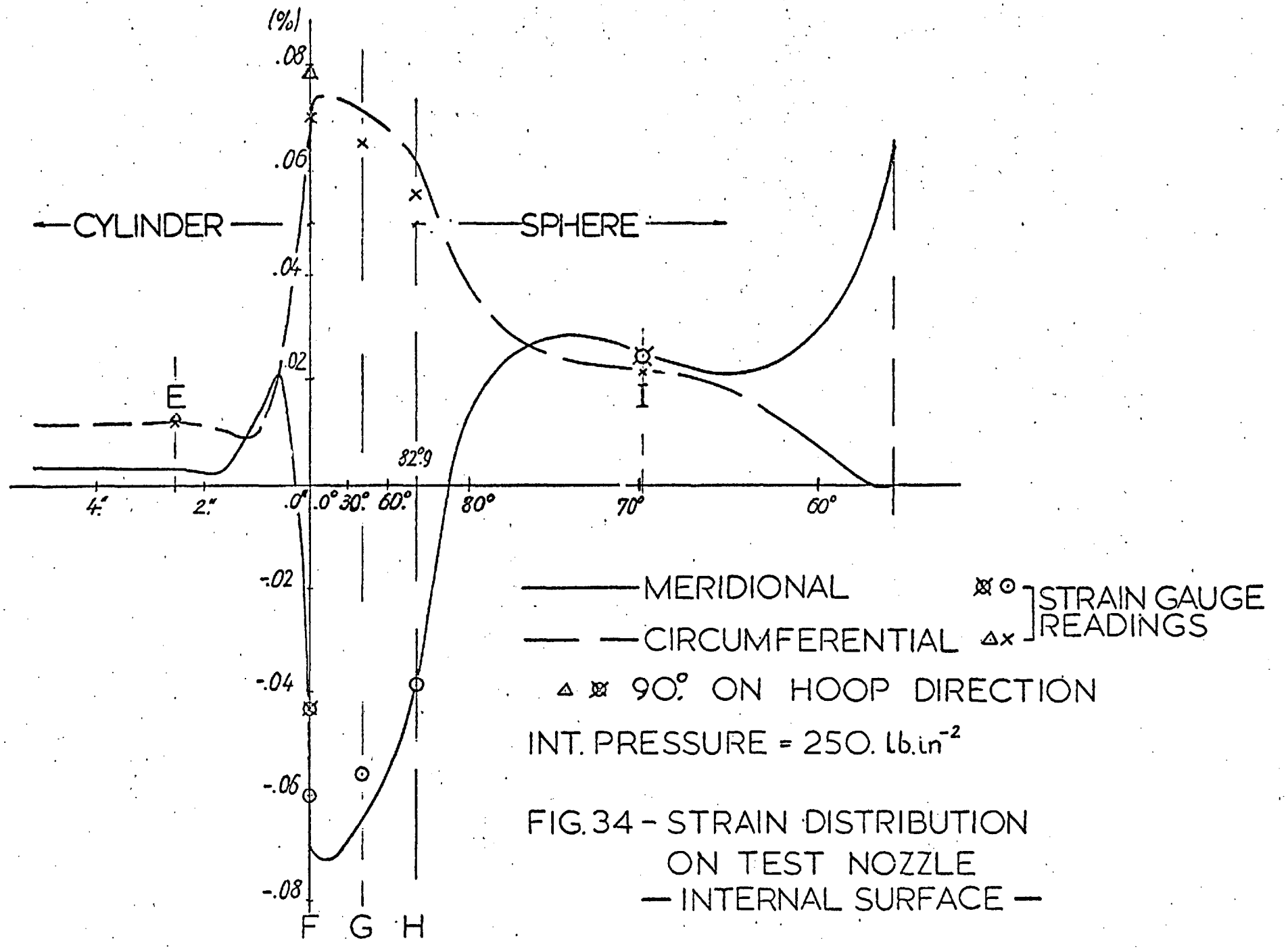

FIG. 34 – STRAIN DISTRIBUTION ON TEST NOZZLE — INTERNAL SURFACE —

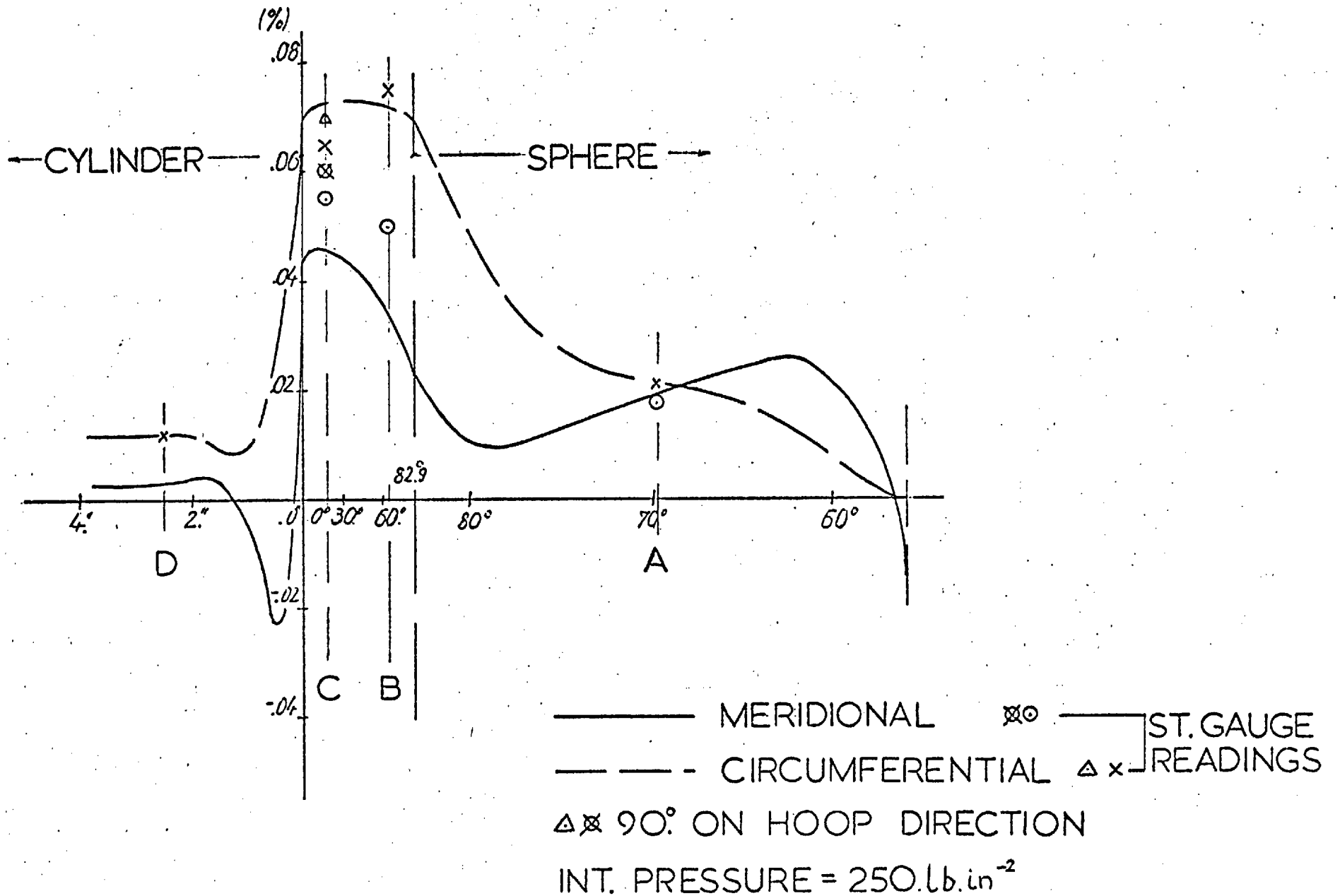

FIG. 35 - STRAIN DISTRIBUTION ON TEST NOZZLE
— EXTERNAL SURFACE —

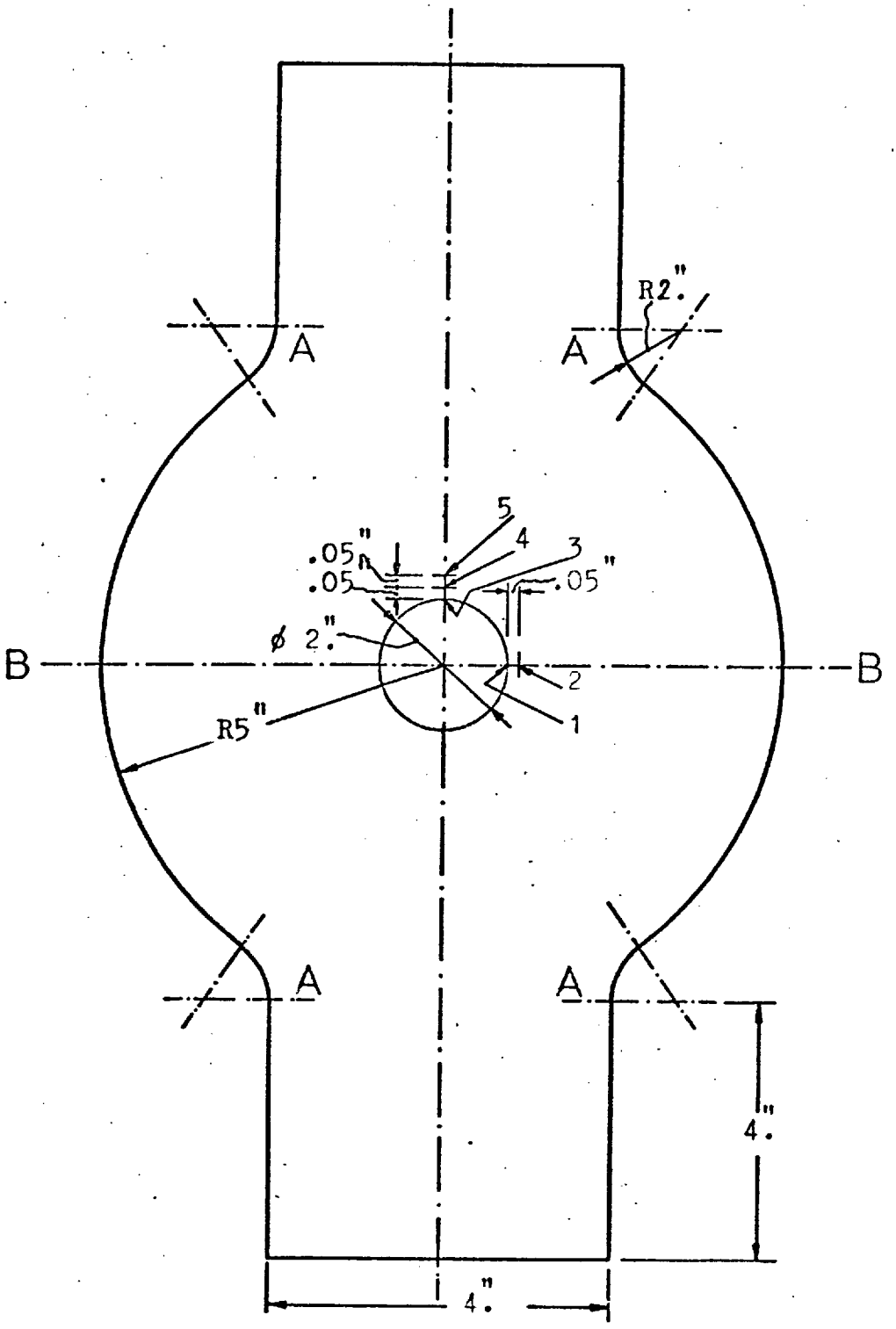

FIG.36

MILD STEEL TEST PLATE

$\frac{1}{2}$" thick

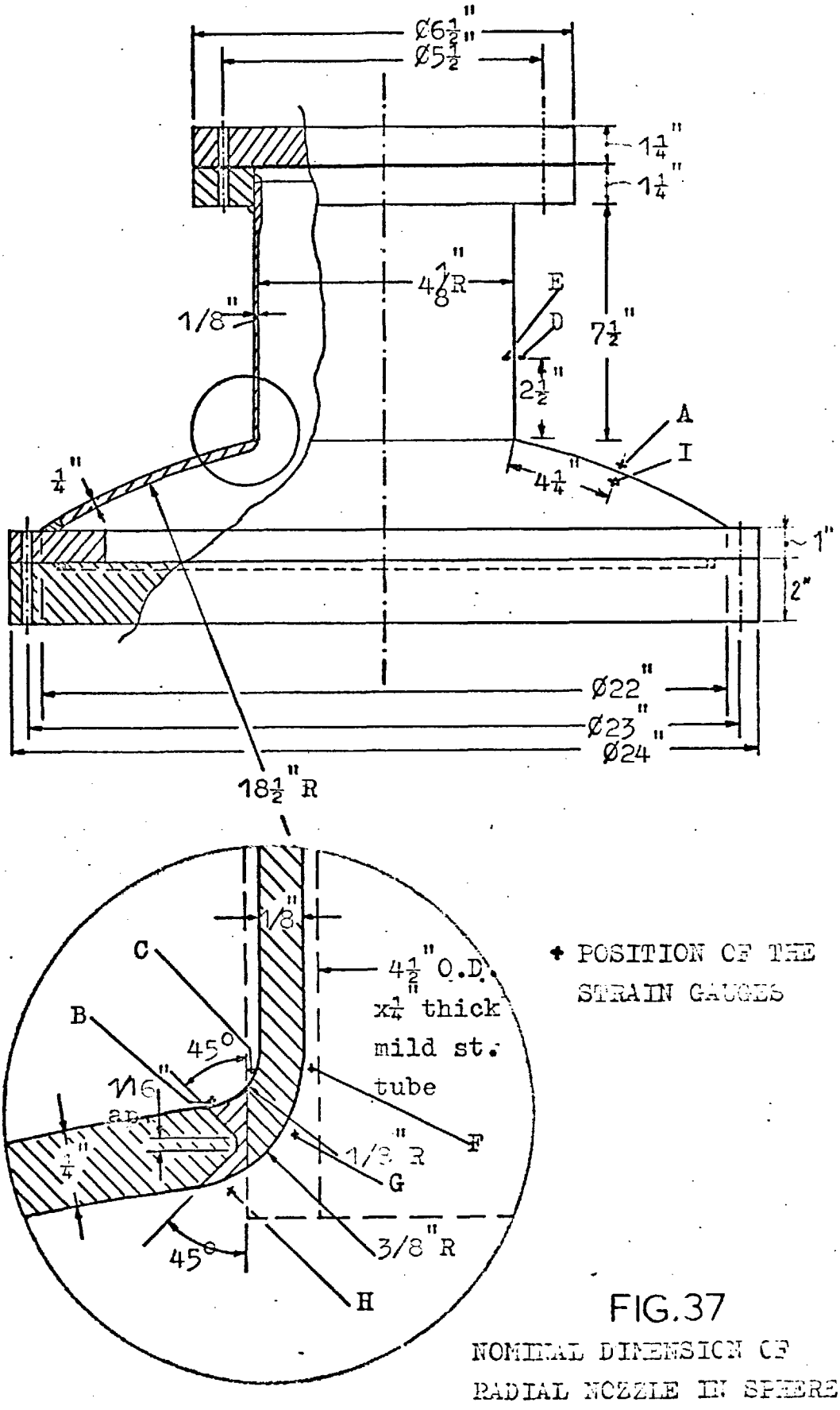

FIG.37

NOMINAL DIMENSION OF RADIAL NOZZLE IN SPHERE AND WELDING - MACHINING DETAILS OF THE JUNCTION

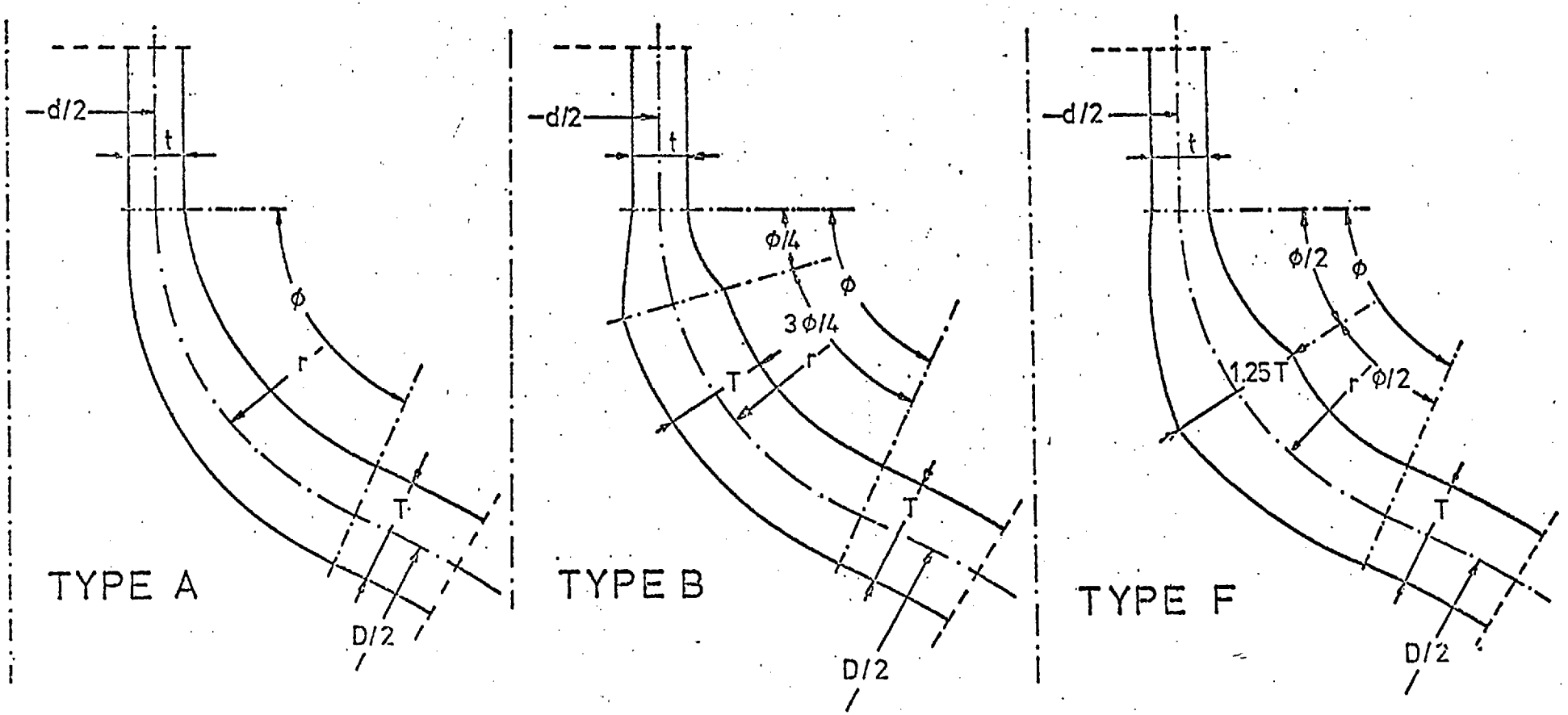

FIG.38

CONFIGURATIONS OF NOZZLES JUNCTION USED FOR VARIOUS NOZZLE COMPUTATIONS

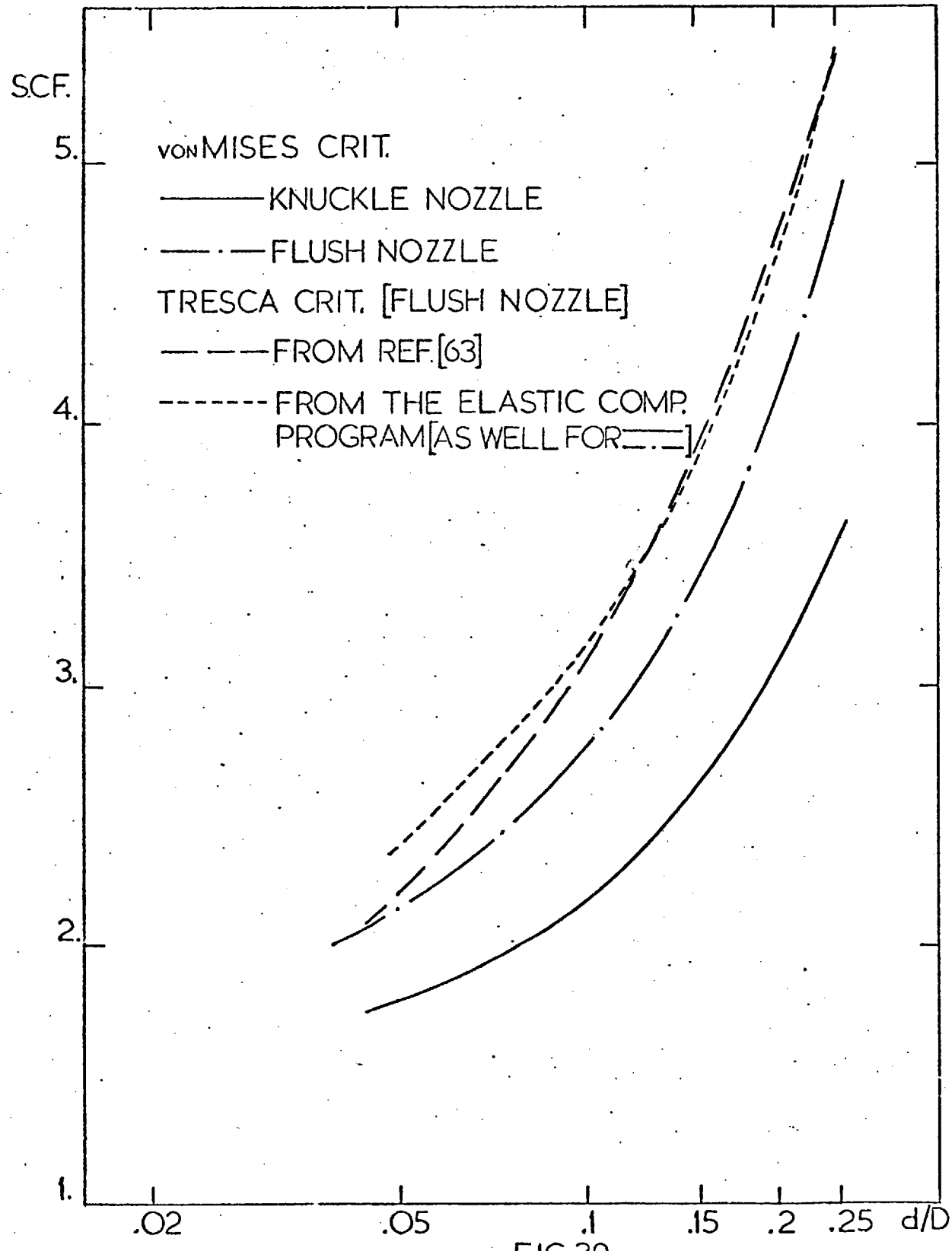

FIG.39

ELASTIC STRESS CONCENTRATION FACTORS FOR A SERIES OF NOZZLES-TO-SPHERE DIAMETER RATIOS

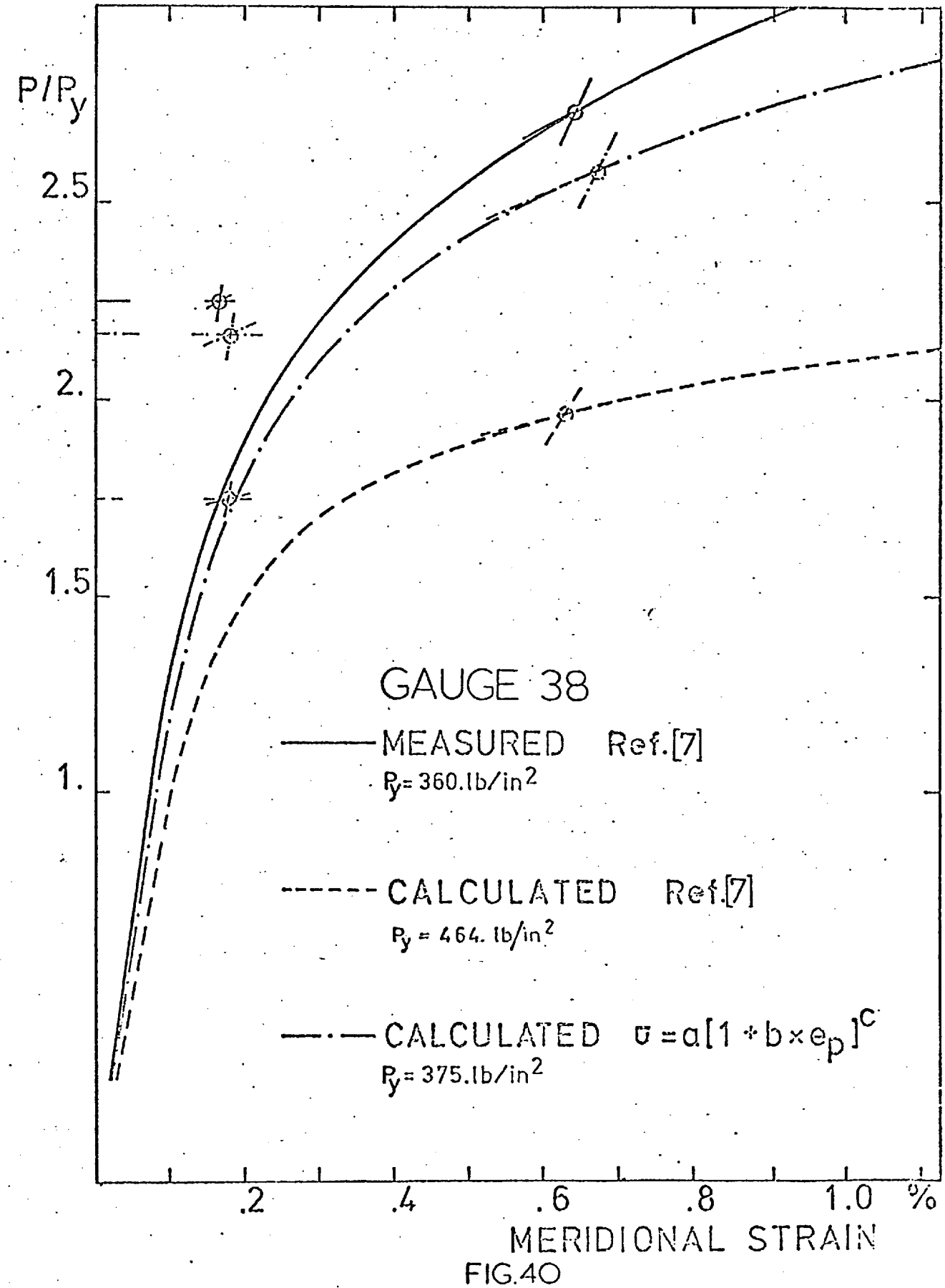

FIG.40

COMPARISON OF EXPERIMENTAL AND COMPUTED ELASTIC-PLASTIC STRAINS ON HEAD A,(ref.[7])

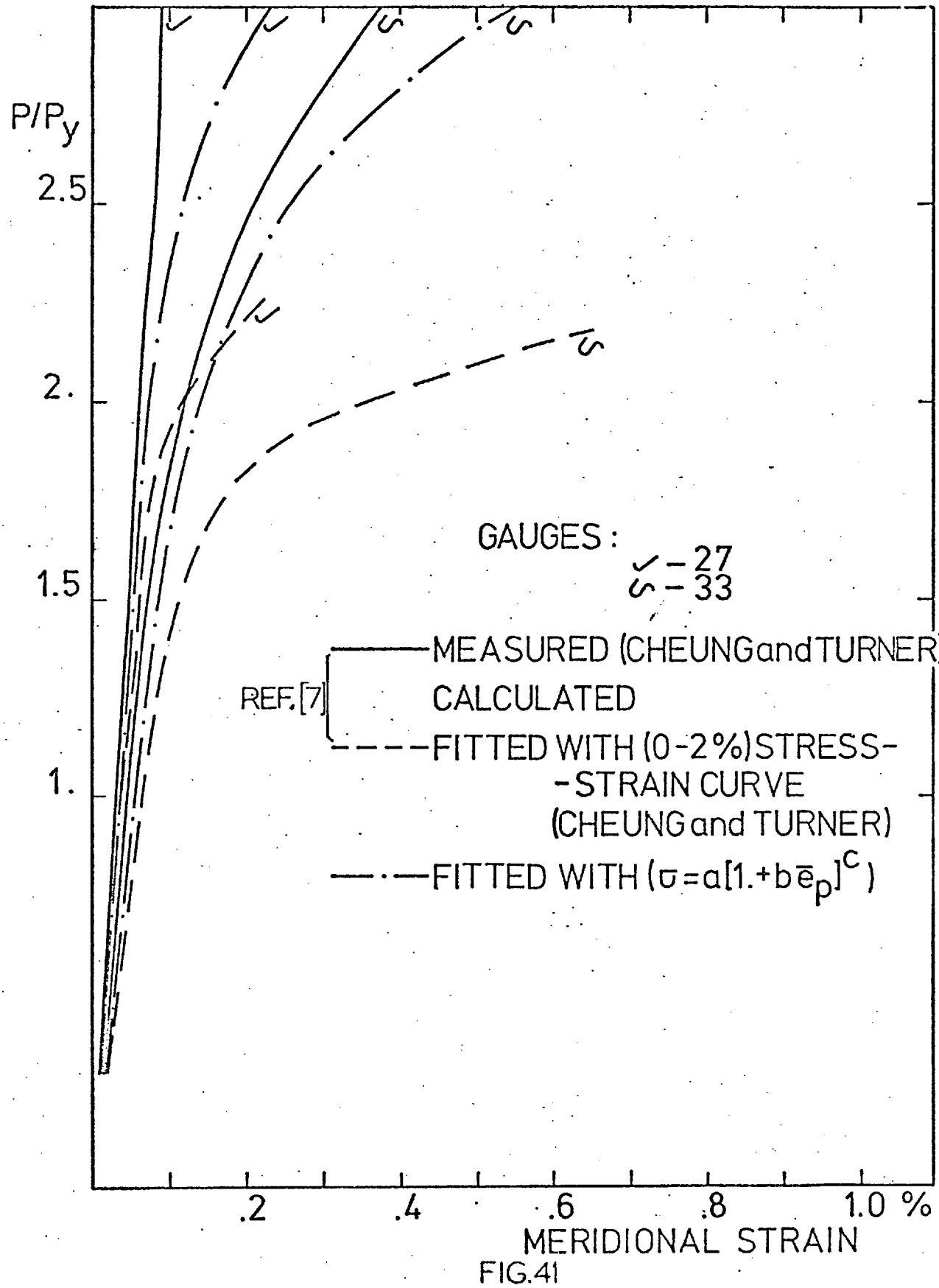

FIG.41

COMPARISON OF EXPERIMENTAL AND COMPUTED ELASTIC-PLASTIC STRAINS ON HEAD A, (REF.[7])

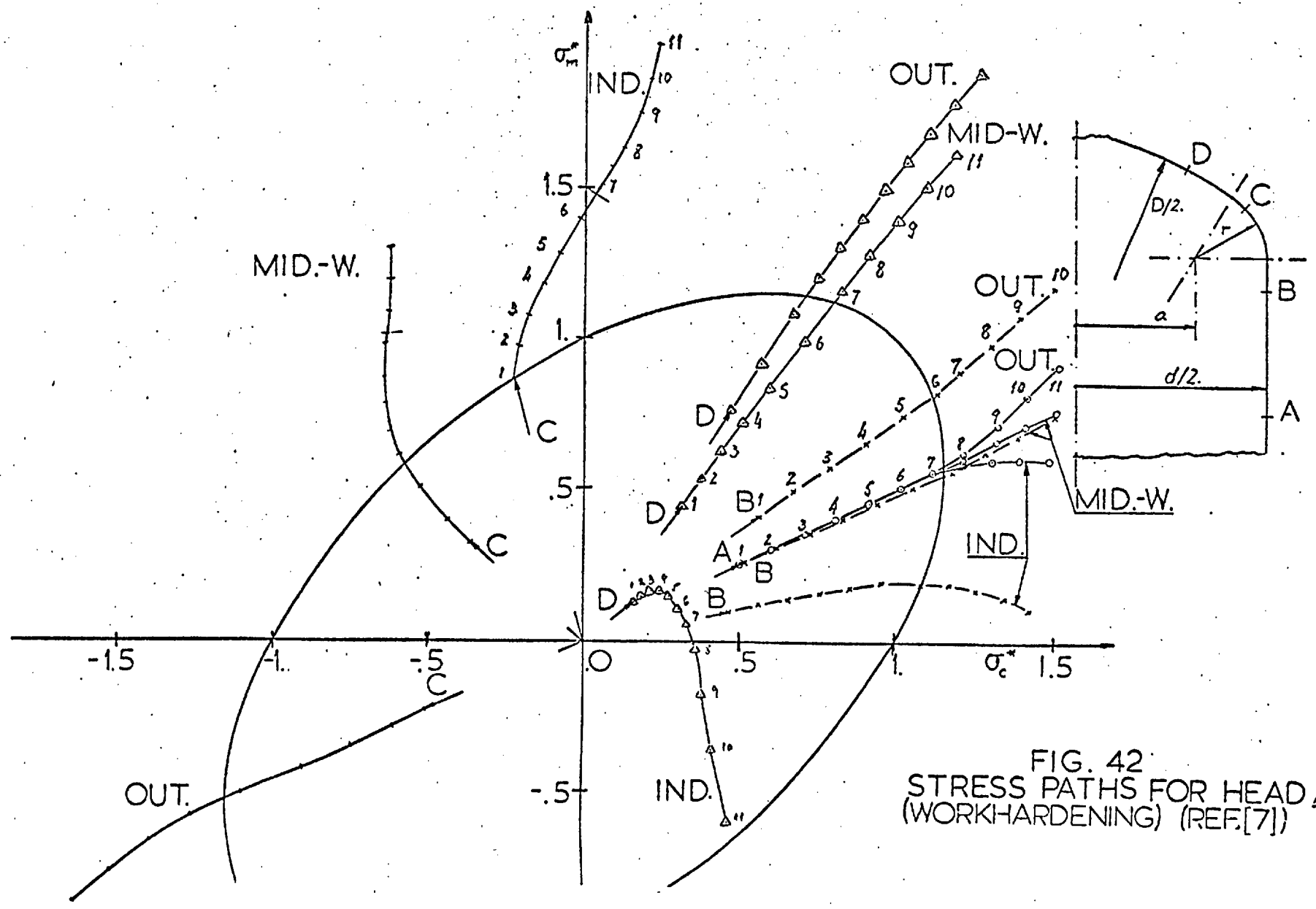

FIG. 42
STRESS PATHS FOR HEAD A
(WORKHARDENING) (REF.[7])

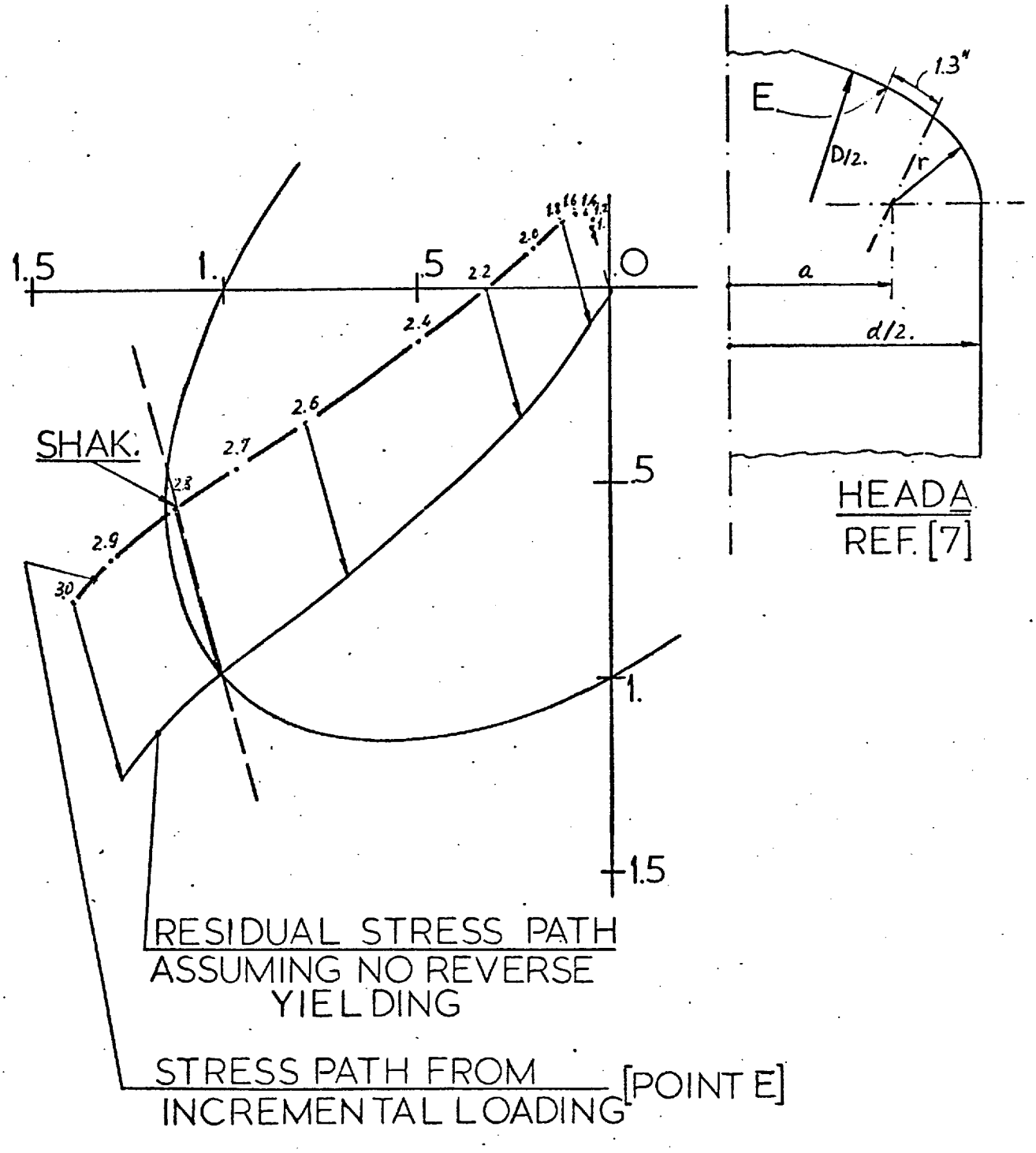

FIG. 43
INTERNAL STRESS PATH
OF THE POINT WHICH WILL
SHAKEDOWN IF WORK-
-HARDENING IS PERMITTED

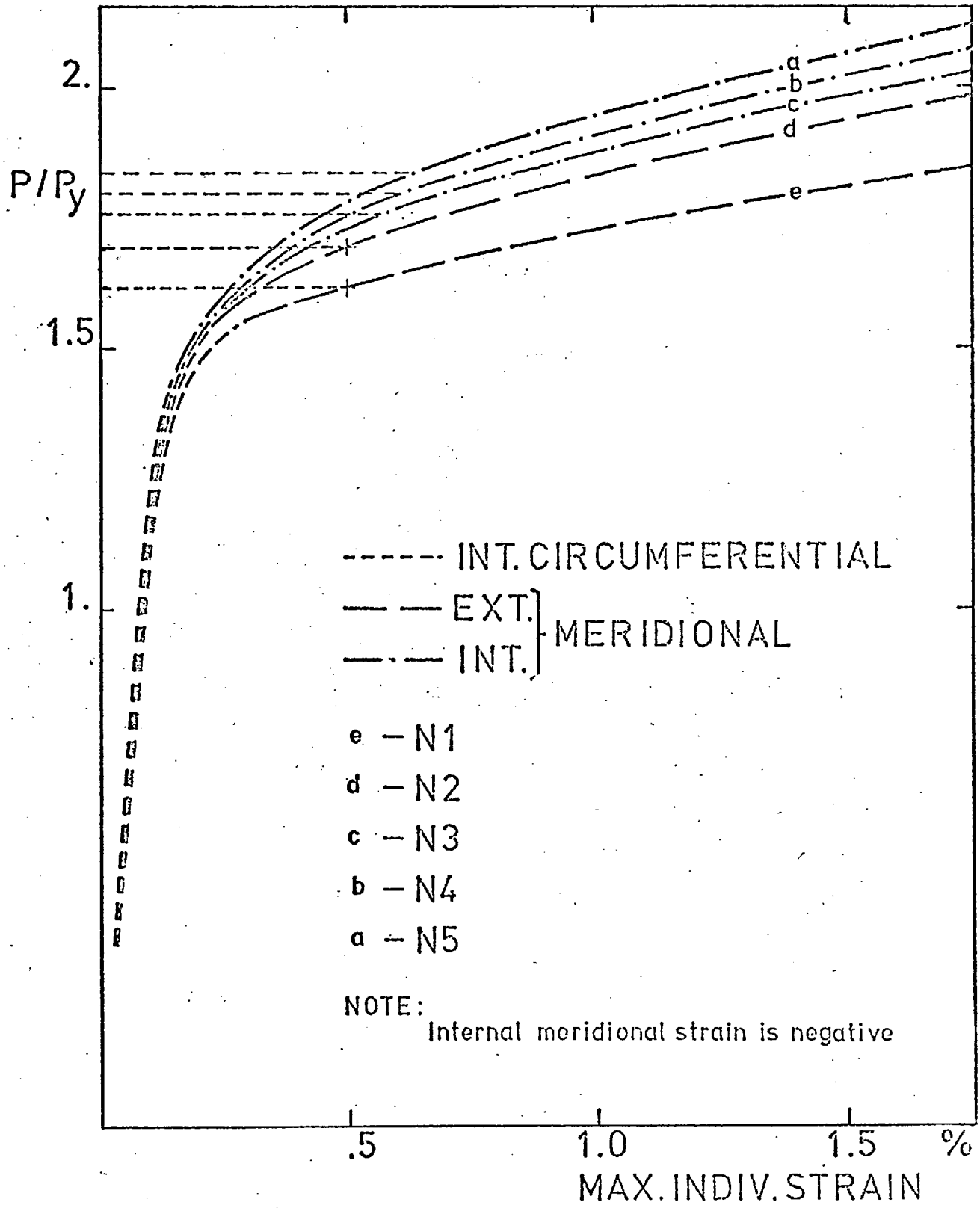

FIG. 44

COMPOSITE CURVES OF MAXIMUM COMPUTED STRAIN AGAINST PRESSURE FOR A SERIES OF NOZZLE-TO-SPHERE DIAMETER RATIOS

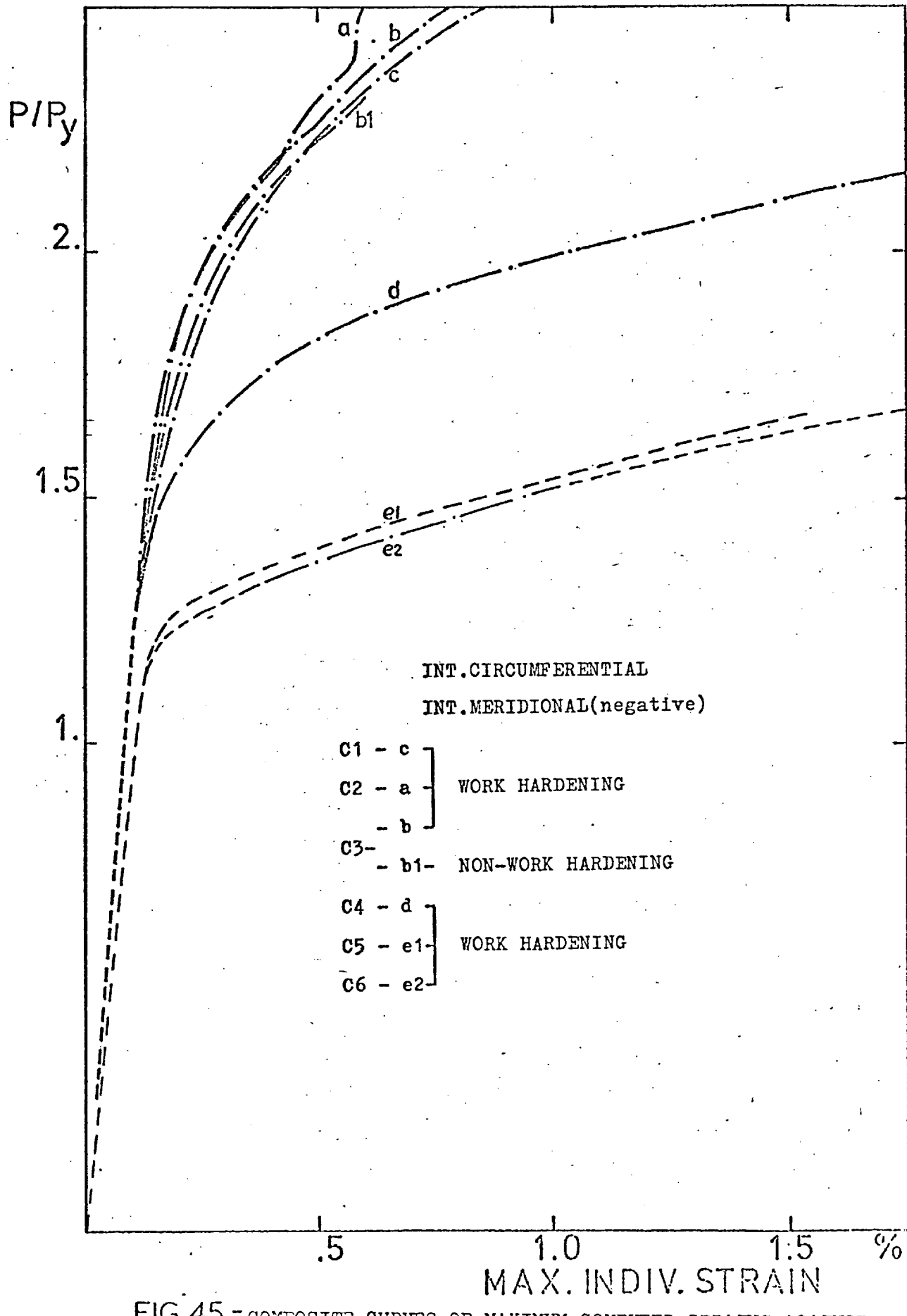

FIG. 45 - COMPOSITE CURVES OF MAXIMUM COMPUTED STRAINS AGAINST PRESSURE FOR SEVERAL CONFIGURATIONS OF NOZZLES JUNCTIONS

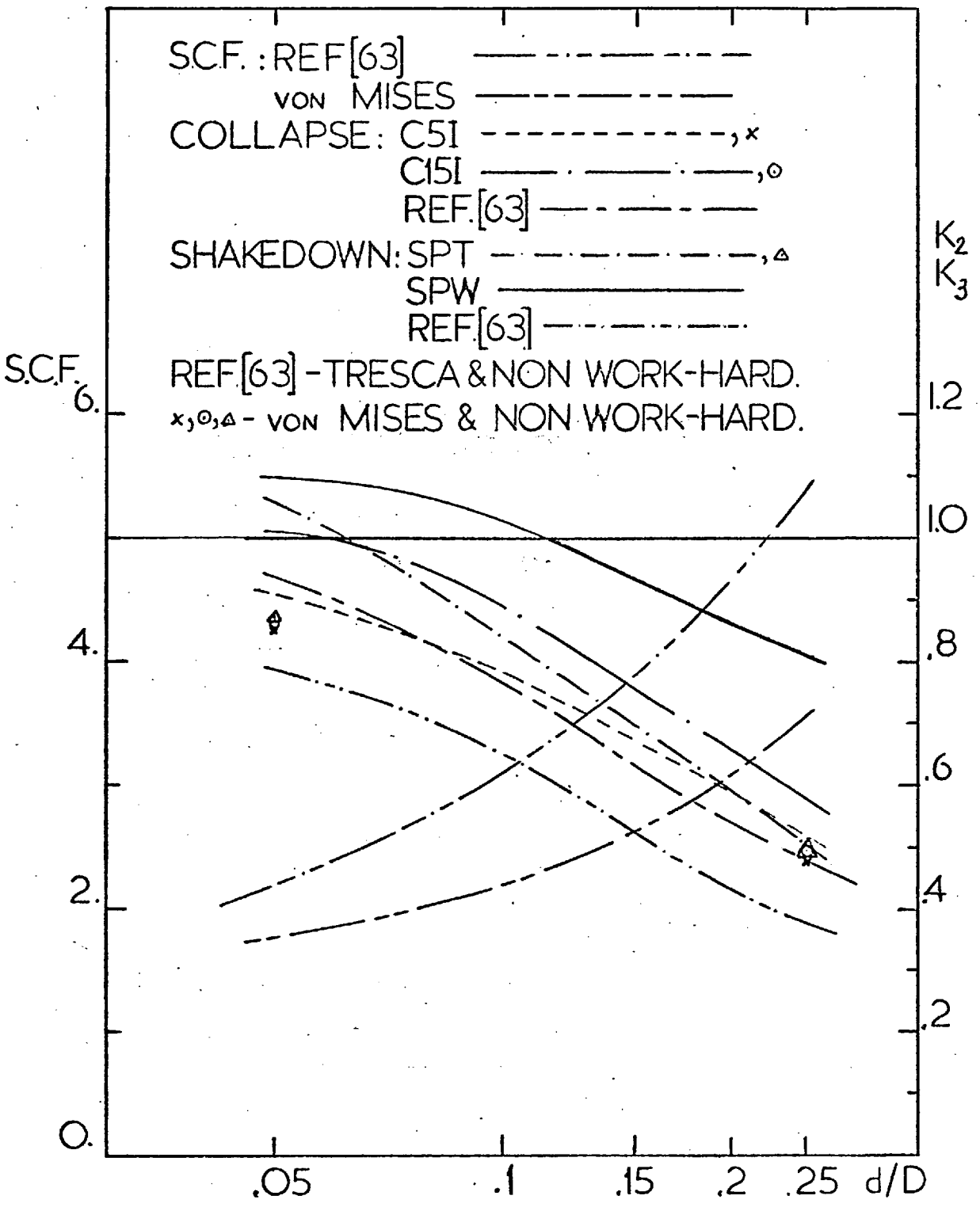

FIG. 46

ELASTIC STRESS CONCENTRATION FACTORS, AND SHAKEDOWN AND COLLAPSE RATIOS FOR A SERIES OF NOZZLE-TO-SPHERE DIAMETER RATIOS

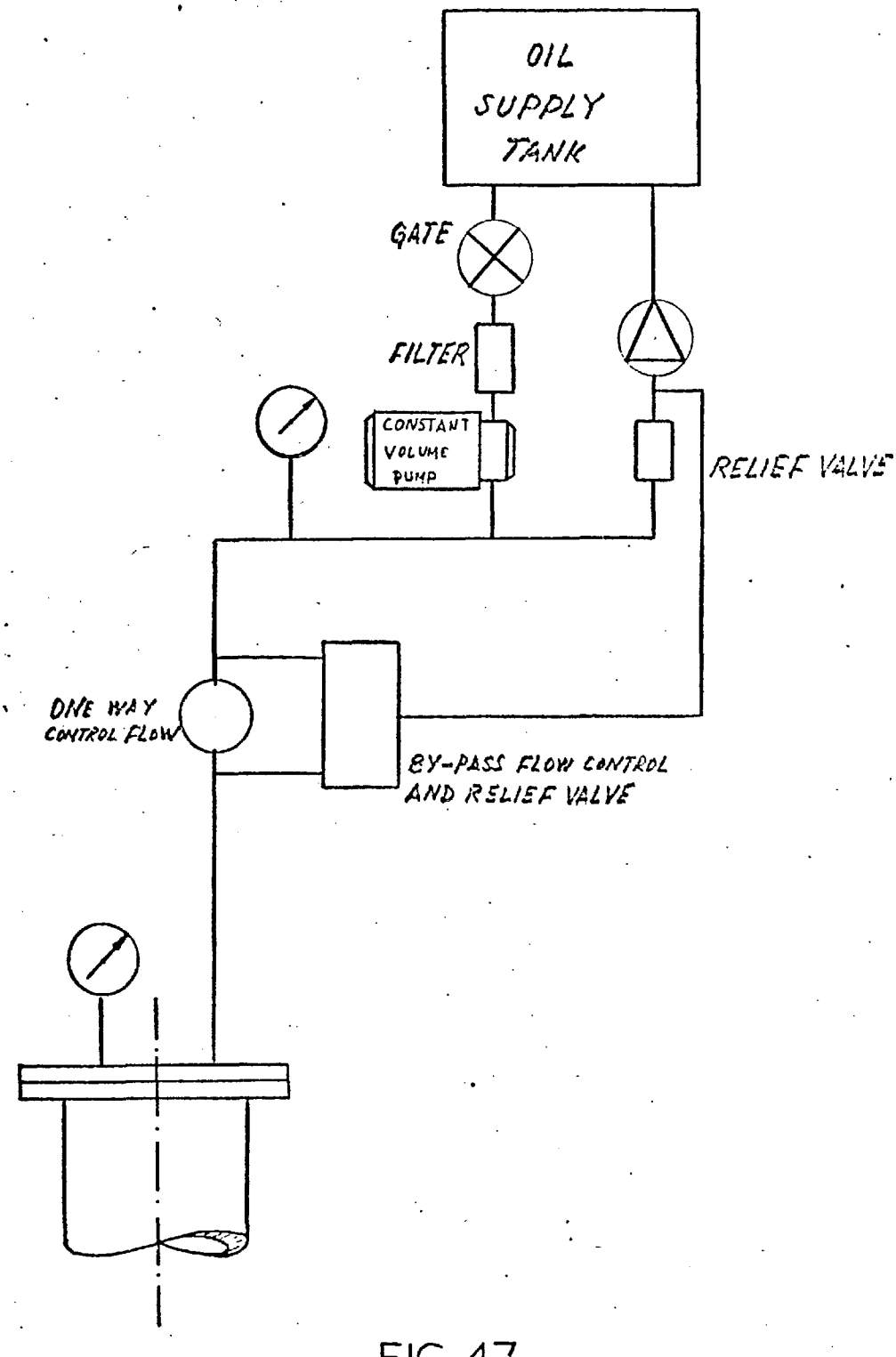

FIG. 47

HYDRAULIC POWER UNIT

KEY:

1...40 CYCLE NUMBER

..... CREEP

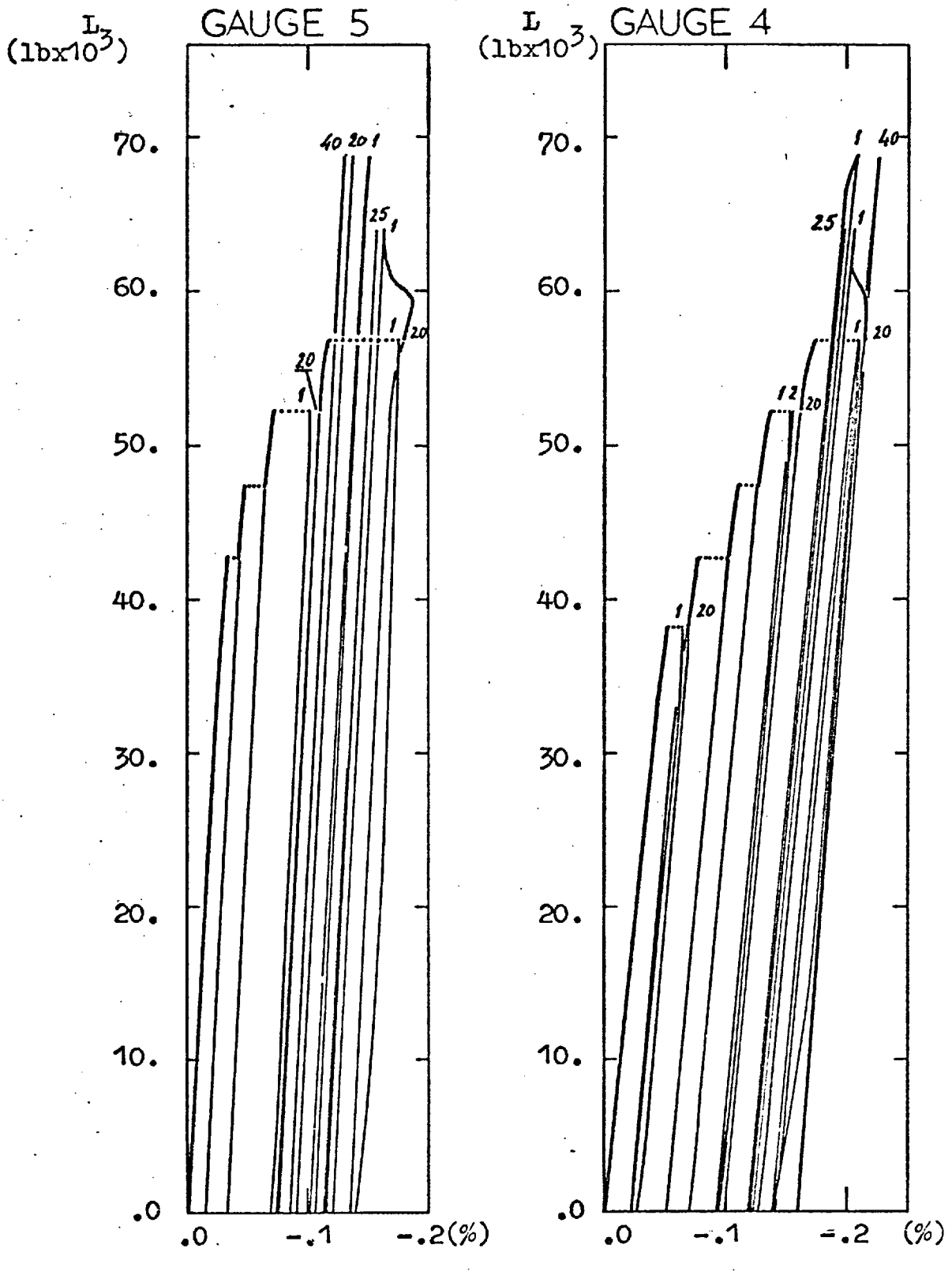

FIG. 48

STRAIN AT POSITIONS 4 AND 5 ON THE PLATE

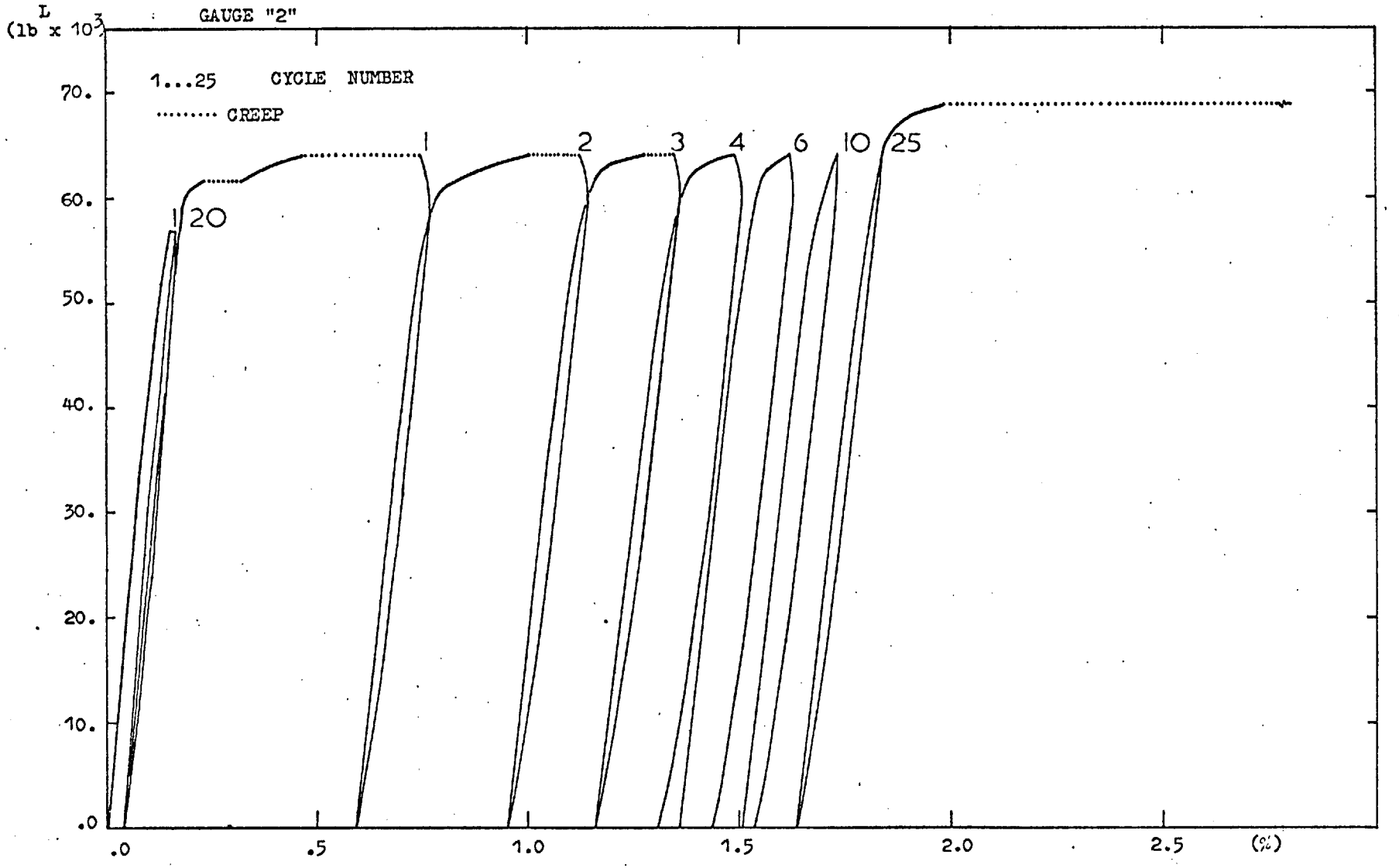

FIG. 49
STRAIN AT POSITION 2 ON THE PLATE

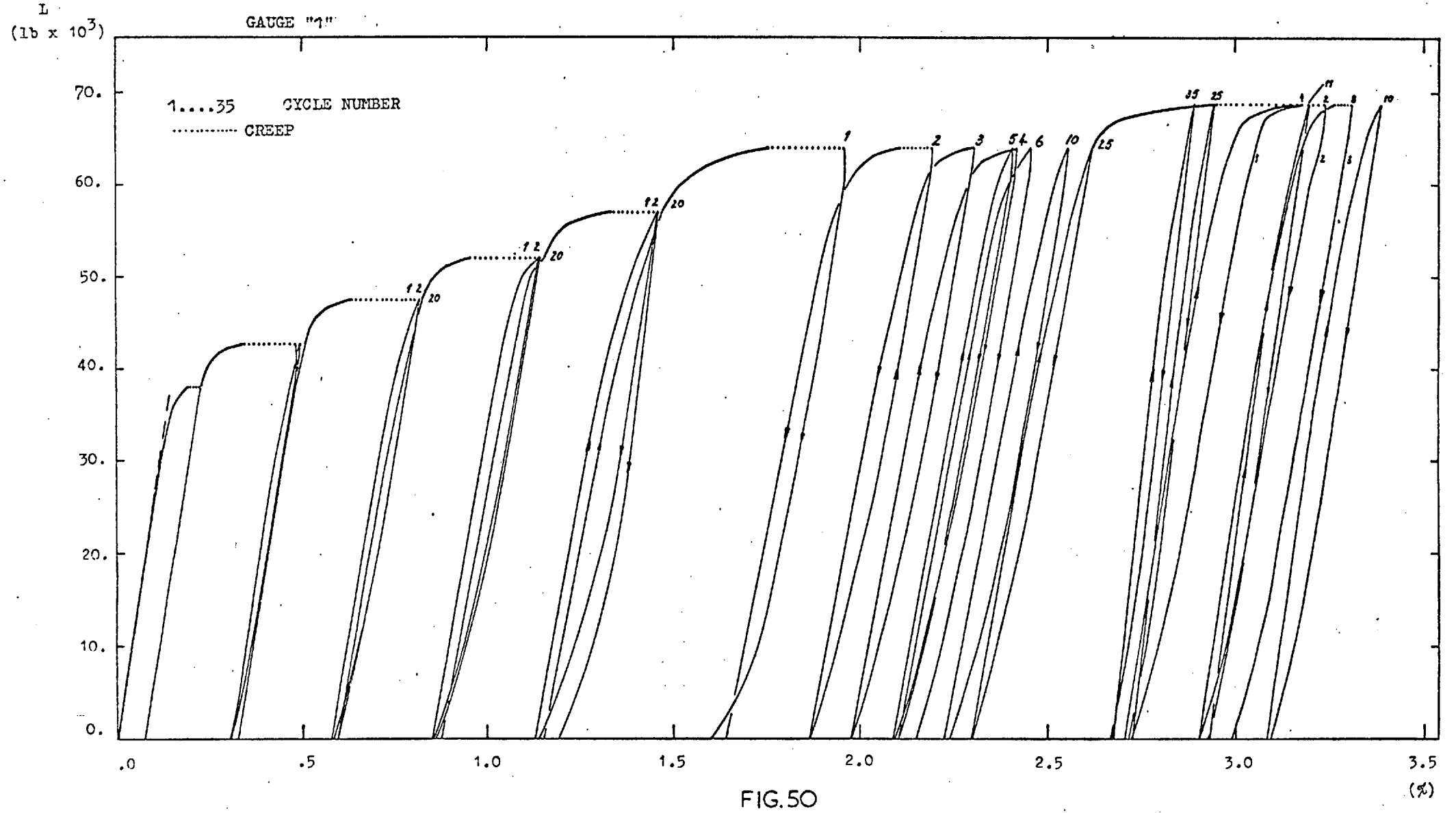

FIG.50

STRAIN AT POSITION 1 ON THE PLATE

KEY:

1...40 CYCLE NUMBER

..... CREEP

GAUGE "3"

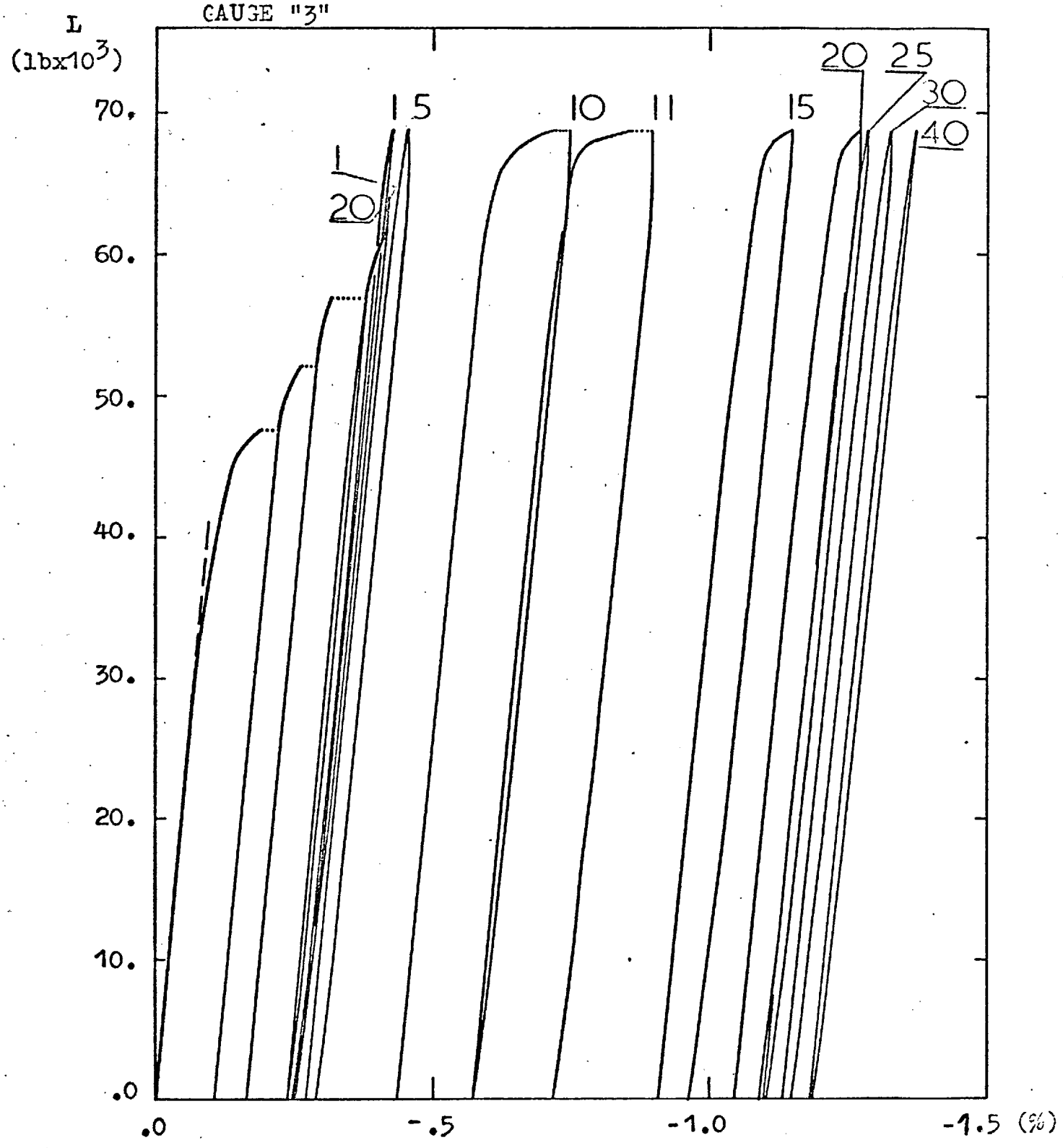

FIG.51

STRAIN AT POSITION 3 ON THE PLATE

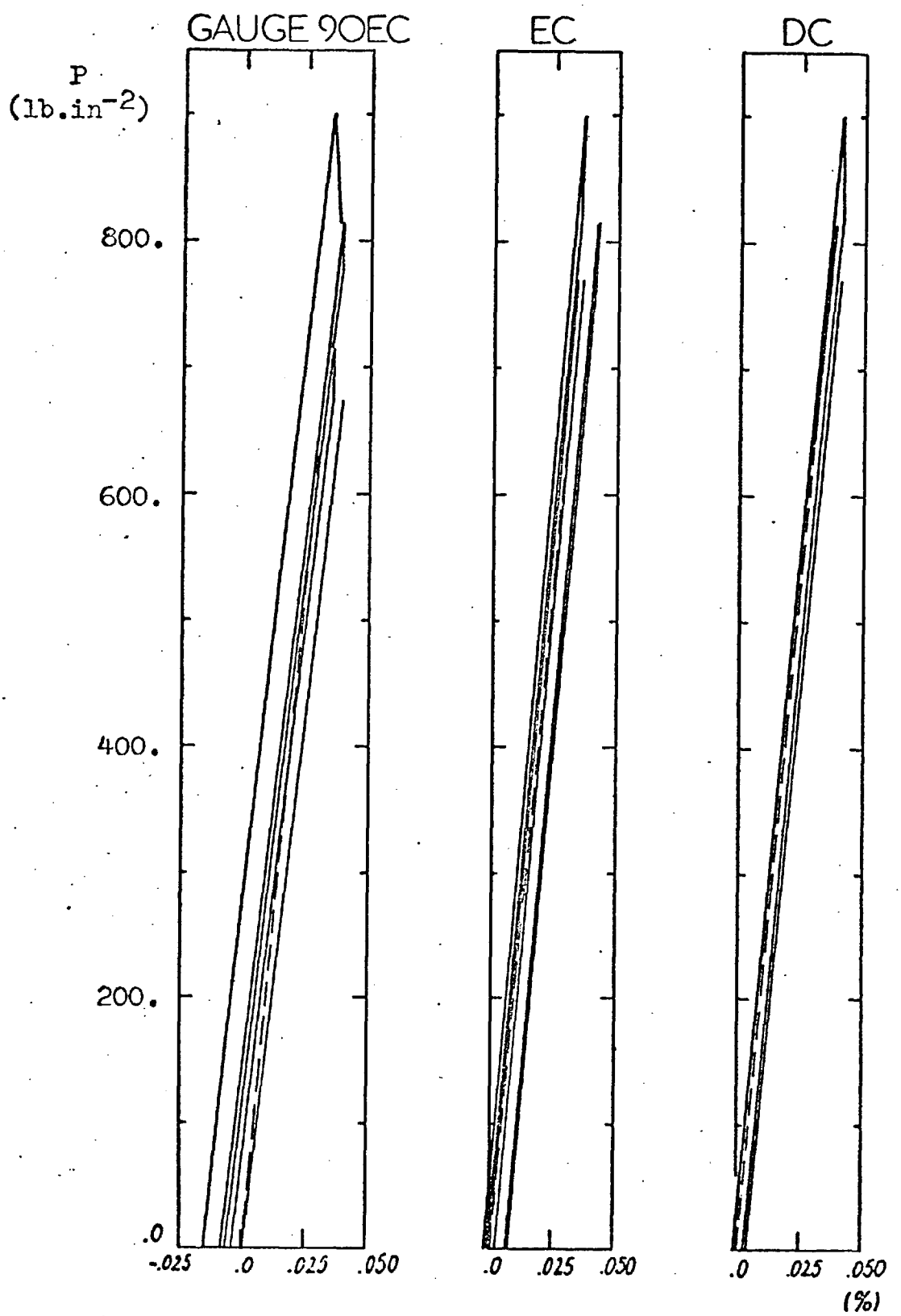

FIG.52

CIRCUMFERENTIAL STRAIN AT POSITIONS C AND D ON THE TEST NOZZLE

KEY:
MEASURED ——
·····CREEP

CALCULATED, – – – WORKHARDENING , –·–·– NON-WORKHARDENING

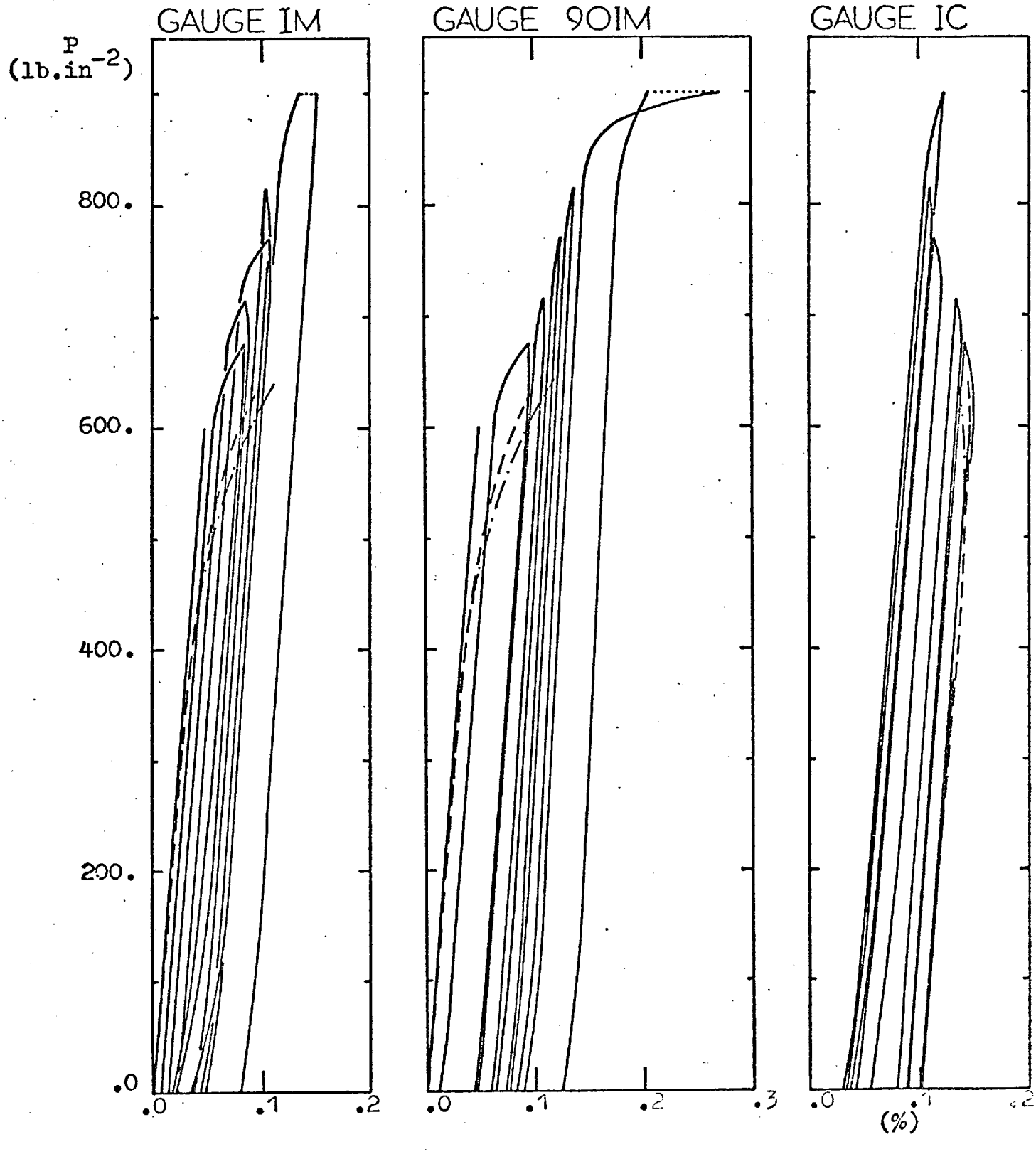

FIG. 53
STRAIN AT POSITION I ON THE TEST NOZZLE

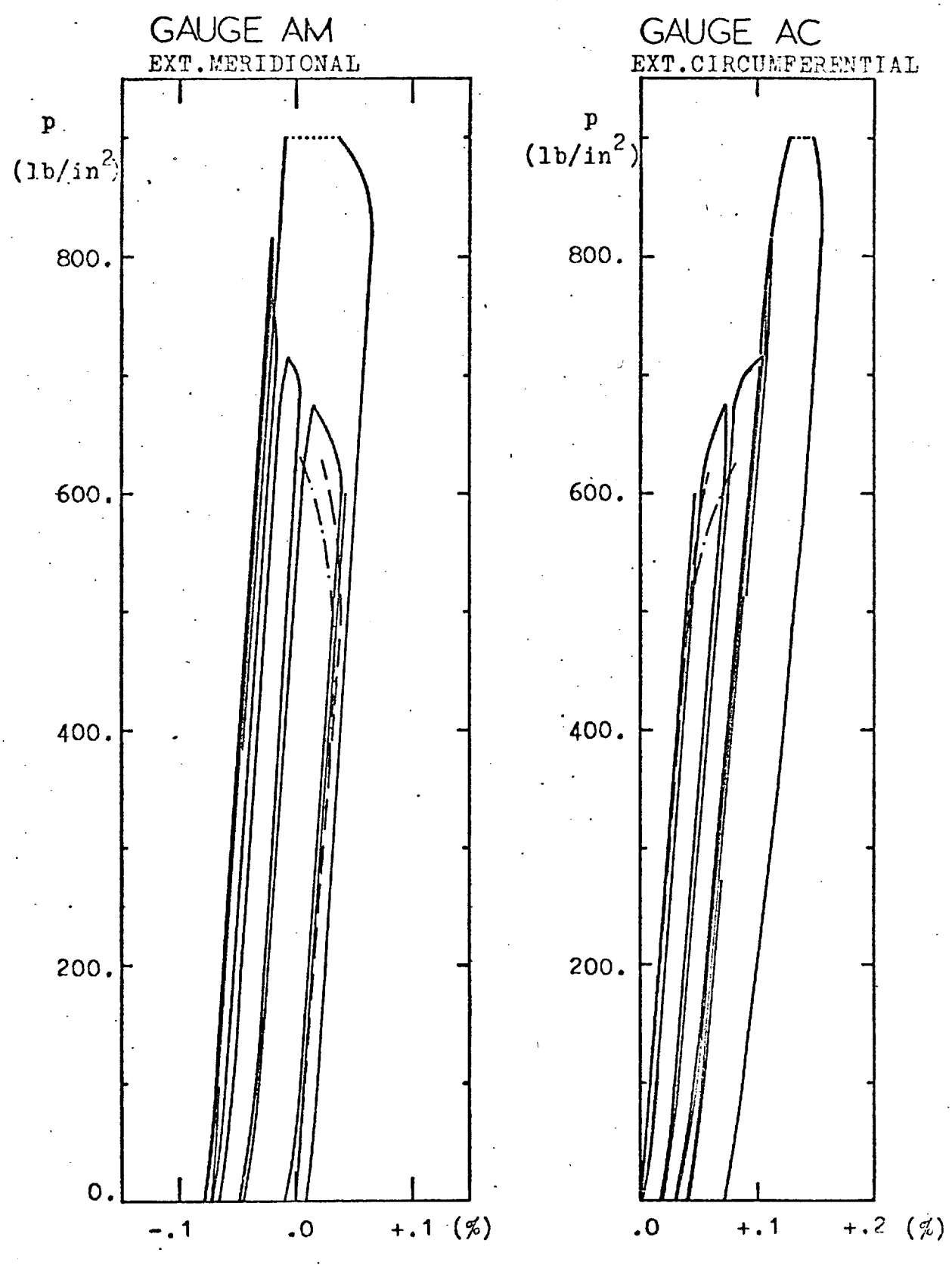

FIG. 54

STRAIN AT POSITION A ON THE TEST NOZZLE

KEY:

MEASURED —— 90C — — — C
····· CREEP

CALCULATED
—·—·— WORKHARDENING
—·—·— NON-WORKHARDENING

1...20 CYCLE NUMBER

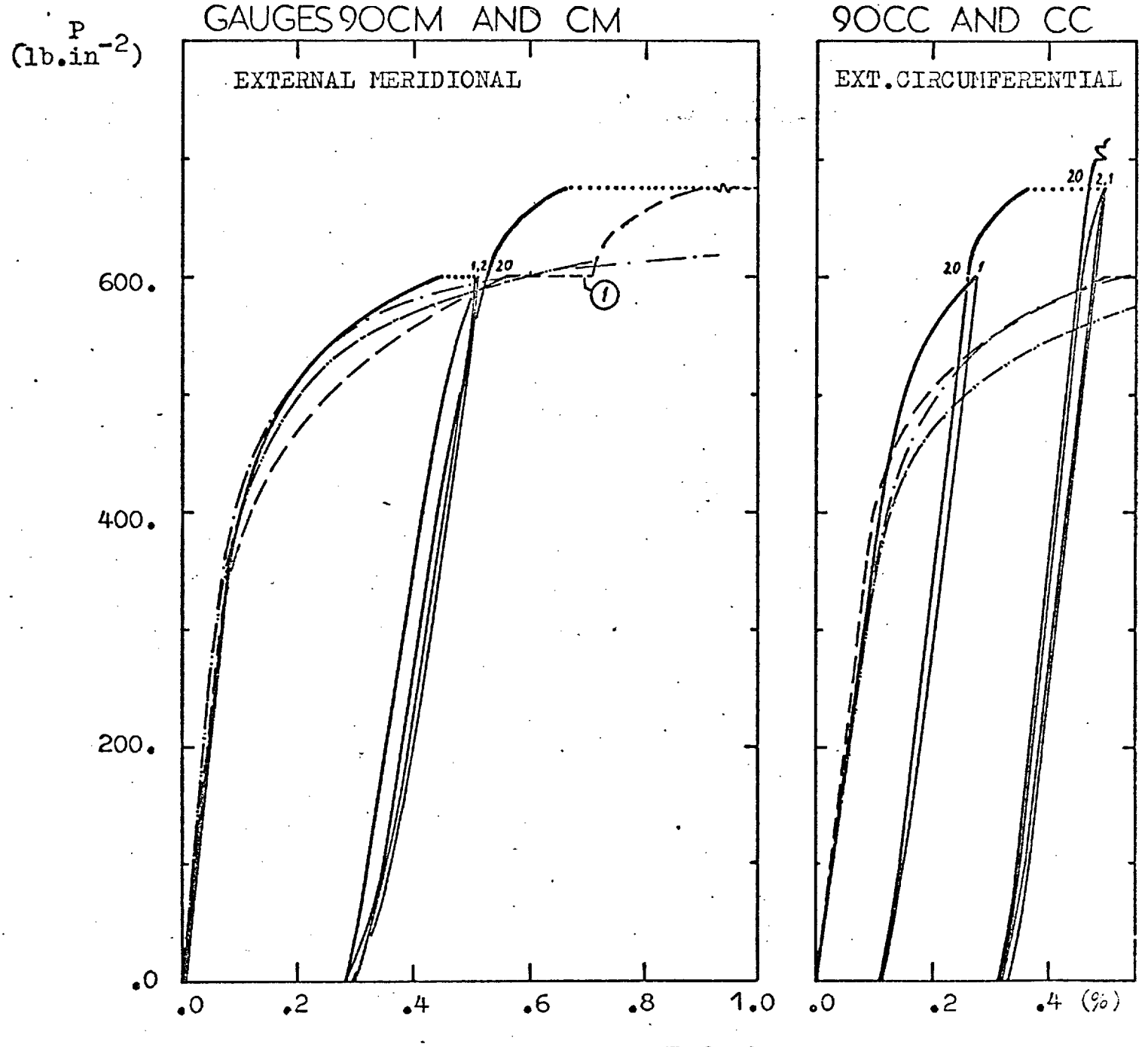

FIG. 55

STRAIN AT POSITIONS C AND 90C ON THE TEST NOZZLE

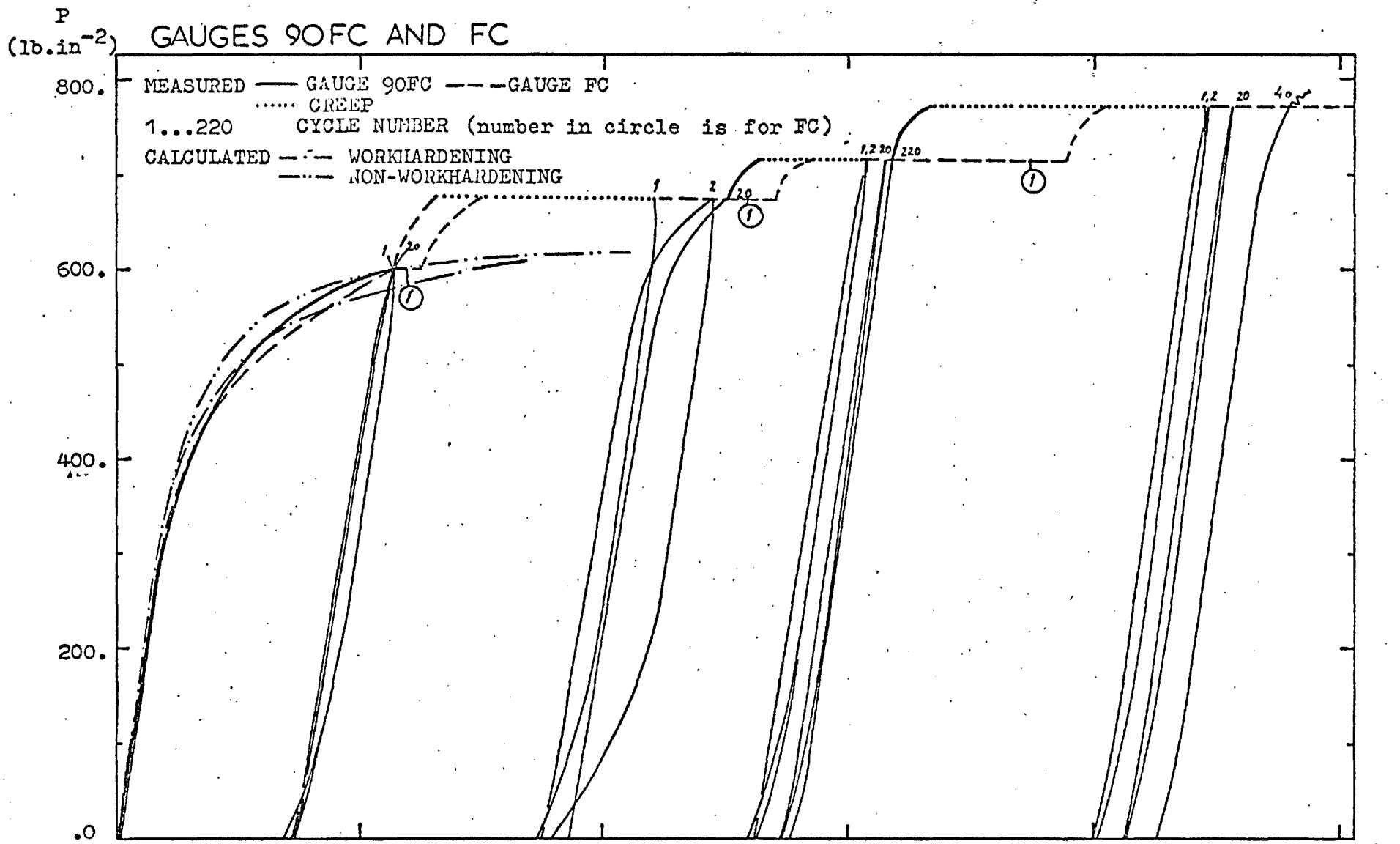

FIG. 56

CIRCUMFERENTIAL STRAIN AT POSITIONS F AND 90F ON THE TEST NOZZLE

KEY:
MEASURED —— GAUGE FM, – – – GAUGE 90FM
····· CREEP
1...220 CYCLE NUMBER (number in circle is for gauge 90FM)

CALCULATED —·— WORKHARDENING
—··— NON-WORKHARDENING

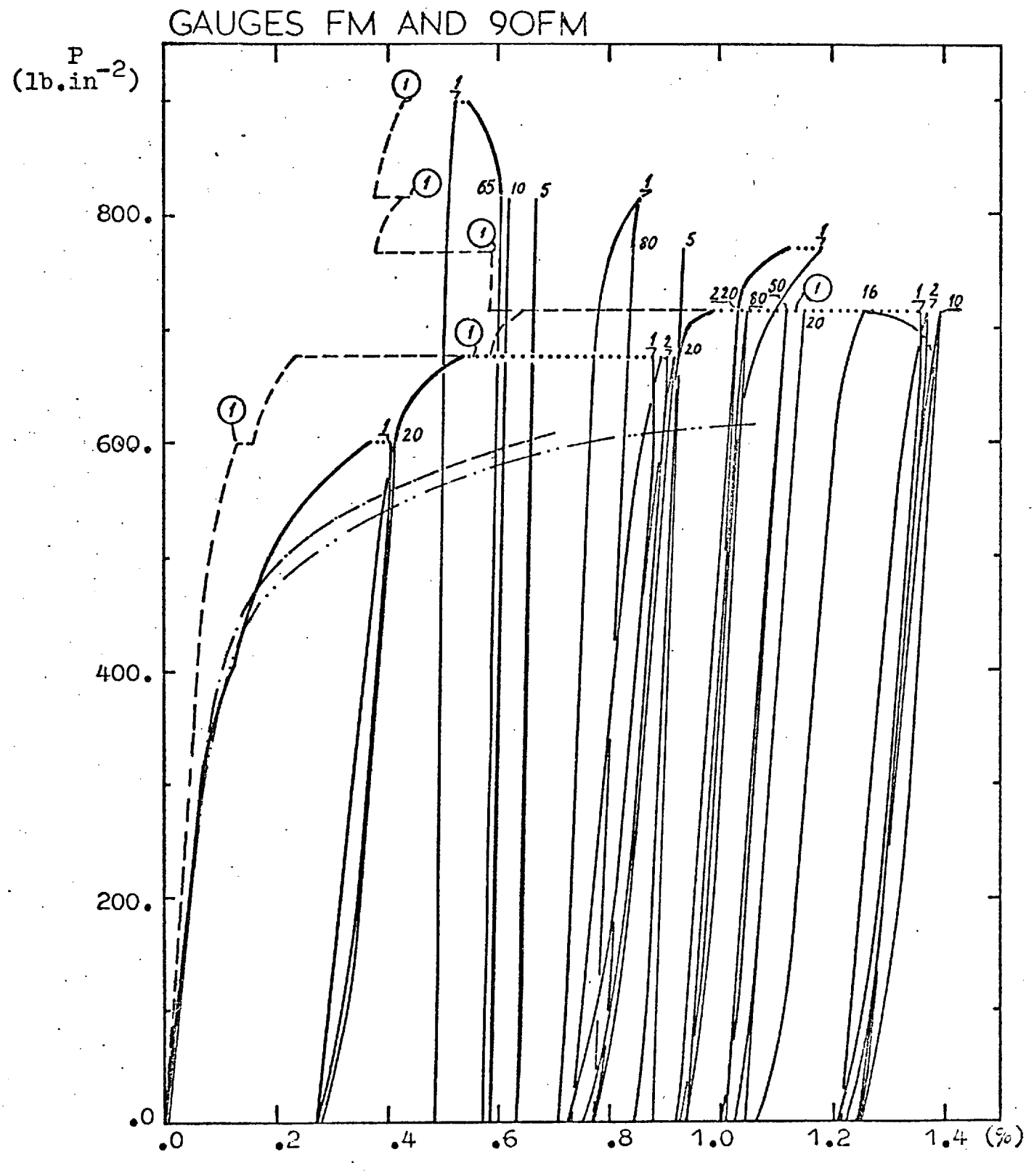

FIG. 57

MERIDIONAL STRAIN AT POSITIONS F AND 90F ON THE TEST NOZZLE

KEY:
MEASURED: —— ;1...220 CYCLE NUMBER
·····CREEP
CALCULATED
– – – – – – WORKHARDENING
—·—·—·— NON WORKHARDENING

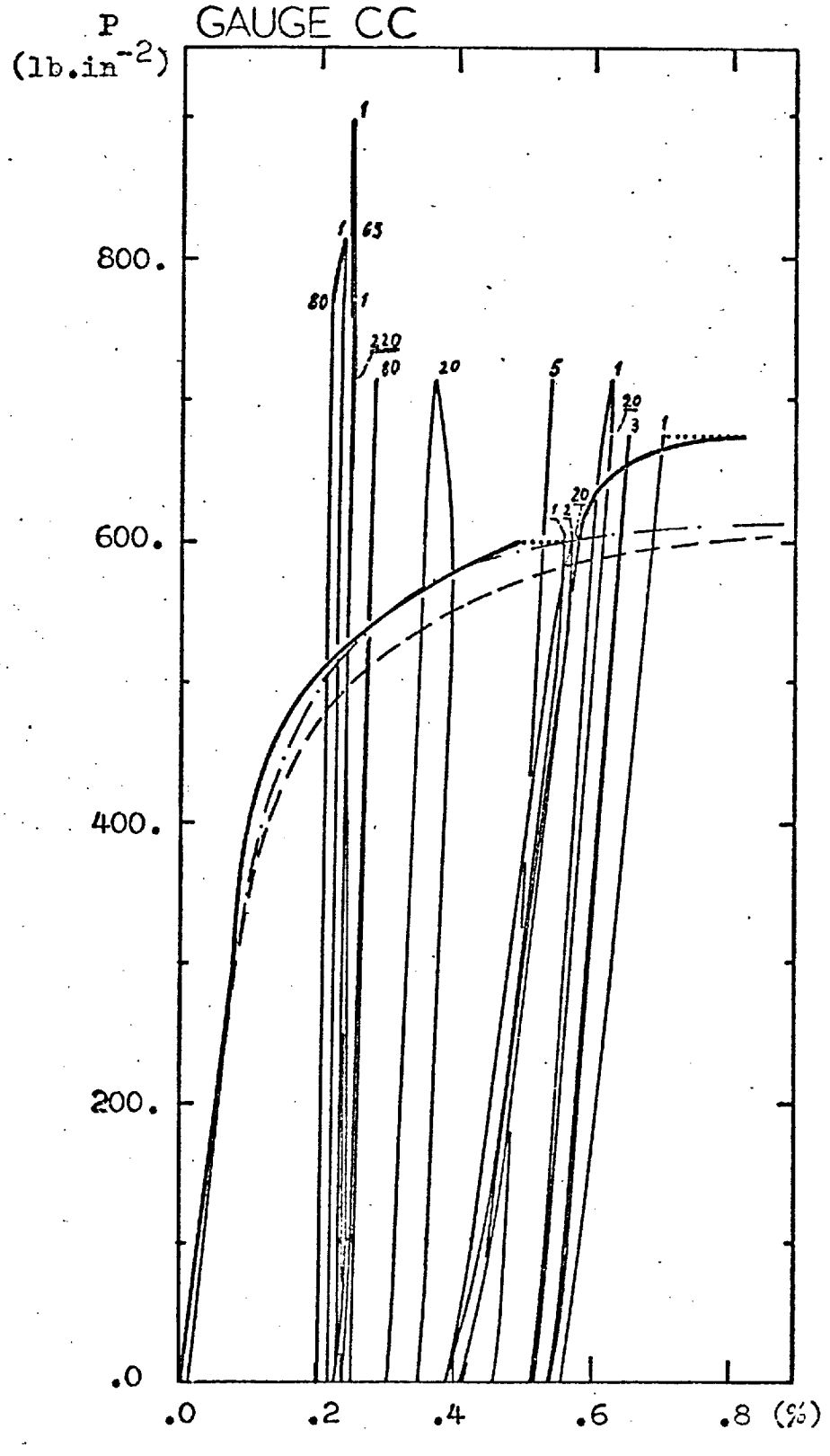

FIG 58
CIRCUMFERENTIAL STRAIN AT POSITION C ON THE TEST NOZZLE

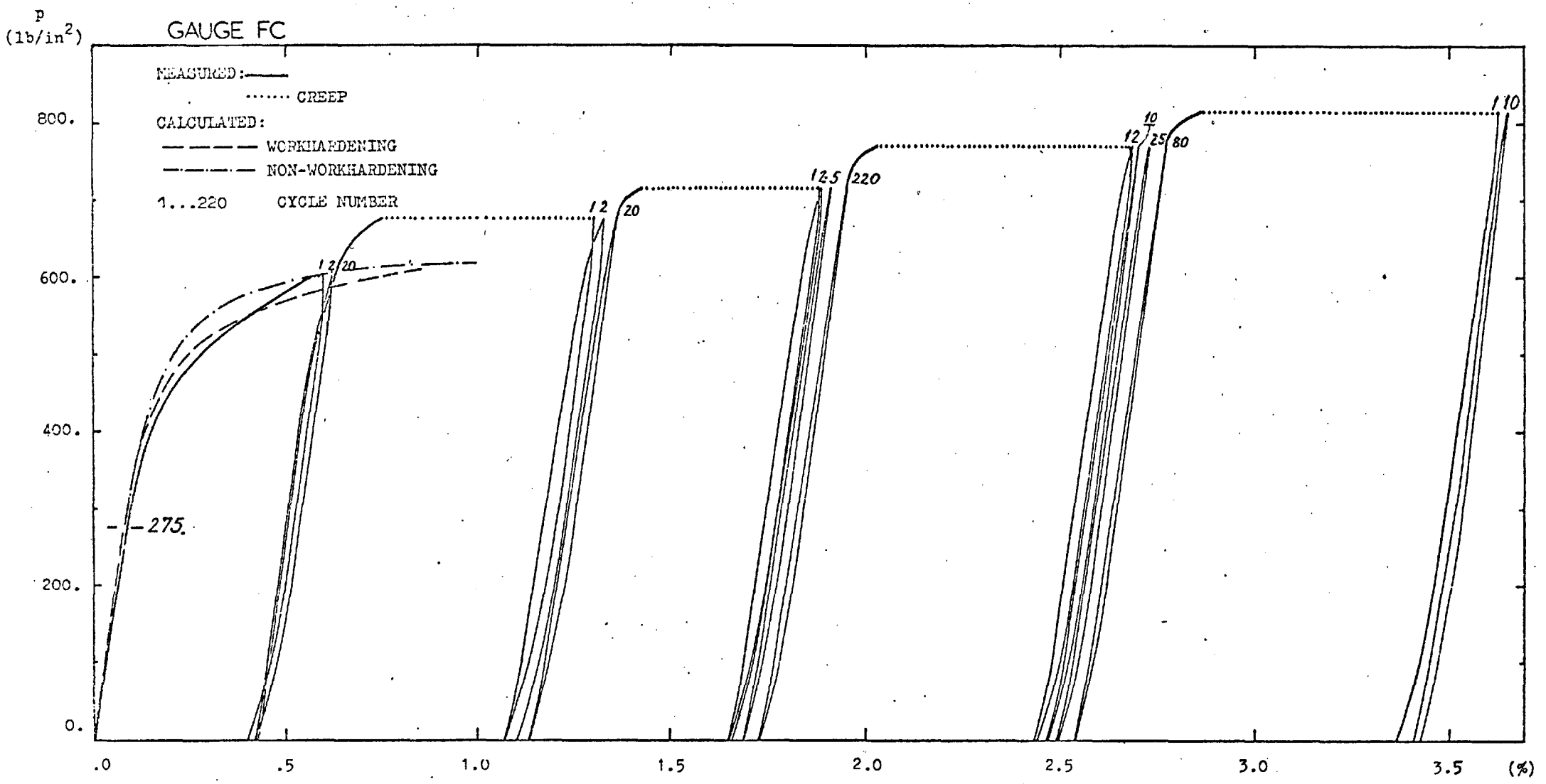

FIG.59-INTERNAL CIRCUMFERENTIAL STRAIN AT POSITION F

o.c.– Overall Creep

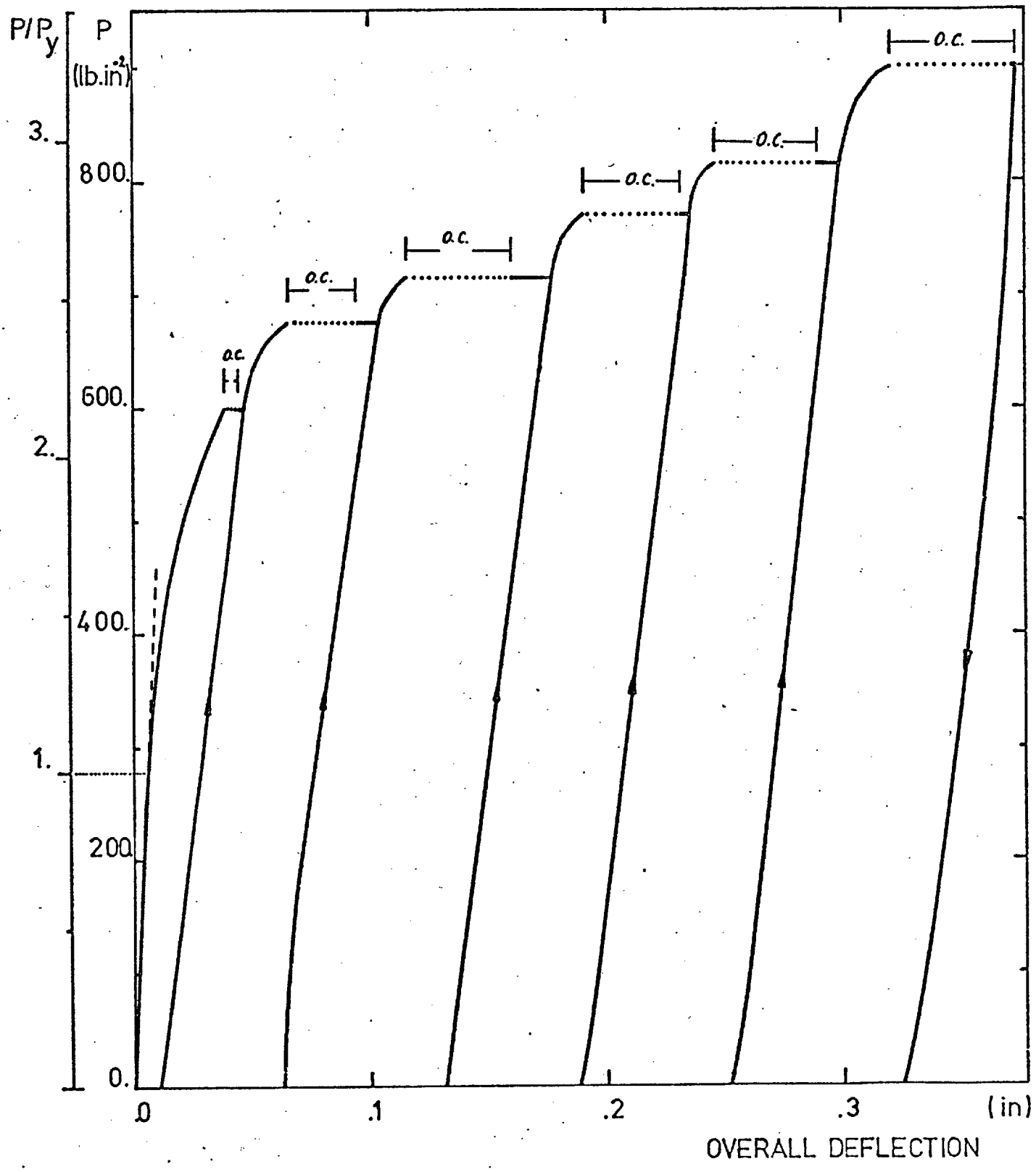

FIG. 60
OVERALL DEFLECTION CURVE

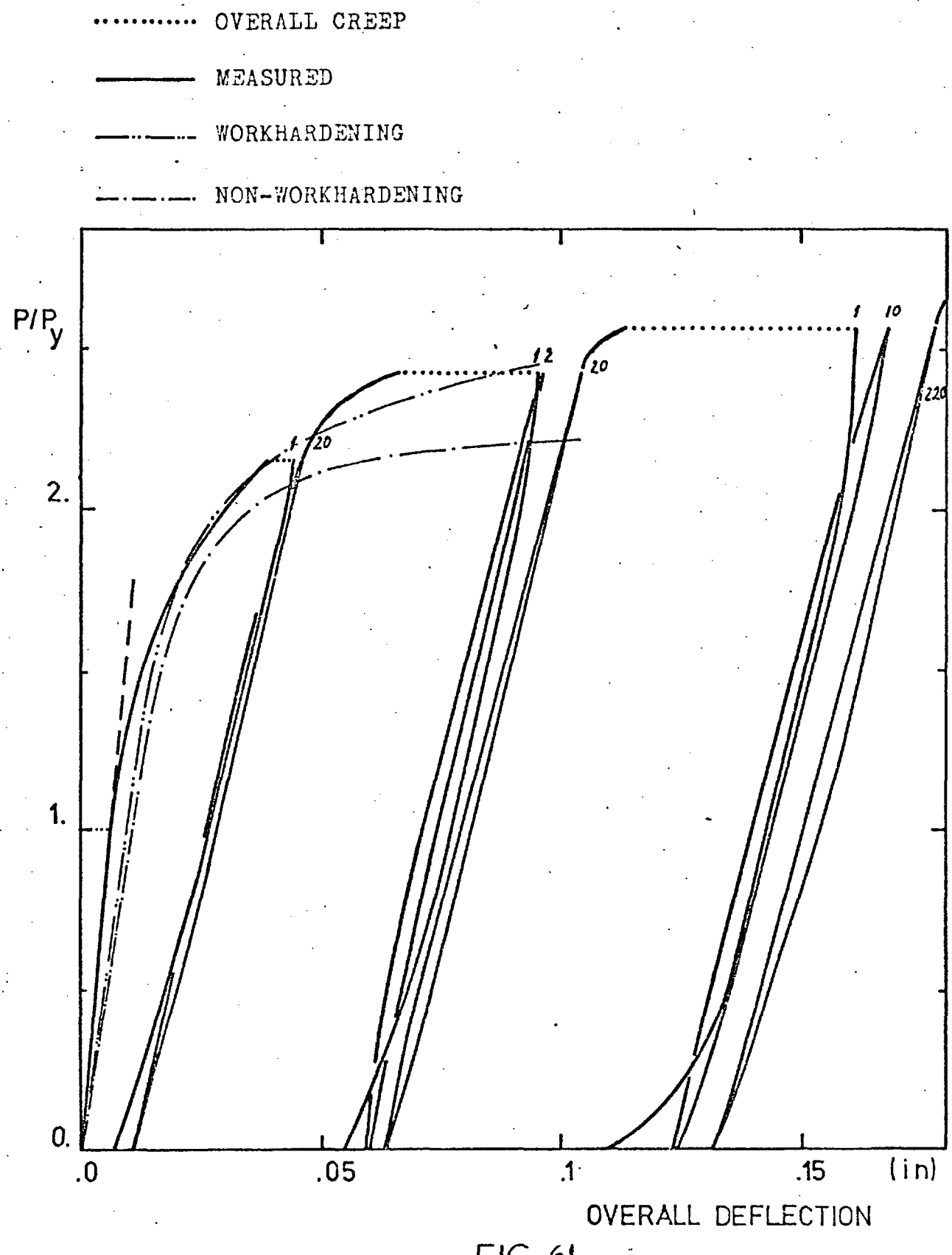

FIG. 61

OVERALL DEFLECTION CURVE